Investigating the role of RNA modifying enzymes in RNA virus infection

Innes Gordon Jarmson BSc.

Submitted in fulfilment of the requirements for the Degree of Doctor of Philosophy in Virology

September 2024

MRC – University of Glasgow Centre for Virus Research
School of Infection and Immunity
College of Medical, Veterinary and Life Sciences
University of Glasgow

Abstract

Viruses, as obligate intracellular parasites, rely heavily on their close interactions with host cells to replicate. To have a successful lifecycle, a virus must subvert the host machinery for its own use, while avoiding inducing an immune response in the cell. One mechanism of inducing an immune response is the sensing of foreign nucleic acid, whether that be through unusual nucleic acid structure or specific motifs on viral RNA and DNA. In the resting cell, all post transcriptional modifications of cellular RNA play an important role in the life cycle of RNA, and these modifications in turn act as a signal in the cell to avoid triggering an immune response. In the eternal battle of viruses and their hosts to adapt and counter adapt to overcome each other, viruses have evolved intricate mechanisms to avoid mounting an immune response. One such method is to mimic the cellular landscape of RNA to avoid being sensed by the host. To do this, viruses hijack cellular RNA modifying enzymes to 'decorate' their genomes. These modifications also serve a functional purpose in viral RNA and can enhance processes like translation of viral mRNAs. However, in the co-evolution of virus and host trying to counter each other, the host cell can also methylate viral RNA to initiate an innate immune mechanism to restrict viral growth. To understand the dynamicity of RNA modifications in viral infection, I have created a CRISPR-Cas9 knockout platform where I systematically knockout each known human RNA modifying enzyme and observe if the lack of the gene increases or decreases viral infection. This allows us to determine whether the gene of interest inhibits or enhances viral infection. Those genes that are identified as necessary for viral infection are subjected to further analysis to identify the function of these RNA modifications and if the same modifications are shared between viruses. Using this platform, I identified several RNA modifying enzymes and characterised one protein that had an antiviral effect against several viruses – NOP2. In the resting cell NOP2 is involved in ribosome biogenesis and I established that after infection it switches its activity to become an antiviral effector. The data in this thesis demonstrates the utility of arrayed CRISPR/Cas9 screening to identify new proteins involved in virus infection and how it can be used as a discovery-based platform to further characterise the host-virus arms race.

Acknowledgements

This PhD has been quite a journey! Borne during the COVID pandemic, dragged through many lows, and then finished with an unexpected change of lab group; it has been very tumultuous. However, when I look back over the last few years, I am struck by the number of wonderful people I have met who made this road more enjoyable.

I firstly would like to thank Professor Sam Wilson for letting me join his group and giving me the chance to complete my PhD at the CVR. I would also like to thank Professor Alfredo Castello for welcoming me into his group in the latter days of my PhD and pushing me to reach the finish line. I have learned a lot from both and have developed my hands on research skills as well as my adaptability, communication and independence.

I received advice and support from numerous people throughout this PhD, whose help I could not have done without. Dr Matt Turnbull had endless advice about flu, a willingness to help and an infinite supply of dad jokes; Dr Elena Sugrue sacrificed a lot of time to provide advice and guidance and generally made working through the pandemic more fun. I would like to thank the other members of the Wilson Group who helped me settle into life at the CVR in the early days and were a fun group of people to work with: Douglas Stewart, Dr Arthur Wickenhagen, Dr Afiq Aziz, Gauthier Lieber, Hollie Jackson Ireland, Emma Davies, Dr Simon Swingler, Vlad Litvin and Yongtao He.

I could not have settled into the Castello group without the support of every single lab member. I am forever indebted and grateful to Dr Azman Embarc, Dr Louie Iselin, Natasha Palmalux and Rozeena Arif for experimental advice and indispensable help with data analysis. Dr Marko Noerenberg, Dr Wael Kamel, Dr Enzo Ruscica, Zaydah Rolande de Laurent and Namah Raut provided on the spot advice as I navigated settling into a new lab and all were a joy to chat and work with. I am very grateful that every member of the group wanted to help me finish this PhD.

On the very first day of my PhD, I met a small group of people who all had completely different personalities, but we ended up becoming a fun group of friends: my cohort.

The five of us felt isolated at the CVR, being disconnected from the rest of the university but their friendship helped me throughout the PhD journey. It has been a great source of joy and encouragement to see all of them successfully submit their theses and pass their vivas. Dr Alex Wilson, who has become a lifelong friend and made living in Anniesland a bit more fun. I will always remember the coffees at beefcake and the random activities she made us take part in. Dr Anna Sims, who truly was a part of the Renaissance of my PhD. Dr Spyros Lytras, possibly the keenest student there ever was and his passion for science was always infectious. Dr Kasim Waraich, the calmest PhD student I have ever met, always has good chat and his sense of humour brightened many days over the last few years. I also need to shout out honorary member Hollie Ireland who is one of the funniest people ever, and an excellent researcher.

I also need to thank my amazing family. My Mum and Dad have always supported me throughout my PhD, and my entire career in general. Karen, Rafał, Louise, Teddy and Thor are my biggest cheerleaders who never bat an eye at my antics. Thank you to all my friends who have supported me from afar and even through periods of radio silence. Particularly to Laura, Georgie, Sam, Sarah and Yana. All brighten my life and thank you for your incredible friendship.

There are countless people I have not named here who helped the ticking over of the PhD. Technical staff, post-docs, students, admin staff, floor coordinators, washroom staff…the list is incomprehensively large. I am forever grateful.

Table of Contents

List of Figures

List of Tables

Chapter 1 Introduction

The innate immune response to viral infection

The immediate response to an infection is based on two coupled processes: pathogen detection and alarm. The main effectors of the 'alarm' in the innate immune response are a group of secreted monomeric cytokines known as interferons (IFNs). The concept of interferon-based immunity was first described in 1957, when Isaacs and Lindenmann reported that the fluid surrounding chick embryos infected with influenza A (IAV) contained a non-viral protein that rendered noninfected cells resistant to IAV challenge (Isaacs & Lindenmann, 1957). Since then, it has been demonstrated that interferons are not a singular entity but a diverse family of proteins which can be classified into three distinct classes: type I, type II and type III (Schoggins, 2019). The type I IFN family encompasses 17 distinct proteins in humans, including 13 IFNα subtypes, IFNβ, IFNε, IFNκ, and IFNω. These proteins exert their effects by binding to the heterodimeric IFNα receptor (IFNAR), thereby initiating a robust intracellular antiviral response (Pestka et al., 2004). Similarly, type III IFNs (IFNλ1-4) activate an antiviral program through the heterodimeric IFNλ receptor (IFNLR1/IL10R2) complex (Sheppard et al., 2003; Kotenko et al., 2003). Distinct from the ubiquitously expressed IFNAR, the IFN-III receptor complex is predominantly expressed in cells at mucosal barrier sites, thus confining the antiviral effects of IFN-IIIs to these localised regions (Sommereyns et al., 2008). In contrast, the type II family is represented solely by IFNɣ, which signals through the IFNɣ receptor (IFNGR). IFNɣ is produced by cells of both the innate and adaptive immune systems and is pivotal in inducing a pro-inflammatory response (Schroder et al., 2003).

This work will focus on the type I IFN (IFN-I) response, principally on specific mechanisms of how it is stimulated by viral RNA.

The induction of IFN-I through pathogen sensing

Viruses, as obligate intracellular parasites, rely heavily on their close interactions with host cells to replicate. During viral infections, host cells detect various viral pathogen associated molecular patterns (PAMPs) as foreign through different classes of pattern

recognition receptors (PRRs). This detection activates distinct signalling pathways, leading to the production of IFNs and proinflammatory cytokines. PRRs can detect viral infections by identifying distinctive features of viral nucleic acids. There are many other features of viruses that PRRs can recognise (Carty et al., 2021). However, I will focus on nucleic acid recognition receptors which includes: The toll-like receptors (TLRs) which sense endosomal DNA and RNA; the RIG-I-like receptors (RLRs) sense cytosolic double-stranded RNA (dsRNA); and the cyclic GMP–AMP synthase (cGAS) and IFI16 which sense cytosolic DNA (Schlee & Hartmann, 2016). Simplified signalling cascades are outlined in Figure 1.1.

Despite each PRR recognising distinct features of nucleic acids, they all stimulate a signal transduction cascade that results in the production of IFN-I (Cai et al., 2021). This level of redundancy in the process is achieved through the convergence of each signalling cascade at the level of interferon regulatory factor (IRF) phosphorylation and homodimerization. This results in the translocation of these molecules to the nucleus where they bind to the promotors of IFN-I genes and initiate transcription (Schlee and Hartmann, 2016). Interestingly the subtypes of IFN-I produced depend on the cell type and IRF dimer composition. IRF3 is expressed in most cell types and drives IFNβ production, whereas IRF7 is highly expressed in plasmacytoid dendritic cells (pDCs) and favours IFNα production (Honda et al., 2005; Honda et al., 2006). These pathways also converge in other processes like the phosphorylation of an Nf-kB inhibitor. Nf-kB is involved in activating transcription of pro-inflammatory cytokines (TNF-α, IL-1β, IL-6, IL-12p40 and cyclooxygenase-2), which reflects the wide range of roles that PRRs contribute to antiviral immunity (Liu et al., 2017).

The toll like receptors (TLRs) are a family of type I transmembrane proteins that have a leucine rich repeat domain which interacts with PAMPs and determines ligand specificity, and a cytoplasmic toll-interleukin-1 receptor (IL-1R) homology (TIR) domain that activates downstream signal transduction (Akira & Takeda, 2004). There are 10 TLRs in humans, however TLRs 3, 7, 8 and 9 reside in endosomal compartments. This means that they primarily recognise incoming viral nucleic acids through endocytosis, however they can also sense nucleic acids of neighbouring cells through autophagy or cell-to-cell transfer of RNA-containing exosomes (Manuse et al., 2010;

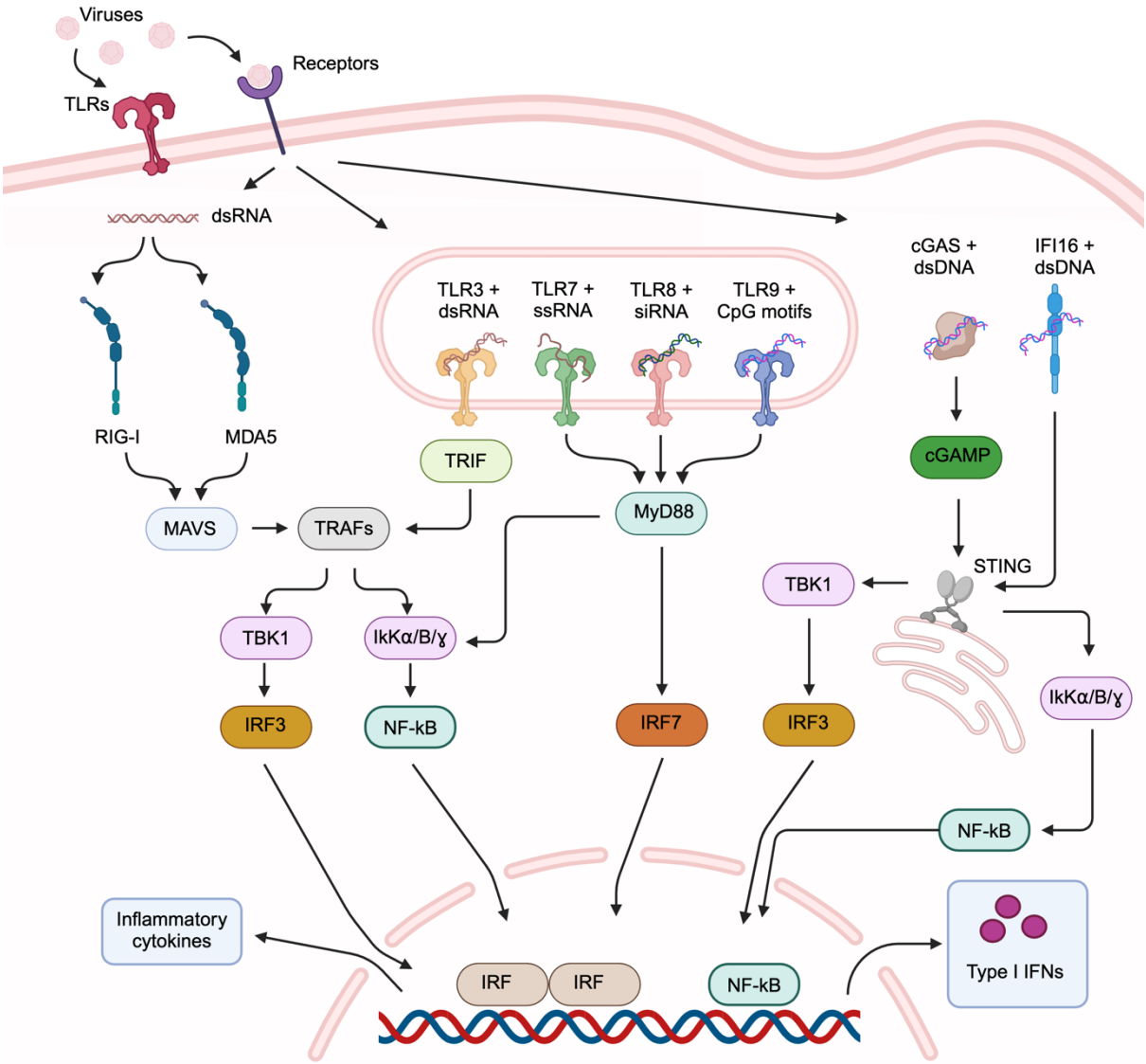

Figure 1.1: Recognition of foreign nucleic acids that induce IFN-I. The RLRs, TLRs and STING pathway all contribute to detection of invading pathogen PAMPs including ssRNA, dsRNA, RNA nucleotides, siRNAs and unmethylated CpG containing DNA. As each receptor binds its cognate nucleic acid on the cell surface, in the cytoplasm or in the lumen of endosomes, signal transduction leads to the activation of Nf-kB, IRF3 or IRF7 which induces the expression of inflammatory cytokines and IFN-I. In the TLR pathway, proteins involved in the signal transduction cascade, including TRIF and MyD88, interact with the cytoplasmic tails of endosomal TLRs after they have bound their associated ligand. The RLRs RIG-I and MDA5 signal via interaction with an adapter protein on the outer mitochondrial membrane protein (MAVS), that activates IRF3 and NF-kB pathways. In the STING pathways, recognition of dsDNA causes cGAS to synthesise cGAMP as its second messenger molecule. cGAMP and IFI16 then bind and activate the ER-resident receptor STING. Activated STING then translocates to the perinuclear Golgi compartment where it takes part in activating IRF3 and NF-kB.

Takahashi et al., 2010). TLR3 was the first characterised nucleic acid sensing TLR. Initially described to be stimulated by a dsRNA analogue, poly I:C, it was later shown

that engagement with synthetic or viral dsRNA of >90bp, which is commonly produced in the cycle of DNA and RNA virus infection, activates downstream signalling by TLR3 (Alexopoulou et al, 2011; Leonard et al., 2008). When TLR3 interacts with synthetic or viral dsRNAs, it triggers the TRIF-dependent pathway that leads to IRF3 phosphorylation (Figure 1.1) (Matsukura et al., 2006). TLR3 is ubiquitously expressed in tissues (Zarember & Godowski, 2002) however is absent from pDCs where TLR7 and TLR9 are highly expressed (Lester and Li, 2014). TLR7 and TLR8 primarily recognise viruses that enter the endosome through endocytosis. They recognise GU- and AU- rich ssRNA sequences of RNA viruses (Diebold et al., 2004). TLR9 is specific for unmethylated CpG motifs that are commonly found in bacterial as well as viral DNA (Latz et al., 2004). TLR7, TLR8 and TLR9 initiate the MyD88-dependent pathway, resulting in IRF7-mediated IFN-I production (Honda et al., 2005; Kawai & Akira, 2011).

RIG-I-like receptors (RLRs) are a family of cytoplasmic RNA helicases that play a key role in the detection of viral RNA, including RIG-I, MDA5 and LGP2 (Yoneyama et al., 2004; Andrejeva et al., 2004). These proteins share several structural features that are crucial for their function. They have a DExD/H Box RNA helicase domain which is responsible for unwinding RNA, a C-terminal domain that recognises and binds to viral RNA, specifically the 5'triphosphate end of RNA, and tandem Caspase Activation and Recruitment Domains which are essential for downstream signalling induction (Kowalinski et al., 2011; Jiang et al., 2011; Cui et al., 2008, Berke et al., 2012). Even though they have similar structures, RIG-I and MDA5 have distinct roles in pathogen sensing because they have different specificities and recognise different features of RNA (Yoneyama et al., 2024). RIG-I recognises short double stranded RNA (dsRNA) and single stranded RNA (ssRNA) with a 5' - triphosphate or - diphosphate end that lacks 2'-O-methylation (Pichlmair et al., 2006; Schlee et al., 2009; Schuberth-Wagner et al., 2015). This is often found in viral genomes and replication intermediates. MDA5 detects long dsRNA, which is typically produced during the replication of many viruses (Dias Junior et al., 2019; Thoresen et al., 2021). Foreign nucleic acid is not the only targets of RLRs; MDA5 is triggered by dsRNA released from damaged mitochondria, which often occurs during infection (Dhir et al., 2018). Upon binding RNA, RLRs undergo a conformation change that exposes its CARDs which interact with MAVS on the mitochondrial membrane to initiate the activation of downstream IFN signalling pathways (Figure 1.1). This cascade ultimately activates transcription factors such as

IRF3, IRF4 and NF-kB, which induce the production of type I interferons and other cytokines (Goubau et al., 2013).

Cytosolic DNA sensors. dsDNA is seldom found in the cytosol and its presence could signal infection or cellular damage. cGAS serves as a pivotal cytosolic DNA sensor, recognising dsDNA within the cytoplasm and has been shown to limit herpes simplex 1 (HSV-1) infection (Sun et al., 2013; Reinert et al., 2016). Upon binding to dsDNA, cGAS undergoes a conformational change that activates its enzymatic function, leading to the synthesis of cyclic GMP-AMP (cGAMP) (Civril et al., 2013; Wu et al., 2022). This second messenger subsequently binds to and activates the adaptor protein STING (Stimulator of Interferon Genes) located on the membrane of the endoplasmic reticulum. IFI16 can also activate STING; it oligomerises on cytoplasmic DNA which interact with STING (Unterholzner et al., 2010; Jønsson et al., 2017). This has been observed against HSV-1 dsDNA (Lum et al., 2019). The activation of STING initiates a signalling cascade culminating in the production of type I interferons and other proinflammatory cytokines through the activation of transcription factors IRF3 and NF-kB (Yu et al., 2021). Additionally, IFI16 shuttles between the nucleus and the cytoplasm, enabling it to sense nuclear DNA that has been damaged or mislocalised (Almine et al., 2017).

STING has also been implicated in the infection of RNA viruses (Ishikawa & Barber, 2008). It interacts with RIG-I and MAVS, which are responsible for viral RNA sensing, and deletion of STING impaired RIG-I mediated innate signalling during infection with Japanese encephalitis virus (Namzi et al., 2012). Additionally, IFI16 positively upregulates RIG-I transcription and binds IAV RNA during IAV infection to promote the production of type I IFN (Jiang et al., 2021). In DENV infection, damage to mitochondria results in release of mtDNA, which is sensed by cGAS (Sun et al., 2017).

In contrast to the wide knowledge of cytosolic sensors of infection, less is known about nuclear detectors of nucleic acids. Detection of single-stranded nucleic acid, like that from a single -stranded nuclear virus like Influenza, or exposed ends of dsDNA may cause the DNA damage response. An example of this is herpesvirus DNA in the nucleus is bound by IFI16 which induces the expression of antiviral cytokines (Lum et al., 2019).

The cellular response to IFN-I stimulation

Following their synthesis and release, IFNs have potent antiviral and growth-inhibitory effects. IFNs induce the expression of hundreds of genes which mediate various biological responses (Der et al., 1998). Some of these genes are regulated by both type I and type II IFNs, whereas others are selectively regulated by distinct IFNs. IFITM1 is induced by all IFNs, whereas expression of 2',5'-oligoadenylate synthetase I (OAS1) is selectively induced by IFNα and IFNβ but not IFN-ɣ (Der et al., 1998).

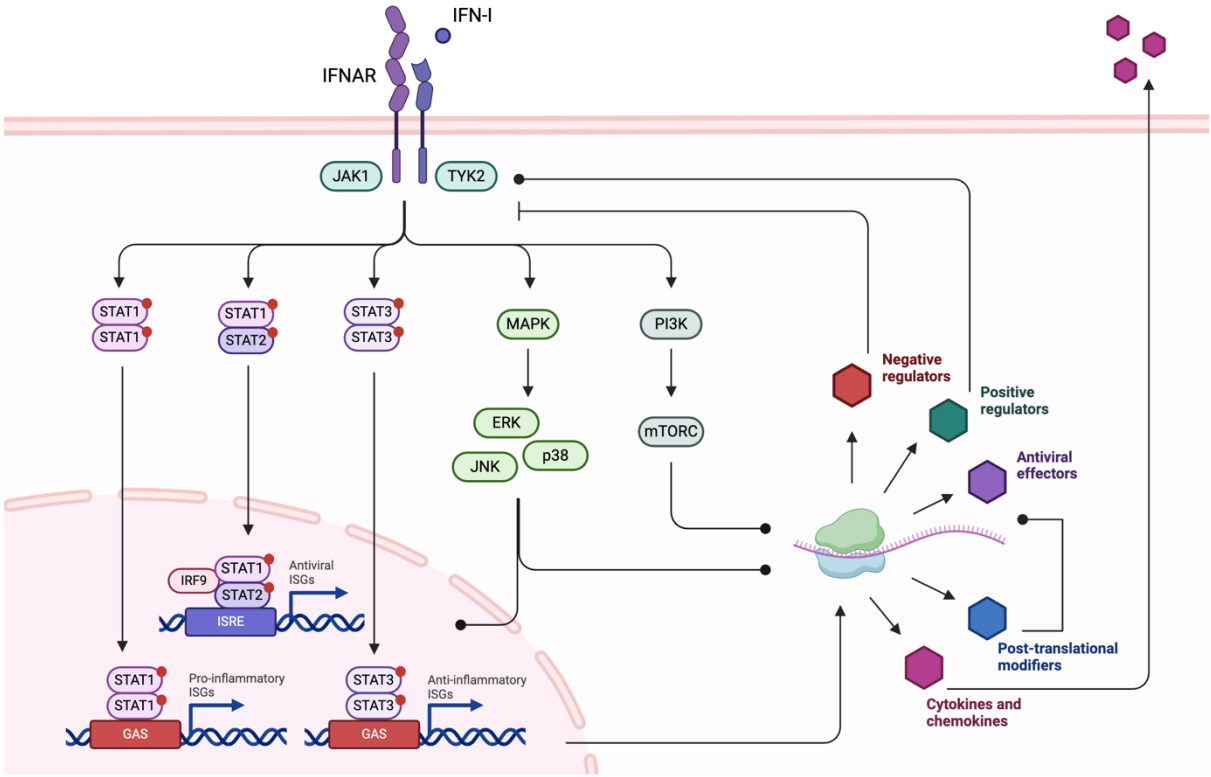

Figure 1.2: Signalling pathways induced by IFN-I. JAK1 and TYK2 become phosphorylated upon IFN-I binding to IFNAR. They then phosphorylate STAT proteins which induces formation of STAT homo- or hetero-dimers. In the nucleus STAT1/STAT2 form a complex with IRF9 to form ISGF3, which binds to ISREs to induce transcription of ISGs. STAT1 and STAT3 homodimers bind to GAS elements in the genome to upregulate expression of inflammatory genes. These STAT induced transcripts can then be translated into various factors involved in the antiviral response. Additionally, MAPK and PI3K pathways can also be activated by IFNAR induced signalling and regulate transcription and translation.

IFN I induced transcription

The first signalling pathway to be discovered was the canonical JAK-STAT pathway which involves the rapid nuclear translocation and initiation of gene transcription of interferon stimulated genes (ISGs) which are responsible for the effects of IFNs

(Schindler et al., 1992). Following their synthesis and release, IFNα and IFNβ bind to IFNα receptor (IFNAR), a heterodimeric transmembrane receptor composed of IFNAR1 and IFNAR2 on the plasma membrane of cells (Ivashkiv & Donlin, 2014). Tyrosine kinases (JAKs) Janus kinase (JAK1) and tyrosine kinase 2 (TYK2) bind the cytosolic portions of IFNAR1 and IFNAR2 receptors, respectively, and upon IFN engagement, a conformational change in IFNAR brings the JAKs into close proximity permitting their trans-phosphorylation and activation (Velazquez et al., 1992). They in turn phosphorylate tyrosine residues in the cytosolic region of the IFNAR subunits (Stark & Darnell, 2012). These phosphorylated tyrosine residues in the IFNAR subunits bind and phosphorylate the latent cytoplasmic STAT (signal transducer and activator of transcription) family, which comprises seven proteins that are all involved in downstream transcriptional regulation of a range of cytokine receptors.

In the canonical IFN-I signalling pathway, STAT1 and STAT2 become phosphorylated. Phosphorylated STAT1 and 2 dimerise and translocate to the nucleus. An important transcriptional complex is formed in the nucleus by STAT1 and STAT2 assembling with IFN-regulatory factor 9 (IRF9) to form a trimolecular complex called IFN-stimulated gene factor 3 (ISGF3) (Levy & Darnell, 2002; Stark & Darnell, 2012). ISGF3 binds to ISREs (IFN-stimulated response elements) that are present in the promoters of certain ISGs, thus initiating their transcription (Platanias, 2005). STATs interact, in the nucleus with several co-activators that have important roles in regulating transcription, like p300, CBP, MCM3 (Platanias, 2005). The recruitment of each of these depends on the phosphorylation of STAT Ser727 (Zhang et al., 1998). Many of these factors are important for chromatin remodelling as regions where ISGs are encoded have low GC content which leads to a high nucleosome content (DaFonseca et al., 2001; Hebbes et al., 1988), and RNA-seq experiments demonstrated binding of ISGF3 increases promoter availability (Bhatt et al., 2012). An ATP-dependent nucleosome complex named BAF is one of these accessory factors, which remodels chromatin and directly interacts with STAT2 (Cui et al., 2004).

ISGF3 can also act in consort with a range of other transcription factors, the best characterised of these is with members of the IRF family (Tamura et al., 2008). ISGF3 directly activates gene expression of IRF1, IRF7, IRF8 and IRF9. The promoter sequences recognised by most IRFs overlap with the ISRE, and so these IRFs can

bind and activate many of the same target genes that ISGF3 can. These newly expressed IRFs can then activate a second group of ISGs (van Boxel-Dezaire et al., 2006). This drives a delayed second wave of ISG induction (Levy et al., 2002).

In addition to the formation of ISGF3 by STAT1 and STAT2, IFNAR can also activate other STATs which induce different patterns of downstream gene expression (leading to parallel transcriptional programs that alter the nature of the antiviral response). These include STAT1 and STAT3 homodimers and heterodimers, and STAT4, STAT5 and STAT6 in some cell types (van Boxel-Dezaire et al., 2006). Such complexes bind another type of element that is present in the promoter of ISGs – the IFNɣ-activated site (GAS) element (Platanias & Fish, 1999). The GAS element is primarily found in the promoters of genes associated with an inflammatory response. Among all the known ISGs, some have only ISREs or only GAS elements in their promoters, while others contain both (Stark et al., 1998). As a result, different combinations of STAT-containing complexes may be necessary for the optimal transcriptional activation of specific genes. The balance between the activation of STAT1/STAT2, STAT1/STAT1 and STAT3/STAT3 dimers by IFNAR is partially determined by relative STAT expression levels and the phosphorylation state of STATs (Hu et al., 2002). For example, STAT1 expression levels can be increased by the ISGF3 pathway and phosphorylation at Tyr701 favours formation of STAT1 homodimers in the type II IFN response (Darnell, 1997). Contrastingly, STAT1 can be phosphorylated by inhibitor of NF-kB kinase-ε (IKKε) at S708 which suppresses homodimer formation but does not disrupt heterodimerisation with STAT2. Thus, this phosphorylation favours ISGF3 formation (Sze-Ling et al., 2011). In contrast to STAT1 homodimers, STAT3 homodimers activate genes that suppress IFN-I response by promoting transcription of negative regulators (Murray, 2007).

In addition to the JAK STAT transcriptional response, there are STAT independent IFN-driven signalling cascades. MAPK and PI3K/AKT/mTOR are the best characterised examples of these. These kinases participate in transcriptional regulation, as has been demonstrated for MAPK-p38. The MAPK pathway is activated by Guanine nucleotide exchange factors (GEFs) that have been phosphorylated, upstream, by IFN-activated JAKs. Inhibition of p38 through gene disruption or a use of a drug, blocked IFN-α dependent transcription of genes that are regulated by ISREs (Uddin et al., 1999) and

GAS elements (Li et al., 2004). Inhibition of p38 did not block tyrosine phosphorylation of STATI or STAT2, nor the formation of the mature ISGF3 complex and subsequent binding of ISGF3 to ISREs, demonstrating that there is an ISRE based mechanism of IFN-driven signalling that is independent of STAT activation (Uddin et al., 1999). P38 also does not act as a serine kinase towards STAT1 in response to IFN-I, further indicating that this mechanism is independent of STAT activation (Uddin et al., 2000).

Upregulation and refinement of the IFN-I response

Regulation of immune genes at the level of translation is essential as many proteins are required within minutes following stimulation. The translation of effectors of host defence, such as ISGs, is maintained and regulated in the context of globally supressed translation, however there are also mechanisms induced by IFN-I signalling which can regulate translation. Eukaryotic initiation factor 4E binding proteins 1 and 2 (4EBP1/2) are translational repressors that regulate the translation of specific mRNAs. They bind eukaryotic initiation factor 4E (eIF4E) to bring about this repression. Mammalian target of rapamycin (mTOR) is a serine/threonine kinase that is activated by TLR ligands through MyD88-TRIF-PI3K-AKT pathways. mTOR phosphorylates eIF4E-binding proteins (4EBPs) which causes them to release eIF4E which is then able to participate in initiating cap dependent translation by interacting with the 5'mRNA cap structure and factors involved in recruiting the 40S ribosomal subunit (Lekmine et al., 2004). 4EBP-depleted cells have increased production of type I IFN following exposure to poly(I:C) or RNA virus infection, showing that it is involved in the repression of ISGs in an unstimulated cell (Colina et al., 2008). Interestingly, genes which have long and highly structured 5'UTRs, like IRF7, depend on eIF4E for translation and are stimulated in cells in which 4EBP1/2 are depleted (López-Pelaéz et al., 2012).

There are also higher levels of regulation of the IFN-I response with examples at the post translational level. Differential phosphorylation of the cellular proteome has been documented in IFN-treated astrocytes and microgila. These proteins were involved in canonical IFN-I signalling but also in other signalling pathways, reflecting the global effect of the IFN-I response (Viengkhou et al., 2021). Proteins can also be ISGylated: this involves the addition of ISG15 to proteins in a post-translational process during the IFN-I response (Durfee et al., 2010). ISG15 is a ubiquitin-like protein that can

regulate the stability and function of viral and cellular proteins and can fine-tune signalling cascades (Mirzalieva et al., 2022). Many of the proteins that are ISGylation targets have not been linked to IFN signalling, suggesting that this regulation is occurring outside of the canonical IFN-I response (Thery et al., 2021). Beyond post-translational modifications of proteins, protein-protein interactions are affected and altered under IFN-I treatment. Most of these novel interactions involved proteins whose abundance was not altered by IFN-I and therefore are probably not ISGs (Kerr et al., 2020). This was also documented in the case of IFIT proteins. They have very few interaction partners under resting conditions, however after IFN-I treatment, they acquired a network of interaction partners (Pichlmair et al., 2011). These changes are perhaps driven by alterations in the post-translational modification landscape and changes in proteins' localisation patterns, however this has yet to be elucidated.

Negative regulation of the IFN-I response

Since many of the gene products characteristic of the antiviral state can cause toxicity in the cell, it is important to suppress the response once viral reproduction has been controlled. This is brought about by negative feedback regulators, some of which are actually ISGs. ISGs, such as suppressor of cytokine signalling (SOCS) and ubiquitin-specific peptidase 18 (USP18) are induced by IFN-I to inhibit the signalling pathways that IFN-I activates. SOCS can inhibit the JAK-STAT pathway by binding to phosphorylated tyrosine residues on IFNAR or JAKs, thus they compete with STATs for binding to IFNAR. This also promotes the ubiquitination of IFNAR and subsequent degradation (Schneider et al., 2014). Gene knockout studies have shown that SOCS proteins are indispensable regulators of important physiological systems. Mice that lack SOCS1 and SOCS3 die early in life, even in the absence of viral infections; they have liver disease, inflammatory lesions, lymphopenia, apoptosis of lymphoid organs and anomalous T cell activation, all probably the result of unrestricted IFN signalling (Starr et al., 1998; Ushiki et al., 2016). USP18 displaces JAK1 from IFNAR2 and causes loss of downstream signalling (Malakhova et al., 2006). USP18 is also partially responsible for removing ISG15 moieties (Durfee et al., 2010). USP18 depletion in mice caused higher levels of ISGylation and increased sensitivity to IFN-I (Malakhov et al., 2002).

When type I IFN is not regulated in humans it can cause interferonopathies which causes chronic inflammation and autoimmune symptoms, for example Systemic Lupus Erythematosus (SLE) and Aicardi-Goutières syndrome (AGS). This can be due to either excessive interferon production, caused by mutations in genes that regulate the immune response or increased recognition of self-DNA, or lack of proper regulation. ISG15 is a key modulator of this balance by modifying key immune proteins and preventing overactivation of the immune system. When this regulation is compromised, e.g. by mutations that impair the ISGylation pathway, it can lead to chronic inflammation and autoimmune activation (Mirzalieva et al., 2022).

There are also negative feedback mechanisms that operate prior to initiation of the ISG transcriptional program. Beyond interfering with IFNAR engagement with internal interactors, a MAPK-p38 kinase mediated mechanism facilitates the internalisation and subsequent degradation of IFNAR (Bhattacharya et al., 2011). When cells are co-stimulated by TLR/ITAM agonists, the phosphatase SHP2 becomes activated and phosphorylates STAT proteins to inhibit their dimerization and downstream signalling (You et al., 1999). PIAS (Protein inhibitor of activated STAT) proteins can also limit the IFN response by regulating downstream STAT signalling capacity. PIAS1 limits STAT1's interaction with ISREs through SUMOylation-dependent and independent pathways (Rogers et al., 2003).

These are just a few examples of the wide regulation of the IFN response.

Antiviral effectors of the immune response

The outcome of the IFN-I signalling cascade is an increase in transcription of hundreds of ISGs. Among these hundreds of IFN-induced genes, many have been ascribed direct antiviral activity: ISGs have evolved to target each stage of the viral lifecycle. There is a certain redundancy of antiviral ISGs, which demonstrates that even in the absence of specific ISGs, a successful antiviral response mounted (Zhou et al., 1999). Additional functions of these proteins, and regular identification of new proteins, means a fully comprehensive discussion of the effectors of the immune response is outside of the scope of this introduction, but what follows is a section detailing illustrative examples against each stage of the virus life cycle.

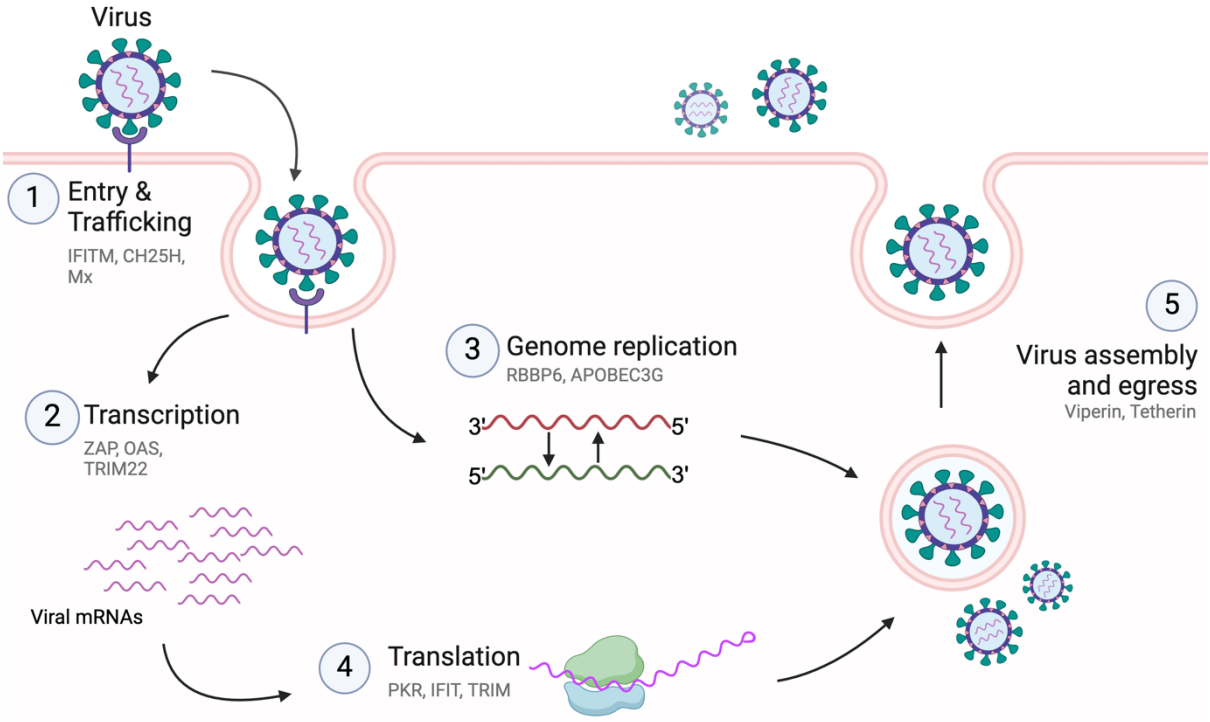

Figure 1.3: ISG mediated antiviral processes. Figure showing the stages of a viral lifecycle that can be targeted by ISGs with example ISGs at each stage.

Entry and Trafficking

To initiate their lifecycle, viruses first have to attach and enter the cell. There are few ISGs that target initial attachment, but several ISGs target viral entry. These ISGs act through disrupting the ability of viruses to initiate membrane fusion or disrupting the endocytic pathway and virus trafficking. The Interferon-inducible transmembrane proteins (IFITM) proteins were identified in genome wide screens to restrict an early step in influenza A viral replication, and some flaviviruses like dengue virus and West Nile virus (Brass et al., 2009). IFITMs are predominantly located at the plasma membrane or in endosomal organelles, thus they primarily affect viruses that enter through the late endocytic pathway. Their mechanism of restriction is still disputed; however, membrane fusion studies suggest IFITM proteins modulate the fluidity of cellular membranes (Guo et al., 2021) or disrupt intracellular cholesterol homeostasis (Amini-Bavil-Olyaee et al., 2013).

The IFN inducible enzyme cholesterol-25-hydroxylase (CH25H), is responsible for cholesterol homeostasis and converts cholesterol to the more permeable 25-hydroxycholesterol (25HC). Cholesterol is important for signalling, membrane

trafficking and viral entry, replication and assembly. 25HC renders the bilayers less rigid and reduces their membrane trafficking and signalling responses (Domingues et al., 2021). The presence of 25HC at the membrane level has been shown to interfere with several viruses' entry into their target cells by blocking membrane fusion, such as VSV, HSV and HIV (Liu et al., 2013). However, recently CH25H has been demonstrated to inhibit HCV through sequestering its NS5A protein, which is essential for genome replication (Chen et al., 2014).

The Mx proteins have been implicated in blocking viral trafficking to the nucleus in IAV infection (Haller et al., 1980). The Mx family GTPases were first identified as mice with mutations in the Mx locus were highly sensitive to IAV infection (Haller et al., 1979). Located near the smooth endoplasmic reticulum, Mx proteins can monitor endocytic events and manage vesicle trafficking to trap essential viral components, preventing viral replication early on (Accola et al., 2002). Mx1 binds to parts of the influenza virus polymerase (PB2 and nucleocapsid protein) to inhibit viral gene transcription (Turan et al., 2004). This is a powerful antiviral feat, as it effectively prevents the viral mutations that can escape Mx-mediated defences and few countermeasures by viruses against Mx proteins have been found (Sadler & Williams, 2008).

Transcription and RNA stability

The stability of RNA is another target that is intimately linked with regulation of translation, and several antiviral factors have been linked to the modulation of both processes. Initially identified to inhibit replication of the gammaretrovirus murine leukaemia virus (MLV) (Gao et al., 2002), ZAP has been shown to restrict a wide range of viruses through targeted RNA degradation and inhibition of mRNA (Guo et al., 2007; Zhu et al., 2011). It does this by binding CpG's, along with its cofactor TRIM25, and mediates RNA degradation by interacting with the putative endonuclease KHNYN (Ficarelli et al., 2019). It can also repress messenger RNA translation by inhibiting the interaction between the translation initiation factor eIF4A and eIF4G (Zhu et al., 2012). Additionally ZAP also directly and indirectly targets a subset of cellular mRNAs to regulate the innate immune response (Ficarelli et al., 2021).

The OAS/RNaseL system is an important factor in vRNA degradation. Upon encountering dsRNA, oligoadenylate synthase (OAS) enzymes oligomerise and

synthesise 2'5'-oligoadenylates that activate the constitutively expressed RNaseL. RNaseL then dimerises and activates, which enables it to cleave global cellular and viral RNA (Clemens & Williams, 1978). This leads to a reduction in vRNA abundance, but the cleaved products are also recognised by RIG-I, which then amplifies pathogen sensing (Krishnamurthy et al., 2010). There are three catalytically active OASs in humans, but depletion of OAS3 in cells increased viral expression compared to depletion of OASs 1 and 2. Thus OAS3 is the main activator of RNaseL in the IFN response, which was attributed to its higher affinity for dsRNA (Li et al., 2016).

Treatment of cells with IFN-I strongly upregulates TRIM22 and inhibits HIV replication. TRIM22 possesses an E3 ubiquitin ligase domain as well as a C terminus that is involved in protein-protein interactions (Pagani et al., 2021). The protein down-regulates transcription from the HIV-1 long terminal repeat (LTR) region. TRIM22 does not bind directly to DNA sequences, in chromatin immunoprecipitation studies it was found that it prevents binding of transcription factor (Sp1) binding to its consensus sites in the HIV-1 LTR (Turrini et al., 2015). TRIM22 also appears to prevent the movement of the HIV gag protein to the plasma membrane and thus TRIM22 can block assembly of the virus as well (Barr et al., 2008).

Translation

The translation of viral proteins is central to the viral life cycle and heavily relies on host translational machinery. Perhaps because of this, this step is very vulnerable to the antiviral activity of ISGs. These antiviral effectors can specifically interfere with the translation of viral RNA, or they can globally suppress translation. Protein kinase R (PKR) was one of the earliest described ISGs with an antiviral function (Lengyel, 1982). PKR is constitutively expressed but is also induced by IFN-I under the control of the IFN-stimulated response element (ISRE) in the promotor of PKR. PKR is activated directly by dsRNA, which is characteristic of viral RNAs, which results in its homodimerization and activation of its kinase domain (Sandler & Williams, 2008). PKR is a part of the phosphorylation of eukaryotic initiation factor 2 (eIF2a) which causes eIF2a to sequester guanine nucleotide exchange factor eIF2b and inhibit its activity (Roberts et al., 1976). This prevents recycling of GDP which is an essential step in translation initiation. Loss of this activity halts translation and causes cellular and viral RNA to accumulate in stress granules (Bogorad et al., 2017).

Some ISGs bind directly to viral RNAs to inhibit their translation. The IFIT family of proteins bind to specific sequences or structures within viral RNA which help to distinguish viral RNA from host RNA: 5'-triphosphate caps or regions with a lack of 2'-O-methylation (Daffis et al., 2010; Züst et al., 2011). IFIT1 binds these caps and prevents the viral RNA from being recognised by the translation initiation factors, effectively blocking translation (Pichlmair et al., 2011). In addition to binding vRNA, IFIT proteins can interact with essential translation initiation factors, such as eIF3, which are necessary for the assembly of the translation initiation complex. IFIT1 blocks HCV replication by targeting eIF3-dependent steps demonstrated when a mutant IFIT1 protein lacking eIF3-binding activity failed to inhibit HCV replication (Raychoudhuri et al., 2011). Some viruses, like mouse and human coronavirus, can overcome the action of IFIT proteins. Many RNA viruses encode a methyltransferase enzyme, which modifies the 2'-O- position of viral RNA to resemble host mRNA. Viruses lacking this methyltransferase are more susceptible to interferon treatment, and this sensitivity is dependent on IFIT proteins (Züst et al., 2011).

While some proteins block translation of viral proteins, other proteins can alter viral proteins co- or post-translationally. Ubiquitination of viral protein components is a common restrictive mechanism of viral inhibition. An example of this is by the TRIM family of E3 ubiquitin ligases, which impart ubiquitin to viral proteins which then targets them for degradation or impacts downstream signalling (Shen et al., 2021). IAV nucleoprotein (NP) is a target for ubiquitination by several TRIM proteins (TRIM14, TRIM41 and TRIM22), which leads to its degradation (Koepke et al., 2020).

Genome replication

Without genome amplification no new progeny virions will be formed. ISGs involved in inhibiting genome replication often degrade or sequester viral proteins. Viruses with an RNA genome usually make use of an RNA-dependent RNA polymerase (RdRp) to transcribe their viral genes from the genome template. This can be inhibited by interfering with transcription elongation which is done by the previously mentioned Mx1 protein (Krug et al., 1985). Another ISG involved in restricting viral transcription is the ubiquitin E3 ligase RBBP6. This IFN-induced gene has been shown to target Ebola virus VP30 which is responsible for RNA synthesis of the virus (Batra et al., 2018). The

interaction between VP30 and NP is important for Ebola viral RNA synthesis (Kirchdoerfer et al., 2016). The ubiquitin ligase RBBP6 is a molecular mimic of the Ebola virus nucleoprotein and binds to the EBoV transcription factor VP30 and blocks vRNA synthesis. RBBP6 outcompetes NP for binding to VP30 since RBBP6 has a 5-fold higher binding affinity than NP. RBBP6 overexpression also reduced the abundance of VP30, which was dependent on the two proteins' direct interaction. Therefore, in addition to its ligase independent molecular mimicry pathway of inhibition, it may also function in a ubiquitin ligase dependent manner (Barta et al., 2018).

Retroviruses use a virally encoded reverse-transcriptase to generate DNA from their RNA genomes, a process which is targeted by ISGs (Baltimore, 1970; Temin, 1970; Schoggins, 2019). The apolipoprotein B mRNA-editing enzyme catalytic polypeptide-like (APOBEC) are C-to-U editing enzymes. A member of this family (APOBEC3G) hypermutates single-stranded retroviral genomes, causing impairment of viral gene expression and replication (Zhang et al., 2003).

Virion assembly and Egress

The late stages of the viral life cycle are generally considered to be assembly, trafficking and egress of the newly formed virions. There are few proteins that have been identified as inhibitors of these processes. Viperin was initially characterised to be antiviral when it significantly decreased the expression of the late viral proteins gB, pp28 and pp65 in HCMV infection (Chin et al., 2001). Since then, it has also been implicated in antiviral mechanisms against a broad range of viruses, like blocking viral particle release of IAV and HIV-I (Wang et al., 2007; Nasr et al., 2012). It does this by affecting membrane fluidity and disrupting lipid rafts by binding an enzyme involved in cholesterol and sterol homeostasis, farnesyl diphosphate synthase (FPPS). By overexpressing FPPS, the effect of viperin was reversed (Wang et al., 2007). Interestingly viperin was also implicated in repressing genome replication. Viperin converts cytidine triphosphate (CTP) into 3'-deoxy-3',4'didehydro-CTP (ddhCTP). Cells overexpressing viperin, or treated with IFN, had high levels of ddhCTP. This ddhCTP is incorporated into newly synthesised vRNA and functioned as a chain terminator for the viral RNA-dependent RNA polymerase of flaviviruses (Gizzi et al., 2018).

Tetherin is another enzyme that impedes viral egress of enveloped viruses (Chemudupati et al., 2019). Tetherin is a transmembrane protein that remarkably anchors budding virions to the cell surface and prevents their release (Neil et al., 2008). Tetherin has broad specificity and primarily affects enveloped viruses like HIV, Influenzas and Hepatitis B. These viruses require a host cell membrane to form their outer envelope during egress. Some viruses can overcome this block, for example, HIV produces the Vpu protein, which binds to tetherin and targets it for degradation, allowing the virus to escape from the infected cell (Neil et al., 2008; Van Damme et al., 2008).

Perspectives on the IFN-I response

A central part in the induction of an IFN response is the sensing of foreign nucleic acid, whether that be through unusual nucleic acid structure or specific motifs on viral RNA and DNA. RNA modifications play a huge part in this process. Viruses can mimic the cellular landscape of RNA to avoid being recognised by RLRs and TLRs by hijacking cellular RNA modifying enzymes. But the host can equally weaponize RNA modifying enzymes to methylate RNA in a way that induces the IFN response or targets the RNA for destruction. While this field or research is expanding, there has yet to be a comprehensive assessment of the role of RNA modifications in the landscape of virus infection. Advancements in the last decade have provided evidence for the central role of RNA modifications in the lifecycle of viruses and in the host cell immune response. What these roles are, and the tools and insights that have been provided so far, along with key features of RNA and RNA modifications, are discussed in the next section.

RNA modifications in the landscape of virus infection

In the IFN response there are many roles for RNA modifications. Unusual RNA signatures are recognised as non self and trigger the antiviral program. Similarly, upregulated ISGs can be RNA modifiers and impart motifs to begin a signalling cascade which can, for example, act as a signpost to block the translation of viral RNA or signpost it for destruction by “reader” proteins which are discussed in more depth below.

Processing of cellular RNA

Most newly synthesised RNAs have to be modified in various ways to be functional (Cooper, 2000). The primary transcripts of rRNAs and tRNAs undergo a series of processing steps, for instance pre-rRNAs undergo fragmentation into functionally active shorter transcripts; tRNA 5’ and 3’ ends are cleaved off and a CAA trinucleotide is added to the 3’ end where the tRNAs amino acid will be added (Aubert et al., 2018; Nakanishi & Nureki, 2005). Primary transcripts of mRNAs similarly undergo extensive modifications, including the removal of introns by splicing, before being transported to the cytoplasm where they act as templates for protein synthesis. All these post-transcriptional steps are regulated which provides an additional level of control of gene expression.

An example of the extensive regulation of RNAs is in the canonical lifecycle of mRNA. As soon as mRNA emerges from RNA polymerase II, it immediately associates with RNA binding proteins and begins to be processed. The first of these processes is mRNA capping. A 7-methylguanosine ‘cap’ is added to the 5’ end of mRNA and then the RNA’s first and second nucleotides are 2’-O-methylated (Gonatopoulos-Pournatzis & Cowling, 2014). This cap is an important attachment point for RBPs throughout the mRNA’s lifecycle. It serves as docking point for the nuclear cap binding complex (CBC), which contributes to RNA stability, splicing regulation, nuclear export and ribosome recruitment for the first round of translation (Gonatopoulos-Pournatzis & Cowling, 2014). In the cytoplasm, the CBC is replaced by the eukaryotic initiation factor (eIF) eIF4E, which interacts with eIF4G. eIF4A and eIF4B (collectively forming the eIF4F complex), promoting subsequent rounds of translation (Querido et al., 2024). As discussed in the previous section, the cap structure and the 2’-O-methylation

prevent binding of PRRs, like RIG-I, which allows the cell to distinguish self from non-self RNA (Schlee & Hartmann, 2016). The final step of transcription is endonucleolytic cleavage, followed by addition of poly(A) at the 3' end by poly(A) polymerase. The poly(A) tail is similar to the cap as it is important for the stability and translational efficiency of the mRNA (Hocine et al., 2010).

In addition, RNAs can be dynamically modified along the length of their sequence. These modifications happen in all four nucleosides: adenine, guanosine, cytidine and uridine. This can be through purine or pyrimidine base modifications including methylation, pseudouridylation and adenosine-to-inosine editing (A-to-I). Like the 2'O-methylation at the 5' cap, the ribose moiety of nucleotides can be methylated. Most, if not all, types of RNA are edited at some point in their life cycle, which affect stability, structure and RNA-protein interactions (Roundtree et al., 2017). Nucleotide modifications are one of the greatest evolutionarily conserved features of RNA and the sites of modifications are under strong selective pressure (Li & Mason, 2014). Abnormal deposition of RNA modifications causes severe diseases such as neurological disorders, and metabolic diseases, including mitochondrial disorders, obesity and diabetes (Delaunay et al., 2024).

Chemical modifications of RNA, such as 5-methylcytidine (m^5C) and pseudouridine, were discovered in the 1950s and 60s (Amos & Korn, 1958; Cohn, 1960). Since then, more than 150 distinct modifications have been described (Boccaletto et al., 2022). The development of high-throughput detection methods to map RNA modifications in a transcriptome-wide manner has advanced our understanding of their functional roles (Delaunay et al., 2024). One method that has been used to measure levels of RNA modifications is liquid chromatography coupled to mass spectrometry (LC-MS), however the sequence positions of the modified nucleosides are lost because the RNA molecule is digested before analysis (Thuring et al., 2017). Next generation sequencing based approaches are able to map the location of the modified nucleoside, however this can only be used on a small number of RNA modifications (N6-methyladenosine (m^6A), 3-methylcytidine (m^3C), 5-methylcytidine (m^5C), 5-hydroxymethylcytidine (hm^5C), N6,2′-O-dimethyladenosine (m^6Am), inosine (I), N7-methylguanosine (m^7G), pseudouridine (Ψ) and 2′-O-methylation (2′-O-Me)) (Wiener & Schwartz, 2021; Motorin & Helm, 2019). Many of these methods depend on probing

the modification with an antibody that upon UV protein-RNA crosslinking leads to truncations during reverse transcription delimiting the position of the modification (Wiener & Shwartz, 2021). Alternatively, other sequencing methods induce chemical conversion of edited nucleotides, which results in high frequency of nucleotide misincorporation during reverse transcription e.g. bisulfite sequencing induces a conversion of cytidines to uridines but this does not occur in m^5C sites as the methyl group protects from the chemical modification (Edelheit et al., 2013). Beyond this, nanopore sequencing allows for direct sequencing of RNA molecules without the need for reverse transcription or amplification (Begik et al., 2021). Begik et al., 2021, successfully used nanopore RNA direct sequencing to detect RNA modifications m^6A, Ψ and 2′-O-Me in cellular RNAs. RNA is passed through a protein nanopore that detects changes to electrical currents that are specific to modified and unmodified nucleotides (Leger et al., 2021).

Ten types of nucleotide modification have been described in eukaryotic mRNAs, which are part of/direct their correct transcription, processing, subcellular localisation and translation (Frye et al., 2018) (Figure 1.4). Alongside the 5'cap described above, m^6A modifications are the most prevalent and best characterised modifications in mRNA. Their addition to RNA requires a complex of proteins known as 'writers,' for instance METTL3, METTL14 and other cofactors deposit the m^6A modification (Figure 1.4). CMTR1, CMTR2, PCIF1 and RNMT are also writer proteins that are responsible for addition of methyl groups to form the 'cap' of RNA. Some modifications are largely irreversible processes. However, some modifications such as ribose methylation and hydroxylation are plastic and reversible being removed by a group of proteins known as 'erasers' (Li & Mason, 2014). For example, ALKBH5 and FTO demethylases can remove the m^6A modification that the METTL3 and METTL14 complex deposit (Zheng et al., 2013).

The RNA modifications can be recognised and bound by a group of proteins known as 'readers' and the fate of the RNA will depend on which 'reader' interacts with the motif (Patil et al., 2018). This can be described by continuing the m^6A modification example. The interaction of the YTH domain family of proteins with m^6A has been well-characterised: the nuclear reader protein YTHDC1 mediates nuclear export of m^6A methylated transcripts, and also regulates mRNA splicing (Roundtree et al., 2017; Xiao

et al., 2016). Additionally, the YTHDF proteins promote general mRNA degradation, although in some instances they can promote transcript specific translation (Zaccara et al., 2020). An interesting example of this is YTHDF3 which suppresses ISG expression under basal conditions by promoting translation of the transcription corepressor forkhead box protein O3 (FOXO3). YTHDF3 does this by recruiting two cofactors, PABP1 and eIF4G2, to promote translation of FOXO3 mRNA. Indeed, mice with YTHDF3 knockout were resistant to several viral infections due to increased ISG levels (Zhang et al., 2019).

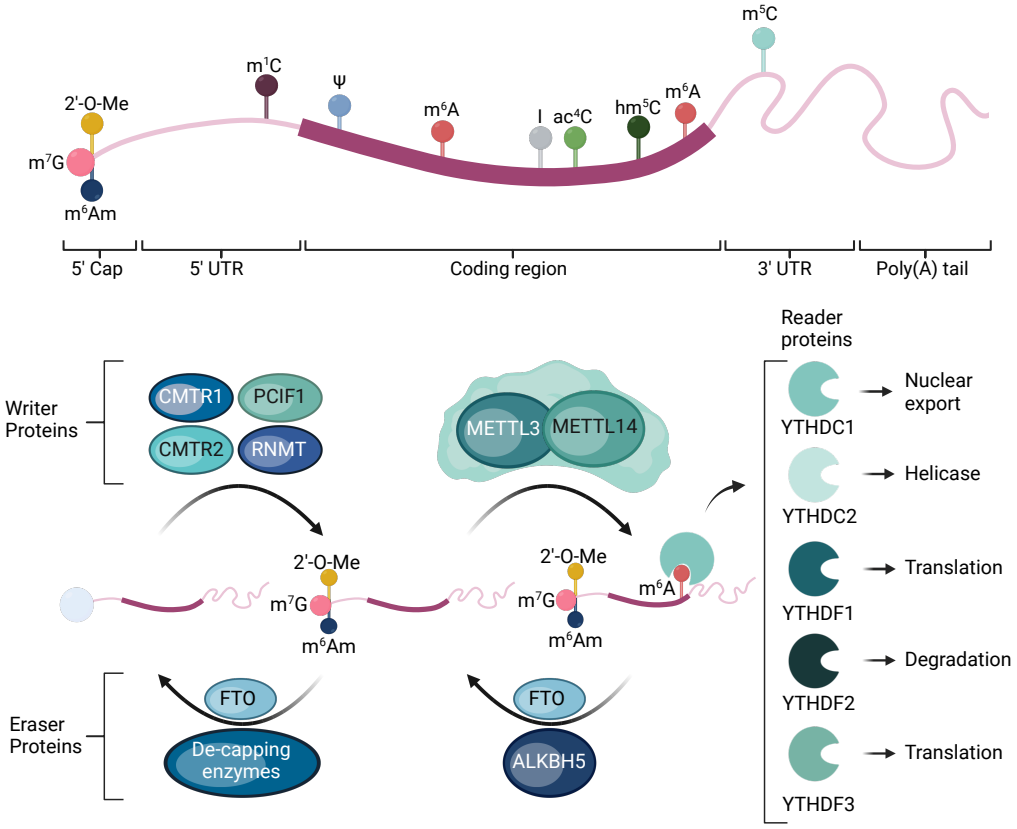

Figure 1.4: RNA modifications. *Top*: an example of RNA modifications of an mRNA molecule consisting of 5' and 3' untranslated regions (UTRs), a coding region, and a poly(A) tail. The 5′ cap is single N7-methylguanosine (m^7G), which is further decorated with 2′-O-methylation (2′-O-Me) at the two nucleotides adjacent to the cap. N6,2′-O-dimethyladenosine (m^6Am) occurs if the first transcribed nucleotide is an adenosine. Other modifications along the length of the RNA include: N6-methyladenosine (m^6A), pseudouridine (Ψ), N1-methyladenosine (m^1A), 5-methylcytidine (m^5C), 5-hydroxymethylcytidine (hm^5C), N4-acetylcytidine (ac^4C) and inosine (I). *Bottom*: 'Writer' proteins can deposit modifications on RNA. CMTR1 and CMTR2 mediate addition of 2′-O-Me at the cap, m^7G is installed by RNMT and PCIF1 adds the m^6Am modification. The m^6A methyltransferase complex contains METTL3 and METTL14 as well as cofactor proteins. m^6Am and m^6A can be removed by 'eraser' protein FTO. The demethylase ALKBH5 is another 'eraser' of m^6A. The YTH domain protein family act as 'Reader' proteins and bind to m^6A modifications in the nucleus or cytoplasm to regulate mRNA molecules (Delaunay et al., 2014).

The addition of RNA modifications is finely regulated by perturbations in the environment, and external signals induce global changes in mRNA editing profiles (Roundtree et al., 2017, Delaunay & Frye, 2019). For example, the host transcriptome has been shown to change during SARS-CoV2 infection (Fan et al., 2024).

It should be mentioned that modifications can occur in many different types of RNAs. Similar to mRNAs, lncRNAs are usually transcribed by RNA polymerase II, 5' capped with N-7-methylguanosine (m^7G), spliced and polyadenylated at their 3' ends (Statello et al., 2021). m^6A, m^5C and Ψ have been reported to occur in lncRNAs such as MALAT1, vault RNAs (vtRNA), HOTAIR, TERRA, 7SK and XIST (Delaunay et al., 2024). rRNAs are also heavily modified throughout their transcription and maturation (rRNA modifications will be covered in more depth in Chapter 5). Small-non-coding RNA, such as microRNAs (miRNAs), PIWI-interacting RNAs (piRNAs), small nuclear RNAs (snRNAs) and small nucleolar RNAs (snoRNAs), are also modified (Li et al., 2021). tRNAs are by far the most widely modified RNA. A human nuclear encoded tRNA molecule has an average of 13 modifications per molecule (Pan, 2018). tRNA modifications have the same effect on stability and processing as discussed for other RNAs (Suzuki, 2021). However, modification of anticodon nucleotides in the wobble position (which is the region mediating the decoding of the mRNA during translation) regulate mRNA translation speed and fidelity by offsetting for codon biases in genes that have an imbalanced distribution of identical nucleotides (Hanson & Coller, 2018). Modifications outside the anticodon sequence but in the anticodon loop, stabilise tRNA-mRNA codon interactions which heightens decoding fidelity and translation efficiency (Nguyen et al., 2019).

Overall, in cellular RNA, discrete sets of regulatory proteins impact RNA modification profiles co-transcriptionally and post-transcriptionally which affects the stability of the RNA. In the context of viral fitness and pathogenicity, RNA modifications are vital for the recognition of self from invading nucleic acid, like viral RNA. Viral RNA is diverse due to the variations and particularities of the different viral lifecycles.

Viral RNA: synthesis of RNA from RNA templates

The genomes of RNA viruses can be unimolecular or segmented, single stranded of positive or negative polarity, or ambisense polarity, double stranded or circular. These diverse genomes have one common requirement – during replication the RNA genome must be copied from end to end with no loss of nucleotide sequence, and viral mRNAs have to be made that can be translated by the host cell protein synthesis machinery. All known RNA viruses, apart from retroviruses, encode an RNA-dependent RNA polymerase (RdRp) to synthesise new genomes and mRNA (Flint et al., 2015). RdRp synthesises RNA complementary to the starting template and is an essential protein for RNA viruses that have no intermediate DNA stage (Koonin et al., 1989; Zanotto et al., 1996). As with any cellular RNA, vRNA is continually packaged into ribonucleoprotein (vRNP) complexes. The components of which can be a range of proteins including RdRp and host factors that have been hijacked by the virus to promote its replication (Giradri et al., 2021).

Viral mRNAs need to be translated by the host cell protein synthesis machinery as their genomes have limited capacity and cannot encode all the proteins and ribosomal RNAs required for translation. Just like cellular RNAs, most viral RNAs undergo 5' end capping and 3' end polyadenylation which ensures efficient translation and protects the viral mRNA from exonucleases and prevents activation of antiviral responses (Flint et al., 2015). A side note here is that some viruses have evolved cap-independent modes of translation. They have internal ribosome entry sites (IRES) that promote translation initiation (Hao et al., 2022). Additionally viral mRNAs can be edited which has multiple effects on the viral lifecycle.

Impact of viral RNA modifications on the virus lifecycle

Recently more and more studies have begun focusing on the roles of RNA modifications in viral infection. In one respect, RNA modifications such as m^6A, m^5C, ac^4C, Ψ, and RNA editing, act directly on RNA which impacts structure, nuclear export, translation, stability and replication (Li & Rana, 2022). In another respect, RNA modifications can regulate the host response to infection by mediating viral RNA signalling, cytokine responses, as well as immune cell functions (Cui et al., 2022).

The role of RNA modifications in regulating immune cell functions in antiviral infection can also be described from two perspectives:

1. RNA modifications on viral RNAs subvert innate immune signalling pathways, e.g., m^6A modified HIV-I and vesicular stomatitis virus RNAs limit the innate sensing efficiency of RLRs and so impair the IFN-I mediated innate antiviral immune response in monocytes and macrophages (Chen et al., 2021).
2. RNA modifications affect the key factors of antiviral immunity in immune cells e.g., m^6A affects antiviral transcripts including CGAS, IFI16, STING, Mavs, Traf3, Traf6 and FOXO3 (Liu et al., 2019; Zhang et al., 2019).

Viruses have evolved several strategies to facilitate their replication and elude host immune surveillance. The repertoire of epitranscriptomic modifications in viral mRNAs is expanding but the most prevalent modifications in the virus genome include methylation (m^6A, m^5C, m^7G, 2'-O-Methyl), and additionally nucleotide editing such as A-to-I editing and pseudouridine (McIntyre et al., 2018). What follows is a short discussion into how viruses utilise these RNA modifications to potentiate their replication.

Capping: 2'-O-methylation and 7-methylguanosine

mRNAs protect their 5' end with an inverted N-7 methylguanosine nucleoside (m7GpppN – cap 1) that is normally modified with a 2'-O-methyl group (cap 2) within the first and second nucleosides downstream of the m^7G cap. This regulates metabolism and stability of the RNA and it is key for discriminating between self and foreign RNA (Schlee & Hartmann, 2016). Pathogenic RNAs without caps trigger the IFN response because they can be recognised by cellular sensors (Züst et al., 2011). Viruses have evolved different strategies to incorporate a modified cap onto viral mRNAs: 1) Bunyaviruses and orthomyxoviruses (such as IAV) utilise a cap-snatching mechanism to hijack m^7G caps from host RNAs. Then viral mRNAs exhibit similar 5' ends as host mRNAs and can compete for the translation apparatus. (De Vlugt et al., 2018). IAV polymerase protein PA targets an actively transcribing host cell RNA polymerase II (Te Velthuis & Fodor, 2016). Subsequently the PB2 domain of the polymerase associates with the 5' end of the cellular mRNA (Gu et al., 2015). The PA uses its endonucleolytic activity to cleave the mRNA, creating a capped 11-12nt primer that is loaded into the active site of the IAV polymerase (Pritlove et al., 1998). A

nucleotide complementary to the second or third residue of the vRNA template is then 3' end of the cap primer and transcription takes place (Gu et al., 2015). 2) Some viruses, such as coronaviruses, encode their own capping enzymes that methylate the 2'-O-postion of the ribose sugar. m^7G and 2'-O-methylation are introduced into coronaviruses by NSP14 and NSP16 respectively (Chen et al., 2011; Chen et al., 2013). Dengue virus and ebola virus also encode proteins for cap methylation (Züst et al., 2011). 3) HIV-1 caps its RNAs by hijacking the host 2′O-MTase RNA 2′-O-methyltransferase 3 (FTSJ3) (Ringeard et al., 2019). Mutating the catalytic core of FTSJ3 or knocking it out caused a reduction in methylation of HIV RNA and a subsequent increase in IFNα and β. In MDA5-silenced U937 cells, type-I interferon induction was reduced when infected with virus produced in absence of FTSJ3 and so lacking methylation. This shows that the FTSJ3 2'-O-methylates HIV RNA, allowing it to avoid MDA5 sensing (Ringeard et al., 2019).

A side note here is that some viruses have evolved cap-independent modes of translation. They have internal ribosome entry sites (IRES) that promote translation initiation (Hao et al., 2022). Some viruses actually lack the cap structure, as is the case of picornaviruses which harbour a protein VPg vrosslinked to their 5' end to protect against degradation and PAMP recognition (Paul et al., 2015).

N^4-acetylcytidine

Ac^4c is found in many human RNAs (Boccaletto et al., 2022) and is deposited by N-acetyltransferase 10 (NAT10) in a process which requires accessory protein THUMPD1 and box C/D snoRNA U13 (Sharma et al., 2015) to acetylate tRNAs and rRNAs. Ac^4c has been found in the genomes of many RNA viruses e.g. Zika Virus, DENV, hepatitis C, poliovirus, HIV-1, enterovirus-71 and IAV (McIntyre et al., 2018; Furuse, 2021; Tsai et al., 2020). EV71 and HIV-1 transcripts are acetylated by NAT10 which enhance viral gene expression (Tsai et al., 2020). In EV71, ac^4c recruits a protein called PCBP2 to its IRES to increase transcript stability to facilitate its interaction with the RdRp (Hao et al., 2022).

Pseudouridine

Pseudouridine has been found in the genomes of several viruses (McIntyre et al., 2018; Furuse, 2021) and is associated with a range of effects: it significantly alters

RNA biology, including changing the coding preference of viral RdRps, mediating alternative splicing and even affecting RNA structures (Pfaller et al., 2021; Netzband & Pager, 2020). Several pseudouridine synthases (PUS proteins) were identified in CRISPR screens searching for host cell factors that target HCV and DENV (Marceau et al., 2016). Pseudouridine modified small RNAs from HCV bind with high affinity to RIG-I but block the conformational change of RIG-I necessary for its activation (Durbin et al., 2016). In Epstein-Barr virus (EBV) infection, disrupting pseudouridylation in an EBV non-coding RNA (EBER2) reduced EBER2 RNA levels and resulted in decreased viral infection (Henry et al., 2022).

5-methylcytosine

Multiple cellular RNA classes have m^5C modifications. It is deposited by the NOL1/NOP2/SUN domain family (NSUN) and DNA methyltransferase family protein (DNMT2) in eukaryotes (Bohnsack et al., 2019). Several viruses have m^5C on their genomic RNA (Cristininelli et al., 2022; Eckwahl et al., 2020) and it impacts nuclear export and viral gene expression. Murine leukemia virus RNAs that harbour m^5C are recognised by a protein called ALYREF to facilitate nuclear export (Eckwahl et al., 2020). There is a discussion about the NSUN enzymes and their impact on viruses in Chapter 4, however depletion of an m^5C writer NSUN2 reduced the levels of methylated cytosines in HIV-1 transcripts which disrupted splicing and translation of viral mRNAs and thus inhibited viral propagation (Courtney et al., 2019; Kong et al., 2019).

DNMT2 has been found to be translocated to stress granules to methylate HIV-1 RNAs (Dev et al., 2017). By affinity RNA pull-down and semi-quantitative RT-PCR of the HIV *nef* gene RNA, HIV-1 was found to interact with DNMT2 during infection of SupT1 cells. HIV co-opts the action of DNMT2 methyltransferase activity because the stability of HIV-1 RNA is improved as the level of HIV-1 RNA (*nef* mRNA) was significantly higher in the presence of DNMT2 in HEK293 cells than depleted cells (Dev et al., 2017).

N6-methyladenosine

m^6A is by far the best characterised of all the RNA modifications. The motif has been found in the genomes of multiple viruses, and generally seems to act as armour to

avoid immune sensing (Gokhale et al., 2020). In Vesicular Stomatitis virus (VSV) infection, METTL3-mediated m^{6}A modification reduced production of viral dsRNA to escape RIG-I or MDA5 detection (Qiu et al., 2021). Rotavirus infection downregulates levels of m^{6}A eraser ALKBH5 to maintain high levels of m^{6}A on its transcripts (Wang et al., 2022).

m^{6}A-deficient viral RNAs generally trigger the RIG-I-dependent innate immune response, compared to methylated transcripts. m^{6}A modifications in HIV-1 reduced RIG-I sensing and type I IFN induction in differentiated monocytic cells, whereas HIV-1 virions produced in FTO (an m^{6}A demethylase) overexpressing HEK293 cells induced high levels of IFN-I expression in a RIG-I dependent manner in monocytic cells (Chen et al., 2021). This same effect has been observed in several families of negative-sense RNA viruses, such as *Pneumoviridae* (hMPV), *Paramyxoviridae* (SeV and MeV), and *Rhabdoviridae* (VSV), which demonstrates m^{6}A is essential to avoid RIG-I sensing (Kim et al., 2020; Lu et al., 2020). m^{6}A modifications in viral RNAs enable the recruitment of m^{6}A reader enzymes, which sequester viral ds/ssRNA by binding to the RNA which prevents RIG-I recognition. m^{6}A in hepatitis B and C viral RNAs suppressed the activation of RIG-I signalling as YTHDF2 bound the RNA, whereas single nucleotide mutation of m^{6}A of viral RNA (A8766C) enhanced RIG-I sensing (Kim et al., 2020).

Above the presence of m^{6}A on viral transcripts and genomes avoiding direct recognition from RLRs, other proteins in the host can interact with the motif in viral infection to elicit different outcomes (Ribeiro et al., 2023). m^{6}A reader YTHDC1 binds HIV-1 transcripts to ensure effective splicing and viral production. This interaction is METTL3 dependent as depletion of METTL3 (an m^{6}A writer) reduced YTHDC1 binding (N'Da Konan et al., 2022). Another reader protein, YTHDF1, participates in EBV viral RNA decapping to cause its RNA decay by recruiting RNA degradation enzymes (Xia et al., 2021).

A-to-I RNA editing

Unlike the previously discussed modifications, A-to-I editing involves the conversion of adenosine to inosine (Pfaller et al., 2021). Adenosine deaminase acting on RNA 1 (ADAR1) converts adenosine to inosine (A-to-I editing) in duplex RNA structures to

destabilise the dsRNA and thus prevent autoimmune activation of MDA-5 and PKR. (Samuel, 2019; Doria et al., 2009). Inosine also base pairs with cytosine as guanosine, so it can change the coding information of transcripts (Alseth et al., 2021). It is believed that ADAR is hijacked by numerous viruses, including IAV (Furuse, 2021), HIV (Doria et al., 2009), DENV (de Chassey et al., 2013), ZIKV (Khrustalev et al., 2017) and SARS-CoV2 (Di Giorgio et al., 2020). Contrasting effects on viruses has been described with ADAR1. Editing of viral RNA by ADAR1 enhances DENV infection by promoting the translation of non-structural proteins (de Chassey et al., 2013), whereas it restricts measles virus replication (Ward et al., 2011). ADAR1 can damage viral RNA genomes by introducing large clusters of mutations, particularly if acting in negative strands (Pfaller et al., 2018). In the case of HIV-1, knockdown of ADAR-1 in human primary CD4+ T cells blocks HIV-1 replication at the protein translation stage (Phuphuakrat et al., 2008). When the level of Gag mRNA expression was correlated to the level of Gag protein expression, there was a clear decrease in protein production per viral Gag transcript observed in ADAR knockdown cells (Cuadrado et al., 2015). This may indicate a post-transcriptional regulation of genomic RNA, which can occur through RNA editing or decreased translation. Thus, ADAR1 facilitates HIV-1 replication in human primary CD4+ T cells by supporting efficient viral protein synthesis (Cuadrado et al., 2015).

Impact of virus infection on the host epitranscriptome

Mass spectrometry has shown that viral infection changes the levels of a range of RNA modifications in cellular RNA. For many of these changes, little is known about the biological function of the change (McIntyre et al., 2018). Viruses may manipulate host RNA modification patterns to alter gene expression and so modulate processes that can undermine infection. m^6A plays a role in regulating translation of ISGs. ISGs such as IFITM1 appear to have their translation enhanced by m^6A and YTHDF1 increased the expression of IFITM1 further (McFadden et al., 2021). At the end of the IFN-I response when infection has been curtailed, demethylase ALKBH5 was shown to demethylate mRNAs of MAVS, TRAF3 and TRAF5 to limit IFN production (Zheng et al., 2017; Ribeiro et al., 2023).

There is increasing evidence that viruses can manipulate the host epitranscriptome to benefit their infection. HIV-1 infection reduced levels of N6,2'-O-dimethyladenosine (m^6Am) modified host mRNAs by degrading the phosphorylated CTD Interacting Factor 1 (PCIF1), an inhibitor of HIV-1 transcription (Zhang et al., 2021). PCIF1 catalyses the addition of m^6A to a 2'-O-methylated A at the 5' end of mRNAs. It was found that during infection levels of m^6Am decreased, with this being due to HIV viral protein R (Vpr) interacting with PCIF1 and inducing PCIF1 ubiquitination and degradation. PCIF1 methyltransferase function restricts HIV replication by methylating the cap of a transcript of a transcription factor - ETS1. When ETS1 is expressed as a protein, it binds to the HIV promoter to decrease viral transcription (Zhang et al., 2021). So, this is a beautiful example of how a virus can escape restriction by degrading a host RNA modifying enzyme and can thus change the epitranscriptome.

Alphaherpes virus infection leads to an almost complete loss of m^6A levels in mRNA by action of is US3 kinase protein which inactivates the m^6A writer complex, independent of its phosphorylation abilities. This causes the METTL3/14-containing writer complex to no longer associate with chromatin and so the m^6a writer complex may no longer be attached to chromatin. The impact or reason for this is unknown as the inactivation of the writer complex was shown not to be essential for virus infection and there were no notable effects on the transcription and translation of ISG transcripts (Jansens et al., 2022).

Viruses can also manipulate and exploit several host ncRNAs and emerging data suggests that tRNA modifications may regulate the immune response. tRNA-derived fragments (tRFs) are a recently discovered family of noncoding RNAs. In response to viral infections, tRNA-derived fragments can be generated. RSV infection causes demethylation of tRNA glutamic acid, with a codon of CTC (tRNA-GluCTC), by ALKBH1. This demethylation causes tRNA-GluCTC cleavage into tRFs, and under RSV infection a 5-fold increase in tRF production was observed which concurrently increased RSV infection. This effect was reduced when ALKBH1 was knocked down. Interestingly, the expression of ALKBH1 was not changed by RSV infection, which suggests that RSV infection alters the activity of the enzyme. How this occurs is still unknown (Choi et al., 2022).

Conversely, ALKBH1 behaves as a host restriction factor that is suppressed during Dengue virus (DENV) infection. A virally encoded NS5 protein modifies ALKBH1 target tRNAs to promote translation of codon-biased pro-viral transcripts. ALKBH1 knockdown reduced the capacity of the tRNA pool to read the UUA codon in mRNAs; this reduced the translation of UUA-enriched transcripts and increased translation of mRNAs lacking UUA and enriched with other synonymous codons for leucine. However, UUA codon frequencies were similar between the genomes of DENV and humans based on gene averages so what this codon bias is for may be gene specific regulation of specific pathways. ALKBH1 reduction also increased expression of human enzymes like FURIN which is involved in the cleavage of the DENV precursor membrane protein to facilitate virion assembly (Chan et al., 2023). The mechanism of how DENV suppresses ALKBH1 expression is also still unknown but is another example of how a virus hijacks the epitranscriptome to promote viral replication.

Despite there being limited examples and incomplete details on how regulation occurs, the examples here support the idea that there is a co-ordinated epitranscriptomic reprogramming in the host cell that regulates translation in infection.

Perspectives on RNA modifications during viral infection

In a cell, all post transcriptional modifications of cellular RNA play an important role in the life cycle of RNA, and these modifications in turn act as a signal in the cell to avoid triggering an immune response. I have discussed and shown that viruses have adapted mechanisms to mimic the cellular landscape of RNA and thus avoid the induction of IFN. While there are an increasing number of examples of RNA modifying enzymes being hijacked by RNA viruses to modify their genome, there has yet to be a comprehensive assessment of the role of all RNA modifying enzymes on viral infection and how this regulates IFN-I induction. To try and understand this further we want to experimentally screen all known human RNA modifying enzymes against a selection of RNA viruses to elucidate the impact of RNA modifications on infection.

Biomedical Relevance of Viruses Studied in this Thesis

Many RNA viruses were used in this project and several of them are discussed in this thesis. Influenza A virus (IAV) is discussed in Chapters 3 and 4, Respiratory syncytial virus (RSV), human metapneumovirus (hMPV) and Semliki Forest virus (SFV) are discussed in Chapter 4. Additionally, Sindbis virus (SINV) is used for investigations in Chapter 5. Biomedically, these viruses cause varying levels of concern for humans.

Influenza A virus (IAV) is a significant pathogen in humans, causing seasonal flu epidemics and occasional pandemics. It belongs to the Orthomyxoviridae family and is responsible for a substantial burden on public health worldwide. IAV is a leading cause of acute respiratory infections during seasonal flu outbreaks, typically in winter months. Severe cases can lead to pneumonia, acute respiratory distress syndrome (ARDS), and death, especially in vulnerable populations (elderly, young children, pregnant women, and those with preexisting health conditions) (Roberts Jr & Krilov, 2022). IAV viruses have subtypes (e.g. H1N1, H3N2) that can undergo antigenic drift (small mutations) and antigenic shift (genetic reassortment), allowing the virus to evade immune recognition and leading to pandemics (Ganti et al., 2021). A notable example is the 2009 H1N1 pandemic, which caused widespread illness globally. The 1918 Spanish flu pandemic, caused by an H1N1 IAV, is estimated to have killed tens of millions of people, highlighting its global impact (Roberts Jr & Krilov, 2022). Antigenic shift (recombination of viral segments from different species) allows influenza A viruses to jump species and acquire new capabilities, making them more virulent or transmissible in humans (e.g., H5N1, H7N9) (Long et al., 2021). Annual flu vaccines are developed based on predictions of circulating strains, but because of constant viral mutation, vaccines may be less effective some years. However, vaccination remains the most effective method for preventing severe disease and reducing transmission (Roberts Jr & Krilov, 2022). Despite advances in prevention (vaccines) and treatment (antiviral drugs), the virus remains a major public health threat.

Respiratory syncytial virus (RSV) is a global pathogen that infects most children under 2 years of age and is responsible for the deaths of 60,000 children annually (Shi et al., 2015). The immune response to RSV causes mucus production which can restrict

airways and cause severe bronchiolitis (Peebles et al., 2005). Human RSV has two subtypes (A and B) which belong to the Orhtopneumorvirus genus of the Pneumoviridae family in the order Mononegavirales. The virus particle is enveloped and pleomorphic but the filamentous form is most common (Ke et al., 2018). There are currently no specific antiviral treatments for RSV infection. Ribavirin, an antiviral drug, may be used in some severe cases, but its use is limited and not universally recommended. Although a vaccine for RSV is highly sought after, developing one has been challenging due to factors like immune response complexity and the risk of vaccine enhanced disease (Shi et al., 2015). Palivizumab, a monoclonal antibody, is used as prophylaxis in high-risk infants to reduce the severity of RSV infection, but it is expensive and limited to wealthier countries (Garegani et al., 2021). The virus has a high mutational capacity, which may contribute to its ability to evade long-term immunity and cause repeat infections. RSV has a high transmission rate and causes seasonal epidemics, typically in the colder months, and results in a substantial healthcare burden globally (Peebles et al., 2005).

Human metapneumovirus (hMPV) is closely related to RSV and causes a range of respiratory illnesses, from mild cold-like symptoms and croup to severe pneumonia and bronchiolitis, particularly in vulnerable populations, and is a significant contributor to hospitalisations due to respiratory illness in children under 5 years old. hMPV circulates in seasonal outbreaks, typically in the winter and early spring months, similar to RSV and influenza (Wang et al., 2020). Symptoms can overlap with other respiratory viruses (RSV, IAV and coronaviruses), making it harder to diagnose based solely on symptoms. There is currently no specific treatment for hMPV infection. Research into antiviral therapies and vaccines is ongoing, but effective prevention and treatment options remain limited (Bakkers et al., 2024). Like RSV, reinfections with hMPV are common throughout life, but they tend to be less severe after the initial infection. Immunity is short-lived and recurrent infections are possible, though they are usually milder in adults compared to children (Wang et al., 2020).

Semliki Forest Virus (SFV) is an alphavirus of the Togaviridae family that is primarily transmitted by mosquitoes, thus is more common in tropical and subtropical regions where mosquito vectors are prevalent (Atkins et al., 1999). It is not a major human pathogen, and cases are relatively rare compared to other mosquito borne viruses like

dengue or chikungunya. SFV can cause mild illness with symptoms such as fever, headache, muscle aches and rash. These symptoms are usually self-limited and resolve within a few days. In rare cases, it can lead to more severe neurological symptoms like encephalitis (brain inflammation) (Ferguson et al., 2015). SFV also has biomedical relevance due to its potential as a model virus for research, especially in studying viral pathogenesis, immune responses and vaccine development. SFV has been studied as a vaccine vector in the development of genetically engineered vaccines. Its ability to replicate efficiently in mammalian cells makes it promising candidate for viral vector vaccines (Atkins et al., 1999). Researchers have used SFV to deliver antigens from other pathogens, e.g. Zika virus and hepatitis B virus, to generate immune responses in mice, making it a valuable tool for vaccine development (Lundstrom, 2020). SFV is an important model for studying alphavirus biology, including its ability to cause neurological diseases, immune evasion and cellular tropism.

Sindbis virus (SINV), is related to SFV, and is an alphavirus from the Togaviridae family. It is a zoonotic virus, meaning it primarily infects animals, but can also cause disease in humans, all be it rarely (Suvanto et al., 2022). While it is not a major global health threat, it has biomedical relevance due to its potential to cause illness, its use as a research model, and its role in vector-borne diseases (Gorchakov et al., 2005). While outbreaks in humans are infrequent, SINV is associated with epidemics in certain regions, particularly in Africa, Asia and Europe. It is transmitted through mosquito bites, but unlike many other mosquito borne diseases, SINV can cause persistent joint pain (arthralgia), which may last for months after the acute infection has resolved, potentially leading to long-term disability in some individuals (Suvanto et al., 2022). This feature makes it particularly relevant in understanding post-viral arthritis and the long-term effects of viral infections on joints. SINV is commonly used in basic research to study viral replication, immune responses, and vector-borne transmission. It is also used as a platform for gene delivery and the development of recombinant vaccines, making it a valuable tool for vaccine development and gene therapy research (Perri et al., 2003; Gorchakov et al., 2005).

The key feature of all these viruses is that they are RNA viruses with well-defined replication systems, particularly SFV and SINV. Thus, they served as models for this

project on investigating the effect of RNA modifying enzymes on RNA virus infection in humans.

Aims

The aim of this project was to improve our understanding of RNA modifications in viral infection. RNA modifications play a central role in the cell, known as the epitranscriptome, and in the last decade it has become apparent that RNA modifications impact the virus lifecycle. We hypothesised that beyond the published examples, other RNA viruses recruit RNA modifying enzymes to alter their genomes and viral transcripts to enable them to hide from the host immune response or desensitise the host cell to infection. Alternatively, the RNA modifying enzyme could act as a restriction factor and the host cell may modify viral RNA in a manner to mark it for destruction. The overarching aim of this thesis was to determine how RNA modifications impact an RNA virus during infection. I sought to explore this by addressing three aims:

1. Create a screening platform of all the known human RNA editing enzymes.
2. Undertake screens using this platform against a range of RNA viruses to identify enzymes involved in RNA modifications of singular viruses and those with broad spanning effects against multiple viruses.
3. Characterise these newly discovered factors and determine what the role of the enzyme and the modification they impart is during infection.

Chapter 2 Materials and Methods

Materials

Reagents and Consumables

Reagent	Supplier
0.5% TrypLE	Thermo Fisher Scientific 12604013
0.5% Trypsin-EDTA	Thermo Fisher Scientific
10x Tris/Glycine/SDS Running buffer	BioRad 1610732
2X Phusion HF PCR Master mix	NEB M0531L
4–15% Mini-PROTEAN TGX Precast Protein Gel	BioRad 4561084
5’ Deadenylase	NEB M0331S
96-well, Cell Culture-Treated, Black Flat-Bottom Microplate	Perkin Elmer
Acetic acid glacial	Fisher Chemical A/0360/PB17
AEBSF	BioChemica A14210100
Agarose	Sigma-Aldrich A9539
Benzonase Nuclease	Millipore E1014
Bovine Serum albumin	Sigma Aldrich
BsmBI	NEB
Colour prestained protein standard, broad range	NEB P7719S
DMEM (no phenol red)	Thermo Fisher 21063029
DMSO	Sigma-Aldrich D2260
DNA midi prep kit	Qiagen
DNA mini prep kit	Qiagen
Doxycycline hyclate (DOX)	Sigma-Aldrich
Dulbecco’s Modified Eagle Medium (DMEM)	Thermo Fisher Scientific 11965092
Dynabeads MyOne Silane	Thermo Fisher 37002D
EDTA	Millipore 324503

Ethidium Bromide	Sigma- Aldrich E1510
EvaGreen	Biotium 31000
FastAP alkaline phosphatase	Thermo Fisher EF0654
Foetal Calf Serum	Thermo Fisher Scientific 16000044
G418 (neomycin analog) 200mg/ml	Invitrogen
Gentamicin 50mg/ml	Melford
HindIII	NEB R0104
Hygromycin 50mg/ml	Thermo Fisher J60681.MD
iBLOT2 nitrocellulose membrane	Thermo Fisher IB23001
IGEPAL CA-630	Sigma-Aldrich I8896
L3 gel extraction buffer	Qiagen 28704
Lipofectamine	Thermo Fisher Scientific
Luria Bertani (LB) Agar	BM5280
Luria Bertani (LB) Broth	E&O Laboratories BM5300
NEB buffer 3.1	NEB B7203
NotI	NEB R0189
NuPAGETM4-12% Bis-Tris 1mm gel	Invitrogen NP0322BOX
OptiMEM	Thermo Fisher Scientific 31985062
Paraformaldehyde, 16% w/v aq. soln.	Thermo Fisher 043368.9M
Penicillin-Streptomycin 5000U/ml	Thermo Fisher Scientific 15140122
PFU Turbo DNA polymerase	Agilent 600252
Phenol:Chloroform:Isoamyl Alcohol	Sigma-Aldrich P3803
Phosphate-buffered saline	Thermo Fisher Scientific 10010023
poly-L-Lysine	Sigma-Aldrich P4832
Polybrene (hexadimethrine bromide) 8mg/ml	Sigma-Aldrich
Polyethyleneimine (PEI)	PolySciences
ProNex	Promega NG2001
Protein Lobind tubes 1.5 ml	Eppendorf 0030108116
Proteinase K	Roche 3115828001
PureLink Quick Gel extraction kit	Qiagen
Puromycin 2mg/ml	Melford

Qubit 1X dsDNA HS Assay Kit	Invitrogen Q33230
Quick ligase buffer	Promega C671B
rCut Smart	NEB B6004
RecJf endonuclease	New England Biolabs M0264S
RiboLock RNase Inhibitor	Thermo Fisher EO0381
RNase I	Thermo Fisher AM2294
RNeasy kit	Qiagen
Sea Block	Thermo Fisher Scientific
SOC	
Superscript IV	Thermo Fisher 18090010
T4 DNA ligase	NEB M0202S
T4 ligation 10X buffer	Promega C126A
T4 PNK	New England Biolabs M0201L
T4 RNA ligase	Thermo Fisher EL0021
TPCK-Trypsin	Thermo Fisher
Triton X-100	Promega H5141
TurboDNase	Thermo Fisher AM2238
Tween-20	Sigma Aldrich P1379
Xho1	NEB R0146S

Mammalian cell lines

Mammalian cell lines, and modified versions of them, used in this thesis:

- Human Embryonic Kidney 293T cells (HEK 293T), received from Paul Bieniasz.
- A549, a human adenocarcinoma alveolar basal epithelial cell line. The derived A549-TMPRSS2 cells express the human TMPRSS2 (Transmembrane protease, serine 2), received from Dr Arthur Wickenhagen.
- HEK-293T FLP-in TREX cells: Thermo Fisher R78007
- MDCK (Madin-Darby canine kidney) cells, received from Dr Matt Turnbull.

Viruses

- Influenza A viruses A/Puerto Rico/8/1934 (H1N1) and A/mallard/Netherlands/10- Cam/1999(H1N1) were rescued from reverse

genetics systems (a kind gift from Prof. Ron Fouchier, and Prof. Laurence Tiley, respectively) as described previously (de Wit et al., 2004, Turnbull et al., 2016).

- Human respirovirus 3 with GFP (PIV3- GFP) was purchased from ViraTree.
- Human respiratory syncytial virus expressing GFP (RSV-GFP) was a kind gift from Prof. Peter Collins (Hallak et al., 2000).
- Semliki forest virus – GFP (SFV-GFP) was a gift from Dr Rute Pinto
- Sindbis viruses: WT, $SINV_{nsp3}$-mCherry and $SINV_{nsp3}$-scarlet, Sindbis virus (SINV) that was produced by in vitro transcription from the plasmid pT7svwt (Castello et al., 2006). Replicative alphaviruses with fluorescent reporters (SINVmCherry and SFVmCherry) were generated by duplication of subgenomic promoter and insertion of mCherry (Garcia-Moreno et al., 2019).

Bacterial cultures

Propagation of DNA plasmids were performed in chemically competent DH10B bacterial cells (lab stocks were grown in house using Thermo Fisher EC0113), using Luria Bertani (LB) agar (E&O Laboratories BM5280) and Luria Bertani (LB) Broth (E&O Laboratories BM5300).

Buffers and solutions

- Protein sample buffer: 12.5% glycerol, 175 mM Tris-HCl [pH 8.5], 2.5% SDS, 70 mM 2-mercaptoethanol, 0.5% bromophenol blue.
- SDS running buffer: For a 20X solution of 500ml add 104.6 g MOPS, 60.6 g Tris Base, 10.0 g SDS, 3.0 g EDTA, pH 7.7.
- Western blot transfer buffer: For a 10X solution of 4 L add 120 g Tris-HCl, 576.9 g Glycine.
- Buffer P1: For 500 ml add 3.03 g Tris, 1.86 g EDTA dihydrate and pH was adjusted to 8.0. RNAse was added before use (100 µg/ml).
- Buffer P2: For 500 ml add 4.0 g NaOH and 25 ml 20 % SDS
- Buffer P3: For 500 ml add 147.25 g potassium acetate and glacial acetic acid until the pH reached 5.5
- TAE Buffer (Gel running buffer): For a 1 L 50X solution add 245.375 g TRIS, 57 ml Acetic Acid, 18.5 g EDTA (dihydrate)

- Agarose gels: Used 1.5 g agarose (Sigma-Aldrich) in 150 ml TAE to make a 1% agarose gel for gel electrophoresis.
- Ethidium bromide: Stock solution of 10 mg/ml in dH2O (Sigma-Aldrich), used for agarose gels at 0.5 µg/ml.
- TB buffer (for preparing competent bacterial cells): To 400 ml dH2O add 1.62g PIPES, 0.93g KCl, 0.83g CaCl2 and adjust pH to 6.7 with KOH (approx. 10 ml of 1M KOH – only after adjusting the pH will the PIPES dissolve), then add 27.5 mL of 1M stock of MnCl2.4H2O and top up to 500 ml with dH2O, filter sterilize and store at 4°C until use.
- Cell freezing mix: Fetal bovine serum containing 10% DMSO, filter sterilized and stored at 20°C until use
- iCLIP 5x PNK buffer: 350 mM Tris HCl pH 6.5, 50 mM MgCl2, 25 mM DTT
- iCLIP high salt buffer: 500 mM NaCl, 1 mM MgCl2, 20 mM Tris HCl pH 7.5, 0.05% NP40, 0.1% SDS, 1 mM DTT, 1x AEBSF
- iCLIP medium salt buffer: 250 mM NaCl, 20 mM Tris HCl pH 7.5, 1 mM MgCl2, 0.05% NP40, 1x AEBSF
- iCLIP PK-SDS solution: 10 mM Tris HCl pH 7.4, 100 mM NaCl, 1 mM EDTA, and 0.2% SDS
- iCLIP PNK buffer: 20 mM Tris HCl pH 7.5, 10 mM MgCl2. 0.2% Tween-20
- RIPA lysis buffer: 10 mM Tris HCl pH 7.5, 150 mM NaCl, 0.5 mM EDTA, 0.1% SDS, 1% Triton X-100, 1% sodium deoxycholate

Antibodies & Dyes

Antibody	**Application**	**Supplier/source**
Mouse monoclonal anti-Actin	WB 1:40	Developmental Studies Hybridoma Bank, University of Iowa
Rabbit monoclonal anti-RNase L (D4B4J)	WB 1:1000	Cell Signaling Technology (27281)
Hoeschst	5ug/ml	Thermo Fisher Scientific 33342
IRDye 680RD Donkey anti-Rabbit IgG	LI-COR Biosciences	926-68073

IRDye 680RD Goat anti-Mouse IgG	LI-COR Biosciences	926-68070
IRDye 800CW Donkey anti-Rabbit IgG	LI-COR Biosciences	926-32213
IRDye 800CW Goat anti-Human IgG	LI-COR Biosciences	926-32232
IRDye 800CW Goat anti-Rat IgG	LI-COR Biosciences	926-32219
SINV Capsid primary antibody	WB	Lab of L. Carrasco
β-actin primary antibody	WB 1:10000	Sigma A1978
MTO1 primary antibody	WB 1:1000	ProteinTech 15650-1-AP
EMG1 primary antibody	WB 1:2000	ProteinTech 11965-1-AP
NSUN2 primary antibody	WB 1:5000	ProteinTech 66580-1-Ig
METTL3 primary antibody	WB 1:5000	ProteinTech 15073-1-AP
Fibrillarin primary antibody	WB 1:2500	Cell Signalling Technologies
NOP2 primary antibody	WB 1:2000	A302-018A, Bethyl
ZC3H11A primary antibody	WB: 1:3000	ProteinTech
GAPDH primary antibody	WB 1:5000	Cell Signalling Technologies
LAMINB primary antibody	WB 1:2000	Cell Signalling Technologies
HIST1H3A primary antibody	WB 1:100	Cell Signalling Technologies
FLAG primary antibody	WB 1:10000	Sigma Aldrich
NOP53 primary antibody	WB 1:2000	Cell Signalling Technologies

Methods

Cell Biology

Mammalian cell culture

All cells were cultured at 37°C with 5% CO_2. Adherent cells were maintained in Dulbeco's modified eagle's medium (DMEM) supplemented with 10% FCS (heat-inactivated foetal calf serum) and 20ug/ml (1X) gentamicin. In addition to standard conditions stable cells lines were kept in 150ug/ml hygromycin (HEK293 Flp/In T-Rex cells) or 2ug/ml puromycin (lentiCRISPRv2-Puro expressing A549 cells). Cells were passaged regularly to maintain a confluence <90%. To do this, cells were washed 1X with 1X PBS, then 1X TrypLE or 1X Trypsin-EDTA was added for 5 min to dissociate cells from the monolayer. Cells were resuspended in DMEM (+10%FCS and 1X gentamicin) and plated at the desired density. Cells were counted by taking a small aliquot, staining with Trypan Blue Stain (0.4%) and using the Countess II FL automated cell counter or a haemocytometer.

Transfection of HEK293 Flp/In T-Rex cells

$2x10^6$ HEK293 Flp/In T-Rex cells were seeded in a T25 flask in DMEM (10% FCS, 1x Gentamicin) 24h before transfection. On the day of transfection media was replaced with fresh DMEM (10% FCS, 1x Gentamicin). 5.33µg pOG44 Flp-recombinase expression vector and 0.67µg pcDNA (9:1 ratio) were added to 600 µL optiMEM and mixed gently. 18ul X-tremeGENE 360 was added in a 1:3 ration was added to the vector-optiMEM mix and incubated at RT for 15min. This transfection complex was added gently to cells. 24h after transfection, media was replaced. After a further 24h, cells were passaged and cell culture media was supplemented with 150ug/ml hygromycin B.

Generation of IAV A/mallard/Netherlands/10- Cam/1999(H1N1)

Plasmids are a set of 8 pDUAL (de Wit et al., 2004) which have the corresponding DNA sequence of the segment (PB2, PB1, PA, HA, NP, NA, M, NS). Pol II and pol I run in opposite directions to generate mRNA and an RNA that resembles vRNA (no 5' cap or poly(A) tail). This leads to production of viral proteins and replication of vRNA

to form progeny infectious virions. The color-flu part of the genome is the segment 8, expressing an NS1-GFP and NEP using a 2A protease.

To generate the P0 stock: 18h before transfection HEK293T cells were seeded at 7.5 x 10^5 cells in 2 ml of D-MEM (9% FBS plus gentamycin) in a 6 well plate. 250ng of each plasmid was added to 200ul serum free DMEM. 4ul of PEI per 1000ng of DNA was added to the plasmid mix and pulse vortexed and incubated for 30min at RT. Media on cells was replaced with fresh DMEM (with 10%FCS and gentamicin), then transfection mix was added dropwise around well. At 18h post transfection, medium was removed and replaced with virus growth medium: serum-free DMEM with 1 ug/ml TPCK-treated trypsin (1:1000) and 0.14% BSA (1:50). After a further 48h, virus was harvested.

To generate a P1 stock in MDCK cells: MDCK cells were seeded (a confluent flask was split 1:3) the night before in DMEM (with 10%FCS and gentamicin). P0 supernatant was diluted 1:10 in virus growth media (serum-free D-MEM with 1 ug/ml TPCK-treated trypsin (1:1000) and 0.14% BSA (1:50)). Cells were washed 2x with serum free DMEM to remove residual FCS, then a low volume of 1:10 P0 virus stock was added (6ml for a T150 flask). Cells were incubated for 1h with regularly tilting to ensure an even overlay. 1h post adsorption, virus growth medium was added (serum-free D-MEM with 1 ug/ml TPCK-treated trypsin (1:1000) and 0.14% BSA (1:50)). 48h post infection virus was harvested by centrifuging at 3000rpm for 5 min at 4^{o}C, aliquoted then stored at -80^{o}C.

All other viruses used in this thesis were kind gifts from colleagues as stated in Materials section.

Platereader Assay

1.5x10^4 cells per well were seeded in 150 µL colourless DMEM (10% FBS, 1x Gentamicin) in a black, clear-bottomed 96 well plate (Perkin Elmer). 24h post seeding, 50 µL colourless DMEM (0% FBS, 1x Gentamicin) containing virus at the desired MOI was added. Cells were then incubated at 37^{o}C with 5% CO_2 in a CLARIOstar

fluorescence plate reader. Fluorescent signal was measured every 15 min over 48h to give a read-out of virus replication.

Confocal Microscopy

Coverslips were placed into the wells of a 24 well plate, washed with 100% ethanol then coated with poly-L-Lysine solution for 5 minutes at 37◦C. HEK293 FITR NOP2-GFP cells were seeded at $2x10^5$ per well onto coverslips in DMEM (10% FBS, 1X Gentamicin) supplemented with 1 ug/mL doxycycline. 24h post induction, cells/coverslips were washed twice with 1X PBS and fixed in 2% PFA for 15 minutes at RT. Cells were washed again with 1X PBS two times and permeabilized using PBS + 0.1% Triton-X100 for 10 minutes at RT. After permeabilization, coverslips were washed with 1X PBS two times and incubated with DAPI at a ratio of 1:1000 for 10 minutes at 37ºC. Cells were washed again in 1X PBS, then in nuclease-free H_2O and mounted on glass slides using SlowFade Diamond antifade mountant. Images were acquired using a 63x/1.40 oil DIC M27 Plano Apochromat objective lens with a total magnification of 630x on a Zeiss LSM 880 Axio-Observer confocal microscope.

Production of lentiviral vectors

Lentiviral vectors were produced by transient transfection of HEK 293T cells.
For 10 cm dish: 5µg of vector, 5µg of GagPol expression vector, and 1µg of VSV-G expression plasmid were added to 500µl serum-free DMEM and vortexed. 4µl PEI per µg DNA used was added to the DNA mix, vortexed and incubated for 30 minutes at RT. Cell medium was replaced with 7 ml fresh DMEM (10% FCS, 1X Gentamicin) then the transfection mixture was added dropwise to the cells. The transfection complex containing media was replaced 16-24 hours post-transfection cell media was replaced with 10 ml fresh DMEM (10% FCS, 1X Gentamicin). Vector-containing supernatants were harvested after 48, 72 and 96 hours and filtered using a 0.45 µm-pore-size-filter before storing at -80ºC.

For 96 well plates (CRISPR library production): HEK293T cells were seeded at a density of $4x10^4$ cells per well 18h before. 50ng of lentiCRISPRv2 vector, 25ng GagPol expression vector and 5ng VSV-g expression plasmid were mixed thoroughly by pipetting in 30ul serum free media per well. 4ul PEI per ug of DNA was added in 30ul

serum free media to each well (3300ul + 68.2ul PEI per plate), mixed thoroughly again and incubated for 2h at room temperature. The transfection mix was then pipetted gently in a dropwise manner onto the HEK 293T cells without changing medium beforehand. 16-24h later, the transfection medium was replaced with 10ml DMEM containing 10% FCS. Vector containing supernatants were collected after 48-, 72-, and 96-hours post transfection and stored at -80^{o}C, and 200ul/well of fresh serum containing media was added to the cells.

To generate stable cell lines, target cells were seeded in 24 well plates at 10^5 cells/well the night before transduction. Cells were transduced with 0.5ml HEK293T lentiviral containing supernatant and spinoculated on to the cells by centrifugation at 1600rpm for 1h at RT. 48h post transduction, cells supplemented with a selection drug until untransduced control cells died. 2ug/ml puromycin, 2mg/ml G418, 200ug/ml Hygromycin and 5ug/ml blasticidin were used for selection.

Screen optimisation titrations

For titration of fluorophore-containing viruses in a lentiviral background, (PIV3-GFP, RSV-GFP, Influenza A viruses A/Puerto Rico/8/1934 (H1N1) and A/mallard/Netherlands/10- Cam/1999(H1N1)), A549 and A549 derived cells were seeded at 6 x 10^3 cells per well (a density to be ~70% confluent the next day) of a 96 well plate. The following day, cells were transduced with a non-targeting guide lentiviral prep (50ul/well) and spinocculated for 1h RT at 1600rpm. 18 hours post transduction, media on the plate was replaced with fresh serum containing DMEM. 72 hours post transduction, cells were infected with serial dilutions of virus for 12h (SeV) 24h (PIV3, SFV), 72h (IAV, RSV). Following incubation, cells were fixed in 2% formaldehyde and the percentage of GFP positive cells was measured using Nexcelom celigo imaging cytometer or cells were trypsinised and GFP positive cells were measured using a Guava EasyCyte cytometer (Luminex).

Arrayed CRISPR knockdown screening

To search for RNA modifying enzymes with novel anti- or pro-viral activity, a library of CRISPR guides targeting all known human RNA modifying enzymes was constructed as described below. Target cells were seeded in 96 well plates at 6x10^3 cells per well

18h before transduction in 100ul DMEM (10% FCS + 1X Gentamicin). The following day, 50ul of DMEM + 4X polybrene was added to each well in the screen. 50ul/well of the lentiviral CRISPR library was then added to each well. To increase success of transduction polybrene (107689, Merck) was added during transduction, and lentiviral supernatants were spin-inoculated onto the cells by centrifugation at 1600rpm for 1h at room temperature. 18-24 hours post transduction, transduction supernatant containing media was replaced with fresh DMEM containing 10% FCS. Cells were incubated for 72 hours post transduction, then media was replaced with 200ul DMEM containing a reporter-encoding virus at a low MOI dose to achieve 8-30% infected cells by the final timepoint. For IFNα14 treated screens, cells were pre-treated for 4h before infection with IFNα14. Infected cells were incubated for 8-72 hours depending on the virus used to allow multiple rounds of replication to be achieved. Cells were fixed in a final concentration of 2% formaldehyde, then nuclei stained with Hoescht so single cells could be detected. The percentage of infected cells (GFP or RFP positive cells) was quantified by the total number of cells (nuclei stained cells) on the Nexcelom Celigo imaging cytometer. Analysis of raw solid state flow cytometry data was analysed using Nexcelom celigo software and downstream analysis was performed using an R statistical programming language script I designed. Each CRISPR guide's ability to impact viral replication (increase or decrease) was determined as a percentage of the medium infectivity from samples per plate of the library. The variability introduced by normalising to the non-target guide condition skewed the results and impacted screening results which is discussed in chapter 4. All screens, unless stated, represent two biological repeats with a single technical repeat. Successful screens were followed up with smaller confirmatory screens using three technical repeats and two or more biological repeats.

Biochemical and Molecular Biology

Molecular Cloning

Open reading frames (ORFs) were either synthesized or digested from a vector stock before cloning into the appropriate plasmid vector. Restriction digests were performed to linearize plasmid DNA vectors for cloning or as control digests to select positive colonies for sequencing. For ligation reactions typically 5µg plasmid DNA was digested with appropriate restriction enzymes and treated with alkaline phosphatase (AP) to

prevent self-ligation of vector fragments. Both vector and insert fragments were gel purified and eluted into 50 µl water. This was achieved by performing gel electrophoresis on 1% (w/v) agarose gels. Agarose prepared by dissolving agarose powder in 1x TAE buffer by microwave heating and adding 8µl ethidium bromide per 150 ml of agarose solution. DNA was extracted and purified from agarose gels was by using the PureLink Quick gel extraction kit (Invitrogen) according to manufacturer's protocols. DNA fragments were eluted in 30-50µl water.

For cloning, digested and purified vector DNA and digested and purified insert DNA were mixed 1:3 respectively, then mixed with 1µl 10x ligation buffer (Promega), 1µl T4-DNA-ligase (Promega) and water to a final volume of 10µl. The ligation mix was incubated at room temperature for 4 hours at RT or overnight at 4°C. After incubation the 10µl ligation-mix was used for transformation of competent bacteria to amplify the cloned product.

Production of CRISPR-Cas9 vectors

Gene editing by CRISPR-Cas9 was performed using the lentiCRISPRv2 one vector system following the established protocols from the Zhang laboratory (Sanjana et al., 2014, Shalem et al., 2014). Seven CRISPR guides per target gene were designed using the CHOPCHOP online tool (https://chopchop.cbu.uib.no) and one non-targeting guide ('NTC': 5′-GTG ACG TAC CGC TGG AGG TA-3′) was used for all targets as control. For a list of CRISPR guides, see Appendix 1. 5ug of LentiCRISPRv2-Puro backbone was digested and dephosphorylated (5ug vector, 3ul BsmBI, 3ul FastAP, 10xFast Digest buffer, 0.6ul 100mM DTT were added to H2O for a total volume of 60ul). CRISPR guides oligonucleotides were ordered from IDT in forward and reverse senses and annealed: 1ul of 100uM of each oligo were aliquoted and 1ul 10X T4 ligation buffer, 0.5ul T4PNK and 6.5ul of H_2O were added then incubated for 1h at 37^{o}C, 95^{o}C for 5 min and the temperature was then ramped down to 25^{o}C at 5^{o}C/min. Annealed oligos were diluted 1:200 then ligated into the lentiCRISPRv2-Puro vector backbone between the BsmBI sites using annealed oligonucleotides with directional, compatible BsmBI overhangs. Ligated plasmids were then transformed in DH10B cells as described above. The produced lentiCRISPRv2 plasmids were packaged into lentivirus by transfecting HEK293T according to the protocol above.

Preparation of chemical competent *E. coli*

Chemically competent DH10B bacteria for heat shock transformation were generated in-house. Parental DH10B bacterial cells were streaked on antibiotic-free agar plates and grown overnight at 37°C. A 10ml 'starter' culture was set up the following morning using a single colony from this plate and grown in antibiotic-free LB for 8 hours with 225rpm shaking at 37°C. The starter culture was then used to inoculate 1L LB culture which was grown for 14-24 hours at 18°C with 225rpm shaking until the culture reached an optical density of OD_{595nm} = 0.6. The culture was then incubated on ice for 10 mins to halt further culture growth, then pelleted by centrifugation at 2000g and 4°C for 10 minutes. The pellet was resuspended in 400ml ice-cold TB and pelleted again by centrifugation at 2000g and 4°C for 10 minutes. The pelleted bacteria were resuspended in TB-DMSO (7% DMSO final concentration) and kept on ice. This suspension is the final competent bacteria. Competent bacteria were aliquoted and snap frozen before being stored at -80°C.

Transformation of *E. coli* by heat shock

DH10B cells were thawed on ice for 30 minutes. For ligation reactions, 50ul DH10Bs was mixed with 5ul ligation mix. For plasmid propagation 50ul DH10B was mixed with 1ul plasmid DNA. The bacteria-DNA mix was incubated on ice for 20 minutes before heat shock for 45 seconds at 42°C in a water bath or on a heat block for 96 well plate transformations. Cells were recovered on ice for 2 minutes before 150ul of SOC medium was added and incubated for 45 minutes at 37°C with shaking. Cultures were then spread on solid LB agar plates containing 200ul/ml ampicillin or 100ug/ml kanamycin and incubated overnight at 30 or 37°C.

Isolation of plasmid DNA

Plasmid DNA was isolated from bacteria using commercially available kits. Plasmid DNA preparations were grown by inoculating 5ml (miniprep) or 50ml (midiprep) LB media including selection antibiotic with a single bacterial colony. Cultures were grown overnight at 30 or 37°C with shaking at 225rpm. Plasmid DNA was recovered using the QIAprep Spin Miniprep kit (Qiagen) or QIAprep Spin Midiprep kit (Qiagen) following the protocols provided with the kits. Plasmid DNA was resuspended in 50ul (miniprep)

or 200ul (midiprep) water and concentration was measured using a NanoDrop (Thermo Fisher Scientific) or a Qubit (Thermo Fisher Scientific).

Western Blots

Cell lysates for protein expression analysis were generated by harvesting a confluent well or plate at the end of an experiment, i.e., for knockout analysis of genes targeted by CRISPR cells were seeded at 1.5 x 10^4 cells/well of a 96 well plate, 18 hours later transduced with lentivirus containing CRISPR condition of interest, and 72 hours post transduction, cells were washed with PBS, lysed with 50ul 1x NuPAGE protein sample buffer. Harvested lysates were denatured at 70^{o}C for 10 minutes and sonicated for 45 seconds at 3.0 magnitude using a sonnicator 3000 (Misonix Inc).

Proteins were separated based on molecular weight by sodium dodecyl sulfate polyacrylamide gel electrophoresis (SDS-PAGE) using pre-cast gradient NuPAGE 4-12% Bis-Tris gel (Invitrogen). Typically, 15ul of sample and 2 ul of PageRuler (Thermo Fisher Scientific) were loaded per lane on a gel. Gels were run for 1h at 140V, followed by wet transfer onto nitrocellulose membranes overnight at 14V. The following day, nitrocellulose membranes were blocked using Sea Block (Thermo Fisher Scientific) for 30mins at room temperature. Then primary antibodies were added at their desired concentration and membranes were incubated for 2 hours at room temperature with rocking. Membranes were washed with PBS+0.1% Tween (v/v) three times, then incubated with secondary antibody for 30mins-1hour at RT. Membranes were washed three times with PBS-T and stored in PBS before scanning on a Li-COR Odyssey CLx machine.

Flow cytometry and imaging cytometry

Cells infected with GFP- or RFP- expressing reporter viruses were quantified using the two-colour flow cytometry machine Guava EasyCyte (Luminex) or the 5 channel colour Nexcelom celigo imaging cytometer. For Guava quantification: cells were trypsinised with 50ul TrypLE (0.5%) [Thermo Fisher Scientific] for 10 mins at 37^{o}C, then mixed by pipetting into a single cell suspension with 50ul PBS and transferred into a round bottom 96 well plates (for use with the Guava EasyCyte) containing 50ul 4% formaldehyde. 10,000 events were acquired on the flow cytometer. Flow cytometry

data was analysed using Guava EasyCyte software before downstream analysis in R. For Nexcelom Celigo quantification: cells were fixed in 2% (final concentration) formaldehyde, then incubated for 10 minutes with Hoescht which stains nuclei blue and allows us to detect individual cells. Plates were imaged on the Celigo with brightfield, GFP or RFP (depending on the fluorophore of the virus) and blue field captured. All celigo data was analysed using the Nexcelom Celigo software and downstream analysis was performed in R.

iCLIP2

Sample harvesting

$10x10^6$ HEK293T cells were seeded per condition in a 10cm dish in DMEM supplemented with 2% FBS. Conditions were either mock infected or cells were infected with MOI=3 of SINV 16 hours before harvesting. The following day, cells were washed twice in 1X PBS and crosslinked at 0.3 J/cm2 UV light irradiation at 254 nm, then lysed in 1 ml RIPA buffer (50 mM Tris pH 7.5, 150 mM NaCl, 1% Triton X-100, 0.1% SDS, 0.5% (w/v) sodium deoxycholate and 0.2mM AEBSF). Lysates were incubated on ice for 30 min, then homogenized by passing through a 27G needle five times. The lysates were then cleared by centrifugation (18000xg for 10 min at 4°C), snap-frozen and stored at -80°C.

iCLIP2

Lysates were thawed and 4U TurboDNase and 5U RNase I were added. Samples were mixed by vortexing and incubated for 3 min at 37°C with shaking (1100 rpm). 200U RiboLock RNase Inhibitor was then added, and lysates were incubated for a further 3 min on ice. Size-matched input (SMI) samples were collected at this point (2x 10ul) and stored at -80^{o}C. Lysates were transferred to fresh tubes and incubated with 25µL of pre-equilibrated Pierce Protein A magnetic beads conjugated to NOP2 antibody for 2h at 4°C with gentle rotation. Beads were washed twice with 900µL of chilled high-salt wash buffer, twice with 900µL of chilled medium-salt wash buffer, and twice with 900µL of chilled PNK wash buffer. RNA 3'-end dephosphorylation was performed using 4ul 5x PNK buffer, 0.5ul PNK enzyme, 0.25ul FastAP alkaline phosphatase, 0.5U TurboDNase and 0.5ul Ribolock RNase inhibitor at 37°C for 40 min with shaking (1100 rpm). Beads were washed once with 500µL chilled PNK wash

buffer, twice with 900µL of chilled high-salt wash buffer, and twice with 900µL chilled PNK wash buffer. L3-IR-App adapter (Zarnegar et al., 2016) ligation was performed overnight at 16°C with 1100 rpm shaking protected from light in the following mixture: 3.6ul H20, 2ul 10X T4 ligation buffer, 1ul T4 RNA ligase I High concentration, 0.5ul Ribolock Rnase Inhibitor, 0.4ul T4 PNK enzyme, 2.5 ul L3-IR-App adapter, 9ul PEG8000 (40%) & 1ul 100% DMSO. Beads were then washed once with 500µL PNK wash buffer, twice with 900µL of high-salt wash buffer, and twice with 900µL PNK wash buffer.

Immunoprecipitated and SMI samples were denatured in 1X NuPage Sample Buffer with 100mM DTT at 70^{o}C for 5min. IP samples were centrifuged and eluate was transferred to a fresh tube. The elution was repeated, and this was added to the first eluate. IP and SMI samples were separated on a 4-15% Mini-PROTEAN TGX Precast Protein Gel for 75 min at 140 V, then protein-RNA complexes were transferred on to an iBLOT2 nitrocellulose membrane using the BioRad Trans-blot Turbo (High Mw protein setting) and imaged using a LI-COR Odyssey imaging system for the RNase concentration trial. For the actual iCLIP protocol, imaging was not performed to avoid contamination. The region corresponding to the RBP-GFP band from the RNase I trial was cut (for IP and SMI) and the protein was digested using 350µg Proteinase K in 180µL PK-SDS solution (10mM Tris-HCl pH 7.5, 100mM NaCl, 1mM EDTA, 0.2% SDS) for 60 min at 50°C with 1100 rpm shaking. RNA was purified by adding 1X volume of Phenol:Chloroform:Isoamyl Alcohol pH 6.6-6.9, then incubating for 10 min at 37°C with 1100 rpm. This was then centrifugaed at 16000xg for 5 min in MaxTract tubes. RNA was cleaned using Zymo RNA Clean & Concentrator-5.

For SMI processing, SMI samples were treated with 4ul 5x PNK buffer, 0.5ul PNK enzyme, 0.25ul FastAP alkaline phosphatase, 0.5U TurboDNase and 0.5ul Ribolock RNase inhibitor at 37°C for 40 min with shaking (1100 rpm). SMI RNA was then cleaned up with MyOne Silane Dynabeads before L3-IR-App adapter ligation was performed using 0.7ul H_20, 2ul 10X T4 ligation buffer, 1.5ul T4 RNA ligase I High concentration, 0.5ul Ribolock Rnase Inhibitor, 2ul 1:10 diluted L3-IR-App adapter, 8ul PEG8000 (40%) & 0.3ul 100% DMSO for 75min at room temperature. Samples were purified using MyOne beads then treated with 0.5ul 5’ Deadenylase and 0.5ul RecJf endonuclease in 1X New England Biolabs buffer 2 with 0.5ul Ribolock RNase Inhibitor

and 20% PEG8000 for 1h at 30°C, then 30 min at 37°C (1100 rpm). Samples were then subject to a MyONE bead clean-up.

RNA from IP and SMI samples were reverse transcribed using Superscript IV reverse transcriptase and hydrolysed by adding 1.25µL of 1M NaOH for 15 min at 85°C, before neutralization with 1.25µL of 1M HCl. cDNA was then purified using MyOne Silane beads. L#clip2.0 adapters with barcodes for multiplexing (Buchbender et al., 2020) were ligated to cDNA in a reaction mix of 2µL of 10µM adapter, 5µL of cDNA, supplemented with 1µL of DMSO, and incubated at 75°C for 2 min before placing on ice. To this 2ul T4 RNA ligase, 2ul 1X RNA ligase buffer and 9ul 40% PEG8000 was added and incubated overnight at 20°C (1100 rpm). cDNA was cleaned up with MyONE beads before PCR amplification. Pre-amplification was performed using 2X Phusion HF PCR Master mix and P5Solexa_s and P3Solexa_s primers for six cycles, proceeded by ProNex size-selective purification. Required number of PCR cycles were determined by Real-Time qPCR, using 0.5ul 20X EvaGreen, 5ul 2X Phusion HF PCR Master mix, and 0.5ul 10uM P5/P3 Solexa primers. Final PCR products were purified in two consecutive rounds of ProNex Size selection.

Oligos used in iCLIP:

L3-App	/rApp/AGATCGGAAGAGCGGTTCAG/ddC/
L01clip2.0	/5Phos/NNNNATCACGNNNNNAGATCGGAAGAGCGTCGTG/3ddC/
L02clip2.0	/5Phos/NNNNCGATGTNNNNNAGATCGGAAGAGCGTCGTG/3ddC/
L03clip2.0	/5Phos/NNNNTTAGGCNNNNNAGATCGGAAGAGCGTCGTG/3ddC/
L04clip2.0	/5Phos/NNNNTGACCANNNNNAGATCGGAAGAGCGTCGTG/3ddC/
L05clip2.0	/5Phos/NNNNACAGTGNNNNNAGATCGGAAGAGCGTCGTG/3ddC/
L06clip2.0	/5Phos/NNNNGCCAATNNNNNAGATCGGAAGAGCGTCGTG/3ddC/
L07clip2.0	/5Phos/NNNNCAGATCNNNNNAGATCGGAAGAGCGTCGTG/3ddC/
L08clip2.0	/5Phos/NNNNACTTGANNNNNAGATCGGAAGAGCGTCGTG/3ddC/
L09clip2.0	/5Phos/NNNNGATCAGNNNNNAGATCGGAAGAGCGTCGTG/3ddC/
L10clip2.0	/5Phos/NNNNTAGCTTNNNNNAGATCGGAAGAGCGTCGTG/3ddC/
L11clip2.0	/5Phos/NNNNATGAGCNNNNNAGATCGGAAGAGCGTCGTG/3ddC/
L12clip2.0	/5Phos/NNNNCTTGTANNNNNAGATCGGAAGAGCGTCGTG/3ddC/
L13clip2.0	/5Phos/NNNNAGTCAANNNNNAGATCGGAAGAGCGTCGTG/3ddC/

L14clip2.0	/5Phos/NNNNAGTTCCNNNNNAGATCGGAAGAGCGTCGTG/3ddC/
L15clip2.0	/5Phos/NNNNATGTCANNNNNAGATCGGAAGAGCGTCGTG/3ddC/
L16clip2.0	/5Phos/NNNNCCGTCCNNNNNAGATCGGAAGAGCGTCGTG/3ddC/
L17clip2.0	/5Phos/NNNNCAACTANNNNNAGATCGGAAGAGCGTCGTG/3ddC/
L18clip2.0	/5Phos/NNNNGTCCGCNNNNNAGATCGGAAGAGCGTCGTG/3ddC/
L19clip2.0	/5Phos/NNNNGTGAAANNNNNAGATCGGAAGAGCGTCGTG/3ddC/
L20clip2.0	/5Phos/NNNNCACCGGNNNNNAGATCGGAAGAGCGTCGTG/3ddC/
L21clip2.0	/5Phos/NNNNGTTTCGNNNNNAGATCGGAAGAGCGTCGTG/3ddC/
L22clip2.0	/5Phos/NNNNCGTACGNNNNNAGATCGGAAGAGCGTCGTG/3ddC/
L23clip2.0	/5Phos/NNNNCACGATNNNNNAGATCGGAAGAGCGTCGTG/3ddC/
L24clip2.0	/5Phos/NNNNATTCCTNNNNNAGATCGGAAGAGCGTCGTG/3ddC/
L25clip2.0	/5Phos/NNNNACTGATNNNNNAGATCGGAAGAGCGTCGTG/3ddC/
P5Solexa_s	ACACGACGCTCTTCCGATCT
P3Solexa_s	CTGAACCGCTCTTCCGATCT
P5Solexa	AATGATACGGCGACCACCGAGATCTACACTCTTTCCCTACACGACGCTCTTCCGATCT
P3Solexa	CAAGCAGAAGACGGCATACGAGATCGGTCTCGGCATTCCTGCTGAACCGCTCTTCCGATCT

Sequencing

Sample concentrations were quantified by Qubit DNA HS and library size was measured using High Sensitivity D1000 TapeStation. Samples were pooled equimolarly and then mixed in a ration of 75% library pool and 25% SMI library pool. Sequencing was performed on a NextSeq 550 with a 75 cycle high-output kit v2.5.

Data analysis

clusterProfiler in R (Wu et al., 2021) was used to perform GO enrichment analyses. A p-value cut-off of 0.01 and a q-value cut-off of 0.05 were used and the Benjamini-Hochberg method was used to correct for multiple testing. Non-unique GO terms were collapsed using clusterProfiler's simplify function.

Raw FASTQ files were demultiplexed using the Je Suite (Girardot et al., 2016) and adapters were trimmed using Cutadapt (Martin, 2011). Reads were aligned using STAR to a concatenated human (GRCh38, ENSEMBL Release 106) and SINV (pT7-SVwt) genome in end-to-end alignment mode (Dobin et al., 2013). Only uniquely aligned reads were retained for downstream analysis and PCR duplicates were collapsed using unique molecular identifiers (UMIs) with the Je Suite. The crosslink truncation site for each read (-1 from the 5' start site of the read) was extracted using BEDTools (Quinlan & Hall, 2010).

HTSeq-clip and the R/Bioconductor package, DEW-seq was used to perform peak calling (Sahadevan et al., 2022). A sliding window annotation of the human and SINV genome was generated using HTSeq-clip (50nt window, 20nt step size) and HTSeq-clip was also used to calculate the frequency of crosslink truncation sites within each window. The differential enrichment of each window relative to size-matched input control samples was calculated using DEW-Seq, with a cut-off of >2 log2 fold change and >0.01 adjusted p-value. Multiple hypothesis correction was performed using the Independent Hypothesis Weighting (IHW) method (Ignatiadis et al., 2016). Overlapping windows were merged to form binding regions.

PCA was performed using DESeq2 (Love et al., 2014). After size correction and variance stabilisation, the 1000 most variable sliding windows were chosen for PCA plotting. Binding site properties, including gene name, biotype, and gene feature, were extracted from the ENSEMBL genome annotation using the GenomicRanges package. Metagene analyses were performed using functions from the cliProfiler package.

For motif and secondary structure prediction, sequences were defined as 50nt regions centred on the peak in the BigWig signal for each binding site. To facilitate motif prediction, a background sequence matching the gene and gene region was extracted for each binding site, enabling differential enrichment analysis. Enrichment analysis was conducted using STREME from the MEME suite (Bailey et al., 2014). The Universalmotif package was utilised for motif processing, while motifStack was employed to cluster and visualise the motifs.

RNAfold from the ViennaRNA suite was used to predict secondary structures, with Forgi, also from ViennaRNA, extracting the specific structural features. To assess enrichment for paired sequences, comparisons were made against 10 scrambled versions of each input sequence.

Using BEDTools (Quinlan et al., 2010), we calculated the SINV genome coverage in reads per million. We then determined the percentage of total signal at each position for both IP and SMI samples. For plotting purposes, the SMI signal was subtracted from the IP signal.

Chapter 3 Designing an arrayed CRISPR screening platform targeting human RNA modifying enzymes

Introduction

CRISPR as an arrayed screening platform

Genetic screening is an incredible approach for discovering genes, pathways and mechanisms that play a role in a phenotype or biological process (Grimm, 2004). In order to ask questions about the role of RNA modifications of viral RNA genomes during infection, we designed and built a platform for screening human RNA modifying enzymes (RME).

Constructing a platform for screening required several key choices early on. We considered a system of over-expressing the genes of interest to get an extreme phenotype or knocking out the gene of interest to gain a loss of function phenotype. There are many disadvantages to both types of screens, principally the time and labour involved. We need to consider that genes involved in editing RNA will reach saturation with the number of targets they have versus the total number of enzyme molecules in the cell, so overexpressing the gene may not have a notable phenotypic change compared to endogenous control levels. However, knocking these enzymes out will have a distinguishable phenotype during infection if they are necessary to aide or prevent pathogenesis. Thus, we decided to design a loss-of-function based platform to question the role of RNA modifications in viral infection. The principal methodologies used in knockdown screening are RNAi and CRISPR, however in the last decade, CRISPR has become the dominant method of creating knockouts as the system is much easier to implement than RNAi. CRISPR screens take advantage of the efficiency and versatility of CRISPR-Cas genome editing (Bock et al., 2022; Jinek et al., 2012).

What is CRISPR? Clustered regularly interspaced short palindromic repeats/CRISPR-associated (Cas) is an RNA-mediated adaptive defence system that bacteria and archaea have evolved to protect themselves from viruses and foreign plasmids. It relies on the incorporation of small fragments of foreign nucleic acids into the host genome between short DNA repeats (Jinek et al., 2012). These sequences are then transcribed and made into small non-coding RNAs (sgRNA) which are incorporated into a multifunctional protein complex composed of Cas proteins. The small RNAs provide sequence-specific recognition of foreign nucleic acid and permit the Cas complex to cut the invading foreign genetic material, thereby silencing it (Bhaya et al., 2011).

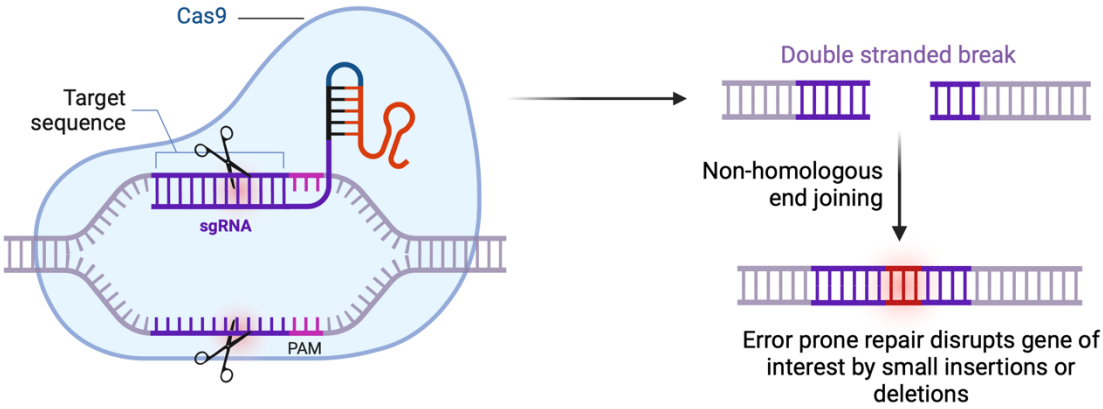

Figure 3.1: Schematic of how CRISPR-Cas9 causes loss-of-function mutations. Guided by a small guide RNA (sgRNA) to specific sequences in the genome, Cas9 has nuclease activity that cuts double stranded DNA. These breaks are repaired by non-homologous end joining which can introduce indel mutations, resulting in compromised gene function.

In the lab the RNA guided CRISPR associated nuclease Cas9 can be used effectively to introduce loss-of-function mutations (Cong et al., 2013; Mali et al., 2013; Shalem et al., 2014). Cas9 can be programmed to introduce targeted loss of function mutations in the genome by inducing double stranded breaks in DNA at specific genomic loci. Errors in the DNA repair process cause frame shift indel mutations leading to a loss-of-function allele (Figure 3.1). The specificity of this targeting is determined by a single short synthetic guide RNA (sgRNA) (Jinek et al., 2012; Shalem et al., 2014), which can be easily generated, meaning it is easy to programme a large-scale arrayed library of oligonucleotides targeting different genes.

There are a range of ways of introducing CRISPR/Cas into cells. We used a derivative of the HIV-1 based retroviral vector lentiCRISPR version 2 (Sanjana et al., 2015,

Shalem et al., 2014). We used a single lentiviral vector to deliver cas9, a sgRNA and a puromycin selection marker (Sanjana et al., 2015, Shalem et al., 2014). It eliminates the need to produce stably expressing Cas9 cells prior to a screen and can allow us to perform knockdowns quickly in different cell types.

CRISPR screens can be defined through four steps: the model the screen is to be performed in, the method of screening/how CRISPR is introduced to the cells, conditions the perturbed cells are then exposed to (i.e. virus infection) which gives us measurable phenotypes, and a measurement of the molecular or cellular effects of the perturbations which are linked to the CRISPR guides (Bock et al., 2022). We had the options of performing arrayed screening, whereby each gene is knocked out separately in a physically compartmentalised way (e.g., different wells on a plate) so we can know the exact cause of a change of phenotype. Or we could perform pooled screening. This involves introducing the CRISPR library in bulk to the cells and following up changes in phenotype with RNA sequencing to see which guide is the cause of the perturbation. Both are powerful techniques, but arrayed screening was already well established in the lab, with methods and protocols for downstream processing already available. There is also a significant cost reduction with arrayed screening.

Results

CRISPR/Cas9 sgRNAs can induce gene knockdown in 72h

To start creating the screening platform, we started at a smaller scale to verify the concept and determine if the platform we wanted to create could yield informative results. We chose several proteins with different enzymatic functions and different levels of characterisation of interactions with viruses:

1. A protein that had been found to interact with viruses, but the role was unknown: EMG1 (a pseudouridine methyltransferase) which was found in datasets to interact with SARS-CoV2 (Samavarchi-Tehrani et al., 2020) and HIV-1 (Naji et al., 2012).
2. A protein that is involved as the catalytic core of a m^6A methyltransferase complex (Yao et al., 2018): METTL3 which has been found to increase viral RNA expression in Influenza A virus (Courtney et al., 2017) and positively

regulate HIV-1 mRNA expression (Kennedy et al., 2016) and viral replication when added to crRNAs (Lichinchi et al., 2016).

3. A m^5C methyltransferase NSUN2 which highly methylates HIV-1 mRNA in infected cells and loss of m5C inhibits HIV-1 mRNA translation (Courtney et al., 2019).
4. We also included a technical control: RNaseL, to ensure cloning and lentiviral packaging were successful as CRISPR guides had been successfully used to knockdown the protein in experiments in the lab (Wickenhagen et al., 2021).

I designed seven CRISPR guides (sgRNAs) per target gene (EMG1, METTL3, NSUN2) using the CHOPCHOP online tool (https://chopchop.cbu.uib.no), then cloned them into the lentiCRISPRv2 vector in tandem with the guides targeting RNaseL as a cloning control. I subsequently produced lentiviral vectors for gene editing.

We had to consider how to set up the knockouts to be manageable at a full screening capacity. The lentiCRISPRv2 system allows us to use antibiotic selection to proliferate cells that have been successfully transduced (Sanjana et al., 2014). Shalem et al., 2014, performed knockouts and selection of screening cell lines for 6 days. However, they undertook pooled screening so could sequence sgRNAs at the end of the experiment and determine the depleted sgRNAs and pinpoint gene targets in negative selection screens. This is not as manageable in an arrayed screen because it unfortunately requires several passages of the cell lines (Shalem et al., 2014). For a screen we want to ideally be able to challenge cells with virus after lentiviral transduction without passaging. I also wanted to probe if the small library of lentivirus I had produced containing crRNAs targeting EMG1, METTL3, NSUN2 and RNaseL could produce knockouts (manifested as a knock down at the cell population level). Thus, we designed an experiment to determine if the small library of lentivirus could reduce expression of the protein in the cell and how long this took.

We set up a time course experiment and assessed the level of gene ablation 24, 48 and 72 hours after transduction using sgRNAs targeting EMG1. Knockdown of EMG1 begun to be seen at 24h, however was more obvious at 72h (Figure 3.2A). This experiment is limited in its scope but covers some important bases. We proved that we see knockdown at 72h and the CRISPR system we have elected to use can

produce this result. The knockdowns would have been more complete if left for a week, but we are aiming to produce a screening system where we can transiently knockdown and then infect the same cells without passaging. We were also considering lengths of time for a multicycle infection during the design phase. In the case of IAV, this is 72h (Eisfeld et al., 2017). Since KOs can be quite deleterious to the cell, perhaps knockdown is better for screening. The phenotypes will not be as extreme, but we'll still see effects/shifts from the norm if a gene is involved in viral infection.

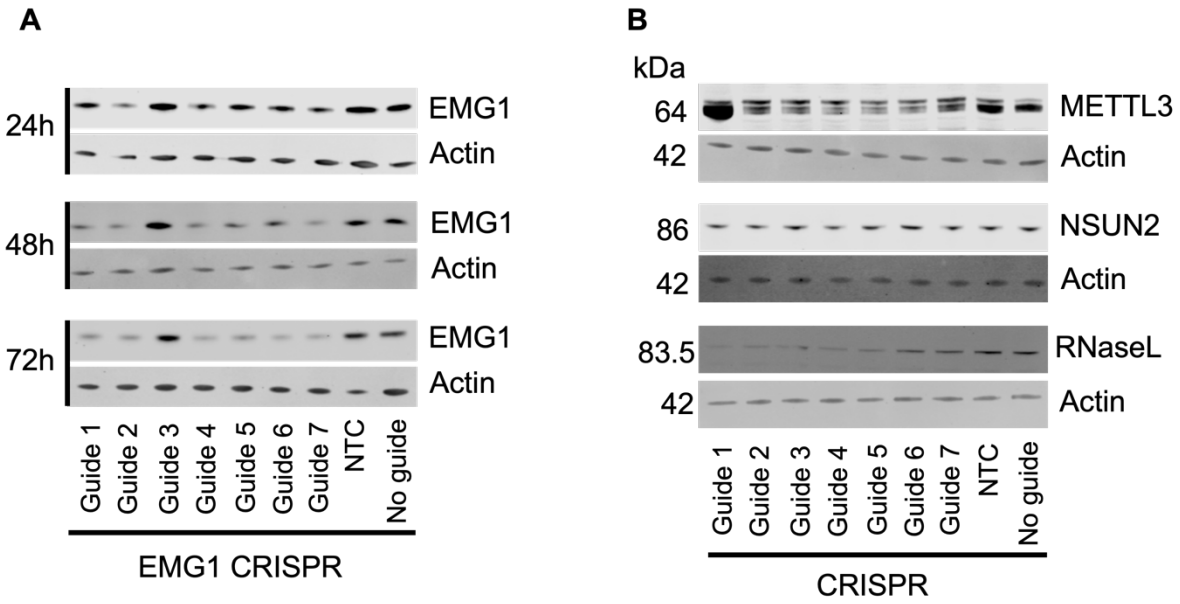

Figure 3.2: Optimising incubation times for transient knockdown after transduction with CRISPR guides. A549 cells were transduced with sgRNAs targeting genes of interest, then harvested and lysed after 24-72h (A) or 72h (B). Lysates were subjected to western blot with antibodies targeting gene of interest and actin as a loading and blotting control.

A. Time trial experiment over 72h that showed reduced expression of EMG1 within 72h. EMG1 molecular weight = 27kDa; actin = 42kDa.
B. transient knockdowns targeting METTL3, NSUN2 and RNaseL for 72h transduction.

Guides 1-7 refer to the small guide RNA targeting the gene, we designed seven for each gene. NTC = non-targeting guide control. No guide = untransduced WT control.

I then transduced A549 cells with CRISPR lentiviruses against METTL3, NSUN2 and RNaseL for 72h and ran westerns of the lysates harvested from this experiment. We can see successful reduction in expression in the first two guide conditions in RNaseL and guides 2-7 of METTL3 (Figure 3.2B). Interestingly in METTL3, guide 1 causes an increase in the expression of METTL3. We are unsure what the explanation for this is. Unfortunately, there was no reduction in expression of NSUN2 in any of the conditions (Figure 3.2B). We designed 7 guides targeted at each gene in the hopes this would increase the chances of having successful knockdowns. In screening, there is a

sizable margin for error, but this raised a concern. Perhaps NSUN2 protein has a slow turnover in the cell and within this experiment, we cannot tell the difference between no editing and slow protein turnover.

The lentiviruses for each gene-editing CRISPR condition were prepared at the same time and used to transduce cells at the same time. As our positive control (RNaseL) worked and we saw a reduction of expression in conditions for the other two genes (EMG1 and METTL3), we thought a technical error was unlikely. An error I had made when designing the guides, was to use the top 7 outputs from the CHOPCHOP script. On analysing the outputs from the programme, I later found that all the NSUNS2 guides target the 3' end of the gene, so perhaps the reason we see no reduction of gene expression is because the gene is not fully targeted. Perhaps a slightly truncated version of the protein was produced but we don't see a shift in the NSUN2 bands on the blot compared to non-targeting control and mock transduced. I also looked at the spread of guides for METTL3 and found they targeted a spread of the gene and were not concentrated at the 3' end. Thus, for designing the full library, we decided to ensure to include guides that targeted the full gene to increase our knockdown successes.

Determining the type of screen to do

To identify human RNA binding proteins involved in viral RNA editing, we wanted to screen a panel of viruses with RNA genomes. We hypothesised we could conduct these screens in two distinct ways. First, to knockdown each RBP of interest using the CRISPR platform we had created and challenge with a fluorophore-expressing virus. Infection then would be measured using flow cytometry (Figure 3.3). This "incoming screening" method would identify RBPs that affect steps of the virus lifecycle preceding fluorophore expression. Second, we would measure the yield of infectious virions by collecting supernatants from cells knocked down with the screening library and subsequently challenged with virus. These supernatants would be used to infect a reporter cell line (Figure 3.3). This "production (or yield) screening" approach would identify RBPs involved in the latter stages of the viral life cycle. For differences in infection to be accurately quantified, i.e., between low infection and superinfection, we aim to infect cells in a range where we can accurately quantify increases and decreases in infection.

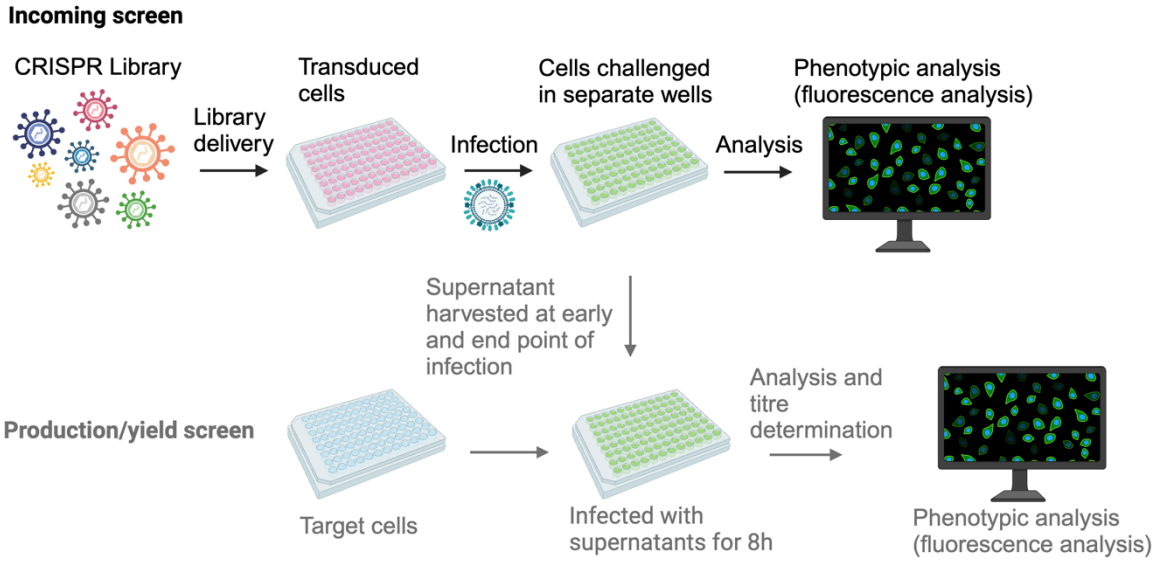

Figure 3.3: Arrayed screening pipelines. In the top workflow, incoming screening follows the process of a canonical arrayed CRISPR screen whereby cells are subjected to CRISPR KD, challenged with fluorescent virus and then numbers of fluorescent/infected cells are quantified and compared to a control KD condition (for this project a non-targeting guide [NTC]). Enrichment or depletion of infection will show potential genes involved in infection.
In the yield screen pipeline, supernatants are harvested from the incoming screen early in infection (4h) and at the endpoint of infection (single or multicycle) and used to infect reporter cells. Differences in titre between the two timepoints can show us conditions that increase or decrease virion production, which could complement hit detection from the incoming screen.

For screen optimisations we chose to use Influenza A/Mallard/Netherlands/10-Cam/1999 (H1N1 NS1-GFP) [from hereon called IAV Mallard] because it can successfully replicate for multiple cycles in mammalian cell lines. We were also interested in finding proteins involved in species restriction, so using an avian virus as part of our screening panel will hopefully produce some interesting results. There were also additional benefits to using IAV for optimisation due to expertise in the lab and readily available reverse genetics systems. Experimentally, a low dose of trypsin is usually added to cultures to aid spreading in cells (Eisfeld et al., 2017), however we want to avoid this for large scale screening to keep the conditions streamlined. To optimise streamlining the screens we decided to test and see if TMPRSS2 (transmembrane serine protease 2) could permit IAV mallard multicycle infection in tissue culture. TMPRSS2 is located on the cell membrane and has been shown to proteolytically activate IAV serotypes H1N1, H7N9 and H3N2 in cells (Limburg et al., 2019; Hatesuer et al., 2013; Tarnow et al., 2014; Sakai et al., 2014). It is also involved

in the entry of SARS-CoV2 (Zhang et al, 2022). Down-regulation of TMPRSS2 can suppress IAV propagation in vivo (Shen et al., 2020). Hence for these optimisations we decided to compare between two cell lines from an A549 background: unmodified A549 cells and A549 cells that (ectopically) expressed TMRSS2.

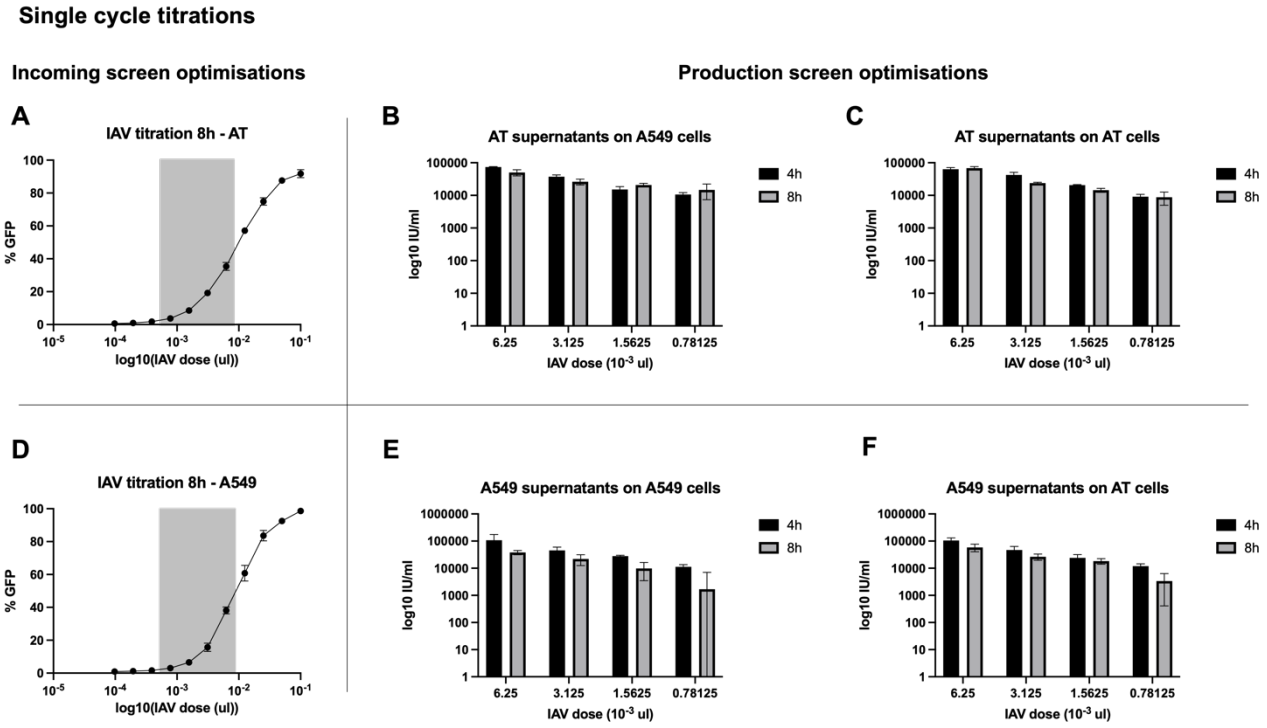

Figure 3.4: Single cycle screening optmisations using IAV mallard. To determine the ideal dose of IAV-mallard to use in single cycle screens, titrations (A and D) were performed in 96 well plates using the cell types stated below. Supernatants were harvested and replaced after 4h and also harvested at 8h, then cells were fixed in 2% formaldehyde. Imaging cytometry was used to determine rates of infection of IAV-mallard by measuring the number of cells expressing GFP as a percentage of the total cell count in a well. 4h and 8h harvested supernatants were titrated over cells stated below to determine if there had been viral production in a single round of infection in A and D (bar charts B,C,E,F). After 8h cells were fixed in 2% formaldehyde and titres were determined using imaging cytometry.
A. Titration of IAV mallard in a TMPRSS2 expressing A549 cell line (A549-TMPRSS2 or AT). X axis = dose of virus, Y axis = rate of infection.
B/C. Bar charts showing viral output (titre – Y axis) from four infection conditions (x axis) in grey box in A. Supernatants were harvested from doses in the grey box in A at 4h (input) post infection and 8h (output). These supernatants were titrated on A549 cells and A549-TMPRSS2 cells and incubated for 8h to see if there was an increase in the titre of virus in the 8h supernatant after a single round of infection.
D. Titration (1:3 dilutions) of IAV mallard in A549 cells. X axis = dose of virus, Y axis = rate of infection.
E/F. Bar charts showing viral output (titre – Y axis) from four infection conditions (x axis) in grey box in D. Supernatants from the grey box in D were harvested at 4h and 8h post infection and titrated on A549 cells and A549-TMPRSS2 cells to see if there was an increase in the titre of virus in the 8h supernatant after a single round of infection.

Incoming screen optimisation

The optimisation of an incoming screen itself is quite simple; we titrated the virus in A549 cells or A549-TMPRSS2 cells transduced with nontargeting guide control (NTC) containing lentivirus several days prior for the period we had elected to use in screens and then quantified infection using imaging cytometry. This allowed us to select a dose where we can accurately quantify increases and decreases in infection to take forward to screening. We did this for a single cycle of IAV infection (Figure 3.4) and a multicycle infection (Figure 3.5). A single cycle infection screen would show us RNA modifications that occur in the first round of infection which act as early restrictors or uncover genes used by IAV previously unknown to aid infection in the first stages. A multicycle assay would show us RME's involved in the increase or reduction of virus infection and later stages of the lifecycle. From these single cycle titrations (Figure 3.4A, D) and multicycle titrations (Figure 3.5A, C) in A549 cells and A549-TMRPSS2 cells, we identified doses of IAV mallard to take forward to screening.

Interestingly we observed viral spreading and foci production in the multicycle assay in the A549-TMPRSS2 cell line (Figure 3.6D). This suggested that 1. That we could use the TMPRSS2 background for IAV screens and 2. Perform screens complementary to imaging cytometry by counting foci instead of quantifying the total GFP expression in the population.

Production screen optimisation

Initially we tried to create a workflow where we could perform an incoming screen and harvest supernatants for a yield screen. We investigated the virion production in the supernatants from the conditions of the incoming titration optimisation. During the single cycle incoming optimisation experiment, we harvested the supernatant 4h after infection before a cycle of IAV had occurred and at 8h to assess if there was production of virions vs the input amount of IAV. To do this we titrated the supernatants so we could ascertain the titre differences between input and 8h single cycle infection (Figure 3.4B,C,E,F). Based on the results of incoming infection, we titrated supernatants from the conditions that had medium to low levels of total infection per well (grey boxes in Figure 3.4A,D). These conditions will be used for the incoming screen and hence would be the supernatants we would collect in the full-scale screen.

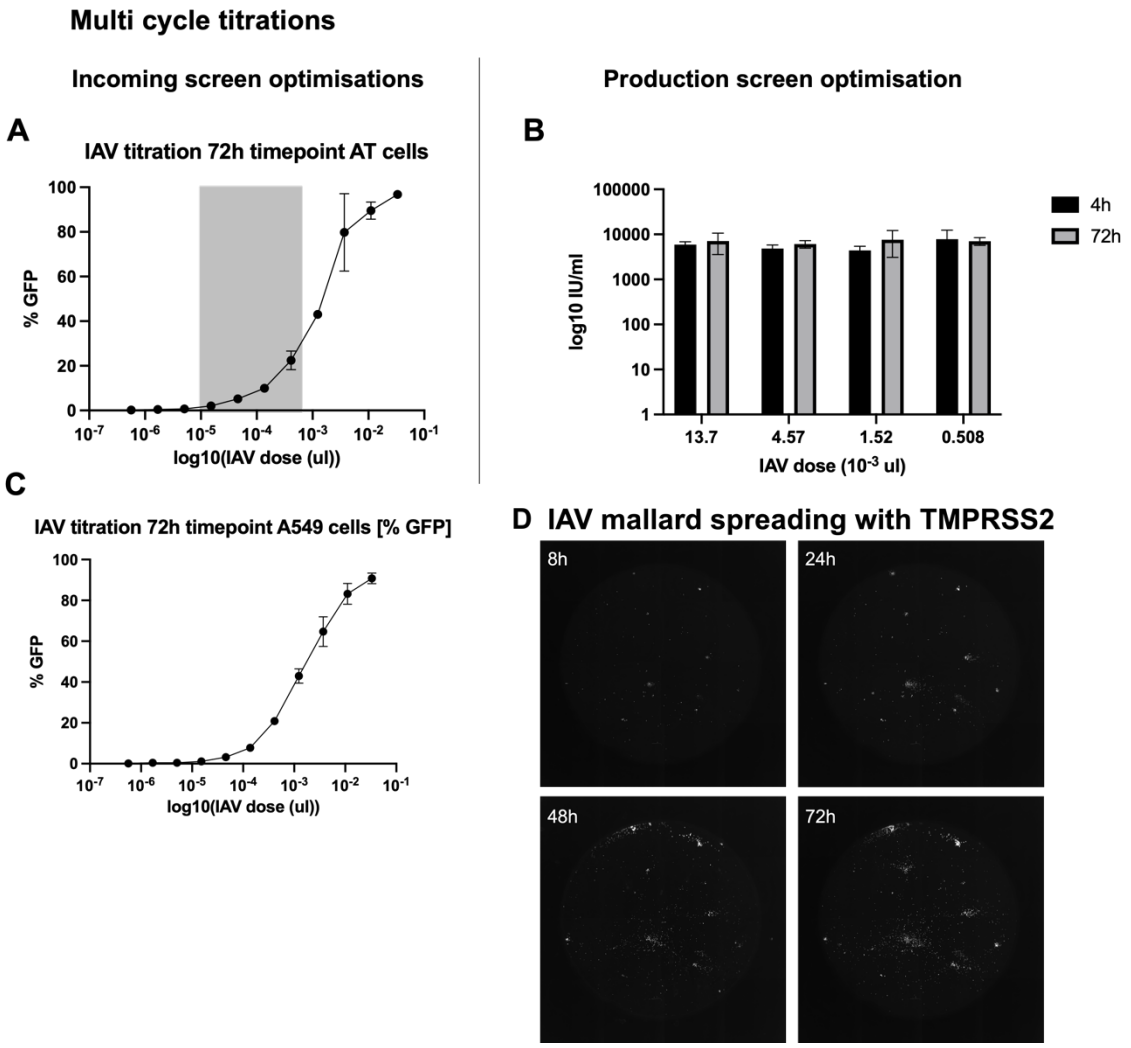

Figure 3.5: Multi-cycle screening optmisations using IAV mallard. To determine the ideal dose of IAV-mallard to use in multi-cycle screens, titrations (A and C) were performed in 96 well plates using a TMPRSS2 expressing A549 cell line (A549-TMPRSS2 or AT)(A) or in A549 cells (C). Supernatants were harvested and replaced after 4h and also harvested at 72h, then cells were fixed in 2% formaldehyde. Imaging cytometry was used to determine rates of infection of IAV-mallard by measuring the number of cells expressing GFP as a percentage of the total cell count in a well.

A. Titration of IAV mallard in a TMPRSS2 expressing A549 cell line (A549-TMPRSS2 or AT).
B. Supernatants from the grey box in A were harvested at 4h and 72h post infection and titrated on A549-TMPRSS2 (AT) cells and incubated for 8h to determine if there had been viral production in multiple cycles of infection in A. After 8h cells were fixed in 2% formaldehyde and titres were determined using imaging cytometry. Bar chart shows viral output (titre – Y axis) from four infection conditions (x axis) in grey box in A.
C. Titration of IAV mallard in A549 cells. We did not follow up with a production screen optimization from this titration because we decided to use AT cells after seeing spreading and similar rates of infection between A549 cells and A549-TMPRSS2 cells.
D. IAV mallard GFP viral spreading and foci production in A549-TMPRSS2 cells. Wells from a medium dose of infection from the titration in A were imaged every at 8, 24, 48 and 72h post infection using a Celigo Imaging Cyometer.

We had supernatants from A549 cells and A549-TMPRSS2 cells. At this stage we still did not know if we would use A459 cells or A549-TMPRSS2 cells, so we titrated the supernatants over several backgrounds: A549 + trypsin and A549-TMPRSS2. We titrated these supernatants from the cell types they were harvested from (A549 → A549 and A549-TMPRSS2 → A549-TMPRSS2) but also over the other cell type (A549 supernatant → A549-TMPRSS2 cells and A549-TMPRSS2 supernatant → A549 cells). Our logic behind this was to see how comparable rates of entry were and if the titres from each were similar in both cell lines, and therefore increase our confidence in A549-TMPRSS2 cells for IAV infection. In all production screen conditions shown in Figure 3.4, we recorded no virion production in this format. There is relatively little difference between 4h and 8h harvests, so there has been very little IAV production during the 8h IAV single cycle screen.

Subsequently, we investigated the virion production from a multicycle IAV infection. During the longer time period, there may have been a greater chance for virion production and release from the cell. As before, we collected supernatants at 4h for the input and another at 72h at the end of the experiment. We had observed in the 72h incoming screen that TMPRSS2 helps IAV spread (Figure 3.5A and Figure 3.5D) and so we eliminated A549 + trypsin conditions from this experiment because we decided to screen using TMPRSS2 cells. I titrated these supernatants on A549-TMPRSS2 cells and left for 8h for a single round of IAV infection to show true yield of virions. We recorded no increase in virions in the supernatants after 72h (Figure 3.5A). This could be because produced virions were stuck in or on the cell and unable to exit or be released.

These results show that we cannot perform simultaneous incoming and production screens. This is probably because the dose of IAV we will use for the incoming screen is too low to produce a detectable level of IAV during the experiment from a well of a 96 well plate or that the IAV lifecycle is not efficiently completed in these cells. However, for the scope of this project we decided to move on from production screening and have not yet revisited the optimisations. For the future it would be useful to revisit this, particularly for follow ups to screens when potential hits are being investigated. One potential solution could be to switch to systems, like using HA and

NA from WSN (influenza A/WSN/33 (H0N1) virus), that propagate more easily in culture (Tian et al., 2019).

Constructing the CRISPR library targeting RNA modifying enzymes

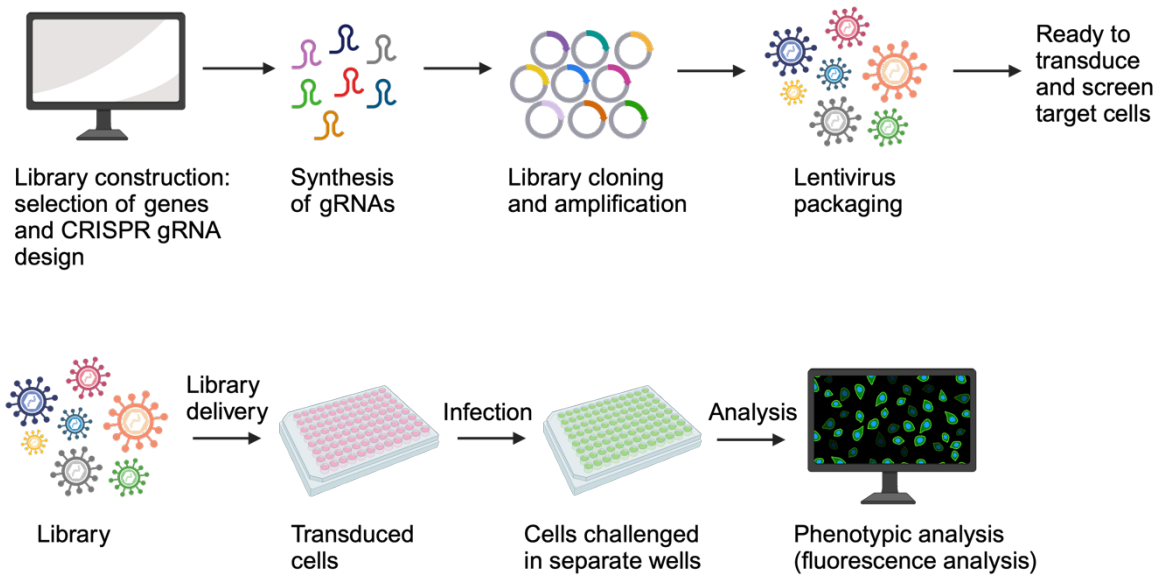

Figure 3.6: Simplified schematic of constructing the CRISPR-Cas9 library targeting human RNA modifying enzymes. Cloning and packaging steps were carried out in bulk in 96 well plates. Library delivery (transduction) is also carried out in 96 well plates using A549 cells or AT cells. Phenotypic analysis is either flow cytometry or imaging cytometry.

To conduct a large scale CRISPR screen, we compiled a list of 72 RNA modifying enzymes (Table 3.1) from a publication that featured all currently known RMEs at that time, that impart some sort of modification or have enzymatic cores that have been described elsewhere (Jonkhout et al., 2017). We designed 21nt CRISPR/Cas9 guides that target each gene and inserted this into a lentiviral vector that contains the Cas9 gene essential for CRISPR located downstream of the guide insert site (Figure 3.6). To account for the unpredictability of a guide having success in knocking down a gene, and to include guides targeted at a range of sites 5'-3' across the length of the gene, we designed at least 7 guides to knockdown each RME, using the CHOPCHOP platform as described before (See Appendix 1 for a list of the all the guides designed). This resulted in 500+ guides (in forward and reverse complements) that had to be annealed, then ligated into a lentiCRISPRv2-Puro backbone in a large scale 96-well plate method and amplified as described in the methods chapter. The identity of

CRISPR guides were confirmed using next generation sequencing of all plasmids constructed, and all errors were corrected. Following this, each CRISPR plasmid was packaged into a lentivirus, again in a large scale 96 well plate format, which was used for screening. By including genes that have been characterised in viral infections previously (e.g., METTL3, ADAR), there are sgRNAs and genes that are expected to be enriched or depleted in the screens so therefore there are positive and negative controls. We then proceeded to full scale screening of a panel of viruses.

Table 3.1: The library of RNA modifying enzymes selected for screening. The description refers to the activity of the enzyme or the motif it enzymatically imparts (Jonkhout et al., 2017).

Name	Description
ADAR	Adenosine to inosine editing
ADARB1	Adenosine to inosine editing
ADAT1	Adenosine to inosine editing
ADAT2	Adenosine to inosine editing
ADAT3	Adenosine to inosine editing
ALKBH1	1-methyladenosine
ALKBH5	N6-methyladenosine
ALKBH8	5-methoxycarbonyl-methyl-2-thiouridine, 5 -methoxycarbonylmethyl-2-thiouridine, 5-methoxycarbonyl-methyluridine
BUD23	7-methylguanosine
CDK5RAP1	2-methylthio-N6-isopentenyladenosine
CDKAL1	2-methylthio-N6-threonylcarbamoyladenosine
CTU1	5-methoxycarbonyl-methyluridine
DIMT1	N6,N6-dimethyladenosine
DNMT2 / TRDMT1	5-methylcytidine
DUS1L	Dihydrouridine synthase
DUS2	Dihydrouridine synthase
DUS3L	Dihydrouridine synthase
DUS4L	Dihydrouridine synthase
ELP3	5-Carbamoyl-methyluridine, 5-methoxycarbonyl-methyl-2-thiouridine, 5-methoxycarbonyl-methyluridine
ELP4	5-carbamoylmethyluridine, 5 -methoxycarbonylmethyl-2-thiouridine, 5-methoxycarbonyl-methyluridine
EMG1	1-methyl-3-(3-amino-3-carboxypropyl) pseudouridine / 1-methyl-pseudouridine / N1-specific pseudouridine methyltransferase
FTO	N6-formyladenosine, N6-hydroxymethyladenosine, N6-methyladenosine

FTSJ1	FtsJ RNA 2'-O-methyltransferase 1 / 2' - O - Methyluridine / 2''-O-methylcytidine / 2'-O-methylguanosine, 2′-O-methyladenosine
FTSJ2	2'-O-Methyluridine / 2''-O-methylcytidine , 2′-O-methyladenosine
FTSJ3	FtsJ RNA 2'-O-methyltransferase 3 / 2'-O-Methyluridine / 2''-O-methylcytidine, 2′-O-methyladenosine
GTPBP3	5-methylamino-methyl-2-selenouridine
HSD17B10	1-methylguanosine, 1-methyladenosine
METTL1	7-methylguanosine
METTL14	N6-methyladenosine
METTL2A	3-methylcytidine
METTL2B	3-methylcytidine
METTL3	N6-methyladenosine
METTL6	3-methylcytidine
METTL8	3-methylcytidine
MRM1	2′-O-methylguanosine
MRM3	2′-O-methylguanosine
MTO1	5-carboxymethyl-aminomethyluridine
NAT10	N4-acetylcytidine
NSUN1 / hNOP2	5-methylcytidine
NSUN2	5-methylcytidine
NSUN3	5-methylcytidine, 5-formylcytidine
NSUN4	5-methylcytidine
NSUN5	5-methylcytidine
PUS1	pseudouridine; pseudouridine synthase that converts uridine to pseudouridine once it has been incorporated into an RNA molecule
PUS3	pseudouridine synthase; trna editor
PUS7	pseudouridine synthase
RPUSD2	pseudouridine synthase
RRP8	1-methyladenosine
TARBP1	2′-O-methylguanosine
TGS1	N2,7-dimethylguanosine, N2,N2,7-trimethylguanosine
THG1L	unknown modified adenosine, G in terminal 5'end
TRIM9B	5-methoxycarbonyl-uridine; Probable tRNA methyltransferase 9B
TRIT1	N6-isopentenyladenosine
TRM6	1-methyladenosine
TRMO	N6-methyl-N6-threonylcarbamoyladenosine
TRMT1	N2,N2-dimethylguanosine
TRMT10A	1-methylguanosine

TRMT10B	1-methylguanosine
TRMT10C	1-methylguanosine, 1-methyladenosine
TRMT11	N2-methylguanosine
TRMT112	7-methylguanosine
TRMT12	Wybutosine (yW) (hypermodified guanosine)
TRMT13	2''-O-methylcytidine
TRMT1L	N2,N2-dimethylguanosine
TRMT2A	5-methyluridine
TRMT2B1	5-methyluridine
TRMT5	1-methylguanosine
TRMT61A	1-methyladenosine
TRMT61B	1-methyladenosine
TRMU	tRNA 5-methylaminomethyl-2-thiouridylate methyltransferase / 2-thiouridine
TYW1	4-demethylwyosine
TYW3	7-aminocarboxypropylwyosine
WBSCR22	7-methylguanosine
WDR4	7-methylguanosine

Discussion

In pilot experiments, I designed conditions to knockdown 3 RMEs (EMG1, NSUN2 and METTL3) and a control gene (RNaseL). I had a major concern about the efficiency of the library when investigating the ability of the knockdowns in the western blots. Whilst the conditions to target EMG1 uncovered transient knockdown success, NSUN2 was not knocked out as strongly, if at all. By going back and redoing the experiments with RNaseL as a control (a collection of guides I designed in the same method for another project in the lab), we found knockdown was most successful in guides that targeted the 5' end of the gene. Subsequently, to design the guides for the full library, I added criteria to favour guides that targeted the 5' end instead of purely focusing on conditions where the number of off targets for the designed guide was low.

I also found that IAV can replicate in a lentiviral background (cells transduced using lentivirus before infection). I titrated the virus in a lentiviral background and selected a low dose which will allow us to record fold-changes in viral growth and subsequently proceeded to screen. This initial optimisation experiment will have to be performed for each virus we intend to screen [these details are in the materials and methods]. I have

not shown that I performed small optimisations in the same format as I did for IAV, for the incoming screens of different viruses. I found the easiest way to optimise a screen was to begin screening and identify the strengths and weaknesses of the method and feed this back into future screens. I will discuss this in the proceeding chapter.

There are also several open questions and concerns on the use of the CRISPR knockdown library I've created:

- Are there conditions where we do production screens by harvesting virions and comparing before/after titres? Beyond a few experiments, we did not fully optimise this.
- How do we normalise the data? What constitutes a hit? And how do we validate screening hits e.g., secondary screens or validation experiments.
- Do these difficulties we have encountered whilst optimising IAV apply to other viruses?
- Would serially passaging cells transduced and selected with the CRISPR library prior to screening improve our ability to uncover novel roles for RNA modifying enzymes?
- Are these optimisations applicable to other cell types, namely suspension cells.
- Targeting only one gene per cell facilitates data analysis but it can mask complex interactions which are typified by redundancy (Dede et al., 2020; Bock et al., 2022).

Despite this, the results we have so far are promising. We invested a significant amount of time to design and clone a library of CRISPR guides that target all known human RNA modifying enzymes. By including numerous guides against each gene and ensuring they target different sites along the full length of a gene, we have hopefully increased the chances of knockdown success. I demonstrated that the packaged lentivirus is capable of knocking down genes of interest in a 72h period. As well as theoretically how simple it will be to perform an incoming screen. These results demonstrate a utility of this screening platform and suggest its potential for uncovering RMEs that are antiviral and proviral and target divergent virus families or that are essential for viral replication.

Chapter 4 Identifying RNA modifying enzymes involved in RNA virus infection

Introduction

To begin exploring our goal of identifying individual RNA modifying enzymes involved in infection of RNA viruses, we selected a panel of viruses that were available in the lab as a starting point to ask two questions: 1. Are any of the enzymes involved in viral infection and 2. Are there enzymes involved in the life cycle of multiple RNA viruses?

Following on from Chapter 3 and optimising screens, we set out to perform incoming screens and assess viral growth after multiple rounds of infection. This chapter is entirely chronological in respect to the timeline of experiments performed, but I chose to do this to showcase some of the initial hurdles and optimisations that we had to configure.

Results

Initial transient CRISPR knockdown screens identified several genes potentially involved in IAV-mallard and RSV-GFP infection

Following the protocol optimised in Chapter 3, we performed transient knockdown screens and challenged KD cells with IAV mallard and RSV-GFP. I performed imaging cytometry and then quantified the number of GFP positive cells as a percentage of the total number of cells. This value was then normalised to control conditions on the plate: cells transduced with a non-targeting CRISPR guide (NTC), then also subsequently challenged with virus.

We initially defined a hit in arrayed screens as two standard deviations from the mean of the bulk population. Looking in Figure 4.1A at the IAV mallard screen we can see a clustering of the population around the median centre line of the screen (at 100 on the

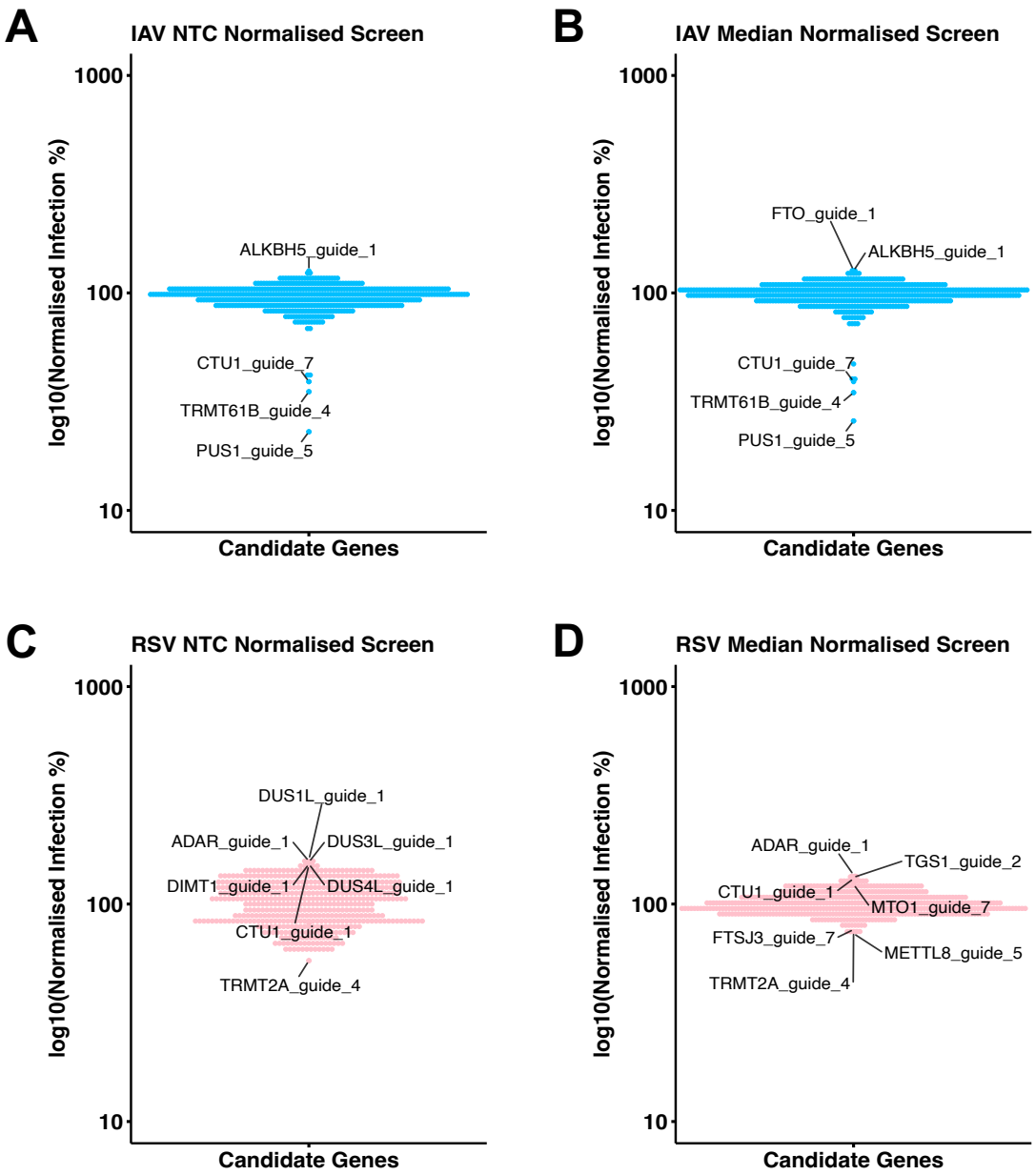

Figure 4.1: Arrayed transient CRISPR knockdown screening using a IAV mallard (A,B) and RSV-GFP (C,D).

A,B. A549-TMRPSS2 cells were transduced with individual CRISPR guides targeting RNA modifying enzymes for 72h then infected with IAV-mallard-GFP for 72h. Cells were fixed in 2% formaldehyde and quantification of infection was measured using Celigo imaging cytometry at 72h post infection. Infection was normalised to the infection rate in the non-targeting control guide (NTC) conditions (A) or to the median (B) of each plate in the screen. NTC conditions are wells transduced with a non-target CRISPR guide for 72h and then also subsequently challenged with virus. Median infection rate is calculated from all wells infected with virus on each plate. Each dot represents the observed infection in the presence of a single CRISPR guide. Normalised infection %'s were $\log_{10}$ transformed and plotted on the y axis.

C,D. A549 cells were transduced with individual CRISPR guides targeting RNA modifying enzymes for 72h and infected with RSV-GFP. Infection was quantified as in A & B and infection was normalised to the infection rate in the non-targeting control guide conditions (C) or to the median of each plate in the screen (D).

log scale). Outside of this we see clear infection rate reduction in the points lower down the y axis; could knockdown of the gene of interest in these conditions be impacting virus replication and thus said gene is essential for viral replication? Or alternatively, in the points towards the top of the y axis, infection rates have increased upon gene knockdown and so perhaps that gene normally restricts virus infection.

On analysis of the RSV screen, I found that normalising to the NTC skewed the data so that the clustering of the bulk population did not occur around the screen average. (Figure 4.1C). I normalised the screen by plate, based on the rates of infection in the NTC guide KD conditions. There is unavoidable intra and inter variation between plates in high throughput experiments (perhaps due to human error in pipetting, etc) and normalising by plate eliminates the inter plate error but can introduce intra plate biases. Within these graphs we did not see a clustering of points based on the plate, however, there is still an error being introduced by normalising to the NTC infection value of each plate. To rectify this, we followed a similar method that has been adopted for over-expression screens performed in (Schoggins et al, 2011; Kane et al, 2016) and in the lab. In these experiments, researchers had found that normalising to the control on each plate caused skews in the data as we see in our knockdown screen. They prevented this from happening by normalising to the median viral expression on each plate of the screen. When I did this, the distribution of the data improved and resolved the skewed infection rates in the RSV screen (Figure 4.1D). Despite there being no issue in the IAV mallard screen, when I compared the NTC normalisation (Figure 4.1A) and the median normalisation (Figure 4.1B), there was very little difference so I decided for consistency from this point onwards, all screens would be normalised to the median rate of infection per plate.

Genes identified in initial CRISPR knockdown screens were found to be false positives.

At this point, we were still optimising the screening process and data analysis pipelines we wanted to use. As such we decided to follow up these initial transient screens with small scale screens of the genes that we had identified from the screens. Follow up experiments would discover if what we had seen were indeed hits and how reliable the platform was. I created fresh lentiviral stocks of the hits to be investigated from the

library of lentiCRISPRv2 vectors and produced stably expressing CRISPR/Cas9 cassette cells by transduction and selection. At this point, I did not test to see if the gene expression had been ablated but proceeded to cell infections. If a hit was confirmed, we would then investigate the gene knockdown level.

In Figure 4.2A we can see that the KD guide conditions identified from the IAV primary screen failed to reach infection levels above background noise in the mini-screens (in 4 biological replicates, each with 3 technical replicates). In the follow ups of hits against RSV (Figure 4.2B), we identified a knockout condition of a gene (MTO1) that caused RSV growth to be greater than the rest of the mini-screen (Figure 4.2B). Of the two guides targeting MTO1 that we took forward for mini-screens, only guide_7 caused a strong knockdown, as seen in western blots (Figure 4.2C). Guide_2 was only partially knocked out and did not cause an extreme phenotype in the mini-screen (Figure 4-2B,C). It was difficult to detect MTO1 without excessive background staining. This could be due to endogenous MTO1 levels being low, or the antibody exhibiting poor binding/specificity or a combination of these. The control actin blots looked consistent, so I reasoned this was not a gel loading, transfer or other methodological error. Despite seeing increased infection in cells with MTO1 knocked-down by guide_7 three times in the mini-screens (Figure 4.2B), I was not then able to replicate the level of RSV infection in independent/further experiments (Figure 4.2C, top panel). I also performed a 'dual' knockout using guides_2 and _7 in the same cells. There was a general increase in infection (Figure 4.2D). However, when I analysed this further, this result became a false positive. The number of cells in the well of the experimental plate was lower in the knockdown condition compared to NTC and non-transduced. When I corrected for the low cell number by using an estimated total cell number based on A549 growth kinetics, the fold-effect disappeared (Figure 4.2E). So, what I had identified as an effect was caused by a much higher MOI due to the low cell number compared to what we had anticipated/calculated for. During cell selection pressure under puromycin, I noticed that the MTO1 KD cell line was growing slightly slower than the NTC line and control WT cells. Despite seeding the experiment at higher densities so there would be a roughly similar number of cells at the point of infection, I think knocking down MTO1 was highly toxic to the cell and had cumulative effects over time. MTO1 is an essential mitochondrial gene involved in tRNA synthesis and protein

translation (Fakruddin et al., 2017), so without it, cellular homeostasis will be affected as well as viral RNA transcription.

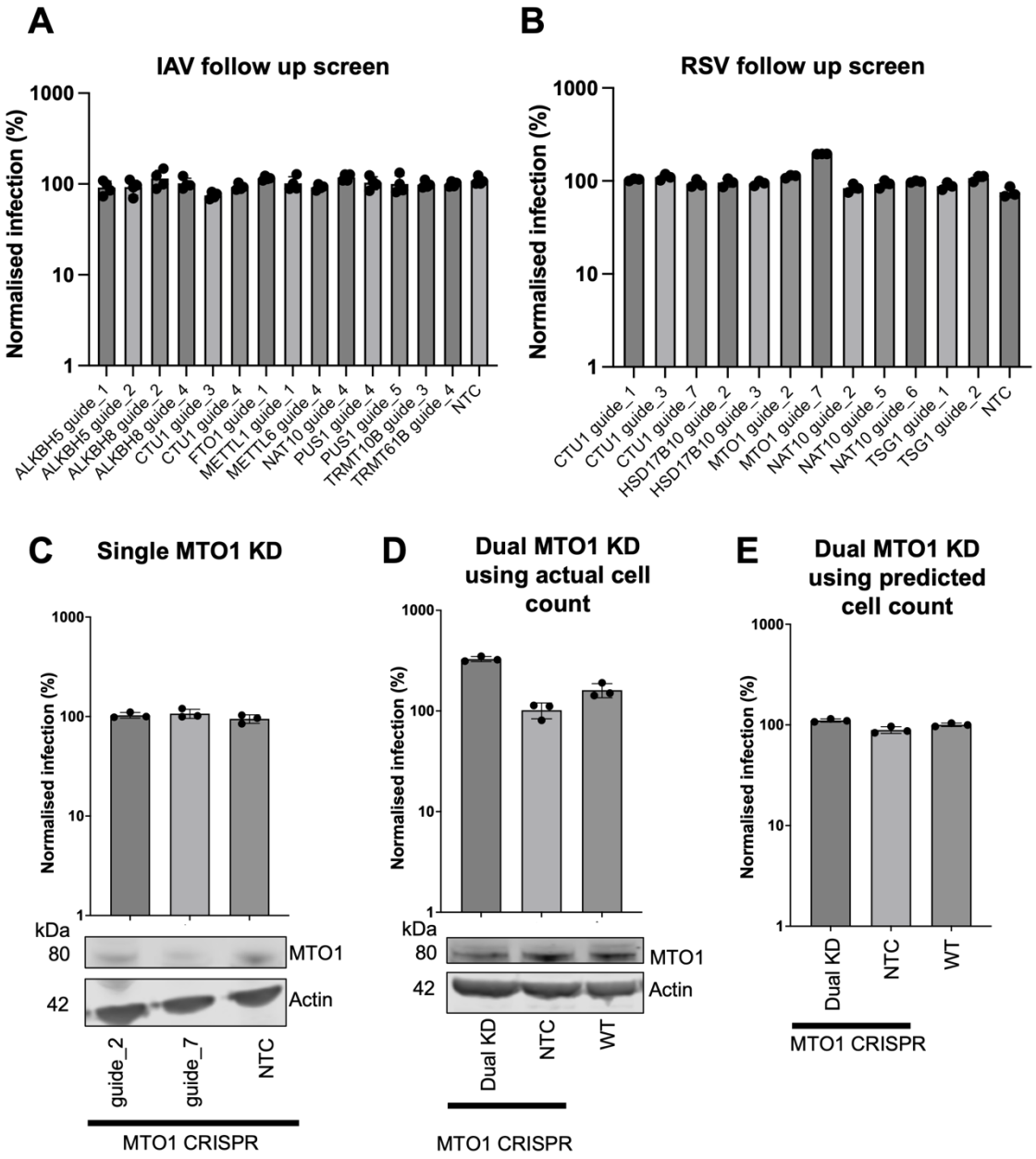

Figure 4.2. Follow up small scale screen of full-scale transient screens in Figure 4.1.

A. Follow up screen of guides against genes that affected IAV mallard growth in Fig 4-1B. A459-TMPRSS2 cells were transduced with CRISPR guides stated on x axis, selected using puromycin, passaged, then infected with IAV-Mallard-GFP. 72hpi, cells were fixed in 2% formaldehyde and rates of infection were quantified using imaging cytometry. Infection rates were normalized to the median rate of infection in the mini screen.

B. Follow up screen of guides against genes that affected RSV-GFP growth in Fig 4-1D. A459 cells were transduced with CRISPR guides stated on x axis, selected and passaged, then infected with RSV-GFP. 72hpi, rates of infection were quantified using imaging cytometry. Infection rates were normalized to the median rate of infection in the mini screen.

C. Bottom: Western blots of A549 cell lysates that were transduced and subsequently selected with lentiCRISPRv2-puro lentiviral CRISPR vectors containing a guide targeting MTO1 or a non-targeting guide control (NTC). Guide_7 reduced MTO1 expression more than guide_2 as seen in the western blots. Top: A549 KD cells against MTO1 were infected with RSV, then rates of infection were quantified 72hpi using imaging cytometry then normalized to the average of the NTC replicates. Infection rates in in the guide_7 KD were not significantly different from the others.
D. Bottom: Western blots of A549 cell lysates which were transduced and selected with both guide_2 and guide_7 as a dual knockout. Top: A549 cells transduced with the dual KD against MTO1 or NTC, and A549 WT cells were infected with RSV-GFP for 72h. Infection rates were then quantified using imaging cytometry and normalized to the average of the NTC replicate conditions. Infection rates in the KD condition were increased, despite MTO1 expression only being slightly reduced compared to control conditions as seen in the western blots.
E. Re-analysis of top graph in D. Due to poor growth of MTO1 dual KD cells observed in D, cells infected with RSV-GFP were calculated as a percentage of the predicted number of cells that would be in the well, instead of the actual number (4.2D). This uncovered that infection rates were not different when MTO1 is knocked down.

These investigations highlighted the need to introduce cell toxicity assays in the future when following up hits to avoid this happening again. Toxicity is something I was aware could happen if we knockdown essential genes within the cell because full knockdowns can be very deleterious to the cell. Conversely, partial knockdowns may be better for uncovering viral phenotypes as the reduction in the expression of the protein could still cause a change in phenotype without being toxic to the cell. I never tried to do partial knockdown follow ups with MTO1 so if it appears in future screens, that would be a starting point to work on.

Full scale primary CRISPR screens using IAV-mallard and RSV-GFP were not replicable

Since the follow ups to the screens did not uncover any true hits or give me positive replication data, I repeated the full transient screens in the same way as I performed the initial screens. When comparing the replicate (y axes) in Figure 4.3 with the initial screen (x axes), there was no significant overlap between the IAV-mallard-GFP screens (Fig 4.3A) or the RSV-GFP screens (Fig 4.3B). In Figure 4.3, there is a cluster of guides around the median mark of each screen. If a hit was replicable, we would see movement of a KD-infection condition away from the bulk population mirrored on both axes. The outliers that have moved down the x axis in Figure 4.3A but remained

at the median on the y axis demonstrate variability/noise in the assay. At this point, we had hit a proverbial wall, because the screening process had not reproducibly identified candidates and follow up experiments were inconclusive. We outlined several potential reasons underlying why the screening process was not replicable:

1. Infection rates were too high. I selected an MOI of virus that resulted in 12-20% infection in optimisations, however in the screens this regularly was upwards of 20-30%.
2. The transductions were not efficient enough to achieve a reduction in target protein expression under the assay conditions used.
3. Errors in seeding and cell handling were causing clumping in the wells which prevented cells proliferating normally. Cells that are actively dividing are typically better infected and transduced.

In efforts to figure out what was going on, and if the platform was useable for screening, I designed some experiments to address the issues.

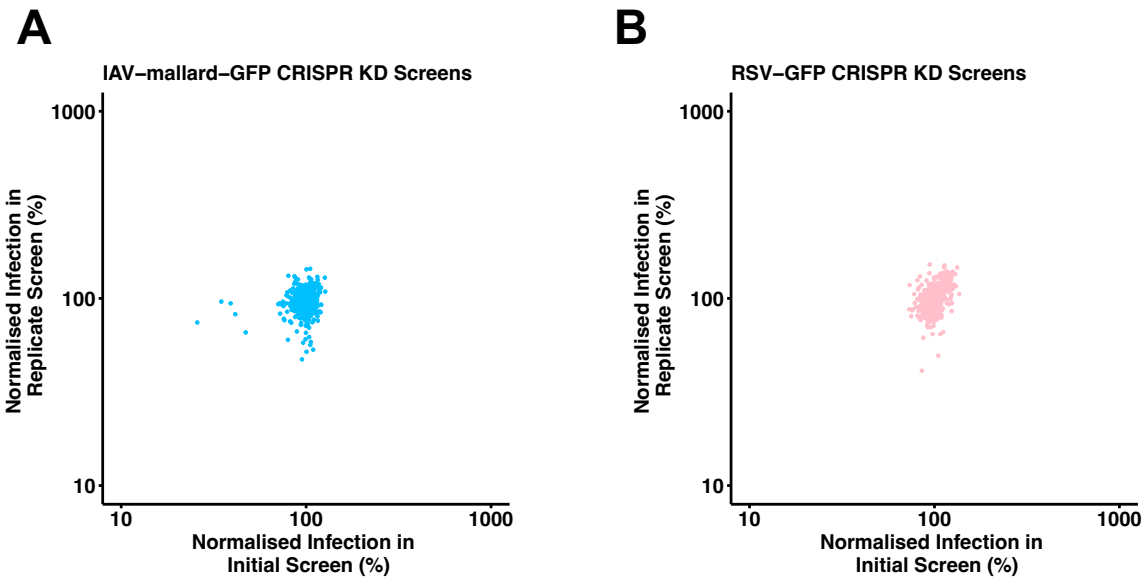

Figure 4.3: Full scale primary CRISPR screens using IAV-mallard and RSV-GFP were not replicable. Initial screens (x axes) which were used for follow-up experiments in Figure 4.2 and replicate screens (y axes) in A549-TMRPSS2 cells infected with IAV mallard (A) or in A549 cells infected with RSV-GFP (B). Experiments were performed and analysed as described in Figure 4.1. Clustering around the median and outliers only moving up one axis shows that screens have not uncovered any potential hits under the conditions used.

CRISPR-Cas9 knockout screens are replicable when a lower dose of virus is used

Unfortunately, there is no simple marker, like the expression of a reporter gene in the CRISPR/Cas9 vector used to make the library, to ascertain whether cell lines are transduced or not in the transient CRISPR knockdown screens. Despite showing that transduction and knockdown was possible in a transient condition (Chapter 3), I questioned how representative this would be on a large screening scale. To determine that the library prep of lentivirus was indeed transducing cells, I decided to deviate from the protocol I had established, and after transducing cells with the CRISPR library for 24h, I put cells under drug selection until control wells containing non-transduced cells were cleared. The vector used to package the CRISPR guide into the lentivirus for the library contains a puromycin resistance gene, hence I selected cells with puromycin. After control wells had been cleared of cells, I passaged the plates of cells so that I could use them for subsequent screens and infections. Across the entire library, there were relatively few wells which had not been successfully transduced and survived drug selection. These wells were eliminated from the final analysis.

I performed screens using these puromycin-selected lineages with IAV mallard and RSV-GFP (Figure 4.4A&B x axes). For the purpose of presenting these data, I have called these screens ‘knockout screens’ to differentiate from transient knockdown screens performed in the rest of the chapter. My reasoning behind continuing to optimise using two viruses was to eliminate the possibility that errors during the screens were virus specific. At the same time, I reduced the viral dose so that fold-changes in infection could be more apparent. In parallel to these knockout screens, I performed transient screens as before but reduced the dose of virus in line with the screens performed in the transduced and selected KD cells. The data from these screens was much more replicable, as seen in Figure 4.4, and the screens showed significant overlap in genes of interest, and genes known to be involved in IAV infection were hits, for example ADAR is known to interact with IAV (Tenoever et al., 2007; de Chassey et al., 2013).

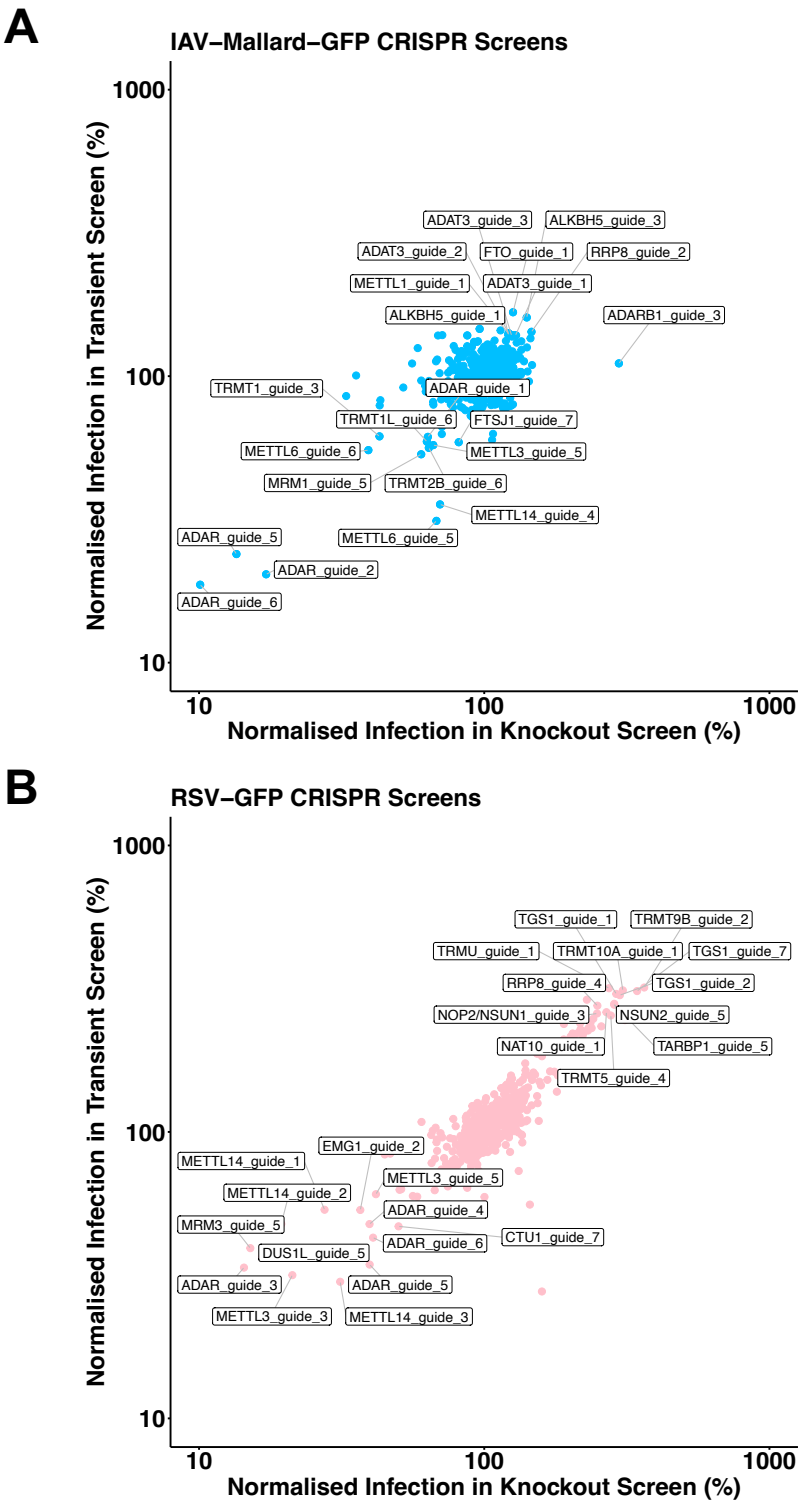

Figure 4.4: Lower dose of virus makes CRISPR/Cas9 screens replicable.
Screens were performed in A549-TMPRSS2 (A) or A549 cells (B) that were puromycin-selected knockout lineages of the CRISPR library (x axes) or transiently transduced for 72h with the CRISPR library (y axes). All screens were then infected with IAV-mallard-GFP (A) or RSV-GFP (B). 72hpi, cells were fixed in 2% formaldehyde and infection rates were quantified using imaging cytometry and normalised to the median infection rates of each plate. Axes display infection rates which were $\log_{10}$ transformed. Each dot represents the observed infection in the presence of a single CRISPR guide.

Pro-viral and antiviral activity of ADAR during IAV infection has been documented previously. The antiviral role of ADAR against IAV was seen as a decrease in viral replication (Ward et al., 2011) and when ADAR was reduced, the number of A-to-G substitutions in the matrix (M) gene decreased which was accompanied by a higher viral titre (Tenoever et al., 2007). Contrarily, ADAR can be pro-viral for IAV, demonstrated by viral growth and neuraminidase activity being reduced when a catalytically inactive ADAR1 form was used (de Chassey et al., 2013). These dual effects on viral growth can be explained as there are two isoforms of ADAR1; p110 acts antivirally and p150 enhances replication because it can supress IFN-B and RIG-I-like receptor signalling (Vogel et al., 2020). P150 prevents hyperactivation of the innate immune response during viral infections. Further to this we have used IAV mallard in our experiments (H1N1), and work has found ADAR1 is upregulated during H1N1 infection. This results in increased A-to-G editing in human epithelial cells (Cao et al., 2018). The appearance of ADAR in these screens is a good positive control for the experiments.

ADAT3 appears several times in the IAV screens, with knockdown upregulating IAV expression, and like ADAR, it is also an adenosine deaminase but it is believed to be tRNA-specific (Torres et al., 2014). ADAT3 having an involvement in IAV has not been described previously.

In consideration of IAV and its nuclear location for replication, finding METTL proteins are implicated in the lifecycle of IAV is not surprising as quite a few METTL proteins are located in the nucleus (Delaunay et al., 2022). Reduction of METTL3 inhibits gene expression and replication of IAV (Courtney et al., 2018) which is observed in our screen (Figure 4.4A). METTL14 is a cofactor of METTL3 so finding KD of this enzyme having the same effect as METTL3 is a positive result (Courtney et al., 2017). METTL3/14 impart an N6-methyladenosine (m^6A) motif; ALKBH5 plays an eraser role and is a N6-methyladenosine demethylase which is also a nuclear protein (Zheng et al., 2013). KD of ALKBH5 in our screen increases IAV gene expression/infection suggesting removal of m^6A modifications on IAV RNA is an antiviral mechanism. Surprisingly, there have not been specific studies carried out onto the effect ALKBH5 has on IAV replication or on other viruses. Courtney et al., 2017, proposed that the m^6A-modification increases the abundance of IAV RNA as it stabilises it or enhances

replication. Thus, removal of m^6A by ALKBH5 would have an opposite effect. FTO (also known as ALKBH9) knockdown notably upregulates IAV infection (Figure 4.4A). It acts like ALKBH5 and demethylates m^6A but its major target is N6,2'-O-dimethyladenosine (Mauer et al., 2017). FTO has not previously been implicated in IAV infection, but the phenotype of FTO depletion is also proviral in HIV-1, KSHV and HBV infection (Tirumuru et al., 2016; Ye et al., 2017; Imam et al., 2018). Methylation of IAV viral RNA is very important for the lifecycle of IAV. In Figure 4.4A METTL3 and ALKBH5/FTO are antagonists, with METTL3 methylating and increasing viral mRNA expression and ALKBH5/FTO removing methylation and causing a reduction in the expression of IAV RNA.

We also saw more reproducibility in the screens using RSV (Figure 4.4B). The general population still clustered around the median but there were a notable number of knockdowns that were further away from the median. Perhaps this is background noise but an interesting thing about the RSV screen is that it has overlap with the IAV screens: ADAR and METTL3/14 KD reduce RSV levels. Studies have not implicated ADAR in the infection of RSV but METTL3/14 appearing in the screen of RSV could be an observation of nuclear shuttling of the N6-methyladensoine transferase complex since RSV replicates cytoplasmically. Xue et al., 2019, found N6-methyladenosine upregulates RSV replication and pathogenesis, however they did not observe a major reshuffling of METTL proteins from the nucleus when they stained each METTL protein individually and visualised with confocal microscopy. Overall, the appearance of METTL3/14 in our screens gives us a similar positive control as ADAR; our results match that of previously published studies and increases our confidence that the screening library can be used as a discovery platform.

I have highlighted genes that were identified in this section that match that of published work to exemplify the utility of the arrayed CRISPR screening platform targeting RNA modifying enzymes and increase our confidence that the screening library can be used as a discovery platform. There are many other genes which have appeared which could be novel factors in IAV and RSV infections, however before discussing these, they would need to be followed up.

Does interferon uncover RMEs involved later in the IAV lifecycle?

Since we had found reproducibility in the screens of IAV and RSV, we began to ask more questions about RMEs and their roles in infection, in this case if interferon impacted the enzymes in IAV infection. Interferon is a group of proteins synthesised and released by host cells in response to infections and stress. After being infected with virus, cells produce IFNs to restrict the virus infection and degrade the virions. IFNs do not kill the virus directly but facilitate the transcription of ISGs and production of proteins that interfere with the lifecycles of divergent viruses (Tong et al., 2022). In turn, the upregulated genes (interferon stimulated genes - ISGs) could be RNA modifying enzymes. The previous screens in this chapter have focused on genes that stimulate, or desensitise, the innate immune response to viruses. To see if IAV may use RMEs to mask itself from interferon stimulated genes or if there are enzymes which sensitise IAV further to eradication by the ISGs, screens were pre-treated with Interferon α14 (IFN α14) for 4 hours before infecting with IAV. IFN α14 is one of the many types of interferon α subtypes belonging to the Type I leukocyte IFN family. The type I IFN family has antiviral and anti-proliferative activities. IFN α14 was chosen because of these broad-spectrum effects and it has been shown to suppress virus replication, like HIV-1 (Abraham et al., 2016). These experiments would highlight RMEs that act after interferon stimulation. We may find RMEs that are upregulated as ISGs by way of a gene knockdown causing an upregulation of IAV. Alternatively, genes that mask virus from the IFN response, would cause reduction in infection upon knockdown.

There is quite a lot of background noise in the IFNα14 treated screens (Figure 4.5) and genes that have strong phenotypes (x axis) are not strongly replicated in a duplicate experiment (y axis). But looking at this preliminary data, there are interesting putative results and there are some overlaps of interest in these datasets. The discussion that follows in this section is mostly speculative; any possible mechanisms discussed need to be followed up. Several of the genes that are significant in the non-interferon treated screens (Figure 4.4A) appear in the interferon treated conditions (Figure 4.5A). These include TRMT1L, ADAR, METTL6, and RRP8. METTL14 is highlighted to show that reduction in protein levels does decrease IAV expression in both screens, despite not being as strong when IFN was used.

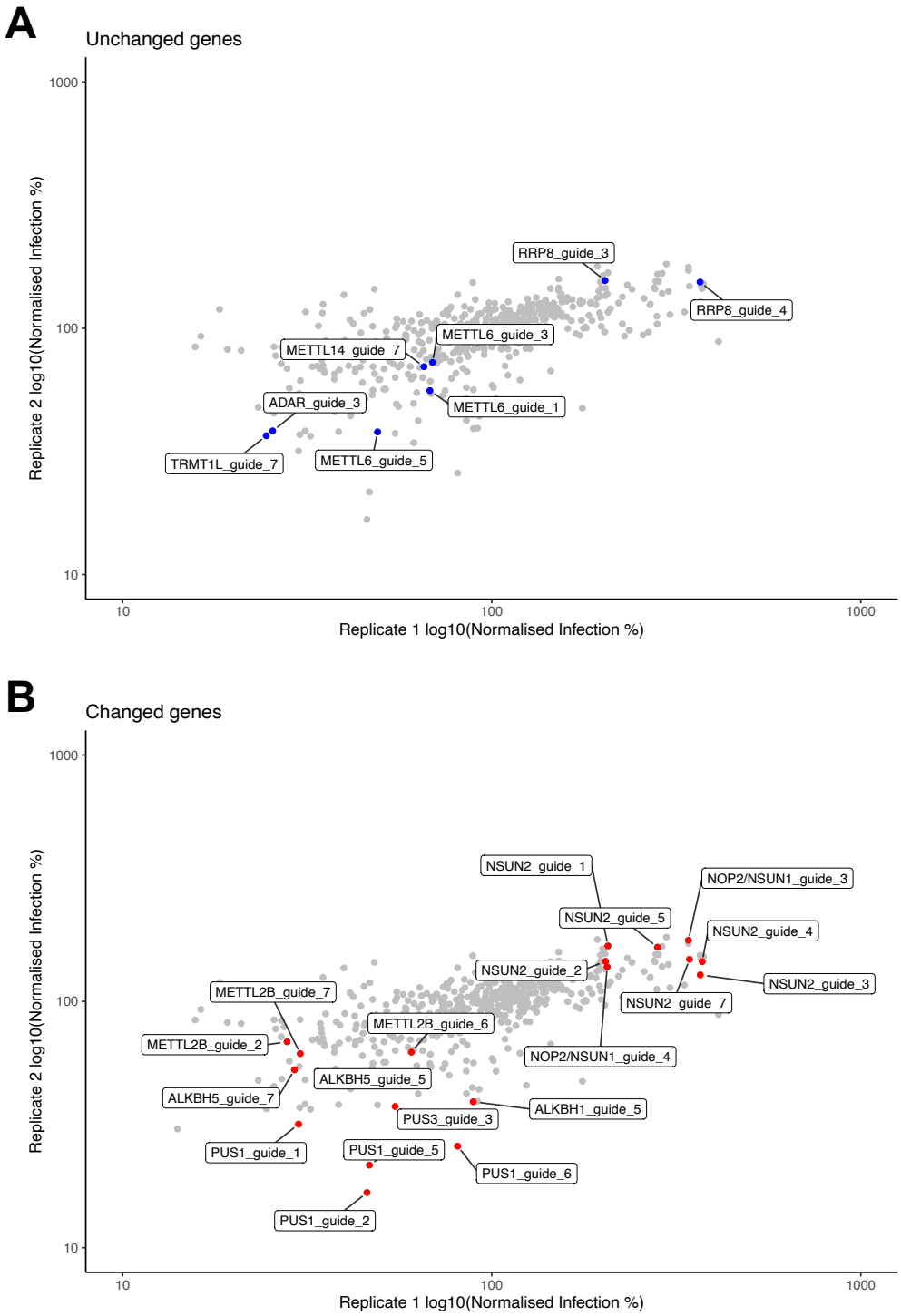

Figure 4.5: Arrayed CRISPR screens performed with IFNα14 treatment before IAV infection. A549-TMPRSS2 cells were transduced with the CRISPR library for 72h then treated with IFNα14 for 4h before being infected with IAV-Mallard-GFP. 72hpi, cells were fixed in 2% formaldehyde then imaged on a Nexcelom celigo imaging cytometer to quantify infection rates. Rates of infection were normalized to the median rate on each plate then converted to a log10 scale. Screens were performed in duplicate.
A: Genes that were also identified in Figure 4.4A to impact IAV growth when knocked down.
B: Genes with different effects that Figure 4.4A or that have been newly identified in the IFN stimulated screen.

However, there are three notable differences in the IFN treated screens (Figure 4.5B) compared to non-interferon treated screens (Figure 4.4A). Firstly ALKBH5 (and ALKBH1) depletion suppressed IAV growth in the presence of IFN (Figure 4.5B). In the screens before (Figure 4.4A), addition of m^6A was pro-viral and removal was antiviral, evidenced by the depletion in IAV when METTL3 and 14 were knocked down and the increase in IAV when ALKBH5 was knocked down. In this screen ALKBH5 depletion reduces IAV expression, inferring m^6A removal seems pro-viral after interferon treatment. This postulation is somewhat bolstered by the lack of extreme phenotypes when METTL3 and 14 are knocked down. They catalyse the addition of m^6A but by not doing so here, IAV growth has not been as negatively affected as before (Figure 4.5A). This contradicts Courtney et al.'s (2017) mechanism that the presence of m^6A stabilises IAV RNA which we would expect to hold-fast after IFN treatment to prevent an increased immune response. However, could IFN be upregulating genes that target m^6A decorated RNAs for destruction?

The reduction of IAV when METTL2B is depleted does not contradict this hypothesis because unlike METTL3 and 14, it is involved in methylation of tRNA as an N(3)-methylcytidine methyltransferase (m^3C) (Mao et al., 2021; Xu et al., 2017). Alongside METTL6 (CRISPR of which reduced IAV expression in Figure 4.4A), METTL2B is involved in m^3C modifications of tRNA. Whilst there are no clear accounts of IAV RNA being modified with m^3C, recent evidence associates infection of RNA virus with alterations in cellular m^3C levels (McIntyre et al., 2018). So perhaps the reduction of global m^3C is responsible for negative IAV growth in the screen and in the interferon response, m^3C in cellular transcripts and RNA attenuates the antiviral response to IAV.

Depletion of PUS1 and PUS3, two pseudouridine synthases that covert uridine to pseudouridine once it has been incorporated into an RNA molecule, decreased IAV growth. Therefore, in the IFN response pseudouridine may desensitise the host to IAV and stabilise IAV RNA. Indeed, pseudouridine decreases the activation of Toll-like receptors (TLRs) by RNA (McIntyre et al., 2018; Karikó et al., 2005), as well as the RIG-I innate signalling pathway (Durbin et al., 2016). Pseuoduridylation stabilises Epstein-Barr virus (EBV) non-coding RNAs and enhances production of EBV viral

genomes in replication (Henry et al., 2022). Pus proteins are nuclear located so an interaction with IAV is more possible (Martinez NM et al., 2022).

Knockdown of NSUN2 increased IAV growth in both replicates in Figure 4.5B. Previously published data states that reduction of NSUN2, an m^5C methyltransferase, significantly inhibits the replication and gene expression of a wide range of RNA and DNA viruses due to an enhanced type I IFN response (Zhang et al., 2022). It is believed that NSUN2 is downregulated in some infections to boost responses for the elimination of viruses (Wang et al., 2023). NSUN2 also has roles in RNA biogenesis, including converting vault ncRNA to vtRNA. The vtRNA can promote IAV replication in A549 cells by repressing PKR activation and the downstream effects of interferon (Li et al., 2015). When NSUN2 is depleted, the host m^5C methylome is decreased, which enhances the RIG-I recognition of RNA polymerase III transcribed noncoding RNAs to trigger type IFN signalling (Zhang et al., 2022). Interestingly, m^5C methylation of IAV viral RNA is not markedly altered by NSUN2 depletion (Zhang et al., 2022). Based on this we would expect when NSUN2 is depleted that IFN levels would increase, and virus levels would decrease. In the case of this experiment (Figure 4.5), IFN levels are already high as cells have been pre-treated with IFN. Thus, we would expect that IAV growth levels would diminish however we are observing a marked upregulation in virus. I think the previous literature disputes how likely this is a true hit. Many growth defects have been reported in NSUN2 knockout/depletion (Zhang et al., 2022; Blanco et al., 2014). NSUN2 also regulates the expression of host cell genes involved in the cell cycle (cell cycle regulator p21 and IL-17A) (Wnuk et al., 2020). Perhaps these hits are a consequence of cell lethality and low cell number, as opposed to uncovering a viral restriction mechanism of IAV.

NOP2 KD increased virus growth in the IFN treated screen (Figure 4.5) as well as the non-IFN treated screen (Figure 4.4A). Like NSUN2, NOP2 is an m^5C methyltransferase and has previously been found to be antiviral against a variety of alphaviruses. When knocked down, NOP2 caused an increase in viral levels (Kamel et al., 2024). This result is more expected than NSUN2, which is interesting considering they impart the same methyl motif. However, NOP2's cellular activities have been shown to be independent of its catalytic abilities (Liao et al., 2022) [discussed in Chapter 5], so perhaps in the response to IAV virus infection, this is also

the case. Considering the knockdown of NOP2 increases IAV growth in the presence of IFN suggests it has an antiviral role against IAV and could be upregulated by the IFN response normally.

It is interesting that the significant genes involved in IAV infection are remarkably different between IFN-treated and non-IFN treated screens. Perhaps part of the IFN response downregulates genes which impart or remove motifs which induce IFN but may upregulate other RMEs to help stem the infection. Downregulation would prevent an over-heightened IFN response constitutively in a resting cell, however we are unable to elucidate if a gene is normally depleted in response to IFN in these screens because we are already reducing the expression with CRISPR. We can infer if a gene upregulated if KD causes an increase in virus. The level of IFN is already high in this experiment, so the cell will already be experiencing a heightened IFN response and we have potentially pushed the cells into shutdown. Perhaps this is why unexpected phenotypes from ALKBH5 and NSUN2 knockdown contradict published data. While the results here may seem exciting, repeated screens using IFN need to be carried out to assess the true nature of these hits.

CRISPR-Cas9 transient knockdown screening reveals several putative genes involved in restriction of multiple RNA viruses

Since we had candidate genes involved in infection of RSV and IAV, we decided to screen more viruses to assess whether the same RMEs are involved in infection of a range of RNA viruses. We selected human meta-pneumavirus (hMPV) and Semliki forest virus (SFV). We also screened Sendai virus and para-influenza 3 virus, but they were not performed in replicate so I have not presented them here.

There is a lot to dissect from these experiments when we look in Figure 4.6. Firstly ADAR (adenosine deaminase that act on RNA) has a key role in the innate immune response to viral infections where adenosine to inosine editing can have a range of pro- or antiviral effects and can contribute to viral evolution (Piontkivska et al., 2021). In our screens KD of ADAR reduces viral expression, thus for all four viruses in Figure 4.6, it potentially has a pro-viral role in a normal cell.

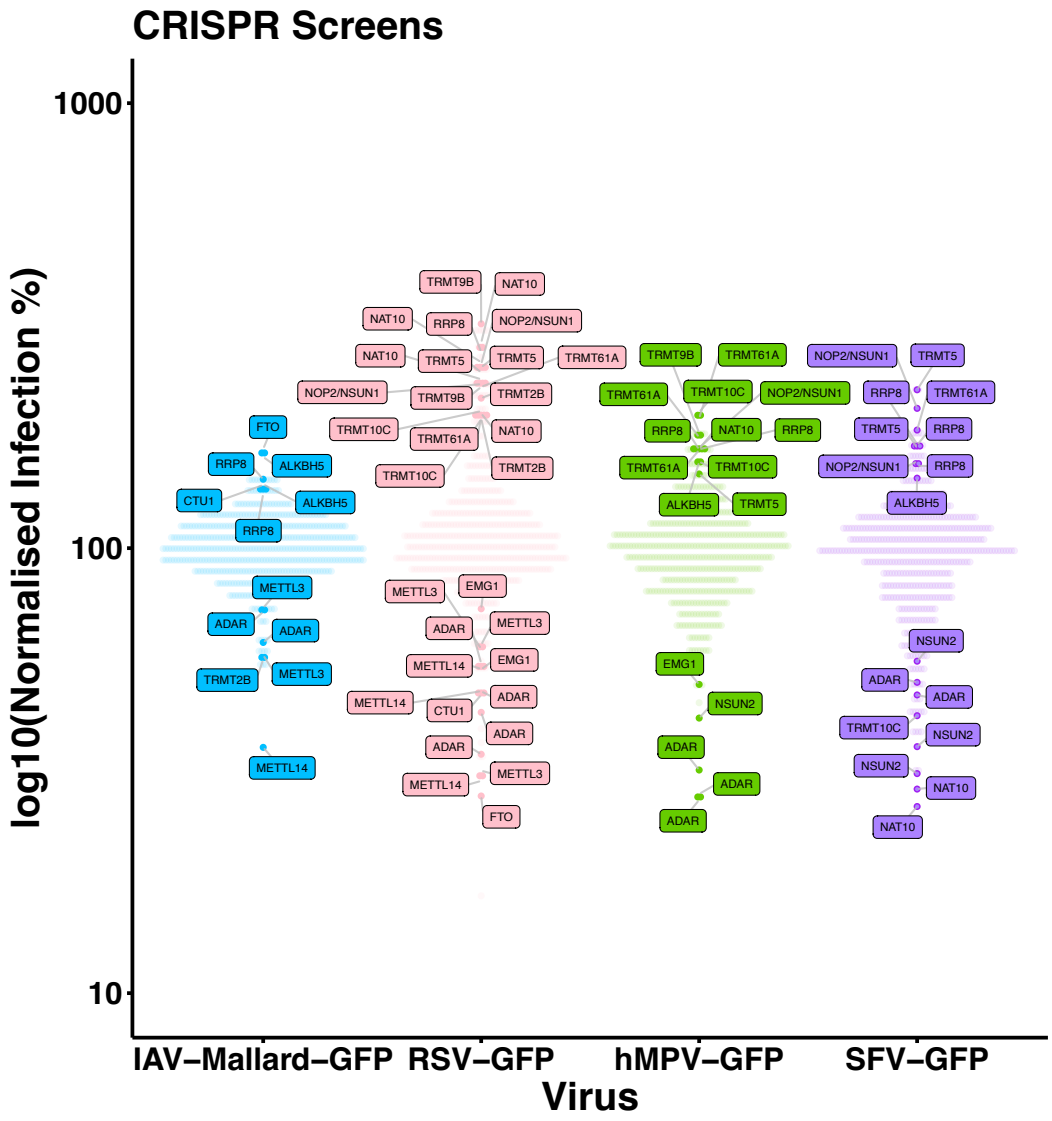

Knockdowns that upregulate infection

Viruses	Knockdowns
IAV RSV SFV hMPV	RRP8
IAV SFV hMPV	ALKBH5
RSV SFV hMPV	NOP2/NSUN1 TRMT10C TRMT5 TRMT61A
RSV hMPV	TRMT9B NAT10
IAV	MRM2/FTSJ2 METTL8 FTO
RSV	TRMT10A

Knockdowns that downregulate infection

Viruses	Knockdowns
IAV RSV SFV hMPV	ADAR
RSV SFV hMPV	TRMT10C
IAV RSV	METTL14 METTL3
RSV hMPV	EMG1
SFV hMPV	NSUN2 NAT10
IAV	METTL6 TRMT1L BUD23 TRMT2B
RSV	CTU1 MRM3 DUS1L FTO
SFV	NSUN4

Figure 4.6: Comparing the CRISPR screens of four RNA viruses. Dot plots of CRISPR KD screens performed in A549-TMPRSS2 cells or A549 cells and infected with IAV-Mallard-GFP, RSV-GFP, hMPV-GFP and SFV-GFP. Cells were transduced with the CRISPR library for 72h, then infected with virus for 72h (IAV-GFP, RSV-GFP), 48h (hMPV-GFP) or 18h (SFV-GFP), then fixed in 2% formaldehyde. Quantification of infection was measured using Celigo imaging cytometry and infection was normalised to the median infection rate of each plate in the screen. Each dot represents the observed infection in the presence of a single CRISPR guide. For ease of visualization, guide identities for each knockdown gene have been removed; when a gene appears multiple times in a plot of one virus, each appearance is the result of a different sgRNA. Tables list the knockdowns in the dot plots that up- or down-regulate virus infection.

Whilst studies have not implicated ADAR in the infection of RSV and hMPV, ADAR activity during alphavirus infection has been described before in CHIKV and VEEV. Since SFV is an alphavirus, we can project these findings onto our data. ADAR overexpression in *STAT1-/-* fibroblasts increased replication of CHIKV and VEEV hinting at a pro-viral role of ADAR in this context (Schoggins et al., 2011). The editing of these viral genomes by ADAR has not been studied at a nucleotide level, nor whether the increased replication with ADAR is due to changes in viral fitness and pathogenicity (Piontkivska et al., 2021). The extent of IFN production varies between alphaviruses and cell models (Her et al., 2010; Piontkivska et al., 2021), so we cannot directly assume the same effect on SFV as CHIKV and VEEV with ADAR. However, ADAR KD causing a reduction in SFV infection suggests it is also pro-viral for this alphavirus too. The appearance of ADAR in our screens is a good positive control. But we should also keep in mind that it is equally likely that KD of ADAR is affecting cellular homeostasis so viruses cannot establish an infection. ADAR is involved in the editing of many transcripts in a normal cell (Nishikura, 2010).

Looking at other genes in Figure 4.5, we find one RME that affects the four viruses. The knockdown of RRP8, ribosomal RNA processing 8 factor, increases the growth of all four RNA viruses suggesting it may have an antiviral role normally. RRP8 catalyses the N1-methyladenosine (m^1A) methylation of 28S rRNA at position 1322 and is involved in ribosome biogenesis (Waku et al., 2016; Zhang and Jia, 2018). RRP8 is located in the cytosol and nuclear lumen and binds to dimethyl lysine at position 9 of histone H3 (H3K9me2) in cells and suppresses ribosomal DNA (rDNA) transcription in response to glucose deprivation (Grummt and Ladurner, 2008; Murayama et al., 2008). Unexpectedly, it does not methylate histones despite binding them (Murayama et al., 2008). Several studies have found viruses perturb RRP8 expression; Ebola virus and SARS-CoV2 increased RRP8 expression, however it is decreased in IAV H5N1 infection (Barret et al., 2013; Furuse, 2021). Based on the increase in viral infection when knocked out in our screens, we can hypothesise that it has an antiviral activity.

On top of finding a protein that affects the growth of all four viruses, when we look deeper into these screens there are some comparable knockdowns that affect viral growth depending on where the virus replicates in the cell and which compartment the enzymes are usually expressed. IAV replicates in the nucleus (Chou et al., 2013)

whereas RSV, hMPV and SFV replicate in the cytoplasm (Garcia et al., 1993, Cifuentes-Muñoz et al., 2017; Acheson & Tamm 1967). With this in mind, we can see several gene knockdowns that increase cytoplasmic RSV, hMPV and SFV viral growth: NOP2 and TRMT61A. Further to this NAT10, TRMT9B and TRMT10C knockdown increase RSV and hMPV growth and KD of TRMT5 increases RSV and SFV growth. METTL3 and METTL14 knockdown reduces IAV and RSV growth. ALKBH5 was found to affect the growth of IAV, hMPV and SFV so it could shuttle from the nucleus to interact with cytoplasmic viruses.

Several of these enzymes are involved in maturation of nuclear and mitochondrial tRNA (TRMT61A, TRMT10C, TRMT5, TRMT9B). TRMT61A is the human ortholog of yeast Trm61, which is responsible for m^1A58 modification of cytoplasmic tRNAs (Ozanick et al., 2005). TRMT61A changes the methylation modification of adenine in position 57 in tRNA glutamic acid, and it also methylates mRNA at low levels and mostly in tRNA loop-like structures. The m^1A modification disrupts base pairing which causes translational repression, most likely by ribosomal scanning or translation issues (Safra et al., 2017). Perhaps the host methylates the viral RNA via TRMT61A to inhibit translation to stop infection. It would be interesting to determine if RSV and other viruses downregulate TRMT61A during infection. However, in retrovirus reverse transcription, m^1A58-modified $tRNA_3$(lys) is a primer for the initiation of reverse transcription, being complementary to the primer binding site on HIV RNA. The methylation of the A58 of the tRNA(lys) removes base pairing and terminates primer binding after 18 bases and limits run-on transcription (Finer-Moore et al., 2015).

TRMT10C is involved in an enzymatic complex in mitochondria for maturation of tRNA which is a key step in mitochondrial gene expression (Meynier et al., 2024). These events occur in RNA granules close to the mitochondrial nucleoid (Rackham et al., 2024), and so perhaps a protein could be displaced and perform a previously unknown antiviral function. Absence of TRMT10C in this enzymatic complex does not stop tRNA maturation and its function is to direct the complex's nuclease domain to the cleavage site, thereby increasing the rate and accuracy of cleavage (Vilardo et al., 2023).

TRMT5 (tRNA methyltransferase 5) encodes a mitochondrial protein with a strong homology to the class I-like methyltransferase superfamily (Powell et al., 2015).

Molecular level detail of this enzyme has not been investigated however whole-exome sequencing identified a mutated form was found to be the cause of a human disorder characterised by poor energy production by the mitochondrial oxidative phosphorylation system (Powell et al., 2015, Wu et al., 2022). There are no previously described roles in virus infection.

TRMT9B has no functional discoveries but recent structural modelling confirms it has methyltransferase function (Hogan et al., 2023).

NOP2 is a very interesting hit in the screens. It is a nuclear protein, but it has been found to be antiviral against several alphaviruses (Kamel et al., 2024), and some of its normal roles in the cell do not require its enzymatic activity (Liao et al., 2022). In these screens, knockdown of NOP2 increases RSV, hMPV and SFV infection, implying an antiviral role. These viruses are all cytoplasmic, therefore NOP2 must have a change in function after infection which causes it to relocate to the cytoplasm.

RSV and hMPV are closely related viruses of the paramyxoviridae family and there is overlap in the sets of RMEs that have effects in the screens against them. In Figure 4.6, NAT10 KD increases RSV and hMPV rates of infection but contrary to this, decreases SFV infection. NAT10 positively regulates Sindbis virus infection by increasing N-acetylation (ac^4c) of cellular RNA (Dang et al., 2024). Like Sindbis virus, SFV is also an alphavirus so it is interesting that NAT10 has the same effects on SINV and SFV. A major difference between these two sets of viruses is that RSV and hMPV are negative strand and SFV and SINV are positive strand RNA viruses. If cellular RNA is acetylated upon alphavirus infection, paramyxovirus RNA may be acetylated directly which is antiviral. Alternatively, acetylation of paramyxovirus RNA may negatively affect the transcription and replication of viral RNA. It may also affect encapsulation of the viral genome or antigenome which affects viral assembly. NAT10 has also been found to increase the stability of HIV-1 transcripts as loss of ac^4c due to NAT10 depletion suppresses HIV-1 replication by decreasing stability of viral RNA (Tsai et al., 2020; Xie et al., 2023). Previous knockouts of NAT10 inhibit IAV development, implying a pro-viral function of NAT10 (Watanabe et al., 2014), however NAT10 did not appear to influence IAV growth in our screen. This may be due to the strain of IAV used (H1N1).

EMG1 knockdown downregulates RSV and hMPV expression. EMG1 is a N1-Specific Pseudouridine Methyltransferase involved in ribosome biogenesis and methylates 18S rRNA base 1248 which stabilises the interaction of the ribosome with tRNA. Despite being a DNA virus, Kaposi's sarcoma-associated herpesvirus (KSHV) enhances the recruitment of EMG1 to newly synthesised pre-40S ribosomal subunits during early stages of KSHV replication. This allows the production of a virally induced specialised ribosome, which preferentially translates viral late proteins. EMG1 depletion reduced the translation of late viral proteins which impacted the formation of new infectious virions and a catalytically inactive form of EMG1 was unable to rescue the expression of KSHV in these depleted cell lines, demonstrating the methyltransferase function of EMG1 is necessary for KSHV lifecycle (Harrington et al., 2024). Perhaps RSV and hMPV also require EMG1 to preferentially translate their viral proteins.

In addition to m^6A being important for IAV and RSV growth (Figure 4.4), our screens found it is also important for hMPV and SFV. METTL3 and METTL14 KD downregulate IAV and RSV infection which shows that the addition of m^6A is important for viral pathogenesis of IAV and RSV (Courtney et al., 2017; Xue et al., 2019). ALKBH5 is an eraser of N6-demethyladenosine (Zheng et al., 2012) and KD of ALKBH5 in our screen increases IAV, hMPV and SFV expression suggesting removal of m^6A modifications is an antiviral mechanism. Since ALKBH5 is also nuclear (Zheng et al., 2012), it could shuttle from the nucleus to perform an antiviral role in the cytoplasm. Previous work exhibited ALKBH5 is downregulated during RSV infection (Xue et al., 2019) and abrogation of m^6A results in attenuation of hMPV in cell culture (Lu et al., 2020). Based on these observations and that hMPV and RSV are closely related viruses, we can extrapolate this to assume that m^6A removal by ALKBH5 would also attenuate RSV and the screen (Figures 4.4B, 4.6) did not capture this.

Even though it is exciting to find genes implicated in the infection of several viruses in Figure 4.6, finding RMEs that are involved in only one virus infection and not shared across the screens is also a very positive result. I have not discussed any of these genes here, but it is good to know we are not just finding global genes that are potentially very toxic to the cell when knocked out, so we can give more value to the results of the screen and begin downstream verifications.

Discussion

Optimising transient CRISPR knockdown screens

For identification of individual RNA modifying enzymes which inhibit viruses with RNA genomes, or enhance growth of said viruses, we used the arrayed library screening method created in previous chapter and initially screened IAV mallard and RSV-GFP using an MOI of 0.5. Through these screens, we followed up several genes that showed strong inhibitory or facilitatory effects. All knockdown conditions that showed a difference in growth of IAV or RSV that was two standard deviations from the bulk population were considered 'candidate' effectors. The process resulted in a panel of genes which were further tested in follow up screens. Unfortunately, during these small-scale mini-screens, all the candidate effectors were dismissed as background noise. Even following up a potent hit in the RSV screens, MTO1, which seemed to have a large effect by increasing RSV-GFP expression when knocked out, did not end up being involved in RSV infection. When the follow up results for MTO1 looked poor and inconsistent, we decided to repeat the screens to see what was causing issues with reproducibility. On repeating the large-scale screens in IAV and RSV, we found the lists of significant genes varied greatly between screens with little overlap. In retrospect, we should have performed replicate screens prior to following up but we wanted to test the robustness of the screens on a more manageable small-scale level and do new experiments to generate definitive data that supported the screening results.

We then outlined several issues in the screen and set out to find what was causing the issue. Firstly, when normalising the data, I had normalised to the non-targeting control conditions, which upon further analysis, varied significantly between plates in a screen. The second issue that could be causing a problem was the dose of virus used. We had selected a dose of MOI 0.5 thinking this would be suitable for us to be able to see fold changes in viral infection, however this perhaps caused fold changes in virus infection to overlap with background noise and so we could not distinguish true hits in the screen. Finally, we considered that perhaps the lentiviral library prep we had produced had failed and we were not transiently transducing cells like we had seen in small scale in Chapter 3.

To start establishing what could make the screens reproducible, I decided to stably transduce the cells in a full screen to see if I could get more consistent results. The CRISPR vectors contain a resistance gene against the drug puromycin so by exposing cells to puromycin, we selected for cells that have been successfully transduced. I confirmed that the lentiviral library was able to transduce the cell lines in the screen, simply by comparing transduced cells to control non transduced cells which died 24h after being exposed to selection drug. This does not mean that each well transduced in the screen is a successful knockout, but we know that scaling up the experiments from chapter 3 is not reducing transduction success.

The high dose of virus had impacted the screens. By lowering the dose of virus used in the infections, and performing duplicate screens, the candidate effectors in a transiently transduced cell line screen had more overlap of candidate genes with 'knockout screens' that I had transduced and subjected to selection and passaging for a period of time. However, ALKBH5 and FTO were hits in the high dose screens of IAV (Figure 4.1B) and low dose screens (Figure 4.4A) and TSG1 was in all RSV screens (Figure 4.1D, 4.4B). In the IFN treated IAV screen in Figure 4.5, I found PUS1 and PUS3 depletion reduced IAV expression and PUS1 depletion had the same effects in the initial high dose screen. This is quite an interesting result for PUS1; perhaps the interferon response in the high dose screens would have been higher than the lower condition which is why we see it also in the interferon pre-treatment screen. ALKBH5, FTO and TSG1 may be very potent antiviral candidates for IAV and RSV causing them to appear in all the screens. The high dose of virus may have overwhelmed the cells and masked genes which have smaller antiviral or pro-viral effects for IAV and RSV, causing these smaller perturbations in virus growth to be lost in the noise of the screen.

RNA modifying enzyme effects are perturbed by interferon treatment of cells

By pre-treating screens with Interferon, we hypothesised we would uncover mechanisms IAV may use to mask itself from interferon stimulated genes or sensitise it further to eradication by the ISGs. Some of the genes that sensitise the virus to eradication may be upregulated as ISGs by interferon treatment, however this would not be distinguishable using knockdowns. The genes that appeared as strong

candidates seem unlikely. NSUN2 depletion is known to enhance the interferon response as a global reduction in m^5C on ncRNAs in the cell is recognised by RIG-I and upregulates interferon (Zhang et al., 2022). And, in fact, NSUN2 is depleted during infection of viruses including SARS-CoV2, Sendai virus (SeV), vesicular stomatitis virus (VSV), herpes simplex virus 1 (HSV-1) and Zika virus (ZIKV) (Wang et al., 2023). Depletion of NSUN2 in the interferon screen enhanced IAV growth, contradicting these published observations. ALKBH5 knockdown reduced IAV expression in this screen which also contradicts previous observations: m^6A stabilises the viral IAV RNA (Courtney et al., 2017). Why would the knockdown of a gene that removes m^6A, thereby destabilising the viral RNA, deplete IAV? We would expect lack of removal of m^6A to enhance IAV infection. PUS1 and PUS3 KD reduced IAV growth, implying pseudouridylation during the interferon response is important for viral fitness. However, PUS1 appeared in the initial screens that I later found to be largely irreplicable. Perhaps this is another case of a false positive or, like I hypothesised above, interferon was high due to excessive levels of infection in the initial high dose screens which is why we see it also in the interferon pre-treatment screen. Looking ahead, it would be important to repeat and further optimise the interferon experiments before following them up.

Screening several RNA viruses uncovered several genes involved in virus restriction or growth

To identify human RNA modifying enzymes with broad anti or proviral activity, and since I had more confidence in the robustness of the screening method (without interferon), before following up candidate effectors, I decided to perform screens against two other viruses: hMPV and SFV. Both have an RNA genome and are from different virus families, although RSV and hMPV are closely related, which would help us to see if there are RMEs that have an impact on RNA viral infection in general. The screening data uncovered both broad acting effectors and specific effectors: we found previously characterised ADAR appearing in all the screens. ADAR is responsible for adenosine to inosine editing which results in an A-to-G mutation in transcripts. We also identified RRP8 as an antiviral factor in all screens because KD of this protein caused an increase in the viral expression of IAV, RSV, hMPV and RSV. RRP8 is a m^1A writer and this methylation affects RNA base pairing which affects the RNA molecule

structure and function (Zhou et al., 2016). M^1A has been found in rRNAs, tRNAs and mRNAs. In mRNA, m^1A is spread throughout the molecule, appearing in coding sequence, 5'- and 3'UTRs (Dominissini et al, 2016). M^1A could alter the structure or protein recognition of translation initiation sites which would influence translation. In mitochondria, m^1A in the 5'UTR or coding sequence repressed translation (Safra et al., 2017). This may be due to m^1A affecting ribosome scanning or translation and perhaps the same happens in virus RNA translation and this is how RRP8 globally affects RNA viruses.

Thinking about where viruses replicated in the cells, nuclear (IAV) or cytosolic (RSV, hMPV, SFV), we found several genes that were involved in cytosolic infection based on the increase in viral infection when the following genes were knocked down: NOP2 and TRMT61A. Knockdown of enzymes that modify tRNAs (TRMT61A, TRMT10C, TRMT5, TRMT9B) affected two viruses in Figure 4.6 and KD all the TRMT enzymes that are candidate effectors increase RSV growth. RSV is known to induce the formation of tRFs from tRNAs so this is an interesting result (Deng et al., 2015). Knockdown of EMG1 decreased and NAT10 increased expression of paramyxoviruses RSV and hMPV. Reduction in expression of METTL3 and METTL14 reduced IAV and RSV growth. These METTL proteins methylate N6-adenosine in RNA and it is already known that m^6A enhances growth of IAV and RSV (Courtney et al., 2018; Xue et al., 2019), so this is another positive result for the utility of the screening platform. An m^6a 'eraser' enzyme, ALKBH5 (Zheng et al., 2012), increased growth of IAV, hMPV and SFV when knocked down which implies that m^6A modification of RNA enhances growth of these viruses.

The next steps would be to investigate all the candidate effectors we have found to have an impact on infection, and to screen other RNA viruses to determine if they are affected by the same genes we have described here. Other IAVs would be a point of interest, to see if there are RMEs involved in aspects of IAV infection. On top of this, other viruses that replicate in the nucleus would also be interesting to see if there is a panel of viruses, like the cytosolic set described in this chapter, that are impacted by the same genes. We could also study the difference between early and late stages of the virus lifecycle. Due to the low levels of infection observed for these viruses in a single replication round (Chapter 3), we assessed multi-cycle infection after 72 hours.

This multicycle assessment of infection creates a potential bias to miss RMEs acting very early in the virus life cycle, so in future work we could design experiments where we measure infection rates at early timepoints post infection and after several rounds of multicycle infection.

While screening experiments are a powerful way to identify candidate antiviral genes, they do not distinguish between genes that act directly on viruses from those that serve a regulatory function in the cell, for example, NSUN2 methylates cellular RNA which impacts IAV infection, however METTL3 methylates IAV RNA directly (Zhang et al., 2022; Courtney et al., 2017). Genes that inhibit one or two viruses are less likely to exert their effects through regulatory or non-specific mechanisms and so we can focus on them having a specific restrictive or proviral effect on a specific virus. That being said, those with broad activity (e.g. ADAR, RRP8) can have important effects e.g. They could have a broader restrictive or pro-viral effect on many viruses or regulate cellular processes involved in eradicating infection. Confirming if RRP8 is active against all these viruses and how (modifying viral RNA directly or influencing global methylation patterns) would be a huge finding and looking ahead on this project, I would follow this up first.

CRISPR screens are simply a snapshot of what was happening in the cell at a specific moment in time. The screens show us candidate effectors, but no screen is perfect. They are good for showing that a virus can establish infection, but it does not allude to how well a virus is doing in the cell. The experiments I have performed so far are designed to look at one parameter: the percentage of GFP at the end point of infection. We are not looking at rates of infectivity but the number of cells successfully infected. For further in-depth analysis, it would be good to perform follow up mini-screens on a plate reader capable of measuring GFP over a series of time points to show us differences in growth rates compared to a control when a gene is knocked out. Knockouts can also lead to inhibition resulting from unnatural perturbation of cell physiology. We found early on in this screening work that MTO1 appeared to have an antiviral effect on RSV however this was an artefact of poor cell growth. Introducing toxicity assays as a step in the hit selection process would avoid this happening in the future.

To investigate each candidate effector in more depth, we should also look at other experiments like the impact of overexpressing the gene and see if this heightens the anti- or pro-viral effect we have found *e.g.* does overexpressing RRP8 ablate the infection of the viruses in Figure 4.6? We could also investigate where the modifications are imparted on the viral RNA and if there are consensus sequences, which if conserved across multiple viruses, would be a huge discovery. Other experiments we could follow up with would be to mutate the active site of the RME and see if this has the same impact as knocking the enzyme out. Some of these proteins may be the same as NOP2, described in the next chapter, and the role of the protein in infection is not wholly reliant on their enzymatic function (Liao et al., 2022).

We then need to consider the perspective that maybe the gene that is knocked out is not the important part of the puzzle, but the modification it imparts. And that compensatory mutations arise masking the effect of knockdown of some genes. The modification itself causes recognition by the innate immune system or allows the viral RNA to mimic the cellular landscape of nucleic acids and avoid sensing. This would mean that knocking out one gene at a time may mask antiviral mechanisms of genes working in consort/pathways together. This is an issue with knockout screening experiments, however using the GO database to assign function and identify pathways could be a way to reduce these artefacts.

Overall, what we have established in this chapter is a platform for use in discovering the role of RNA modifications in the lifecycle of RNA viruses. I have ironed out some early hiccups but there are more issues to address. The utility of it could be expanded to look at the titres of viruses produced in knocked down cells by infecting reporter cells with supernatants from the screen. I began optimising this in the previous chapter and it would be an interesting facet to return to. I think the platform will be of use to other researchers in the lab who want a CRISPR screening method that does not rely on sequencing, making it cheaper and more accessible to researchers with limited bioinformatic skills. This method of arrayed CRISPR screening has already been used and described by other groups (Kim et al., 2018), demonstrating the impact of this and how it could be applied to many other types of genes and not just limited to RNA modifying enzymes.

Chapter 5 Elucidating the role of NOP2 in virus infected cells

Introduction

NOP2/NSUN1 is a 120kDa protein that was initially characterised as a proliferating-cell nucleolar antigen (p120) found over-expressed in a range of precipitously dividing cells and malignant cancers (McGrath et al., 1994). NOP2 has 4 four RNA binding domains and an S-adenosyl-L-methionine-dependent methyltransferase domain. It's one of three C5 methyltransferases that are conserved in all eukaryotes, the other's being NSUN2 and NSUN5 (Bohnsack et al., 2019). C5 methylation of cytosines (5-Methylcytosine or m^5C) is a common modification found on a wide variety of RNA molecules; from ribosomal rRNAs (rRNA), transfer RNAs (tRNA), messenger RNA (mRNA), vault RNAs (vtRNA) to non-coding RNAs. The NSUN proteins play a role in the regulation of nuclear and mitochondrial gene expression through their methylation and RNA binding properties (Liao et al., 2022).

Ribosome biogenesis is initiated in the nucleolus (a specialised sub-compartment of the cell nucleus where rRNA precursors are synthesised by RNA polymerase I) (Drygin et al., 2010). Precursor-rRNAs (pre-rRNAs) are heavily modified post-transcriptionally (Decatur et al., 2002) and the methylation of rRNA by NOP2 is one step in the complex process of ribosome assembly. In budding yeast NOP2 is essential for pre-RNA processing and 60S ribosome subunit synthesis. Additionally, in *S. cerevisiae* NOP2 catalyses m^5C deposition on the 25S rRNA at position 2870, near the peptidyl-transferase centre of the ribosome (Sharma et al., 2013). The equivalent site in human 28S rRNA is C5-methylated at position 4447 by NOP2 as well (Liao et al., 2022). This methylation process is crucial for the correct structure and function of ribosomes (Sharma et al., 2015).

Liao et al., 2022, established further functions of NOP2 in ribosome biogenesis beyond catalysing rRNA methylation. NOP2 is involved in non-catalytic pre-rRNA processing

by recruiting the box C/D small nucleolar RNAs (snoRNA) U3 and U8 to the pre90S ribosomal particle to form small nucleolar ribonucleoprotein (snoRNP) complexes. SnoRNAs are a type of non-coding RNA which are 60-300nt long and are present in the nucleoli of eukaryotic cells and regulate rRNA modification. U3 and U8 are needed for pre-rRNA processing reactions by recruiting catalytically active proteins to sites of modification or cleavage, thereby directing synthesis of the small and large ribosomal subunits respectively (Cléry et al., 2007; Watkins et al., 2012). In addition to interacting with RNA, NOP2 also interacts with protein components of the small nucleolar ribonucleoprotein (snoRNP) complex: Fibrillarin, NOP56/58 and 15.5K. These proteins are also involved in post-transcriptional modifications of rRNA. Fibrillarin is a methyltransferase that directly catalyses the 2'-O-methylation of rRNA residues guided by snoRNAs. NOP2 binds the U3 snoRNA involved in guiding Fibrillarin catalysed 2'-O-methylation on rRNAs (Liao et al., 2022). NOP56/58 are essential for snoRNP assembly and stability and interact with NOP2 to facilitate its recruitment to the nucleolus (Watkins et al., 2004).

Depletion of NOP2 in human cells leads to a severe rRNA processing defect causing an accumulation of 47S pre-rRNA. These defects are similar to that when U3 and U8 box C/D snoRNAs are depleted (Langhendries et al., 2016). The recruitment of U3 and U8 to pre-ribosomes and their complex formation with NOP56 and 15.5K was compromised in the absence of NOP2 (Liao et al., 2022).

Beyond these established functions, NOP2 has been implicated in viral infections. As presented in Chapter 4, I found in CRISPR screens that NOP2 knockdown increased the growth of SFV, an alphavirus, as well as two pneumoviruses, hMPV and RSV. This suggests it has an antiviral function. Given NOP2's crucial role in ribosome biogenesis, it is possible that it could indirectly influence viral replication through:

1. Ribosome availability: viruses rely on host cell machinery, including ribosomes, for protein synthesis. If NOP2 is involved in regulating ribosome biogenesis, it could potentially impact viral replication. However this is unlikely due to timing as there will be many ribosomes in the cell at the start of infection.

2. Cellular stress response: viral infections often trigger cellular stress responses. NOP2 might be involved in the cellular response to stress which could indirectly influence viral replication.

However, more specific NOP2-viral interactions have been characterised. NOP2/NSUN1 was recently shown to restrict HIV-1 replication and promote latency by participating in the methylation of the HIV-1 TAR RNA (Kong et al., 2020). In the Castello group, Dr Wael Kamel found that NOP2 is in the vRNA interactomes of a range of cytoplasmic RNA viruses. He also found that NOP2 is one of a panel of nuclear proteins that shuttle to the cytoplasm during viral infection (Kamel et al., 2024).

Most research on NOP2 has focused on its role in normal cellular processes, particularly ribosome biogenesis. In this chapter, I set the foundations to unveil the role of NOP2 in virus infection, by applying:

- A comparative analysis between NOP2 expression and activity in infected and uninfected cells
- interaction studies investigating the RNA interactome of NOP2 in infected and uninfected cells
- functional studies further analysing the impact of NOP2 knockdown on viral infection.

A note on this chapter

This chapter marked the end of my time in the Wilson lab and an abrupt move into Professor Alfredo Castello's group, as my primary PhD lab moved to Cambridge. This move was somewhat unwelcome and traumatic in the last stretch of a PhD, but fortunately I was able to move into a group with one of the greatest expertise in RNA biology in the UK. I had intended to do further screens on several more viruses, perform various verification experiments and then follow up RRP8, along with several other proteins that were interesting in the screens. Naturally the disruption from this move had a greater impact than I initially foresaw (who knew basic procedures like a western blot could differ so hugely between lab groups) but I made the most of it and was able to follow up one of the hits from the screens in Chapter 4 – NOP2/NSUN1. The project pivoted a little and there are small inconsistencies from the previous chapters, including having to switch viruses to Sindbis virus (SINV). Fortunately, I had the help of many members of the Castello group and some of the experiments were carried out in collaboration with Dr Wael Kamel, Dr Azman Embarc, and Dr Vincenzo Ruscica. Rozeena Arif kindly helped with the iCLIP data analysis. Further to this Dr Louisa Iselin and Natasha Palmalux provided on the spot help and guidance through settling into the lab and learning new ways of carrying out standard procedures that differed from the Wilson group, as well as essential advice into the experimental side of iCLIP.

Results

NOP2 translocates to the cytoplasm

To begin characterising what NOP2 does in infection, experiments were performed to validate the nucleo-cytoplasmic translocation of NOP2. Firstly, nucleus and cytoplasm were fractionated and probed by Western blotting for the presence of NOP2 (Figure 5.1). Cytoplasmic (GAPDH) and nuclear envelope (LamininB) controls confirmed the successful fractionation of the nucleus. Controls to confirm that nuclear envelope integrity is maintained on infection were also assessed, including nucleolar Fibrillarin and nucleoplasmic ZC3H11A. Notably, we observed an accumulation of NOP2 in the cytoplasm 24h after SINV infection. Neither Fibrillarin nor ZC3H11A shuttled from the nucleus, as previously reported (Younis et al., 2018). Fibrillarin is known to interact with NOP2 (Liao et al., 2022), however it does not shuttle to the cytosol with NOP2. We can thus infer that the partners of NOP2 may change after infection, consistent with our observed accumulation of NOP2 into the cytoplasm 24h after SINV infection Figure 5.1).

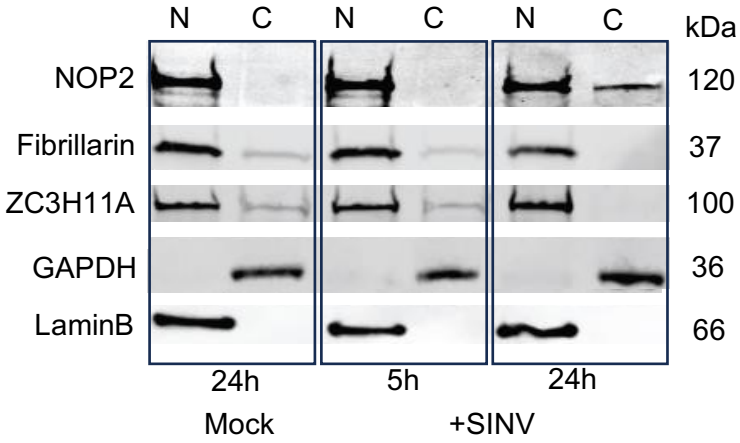

Figure 5.1: Western blot showing nucleus to cytoplasmic translocation of NOP2 during infection. HEK293 cells were infected (+SINV) or not infected (mock) with SINV, then harvested after the time shown in the figure. Cells were fractionated into cytoplasmic (C) and nuclear (N) fractions, then Western blotting of NOP2 and control proteins for shuttling (nucleolar Fibrillarin and nucleoplasmic ZC3H11A) and fractionation (cytoplasmic GAPDH and nuclear envelope protein Lamin B) was performed and imaged on a Li-Cor instrument.

Cytoplasmic shuttling of NOP2 was further validated by confocal microscopy. In experiments performed with Dr Azman Embark Buh and Dr Vincenzo Ruscica, cells were infected with SINVnsp3-mScarlet and the location of NOP2, and two controls (cytoplasmic PURB and nucleoplasmic ZC3H11A) was determined.

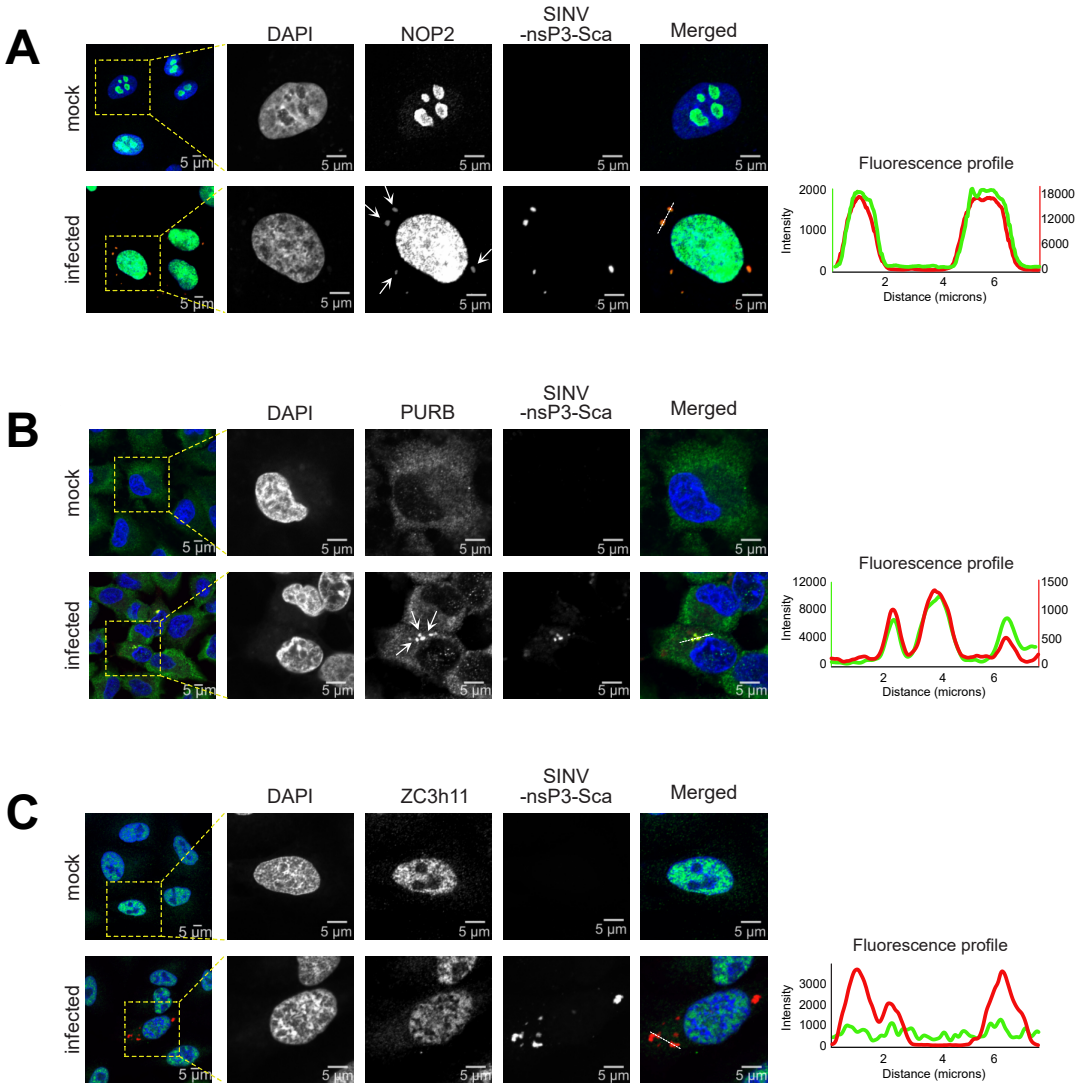

Figure 5.2: Analysis of the subcellular location of NOP2 after SINV infection by immunofluorescence.

A549 cells were infected with SINVnsp3-mScarlet at an MOI of 3 and after 24h were analysed by immunofluorescence using nsP3-mScarlet as a marker of viral replication organelles and DAPI to define the cell nucleus.

A. Nucleolar NOP2 shifts to the cytoplasm after infection. NOP2 is located in the nucleus in mock infected (top), but a portion can be seen to move to the cytoplasm in infected cells (bottom).
B. Cytosolic SINV RNA-binder PURB relocates to SINV replication organelles (RO's) following infection.
C. Nuclear ZC3H11A does not move to the SINV ROs following infection.

This experiment was performed by Dr Ruscica and Dr Embarc and the figure is an edited form of what will be published in WK's upcoming paper "Alphavirus infection triggers selective cytoplasmic translocation of nuclear RBPs with moonlighting antiviral roles."

Upon infection, NOP2 went from a nucleolar location in uninfected cells, to being diffusely spread in the nucleus and present in the cytoplasm following infection. This is in part due to nucleolus disruption under cellular stress, which leads to a redistribution of nucleolar proteins to the nucleoplasm (Yang et al., 2018). In addition to this redistribution of NOP2, the cytoplasmic portion of NOP2 completely co-localised with nsP3-mScarlet, which supports the engagement of NOP2 with SINV replication organelles (ROs). PURB, which is a cytoplasmic effector known to interact with SINV RNA, redistributed from the cytosol in uninfected cells to the ROs upon infection. ZC3H11A is a nuclear protein, and negative control since it does not interact with either SINV RNA or nsP3-mScarlet. As expected, it did not shuttle from the nucleus to engage with SINV ROs, implying that the relocation of NOP2 is due to viral infection.

NOP2 suppresses SINV infection

To investigate the antiviral role of NOP2 in the cells, we probed the fitness of SINV when NOP2 was knocked down. Using the panel of NOP2 CRISPR guides I created in Chapter 3 and used in Chapter 4 in screens, I probed the different NOP2 sgRNAs for the strongest KDs (Figure 5.3A). I focused on the most potent guides (guides 2, 4 and 5) to create knockdown cell lines for viral fitness experiments. Unfortunately, the cells transduced with guide 4 did not survive. This is likely because NOP2 is essential for cell proliferation (de Beus et al., 1994) and a full knockout is likely very toxic and deleterious for the cell. In Figure 5.3B, guides 2 and 5 reduced expression of NOP2 compared to a non-targeting control to different extents: guide 2 caused partial knock down whereas guide 5 caused a much greater depletion of NOP2. In both conditions the reduction in NOP2 increased the levels of SINV capsid 24h post infection. Interestingly the stronger knockdown (guide 5) caused increased levels of SINV capsid compared to guide 2. This suggests that under normal levels of NOP2, NOP2 acts antivirally, and its depletion allows greater levels of SINV infection, reflected in the increase in SINV capsid in the western blot.

I then used the cell lines that were stably transduced with guides 2 and 5 for a viral growth assay and tracked the increase in either $SINV_{nsp3}$-mCherry and $SINV_{nsp3}$-scarlet in 15 min increments over a 48h period (Figure 5.3C). Compared to a non-target sgRNA control (NTC) condition, NOP2 knock down by guide 5 showed a slight increase in SINV-nsP3-mCherry growth. Conversely, CRISPR knockdown by guide 2

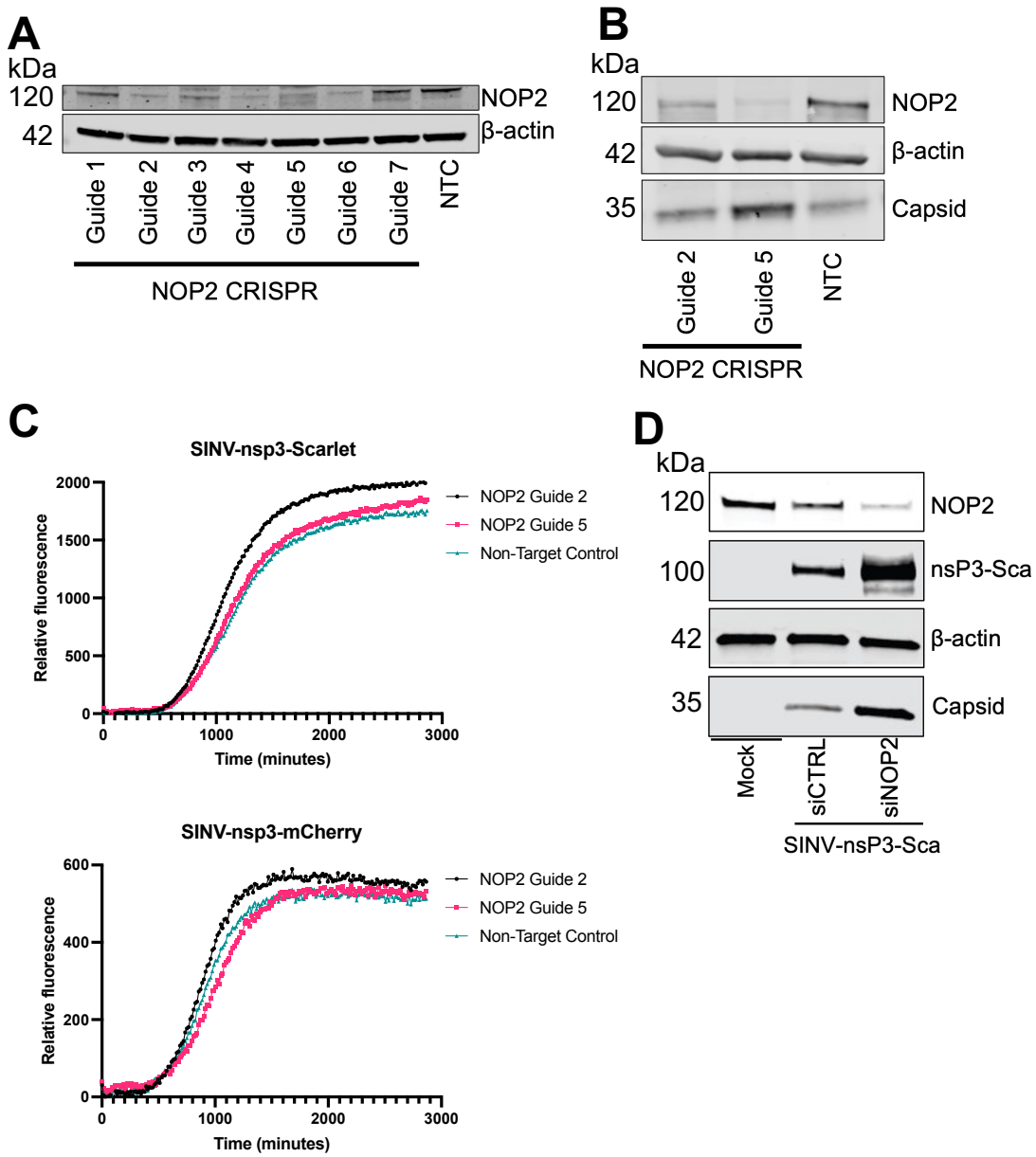

Figure 5.3: NOP2 is putatively antiviral.

A. HEK293 cells were transduced with CRISPR guides against NOP2, then harvested and an immunoblot was performed against NOP2 CRISPR knockdowns (Guide 1-7), non-target control (NTC) with β-actin as a loading control.

B. Immunoblot probing levels of capsid as a measure of viral fitness upon NOP2 CRISPR knockdown. Cell lines from guides 2 and 5, and a non-target control (NTC) in A were infected with SINV-nsp3-scarlet at MOI = 3 for 24h, then harvested for western blot.

C. Growth curves of SINV fitness upon NOP2 knockdown. HEK293T cells from A transduced with CRISPR guides 2 and 5 were infected with SINV-nsp3-scarlet (top) or SINV-nsp3-mCherry at MOI = 0.5 and fluorescence intensities were recorded every 15 minutes for 48h.

D. SINVnsP3-mScarlet gene expression upon siRNA knock down of NOP2 in HEK293 cells at MOI= 0.5 for 48hpi. siCTRL: control siRNA, siNOP2, siRNA against NOP2. Western blot against viral proteins.

caused a strong and reproducible increase in SINV gene expression. While the results are promising at showing NOP2 antiviral activity, the experiments should be repeated with other guides and experimental approaches to confirm the results.

These blotting and growth curve experiments were corroborated with data from Dr Wael Kamel. As part of a larger experiment, Dr Kamel performed an siRNA knockdown experiment of NOP2. Transient KD of NOP2 using siRNA did not affect cell viability (data not shown). Depletion of NOP2 caused a robust increase in SINV protein levels (Figure 5.3D) as well as RNA levels and virus titre (data not shown). He also probed a cytosolic RBP that interacts with SINV RNA (MKRN2) and a nuclear RNP that neither relocates to the cytoplasm nor interacts with SINV RNA (ZC3H11A). KD of the cytosolic protein increased SINV expression and negative control ZC3H11A had no effect. These differential phenotypes support a specific antiviral effect for NOP2 that is not recapitulated when knocking down other RBPs.

Using iCLIP to define NOP2's RNA substrates during infection

NOP2 has essential roles in the cell, and total depletion of NOP2 is deleterious. The majority of NOP2's functions rely on its RNA-binding activity, and we have found that under viral infection it localises with virus ROs. This led me to hypothesise that NOP2's antiviral activity may involve its interaction with vRNA or altered interaction with cellular RNA targets. To determine whether NOP2 exhibits a specific pattern of binding to vRNA or if it has a different interaction with cellular RNA during infection, I used iCLIP2. iCLIP2 enables us to identify RNA-binding sites with single nucleotide resolution (Hafner et al., 2021).

It works on the basis of stabilising protein-RNA interactions by UV crosslinking, then treating with RNases to narrow down the footprint of the RBP on the RNA (Figure 5.4). The protein under investigation is then immunoprecipitated under stringent wash conditions. Protein-RNA complexes are separated and extracted by SDS-PAGE and nitrocellulose membrane transfer, then the protein is digested, resulting in RNA fragments with a small protein fragment at the site of crosslinking. This short polypeptide causes termination during reverse transcription in >80% of cases, with the 5' end of the produced cDNA representing the nucleotide following crosslink site

(Buchbender et al., 2020). These cDNAs are then processed and sequenced to identify NOP2's binding sites.

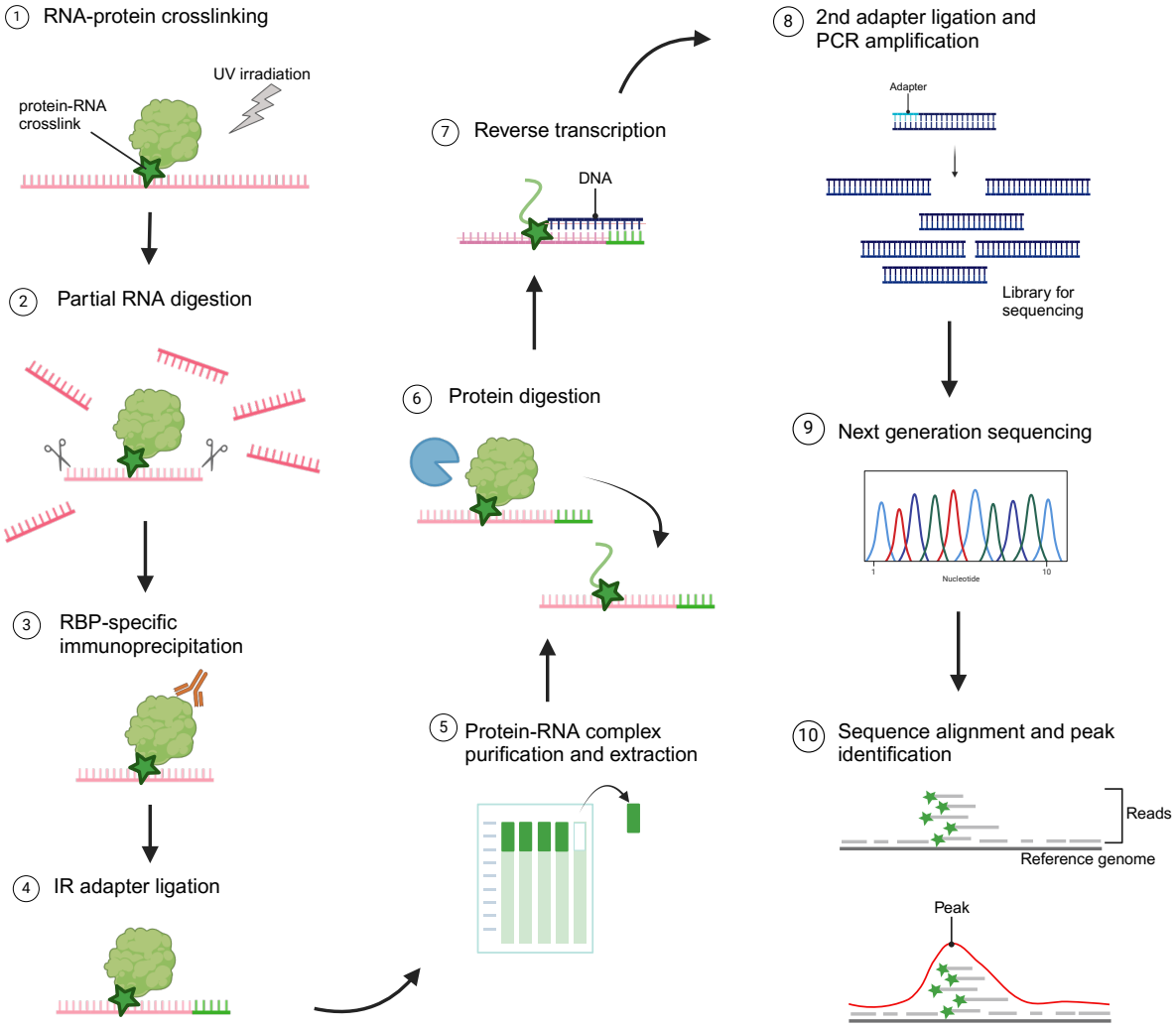

Figure 5.4: The iCLIP2 workflow.

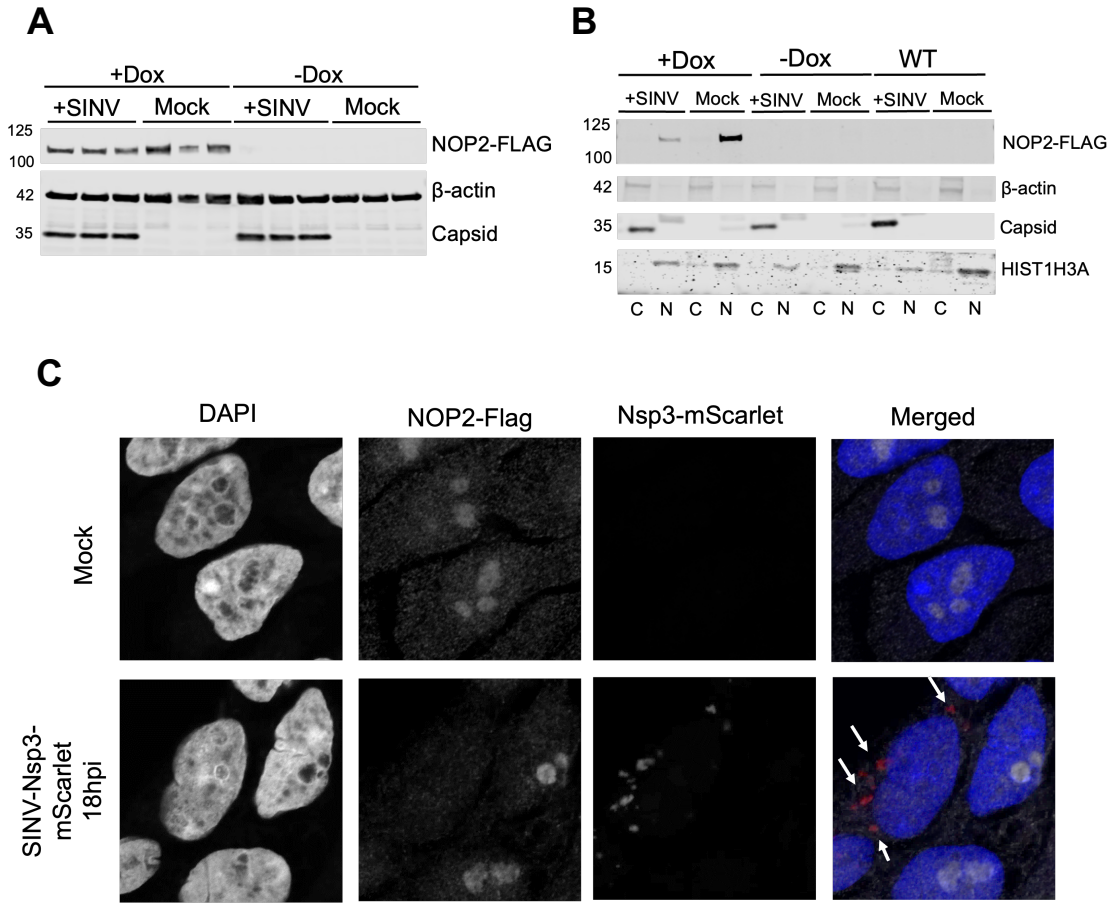

Figure 5.5: NOP2-FLAG is trapped in the nucleus.

A. Levels of capsid were not affected by NOP2-FLAG overexpression. NOP2-FLAG expression was induced (+Dox) or not (-Dox) using doxycycline for 24h in HEK293T FLP-IN TRX cells. Cells were then infected with SINV-nsP3-mScarlet or mock infected for 18h then harvested for western blotting.

B. NOP2-FLAG does not shuttle to the cytoplasm. NOP2-FLAG expression was induced (+Dox) or not (-Dox) using doxycycline for 24h in HEK293T FLP-IN TRX cells. Cells were then infected with SINV-nsP3-mScarlet or mock infected for 18h. Cells were fractionated into cytoplasm (C) or nucleus (N), demarked by nuclear protein HIST1HA and β-actin respectively. Levels of capsid were probed to assess viral fitness.

C. Confocal microscopy showing that NOP2-FLAG doesn't shuttle to the cytoplasm under SINV infection. A549 cells were infected with SINVnsp3-mScarlet at an MOI of 3 and after 24h were analysed by immunofluorescence using nsP3-mScarlet as a marker of the replication organelles and DAPI to define the cell nucleus.

Attempt to make a NOP2 FLAG-tagged over-expression cell line

To employ iCLIP2, it can be preferable to use an overexpressed protein to maximise the capture of RNA of interest, especially if endogenous levels of the protein are low. I also thought it would be beneficial for immunoprecipitation to use an over-expressed

tagged construct of NOP2 since it would increase chances of IP being successful and allow me to IP the protein using the polypeptide tag. I thus created a FLAG-tagged NOP2 (NOP2-FLAG) overexpression cell line. Utilising the FLP-in TRX system, the FLAG tagged NOP2 construct is under a doxycycline inducible promoter. When I tested the expression of this cell line (Figure 5.5A) and probed for the FLAG tag, I found expression of NOP2-FLAG was successful, however under high levels of NOP2-FLAG, SINV capsid expression was unchanged compared to uninduced NOP2-FLAG. While I expected a suppression of viral gene expression, these results could be explained by the fact that NOP2 is an abundant protein, and endogenous levels might suffice to exert its antiviral role as described for other RBPs (Iselin et al, in preparation). I investigated this further by fractionating cells that were either infected or mock infected from populations where NOP2-FLAG expression was induced or not (Figure 5.5B). In this experiment, I saw no shuttling of the tagged construct from the nucleus. In retrospect I should have probed the same membrane for endogenous NOP2, to see if there were small shifts in endogenous NOP2 under SINV+ conditions and that it was indeed the tagged construct that wasn't shuttling.

We also sought to see if we could recapitulate the localisation of NOP2-FLAG to the cytoplasmic RO by confocal microscopy. The NOP2-FLAG construct located in the nucleolus of uninfected cells and disappeared in infected cells, leaving a faint stain in the nucleus (Figure 5.5C). However, it was not observed in the ROs, which is opposite to what we saw with the endogenous NOP2 protein. Only a subpopulation of the endogenous NOP2 locates at the ROs (Figure 5.2A). Hence, a plausible explanation for the lack of NOP2-flag in the ROs is that the expression of the protein is insufficient to promote a detectable mobilisation to the ROs, which is indeed compatible with the lack of antiviral effect. Alternatively, the heavily charged Flag motif may alter the localisation of NOP2 impairing its relocation to the cytosol.

Immunoprecipitation of endogenous NOP2

Since NOP2-Flag was not behaving as expected, I decided to focus on the endogenous NOP2. I conjugated a NOP2 antibody (A302-018A, Bethyl) to Pierce Protein A magnetic beads and incubated a cell lysate from non-infected HEK293T cells to IgG conjugated beads and non-conjugated beads. In Figure 5.6 we can see that high levels of NOP2 were captured in the immunoprecipitation compared to mock-

conjugated beads. Thus, I decided to perform iCLIP2 immunoprecipitations using the endogenous NOP2.

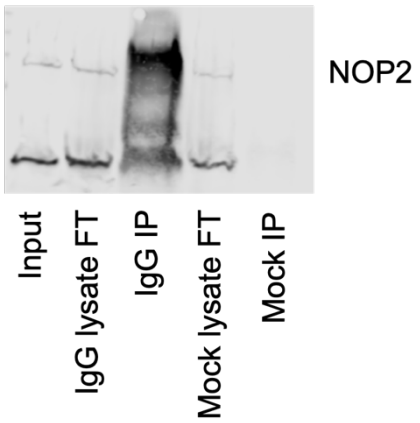

Figure 5.6: Endogenous NOP2 can be precipitated. A confluent 10cm dish of HEK293T cells were harvested and lysed and endogenous NOP2 was immunoprecipitated using antibody (A302-018A, Bethyl) conjugated to Pierce Protein A magnetic beads (IgG), or mock conjugated beads. Beads were boiled in NuPAGE loading buffer, spun down and supernatants collected. The input, flow through (FT) and IP supernatants were probed by Western blot to assess if NOP2 is immunoprecipitated by the NOP2 antibody. A clear smear of NOP2 can be seen in the IgG IP column where NOP2 has successfully been captured on the beads.

Determining the ideal concentration of RNase I for iCLIP

RNA digestion by RNases is dependent on the RBP mode of binding and the resulting RNA accessibility for cleavage. Therefore, before I could perform iCLIP2 I had to optimise the concentration of RNase I to produce RNA fragments of an optimum size, which is 50-70nt (Figure 5.4 step 2). In a previous study, the distinct size ranges acquired from different regions of the nitrocellulose membrane show that 50-70nt of attached RNA shift the migration of protein-RNA complexes by approximately 15-20kDa (Ule et al., 2005). I used RNase I to avoid sequence cleavage bias. As expected, the lower the RNase concentration was, the wider the distribution of RNA sizes because the cleavage is random. Long RNA fragments cannot be used because sequencing (75 cycles) would fail to analyse the barcodes at the two ends of the cDNA that are included during sample preparation. We therefore want to homogenise the size of the RNA fragments to 50-70nt to minimise the incidence of unassigned reads. On the other hand, an excess of RNase may lead to short RNA fragments that cannot be mapped back to the genome unambiguously.

To optimise this for NOP2, I performed a dilution series of partial RNA digestions using dilutions of RNase I from 1:5 to 1:250 (Figure 5.7). After digesting the RNA, an IR adapter was ligated to the 3' end of the RNA to allow us to visualise the RNA on the membrane. The 1:5 dilution displays the size of the immunoprecipitated NOP2A, as under high RNase I concentrations, the protein is bound to very short and homogeneous RNA fragments, which only induces a shift of ~5kDa above the expected molecular weight. The excess of RNase enables that all accessible RNA tracts are digested reducing the "at random" effect in RNA lengths. The position of this band determines position of NOP2 with the minima RNA and setting a reference to later excise the RNA containing nitrocellulose membrane. In the experiment, the optimal digestion was observed with the 1:100 dilution, which generated a diffuse signal of protein-RNA complexes, starting close to the molecular weight of NOP2 (~100 kDa). The diffuse signal in 1:150 and 1:250 was weaker indicating there were perhaps RNA molecules longer than 200nt and increased the dispersion of the smear which therefore reduces the intensity per surface area. The reduced signal could also be because the size of protein-RNA complexes obstructed gel migration and transfer to the nitrocellulose membrane (Huppertz et al., 2014). This shows why it is important to optimise the RNase concentration to increase yield of RNA.

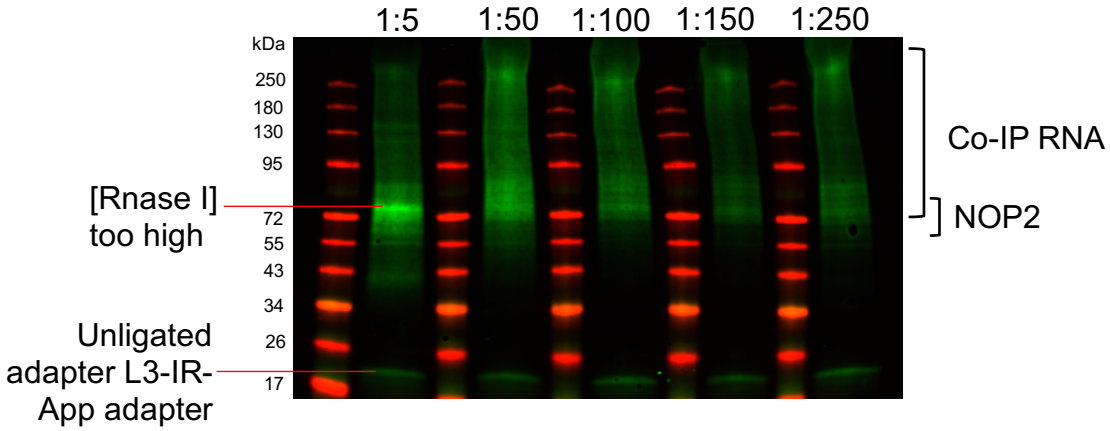

Figure 5.7: RNase concentration optimization. Immunoprecipitated NOP2-RNA complexes were subjected to a range of RNase I concentrations to partially digest the RNA bound to NOP2. An IR 3' adapter was ligated to the NOP2-bound RNA fragments then samples were separated by SDS-PAGE, transferred to a nitrocellulose membrane then imaged using a Li-Cor.

Further experiments that may have made these optimisation experiments more robust would have been to separate RNA from the excised regions of the nitrocellulose membrane by gel electrophoresis to visualise the range of different RNA fragments. This would have allowed me to see the range of different RNA lengths and pick an RNase I concentration that produced the ideal RNA length. Despite this, this experiment endorses the following:

- The size of the immunoprecipitated NOP2-RNA complex,
- The region to cut from the gel: To collect a RNAs with a range of sizes between 20-70nt, I cut a wide region corresponding to the sharp band in the 1:5 condition to ~20kDa above this.

iCLIP of NOP2 in mock and SINV-WT infected cells

Following the setup experiments, I performed iCLIP2 on mock and SINV infected samples from HEK293 cells to determine how NOP2's RNA targets change after infection. SINV-infected cells were harvested 16 hours after infection. As a control, the size matched input (SMI) samples were taken directly from the input used for the IP. SMI samples are processed through a parallel pipeline in which no protein is immunoprecipitated, but the same size-matched region of the membrane is extracted, providing background signal for all the RBPs that migrate in the same region of the gel. This helps to remove potential contaminants that may co-precipitate with the antibody.

Throughout the iCLIP protocol there are few points where quality control can be performed to see if we have successfully isolated RNA. I tested if SINV capsid and NOP2 were present in SINV and mock infected samples (Figure 5.8A). I checked the input and flow through of the immunoprecipitation (Figure 5.8B) and observed, despite fluctuations in abundance, that there was a decrease in NOP2 following IP which shows I had isolated NOP2.

The nitrocellulose membrane (step 5 in Figure 5.4) could not be blotted against NOP2-RNA complexes to avoid contaminating the samples and degrading the RNA, so from this point forward no intermediate quality controls are available until the qPCR to optimise PCR amplification of the RNA (step 8 in Figure 5.4).

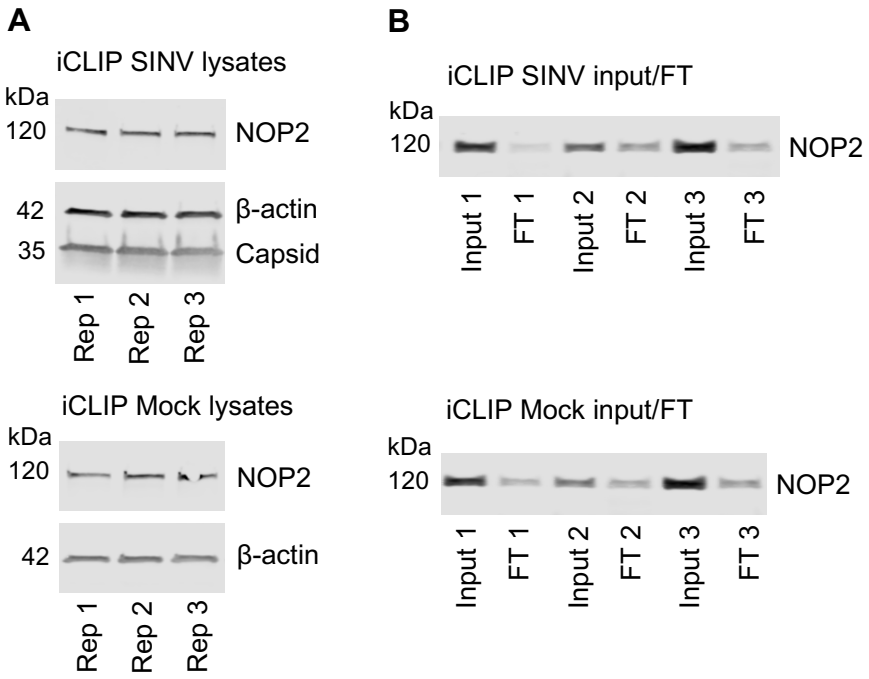

Figure 5.8: iCLIP quality control part I. A. HEK293T cells were infected with SINV or mock infected in 3 replicates and harvested 18hpi. Cells were lysed for immunoprecipitations to be performed and a small aliquot taken for Western blots. These aliquots were probed for presence of NOP2 in both conditions (infected and mock) and the presence of SINV capsid in infected conditions to confirm successful infection (top blot). B. NOP2-RNA immunoprecipitation inputs and flowthroughs (FT). Small aliquots of lysates from the input of immunoprecipitations and the flowthrough after IP were collected. Western blots were performed using these aliquots to determine if NOP2 levels had decreased in the lysates to confirm IP on the NOP2 antibody conjugated beads.

It is necessary to increase the concentration of libraries to enable sequencing, which is achieved by PCR. For this I optimised the number of PCR amplification cycles to avoid formation of secondary products or overamplification (Huppertz et al., 2014). However, it should be noted that the random barcode present in the PCR primers enables later removal of PCR amplification events. I collected a small aliquot of each SINV and mock infected reverse transcribed DNA samples as well as their sized-matched inputs, and used water as a negative control, and performed a qPCR (Figure 5.9). The required cycles reflect the performance of protein-RNA complex purification, which depends on antibody quality, UV cross linking efficiency as well as protein abundance. Boosting the abundance factor was the reason I wanted to use an overexpressed NOP2 construct. This experiment shows that iCLIP worked and I had successfully isolated RNA and transcribed it into cDNA as the sample curves amplified

many cycles earlier than the -RT (H2O) negative control (Figure 5.9). It also let us determine how many cycles are required to increase the cDNA concentrations in a PCR of the library to prepare for sequencing without overamplifying. The Cq number (the cycle number where fluorescence first rises above the threshold level) – 4 is the ideal number of cycles for PCR amplification of the library based on previous experiments.

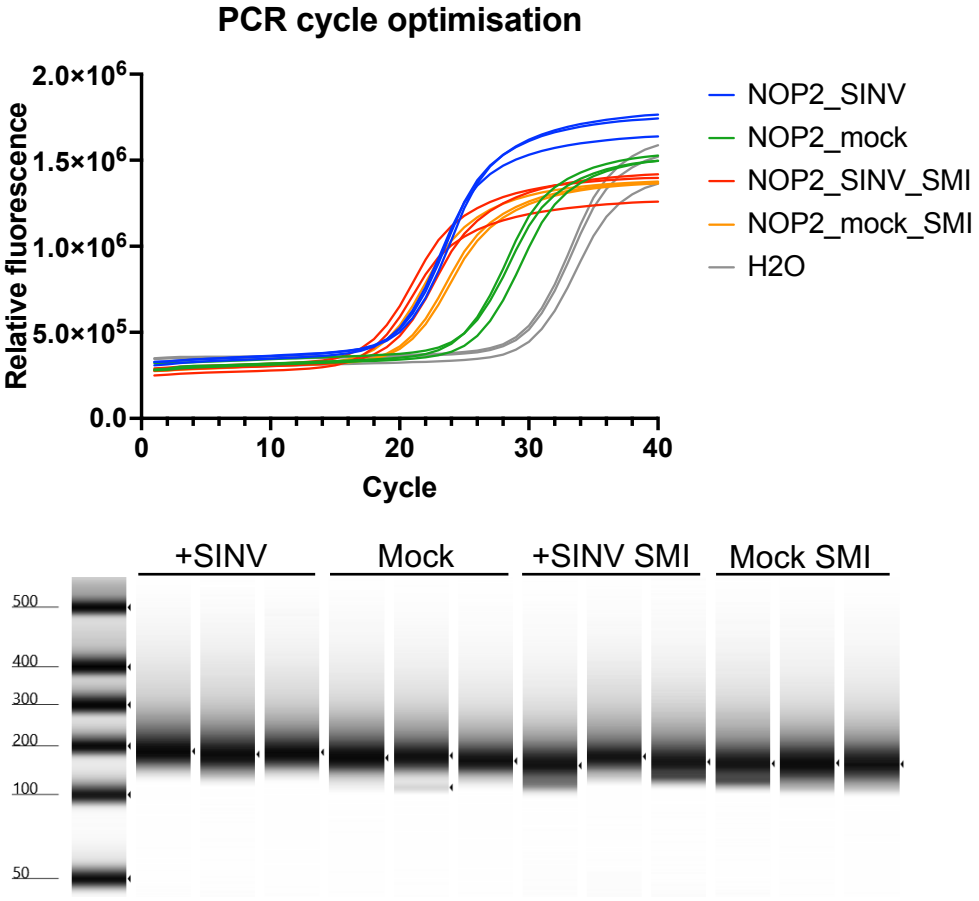

Figure 5.9: iCLIP quality control part II. Top: qPCR showing amplification curves from samples stated in legend after reverse transcribing captured RNA in the iCLIP protocol. Bottom: TapeStation capillary electrophoresis of samples before they were normalized for next generation sequencing. Numbers on left indicated size of DNA in basepairs. Arrows indicate size of isolated PCR products from library amplification and corresponds to part 8 in Figure 5.4. See text for detailed experimental descriptions. +SINV = infected samples, Mock = mock infected samples, SMI = size-matched input (background control samples) corresponding to the sample taken from.

In the qPCR, the amplification cycles for all but the NOP2 mock infected samples were the same, beginning exponential increase around 20 cycles. NOP2 mock required several more rounds of PCR, perhaps due to sample handling, I lost nucleic acid

quantity in these samples. Following amplification, the library size was determined using TapeStation gel electrophoresis (Figure 5.9) which showed us the average size of the samples were ~200bp. Whilst used to calculate the average PCR product length (which is longer than the harvested RNA because of the addition of barcodes and primers during the iCLIP protocol) and concentration of DNA in each sample so we can normalise concentrations for pooling the samples for sequencing, the TapeStation gel shows us that we have successfully amplified the cDNA library free of primers and without secondary products.

Characterising NOP2's interaction with RNA during infection

iCLIP2 data analysis was performed in collaboration with Rozeena Arif using an in-house analysis pipeline created by Drs Jeff Lee and Louisa Iselin as well as customised analysis. Sequencing data was aligned to a combined human and SINV genome annotation and 'crosslink sites' were defined as the first nucleotide before the start of each read (Huppertz et al., 2014). We used the ht-seqCLIP/DEWseq analysis pipeline to identify regions with significant enrichment of crosslink frequencies over the SMI control.

We performed a Principal Component Analysis (PCA) for sample quality control purposes (Figure 5.10). SINV SMI sample 3 was an outlier in the PCA and a close inspection revealed substantially reduced read amount, suggesting a technical issue (Figure 5.10 *left*). It also affected downstream analyses because there wasn't significant enrichment in reads for this sample. Because of this sample being technically faulty, we thus filtered it out of the analyses and repeated the PCA observing strong differences between IP and SMI samples, and between infected and uninfected settings. Replicates of each condition clustered together which demonstrates a low degree of technical variation in the experiment once the SINV SMI sample 3 is removed.

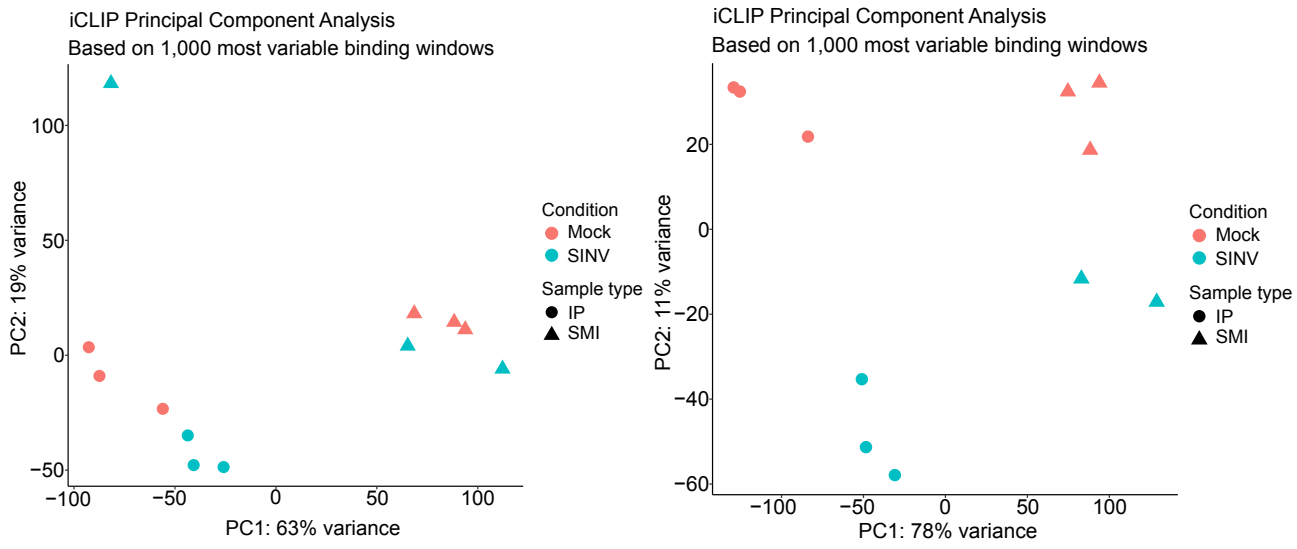

Figure 5.10: Principal Component Analysis of NOP2 iCLIP samples. The first two principal components were plotted as a 2D scatter plot. The percentage of variance described by each component is shown in the axes titles. Mock infected samples are orange; SINV infected samples are blue. Immunoprecipitated and SMI samples are shown as circles and triangles, respectively. Left: PCA with SINV SMI replicate 3 skewed the data. Right: SINV replicate 3 was removed and the distribution of sample type and condition (infected or not) became distinct.

When we compared the list of genes with NOP2 binding sites in mock and infected cells (adjusted p-value <0.01), there was a small overlap between target genes under the two conditions (Figure 5.11). These genes perhaps reflect the core interaction partners of NOP2. The staggering difference between the interaction partners between mock and infected conditions could be due to NOP2 shuttling from the nucleus under infection. Since the list of genes interacting under both conditions was so small, I manually assessed the role of each gene (Table 5.1). Of these RNA interactors, there are protein coding RNAs as well as non-coding RNAs and mitochondrial RNA. The protein coding RNAs produce proteins involved in regulating the expression of apoptosis associated genes and translational repression, histone proteins (nucleosome assembly) and a subunit of a nuclear import complex. The ncRNAs are involved in splicing and DNA damage repair. There are also two mitochondrial RNAs and a ribosomal RNA pseudogene. This indicates the overlapping roles of NOP2 is in apoptotic signalling pathways, splicing of cellular transcripts and DNA damage repair. However, it should be noted that this stage we had not assessed binding to ribosomal RNAs. The in-house CLIP processing pipelines filter out rRNA because they are multi-locus genes that are incompatible with unique mapping.

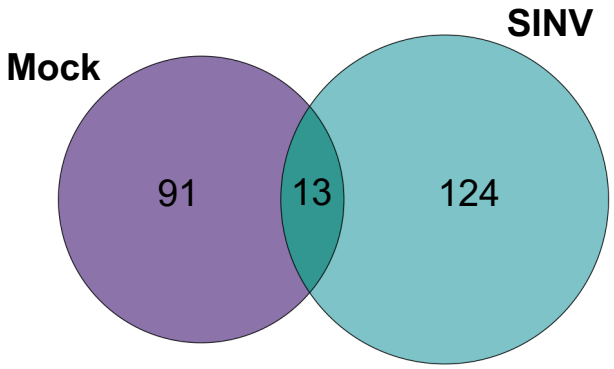

Figure 5.11: NOP2 targets in mock and infected cells. Venn diagram showing the overlap of NOP2 target genes in mock and infected cells. Target genes are defined as genes with at least one significant binding site.

Table 5.1: Functions of overlapping genes in Figure 5.11

Gene	*Type of RNA*	*Function of gene*
YBX1	mRNA	Regulates expression of apoptotic associated genes by cooperating with RNA m6A reader proteins to stabilise mRNA transcripts in an m6A-dependent manner (Chai et al., 2022). Translational repressor which can bind the capped 5' mRNA terminus (Evdokimova et al., 2006).
USP53	mRNA	Non-catalytic involved in cell cycle regulation and promotes apoptosis (Yao et al., 2022).
H1-4	mRNA	Linker histone H1 subtype 4
H1-2	mRNA	Linker histone H1 subtype 2. Histone 1-2 translocates from the nucleus to the cytoplasm following dsDNA breaks and induces the release of cytochrome *c* from mitochondria and subsequent apoptosis of the cell (Konishi et al., 2003).
KPNA4	mRNA	Karyopherin subunit alpha 4 or importin subunit alpha 3, is involved in the nuclear import of proteins. KPNA4 translocates NF-kB into the nucleus. MERS-CoV accessory protein 4b binds to KPNA4 to compete with NF-kB translocation into the nucleus to interfere with the NF-kB mediated immune response (Canton et al., 2018).
AL356488.2	ncRNA	Detailed functional information is limited.
MALAT1	lncRNA	Predominantly expressed in the nucleus (Hutchinson et al., 2007). Involved in RNA processing and regulation of alternative splicing (Mazarei et al., 2023) as well as chromatin remodelling and gene expression (Piórkowska et al., 2024).
FP671120.5	lncRNA	Involved in regulation of gene expression, however the exact mechanisms and target genes have not yet been found (Wang et al., 2020).
RNA5-8SP6	ncRNA	5.8S ribosomal RNA pseudogene.

SCARNA2	scaRNA	Small Cajal body-specific RNA 2 is involved in the regulation of DNA damage repair by facilitating efficient DNA end resection and promoting homologous recombination over non-homologous end joining (Chen et al., 2023).
SCARNA7	scaRNA	Small Cajal body-specific RNA 7 plays a role in the 2'-O-methylation of U1 and U2 snRNAs, which are crucial for the splicing of pre-mRNA (Izumikawa et al., 2019). This modification is essential for the proper function of the spliceosome.
MT-TF	tRNA	Mitochondrially encoded tRNA phenylalanine.
MT-ND6	mRNA	Mitochondrially encoded NADH dehydrogenase 6 is a subunit of the NADH dehydrogenase, which is a part of the complex I of the mitochondrial respiratory chain (de Vries et al., 1996).

The properties of NOP2 binding sites in cellular RNA were assessed to ascertain if there were general differences in NOP2 binding behaviour following infection. Most of the binding sites in each condition (mock or infected) are in protein coding genes, with a small fraction of lncRNAs, scaRNAs, pseudogenes and mtRNA (Figure 5.12A). Interestingly, the diversity of RNA bound in the infected condition is greater than mock which is compatible with the NOP2 release from the nucleolus in SINV infected cells. Notably the levels of lncRNA, pseudogenes and mtRNA increased and the levels of snoRNA, snRNAs, mt-rRNA and other RNAs became detectable in infected conditions. An interesting RNA in the infected condition is TR J gene RNA which is a T cell receptor gene – indicating that NOP2 may switch to regulate the processing, stability and/or translation of RNAs involved in an antiviral response. The increase of snRNA and snoRNA, which are involved in the processing of pre-mRNAs and RNA post-transcriptional editing, respectively, could support the role of NOP2 being involved in the expression of antiviral genes. The levels of mt-tRNA and mt-rRNA increase in infected conditions which suggests levels of cytoplasmic NOP2 have increased. The decrease in binding to protein coding RNA and an increase in other RNAs, suggests levels of NOP2 do not increase in infection, but there is a redistribution of its activity.

Among the RNA of protein-coding genes that NOP2 interacts with, half of the binding sites were in introns and >25% in coding sequences (Figure 5.12B). This is similar to the average proportion found across RNA binding proteins globally (eCLIP superset in ENCODE). There is a slight decrease in intron binding in infected conditions which is

consistent with NOP2 shifting from the nucleus to the cytoplasm in infection, however the change is only partial. NOP2's pattern of binding to transcripts does not notably change between mock and infected conditions when the signal peak distribution across the gene is plotted (Figure 5.12C). There is a slight increase in the binding to coding sequence, which may reflect a role for NOP2 in regulating transcripts, perhaps its known role in methylation of cytosines (Liao et al., 2022). It should be noted that these results are for cellular RNA and binding to viral RNA is discussed later.

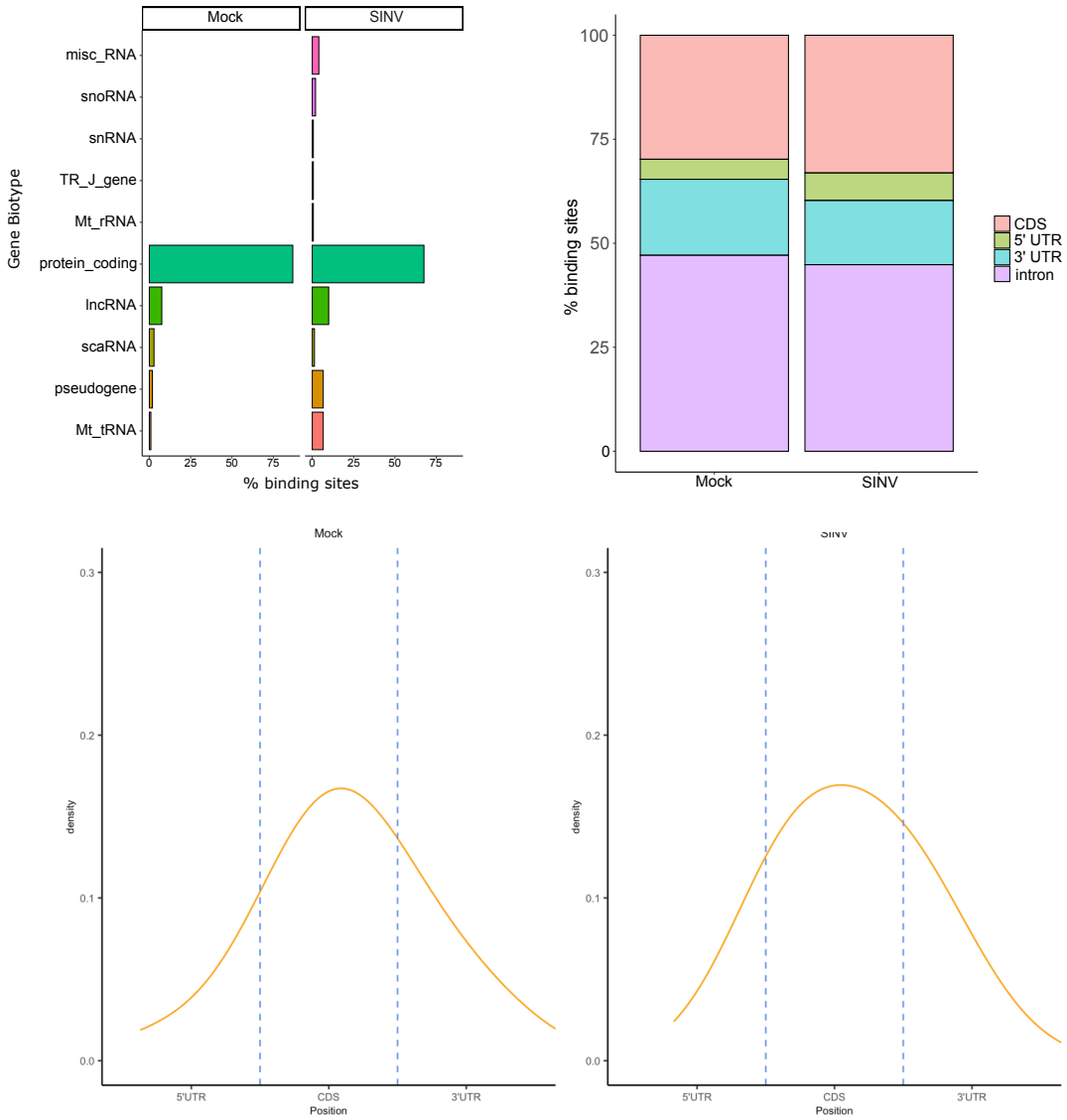

Figure 5.12: NOP2 primarily binds to protein-coding mRNA.
A. Bar plots displaying the proportion of different RNA biotypes that are targets of NOP2 in mock and infected conditions.
B. Stacked bar charts indicate distribution of NOP2 binding sites within each transcript feature of protein-coding genes.
C. Meta-gene profiles of binding site distribution across 5' UTR, CDS and 3'UTR.

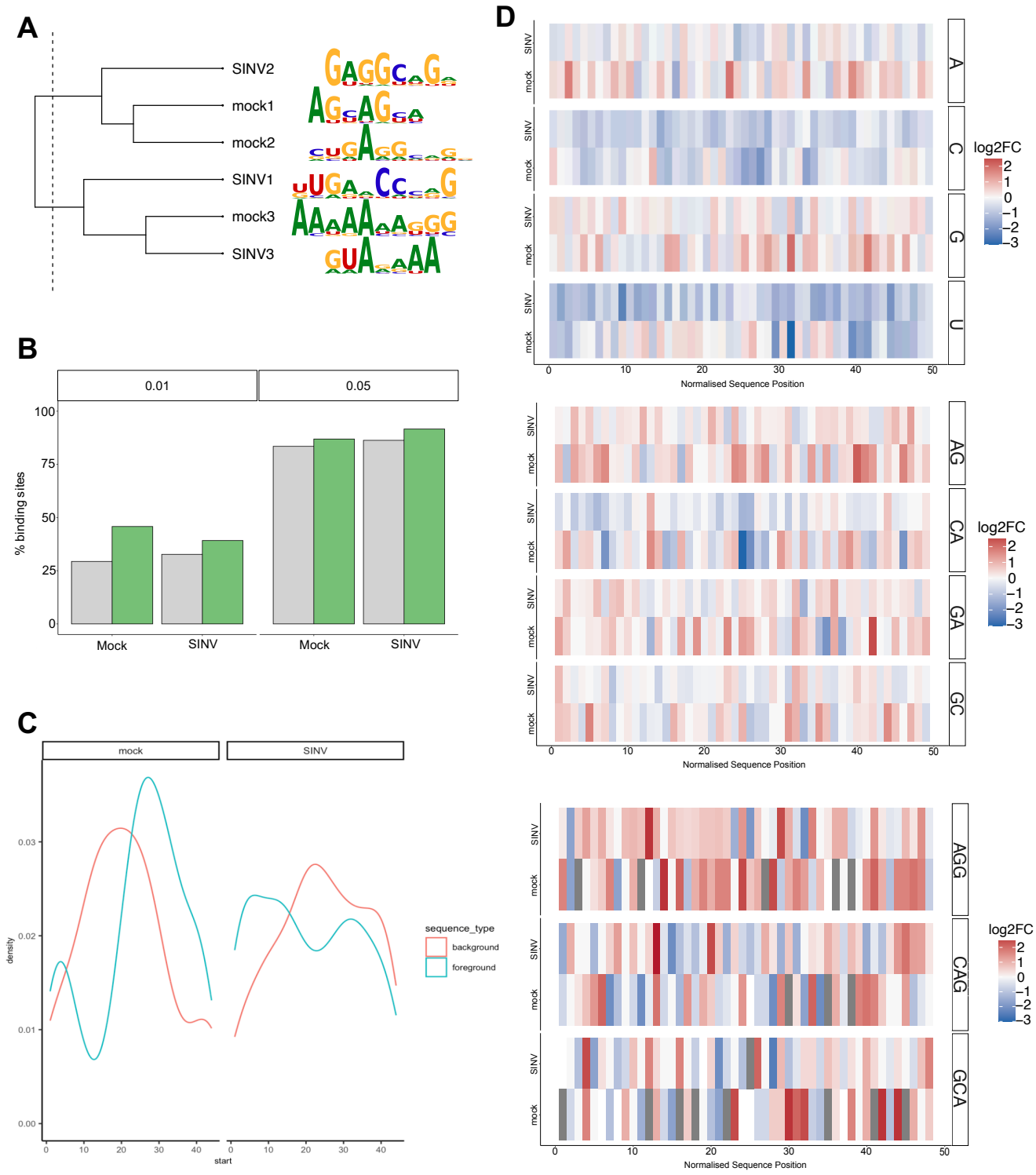

Figure 5.13 NOP2 binds to purine abundant regions.

A. Hierarchical clustering of the top three enriched motifs in mock and infected binding sites. Motif enrichment was done on 50nt windows centred around the signal peak of each binding site. Enrichment was over gene and gene region-matched sequences generated for each binding site and calculated using STREME from the MEME package.

B. Percentage of input sequences containing at least one motif at two motif similarity thresholds (0.01, 0.05). Percentage of binding sites is represented by the green bars and percentage of background sequences by the grey bars.

C. Profiles of motif start site distribution in the 50nt windows of binding and background sequences at a motif similarity threshold of 0.05. Red lines depict the background sequences and blue lines show the NOP2 binding sequences as 'foreground.'
D. Heatmaps of the occurrence of nucleotide bases in NOP2 binding sites. Increased occurrence is represented as red on the log2 fold change scale, and blue as decreased. Top: nucleotide, middle: di-nucleotide, bottom: tri-nucleotide.

We next sought out whether NOP2s binding specificity changes following infection. To do this we selected a 50-nucleotide window for each binding site in cellular RNA, with the binding site signal peak as the window's centre, and performed a motif enrichment analysis for each replicate using STREME to search for enrichment over a set of gene and gene (matched) background sequences (Bailey et al., 2015). Hierarchical clustering of the top 3 motifs allowed us to see if there were multiple different motifs enriched. The motifs in cellular RNA targets in mock and SINV infected samples cluster together, implying that there is not a change in binding specificity following infection (Figure 5.13A). In mock and infected conditions, the proportion of sequences containing a motif over background matched sequences was low (Figure 5.13B), this is also reflected by the large variation in the motif composition where the only apparent signature was the enrichment for purines. When the threshold was increased to p=0.05, the percentage of binding sites containing a motif was greater than 80%. However, this was not substantially above the occurrence rate in the background, probably because the low sequence definition of the motif. From this it does not seem that NOP2 has a specific binding site motif, beyond preferring purine-rich regions on cellular RNAs. To confirm this, we assessed the distribution of motifs across the normalised 50nt window (Figure 5.13C). In background sequences, there is a peak at the centre of the sequence, whereas in NOP2 binding sites, there are two peaks at the start and mid-to-end of the sequence. This suggests that crosslinking is not frequently occurring at the site of the motif but in its proximity. This approach did not identify a conserved binding motif, but it showed that NOP2 seems to have a preference of AG enriched regions (Figure 5.13A). It also showed there is a conserved adenine binding residue in the middle of putative motifs in mock infected cells, however this signal isn't as strong in SINV infected samples. To explore this further, we assessed nucleotide frequencies in the binding sites which showed that there is a slight preference for purine rich sequences, with levels of cytosine and uracil being lower, particularly in infected samples (Figure 5.13D-top). In another approach to find a short motif, we then

assessed di-nucleotide and tri- nucleotide frequencies. The level of binding to AG or GA was slightly higher than cytosine containing control di-nucleotides. In three tri-nucleotides, AGG, CAG and GCA, binding in the pyrimidine-free AGG was more likely than the latter two. Overall, from the data there is not a clearly definable NOP2 binding motif. In agreement with this, we can see that there is a slight enrichment of AG sequences (Figure 5.13D). A binding motif for NOP2 has not been defined previously so perhaps this shows that there is not one. However, this could reflect a broad range of RNA binding activity by NOP2, which has been previously described (Liao et al., 2022). Perhaps its binding specificity is defined by non-coding RNAs that target it to a specific gene or site or it could be defined by protein interaction partners, rather than a specific sequence.

NOP2 is a m^5C-methyltransferase with known methylation activity in ribosomal RNA (rRNA). The lack of enrichment in cytosines in putative motif recognition sites was puzzling. As a quality control in the NOP2 iCLIP analysis, I decided to investigate if we recapitulated known binding of NOP2 to ribosomal RNA. Human rRNA is transcribed by RNA Pol I as a long precursor transcript (47S), which is cleaved and modified through a series of steps to generate the mature rRNAs (18S, 28S and 5.8S) (Drygin et al., 2010). 5S is transcribed separately by RNA pol III (Ciganda et al., 2011). Aligning the iCLIP reads to the 47S precursor rRNA showed that NOP2 has a similar binding pattern to the 5' external transcribed spacer (5'ETS) region, which includes the 01/A', A0 and 1 endonucleolytic cleavage sites for 47s processing (Figure 5.14). Additionally, there is a peak on the 28S rRNA that maps to C4447 which corresponds to the predicted NOP2 methylation site based on data from the yeast orthologue and the recently defined site in human 28S rRNA (Sharma et al., 2015; Liao et al., 2022). These binding enrichments recapitulate pervious data and are a good control that we're capturing known properties of NOP2 RNA interaction. The appearance in mock and infected suggests only a fraction of NOP2 performs the antiviral activities we have hypothesised and agrees with the partial re-localisation of NOP2 in infected cells (Figure 5.14). In addition to these previously characterised bindings of NOP2, we saw a highly enriched peak in the 5.8S rRNA, as well as others in the 18S region and the boundary between Internal transcribed spacer 2 (ITS2; between 5.8S and 28S) and 28S. Interestingly, the two peaks in 18S and 5.8S are cytosines, so we have identified more regions of potential methylation. We then assessed if there is a binding motif on

rRNA for NOP2. Again, performing a motif enrichment analysis on rRNA for each replicate using STREME (Figure 5.14B), we did not find a clear binding motif, but cytosine appeared more enriched in potential rRNA motifs than for all cellular RNA, suggesting a role in m^5C methylation (Figure 5.13A).

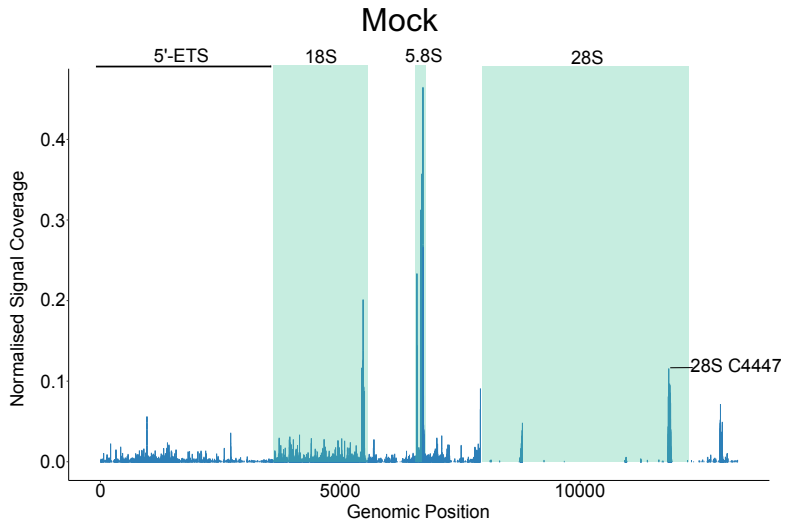

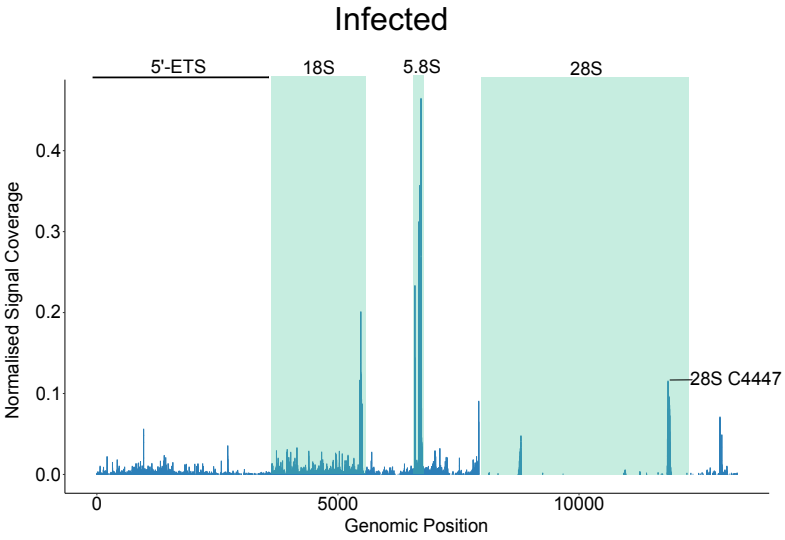

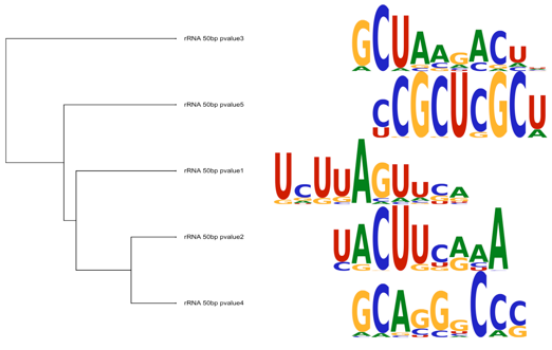

Figure 5.14: NOP2 binding profiles on 47S precursor ribosomal RNA (45S-pre-rRNA). A line plot of NOP2 signal from iCLIP crosslinked sites on 45S-pre-rRNA. The density of crosslinked sites at each position is a percentage of total signal across the genome. Signal coverage was normalized by subtracting SMI from IP to give the NOP2 binding profile. B. Hierarchical clustering of the top three enriched motifs in ribosomal binding sites. Motif enrichment was done on 50nt windows centered around the signal peak of each binding site. Enrichment was over gene and gene region-matched sequences generated for each binding site and calculated using STREME from the MEME package.

To further assess how rRNA binding differs between infected and mock samples, we plotted the number of reads aligning to rRNA and to all other RNAs (Figure 5.15). In these bar blots, we can see a high level of rRNA binding compared to all other RNA in mock IP samples, and their respective SMI samples. In infection, the percentage of rRNA reads decreases compared to mock and the number of reads mapped to other RNAs increases. This shows that there is a clear change in the binding targets of NOP2 after infection which is consistent with the dissolution of the nucleolus and a redistribution of NOP2 (Figure 5.2).

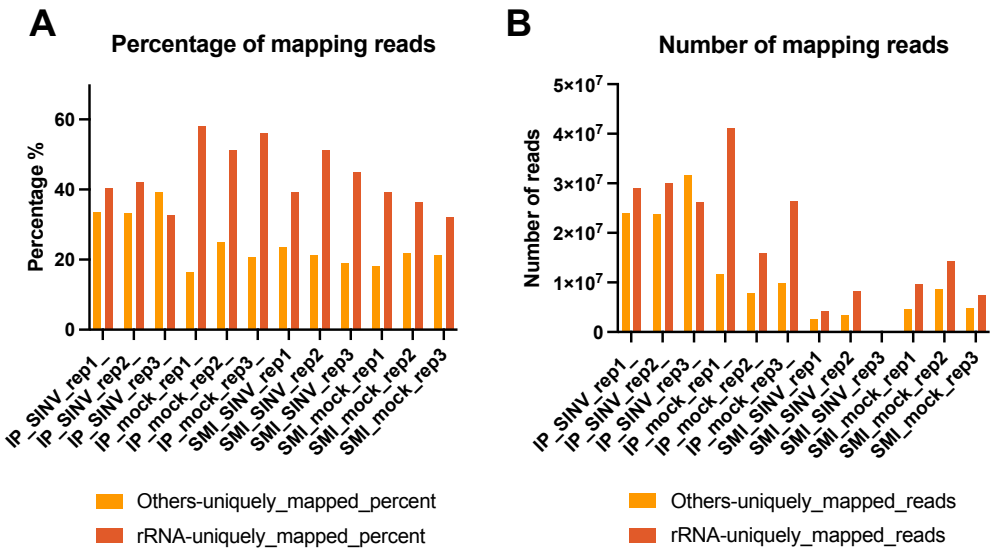

Figure 5.15: Number of reads mapping to rRNA compared to all other RNA. A. Proportion of reads represented as a percentage of each sample. B. The raw number of reads mapping to rRNA or other RNA per sample. IP = immunoprecipitation, SMI = size-matched input (background control samples) corresponding to the sample taken before IP, SINV = infected samples, Mock = mock infected samples, rep = replicate (all conditions have 3 biological replicates). Red bars = NOP2 binding rRNA, orange bars = NOP2 binding off all other RNA that is not rRNA.

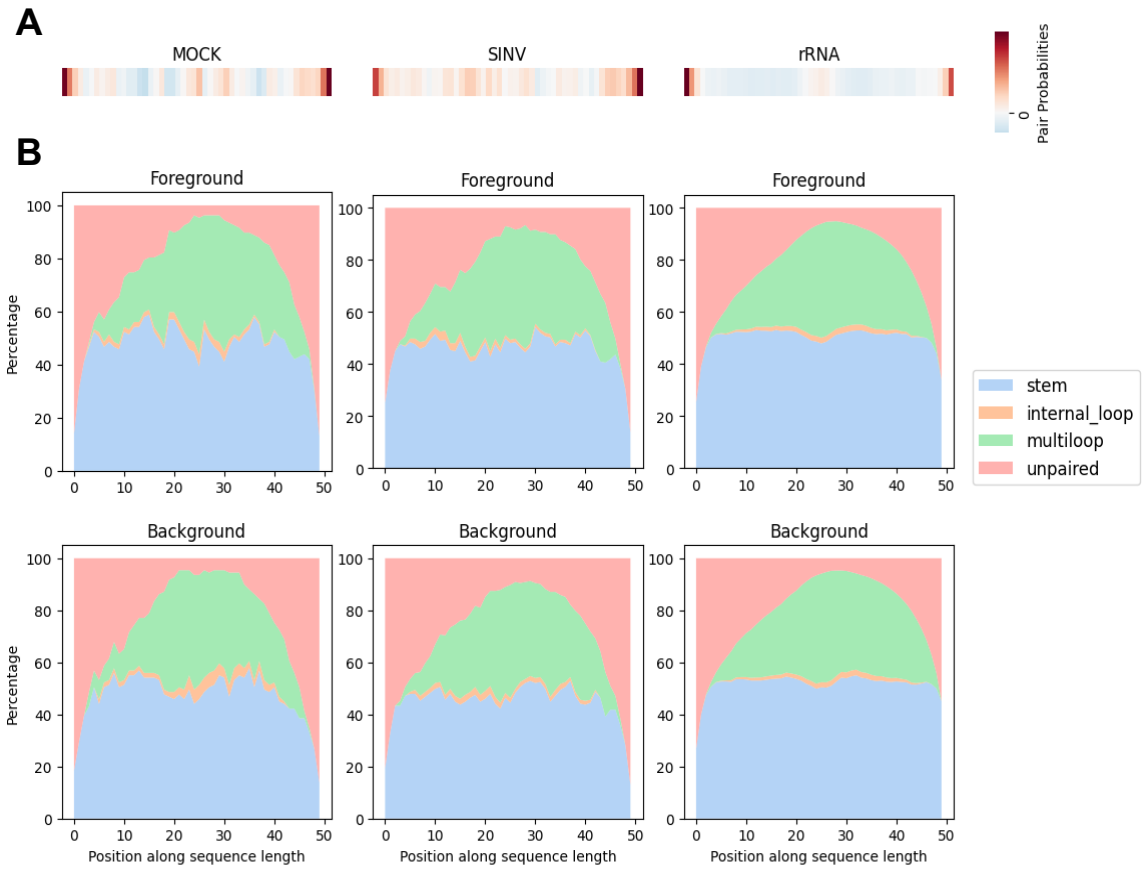

Figure 5.16. Secondary structure preferences of NOP2. A. Secondary structure likelihood calculated by RNAfold. Heatmap of the % of paired nucleotides in NOP2 binding sites versus motif prediction background. Binding sites were defined as binding site peak with 25 nucleotides on either side. The scale for these heatmaps is in line with the x axes on the graphs in B. B. Stacked bar chart plotting percentage of each structural feature predicted by Forgi at each nucleotide position in foreground and background sequences.

We then wanted to understand that since NOP2 does not have a motif preference, does it have a secondary structure preference. To this end we used RNAfold to fold each input sequence used for motif prediction, i.e., binding site peak with 25 nucleotides on either side, for mRNA and rRNA. This indicated that NOP2 has no preferential binding regions in mRNA since the central regions (of the heatmaps at the top of the figure) are not enriched in paired nucleotides, nor unpaired nucleotides (Figure 5.16A). This was supported by using the forgi package to see what features they were probable to belong to, which also showed no absolute preference for a type of structure as there was no clear differences from random background sequences (Figure 5.16B). In contrast in rRNA, there was a clear enrichment of paired nucleotides at the binding site in the heatmap from RNA fold, indicating NOP2 preferentially binds

to structured regions in rRNA (Figure 5.16A). However, there was no clear preference for specific structural features compared to background sequences (Figure 5.16B). Overall, these structural analyses suggest that after the nucleolus disassembles and NOP2 redistributes, it does not have a specific function, and that most of its binding partners outside of rRNA or vRNA are random.

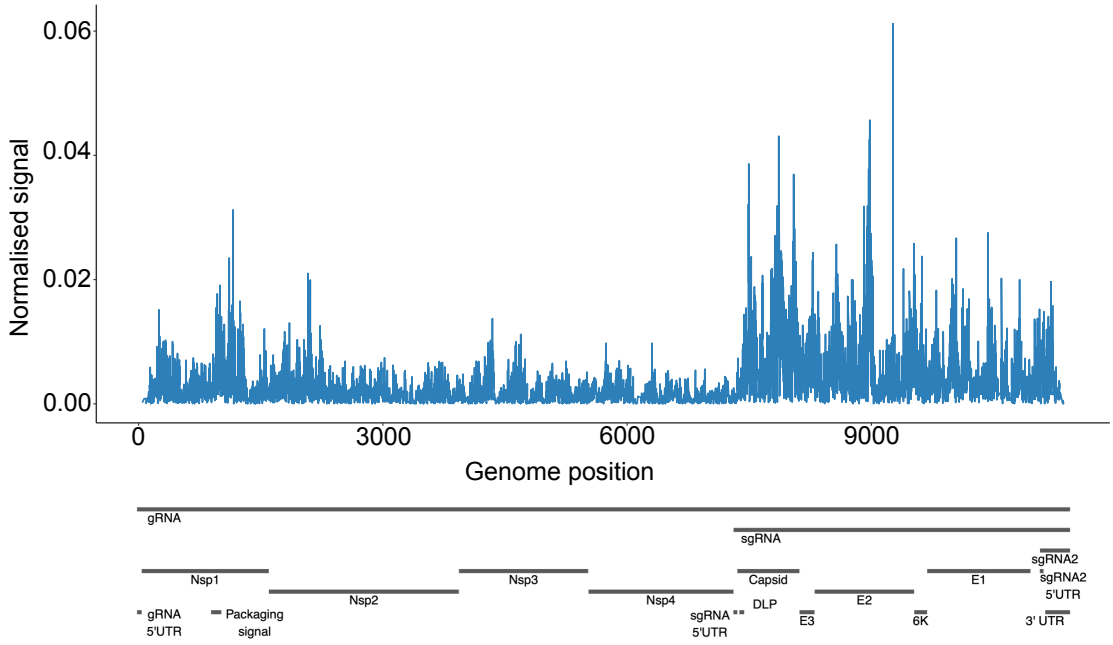

Figure 5.17: A line plot of NOP2's binding profile on SINV RNA. The density of crosslinked sites at each position is a percentage of the total signal across the genome. Percent signal at each position in the SMI was subtracted from IP to give the NOP2 binding profile (normalised signal).

The most significant difference between mock and infected samples is NOP2 binding to SINV RNA. So far, all the analyses have explored the differences in binding to cellular RNA between the two conditions. Looking at the signal pattern on SINV RNA, we can observe a NOP2 pattern of binding (Figure 5.17). NOP2 does not bind to a single site within the viral genome, but multiple sites throughout viral RNA. There is a strong peak in the 5' regions of the genome where Nsp1 is encoded. Moreover, there are several sites mapping to the sub-genomic region. Note that overall signal is higher at the last 1/3 of the genome because 1) sub-genomic and genomic RNA overlap at this region and 2) because the sub-genomic RNA is higher in abundance than genomic RNA in SINV infected cells. This shows that NOP2 interacts with vRNA in the cytoplasm during infection and has no preference for genomic or sub-genomic RNA.

Discussion

In CRISPR knockout screens in the previous chapter, I identified several RNA modifying enzymes that may have an impact in viral infection, some solely on individual viruses, and others on several viruses. A protein which had an effect on multiple viruses was NOP2. Knockdown of NOP2 enhanced viral replication in the cytoplasmic RSV, hMPV and SFV. Orthogonally, NOP2 was found to be one of the three hundred RBPs that interact with SINV (closely related to SFV) viral RNA using a proteomic approach called viral RNA interactome capture (vRIC). Many of these RBPs were nuclear proteins and they were shown by nucleo-cytoplasmic fractionation coupled to proteomics that they shuttle to the cytosol in SINV infected cells (Kamel et al., 2024). With this base of finding NOP2 knockdown to increase viral infection, and data supporting its interaction with viral RNA, I set out to characterise its role in viral infection more clearly.

By performing functional assays, we found that NOP2 effectively quells SINV infection. After 24h of infection, levels of NOP2 become detectable in the cytoplasm by western blot. This was further backed up by confocal microscopy whereby NOP2 localised to SINV ROs in the cytoplasm at 24hpi, whereas a control nuclear protein (ZC3H11) did not translocate ruling out an increase in general nuclear permeability. By using siRNA and CRISPR knockdown, I found that SINV capsid levels increased when NOP2 was depleted, indicating an increase in viral fitness. I found that virus expression increased over a non-target control guide when I infected the CRISPR KD cell lines and recorded the growth of two fluorescent chimeric SINV. However, a guide that caused an almost full knockdown had limited effect in SINV infection when compared to the non-target control, and I reason this is likely due to NOP2 ablation being toxic to the cell and reducing the cell's ability to support infection. Dr Wael Kamel analysed levels of SINV RNA by RT-qPCR and found that levels of SINV gRNA increased on knockdown of NOP2 by siRNA. He also found that virus production and release from these knockdown cells increased by analysing viral titre in the supernatants by plaque assay (Kamel et al., 2024).

Having demonstrated the shift of NOP2 to the cytoplasm from the nucleus under infection and that it has antiviral activity against SINV, I wanted to characterise what

its role in the antiviral response is. Since it is an interactor of SINV RNA, and it has methylation activities (Bohnsack et al., 2019), I wanted to characterise if there was a change in its RNA targets under infection and characterise its interactions with RNA in more depth. For this I performed iCLIP. I found that NOP2 indeed does interact with both positive stranded SINV RNAs, genomic and subgenomic, and has many discrete binding sites across the vRNA (Figure 5.17). I found NOP2s binding specificity difficult to characterise. Probably because it likely lacks specificity and binding might be promoted by deposition through protein-protein interactions in analogy to the exon junction complex (Hentze et al., 2018). However, we noticed that NOP2 has a preference for purine-rich regions, and that those sites within rRNAs also contain "methyl-able" Cytidines (Figure 5.13). CLIP methods have a general bias for crosslinking at U nucleotides (Hafner et al., 2021). The low level of Us in the binding motifs detected indicates that the dataset is of a good quality, however, it also explains that crosslinking tends to occur outside the purine-rich motif itself perhaps due to the presence of incidental Us. The in-house CLIP processing pipelines filter out ribosomal RNA because they are multi-locus genes that are incompatible with unique mapping. To assess the quality of the NOP2 iCLIP dataset, in a separate pipeline, we tested NOP2's interaction with rRNA because it has been characterised as a critical factor of ribosome biogenesis in humans and yeast (Liao et al., 2022; Sharma et al., 2013). We observed that rRNAs are the main target of NOP2, and that it binds at the 5' ETS region of 47S rRNA as well as at the C4447 of 28S rRNA, which are known NOP2 binding sites. In addition, we found a highly enriched peak in the 5.8S segment (Figure 5.14) that was not identified in a previous CLIP study of NOP2 (Liao et al., 2022). A study performed a miCLIP-seq (methylation individual-nucleotide-resolution crosslinking and immunoprecipitation-sequencing) approach to identify methylated targets of NOP2 in human cells (Hussain et al., 2013). They used a mutant version of NOP2 with a catalytic cysteine mutated to alanine which results in longer binding times on the RNA due to the lack of catalytic activity. They also found binding to the 5' ETS region of 45S rRNA and proved that this binding is non-catalytic. They did not find an enriched peak around the 5.8S segment, however we found it separately in infected and mock infected samples. Moreover, our protocol employs an enhanced experimental pipeline that enables detection of binding sites bound with lower propensity. When we searched for a binding motif on rRNA, a clear sequence motif was not detected (Figure 5.14), however a cytidine residue was enriched in each

predicted site, which could suggest that NOP2's binding activity on rRNA is driven by its m^5C-methyl transferase activity, whereas the binding of other cellular RNA is not driven by its catalytic properties.

We found NOP2s binding targets change hugely following infection (Figure 5.11), with a shift from nuclear and nucleolar targets to cytoplasmic targets. This could reflect NOP2s relocation to the cytoplasm, however, as a large proportion remains nuclear under infection (Figure 5.1), it is expected that the shift towards cytoplasmic RNA should not be complete. I suspect that since we filtered out rRNA in the initial data analysis, NOP2s primary roles in ribosome biogenesis and binding to other transcripts is residual in non-infected cells. Despite this, the range of RNAs bound after infection increased, including ncRNAs and mt_RNAs (Figure 5.12A). The appearance of mitochondrial RNA provides more evidence that NOP2 is nuclear under these conditions. It could be the case that NOP2 dictates RNA function in the nucleus, demonstrated by its essential role in editing rRNA, but RNA can also riboregulate NOP2 which influences its shift to the cytoplasm under infection (Iselin et al., 2021).

RBPs can also exhibit preferences for specific structural motifs on RNA, in combination or independent of sequence specificity. Since we did not identify a specific NOP2 binding motif, I considered that perhaps NOP2 exhibits a structure binding preference. Thus, we assessed the likelihood that the crosslinked sites identified in iCLIP are predicted to be in a structured region. This identified no clear preference for RNA structure in cellular RNA, however we putatively identified that the crosslinked binding site in rRNA is in a paired nucleotide (Figure 5.16A). Further analysis of the validated binding sites on rRNA and putative binding sites on the viral RNA should be performed to determine if there is any structural preference compared to other cellular RNAs.

Where do we go from here? We have established some core results of NOP2 being antiviral and its direct interactions with RNA. To establish a working model of NOP2s antiviral function, there are some outstanding pieces of the puzzle left to figure out. How NOP2 interacts with pulled down RNA would be a first point of interest: is it due to methylation or another RNA binding property? This could be achieved in several different ways. Firstly, we could do an RNA bisulfite sequencing method in cells

normally expressing NOP2 and depleted by CRISPR and/or siRNA. This technique works by treating RNA with sodium bisulfite and then sequencing. This identifies methylation as methylated cytosines are bisulfite resistant, whereas other cytosines are deaminated to uracil (Li & Tollefsbol, 2011). This could be done in infected and non-infected samples to also establish if viral infection influences methylation. An analogous experiment to this would be to mutate the catalytic core as in Liao et al., 2022, and determine, via miCLIP with antibodies against m^5C, if NOP2 crosslinks on RNAs in the cytoplasm, including viral RNA, following infection to see if it is methylating its targets under infection. If the methylation activity is not involved, we could mutate NOP2s RNA binding domains and see how this impacts infection, as in Figures 5.1 and 5.3, and if it still relocates to SINV ROs in the cytoplasm as in Figure 5.2. Finally, it would be interesting to establish the exact RNA targets of NOP2 in the nucleus and cytoplasm following infection instead of the whole cell as in this chapter. I suspect that a fraction of NOP2 is cytoplasmic under normal cellular conditions due to the presence of mitochondrial RNA in mock infected iCLIP samples (Figure 5.12), however if we performed iCLIP as in this chapter but fractionated the cells after UV crosslinking (step 1 in Figure 5.4), we could establish the RNA targets in both compartments to better understand how much NOP2s activity changes following infection. Finally, it would be good to understand if these effects are replicated with other viruses, since I found it is putatively antiviral against several RNA viruses in the screens in Chapter 4.

In conclusion, in this chapter I have presented the results of functional assays of NOP2s antiviral activity and RNA interaction analyses for NOP2. These results indicate that NOP2 acts antivirally and alters its RNA interaction partners following infection. By exploring these altered interactions, we can begin to create investigable hypotheses of what its antiviral function may be.

Chapter 6 Discussion and Conclusion

The overall aim of this PhD was to increase our understanding of RNA modifications in RNA virus infection. For this, I created an arrayed CRISPR/Cas9 knockdown library to test the role all known human RNA modifications in RNA virus infection. After identifying a putative antiviral candidate effector against several cytoplasmic replicating viruses, I proceeded to characterise the mechanism of the discovered RNA modifying enzyme. The data in this thesis demonstrates the utility of arrayed CRISPR/Cas9 screening to identify new proteins involved in virus infection and how it can be used as a discovery-based platform to understand more about the complex interplay of virus and host in infection.

Viruses, as obligate intracellular parasites, rely heavily on their close interactions with host cells to replicate. To have a successful lifecycle, a virus must subvert the host machinery for its own use, while avoiding inducing an immune response in the cell. One mechanism of inducing an IFN response is the sensing of foreign nucleic acid, whether that be through unusual nucleic acid structure or specific motifs on viral RNA and DNA. In the resting cell, all post transcriptional modifications of cellular RNA play an important role in the life cycle of RNA, and these modifications in turn act as a signal in the cell to avoid triggering an immune response. In the eternal battle of viruses and their hosts to adapt and counter adapt to overcome each other, viruses have evolved intricate mechanisms to avoid mounting an immune response. One such method is to mimic the cellular landscape of RNA to avoid being sensed by the host. To do this, viruses hijack cellular RNA modifying enzymes to ‘decorate’ their genomes. These modifications also serve a functional purpose in viral RNA and can enhance processes like translation or viral mRNAs. However, in the co-evolution of virus and host trying to counter each other, the host cell can also methylate viral RNA to initiate an innate immune mechanism to restrict viral growth. At the start of my PhD there had yet to be a comprehensive assessment of the role of RNA modifications in the landscape of virus infection. To dissect this, we decided to experimentally screen all

known human RNA modifying enzymes against a selection of RNA viruses to elucidate the impact of RNA modifications on infection.

In Chapter 3, I described how we created a CRISPR knockout library targeting all known human RNA modifying enzymes based on Jonkhout et al., 2017. Creating a screening platform comes with many hurdles and I managed to optimise several facets of using the library to successfully probe the impact of knocking out RNA modifying enzymes on RNA virus infection. A key piece of knowledge we gained early on, is to ensure there is a spread of guides targeting a gene to avoid 3' guides that do not disrupt gene expression. I then optimised a use of the library that we described as 'Incoming Screens.' This simply questions how well a virus establishes infection in a cell in the presence of a knockout. The utility of the arrayed approach meant that as we had physically set a barrier between the conditions of each guide, the output of the screens was immediately interpretable as a measure of a virus establishing an infection, since we used fluorophore expressing viruses for visualisation. A way that this could have perhaps been improved would be to measure the increase in the intensity of the fluorescence to determine rates of infectivity as opposed to number of fluorescent cells at the end point of infection. This would allow us to observe how quickly a virus can establish an infection, and if the block to replication caused by the gene of interest is earlier or later in infection. Measuring fluorescence intensity was a very useful approach in the early stages of characterising a 'hit' (Chapter 5). In the future the utility of the library can be expanded; supernatants of cells at the end of a screen could be harvested and used as an assessment of viral output by measuring the titre in a follow up screening pipeline.

I used the CRISPR screening platform against several viruses (IAV, RSV, hMPV and SFV). The success of the screens can be demonstrated by known effectors in IAV infection (the METTL3/METTL14/ALKBH5 proteins) appearing as 'hits' in the screens. We only found one 'universally' acting enzyme in all virus infections - RRP8. This protein is involved in ribosome biogenesis. In the future it would be interesting to determine if it appears in the screens against other viruses, and to characterise its role in infection. It may be that the knockdown is deleterious to the cell and knockdown impairs cellular function so the virus can dominate. However, our method of transiently transducing cells with the CRISPR library, means residual protein will remain that can

perhaps maintain the function the cell requires to reduce cellular toxicity. Future work for characterising hits could look at the impact of overexpressing the gene and see if this heightens the anti- or pro-viral effect we have found *e.g.* does overexpressing RRP8 ablate the infection of the viruses in Figure 4.6? We could also investigate where the modifications are imparted on the viral RNA and if there are consensus sequences, which if conserved across multiple viruses, would be a huge discovery. Other experiments we could follow up with would be to mutate the active site of the RME and see if this has the same impact as knocking the enzyme out.

A key consideration in characterising a hit is where the virus replicates in the cell (cytosolic or nuclear) and the location of the RME. This was counteracted when I established that NOP2 shuttles from the nucleus to the cytoplasm during SINV infection, however NOP2 and TRMT61 knockdown both increased replication of cytoplasmic replicating viruses only. Another consideration in the impact of an RNA modification on virus infection, is that the modification may change the host epitranscriptome which can result in pro and antiviral effects for the virus. This screening platform does not distinguish between genes that act directly on viruses from those that serve a regulatory function in the cell, for example, NSUN2 is known to methylate cellular RNA which impacts IAV infection, however METTL3 methylates IAV RNA directly (Zhang et al., 2022; Courtney et al., 2017). Changes in the epitranscriptome therefore need to be considered when following up a hit, as some studies relatively ignore the impact of this on infection and focus on viral RNA.

I decided to follow up NOP2, which was a putative antiviral candidate identified in the CRISPR screens. Concurrently in vRIC experiments, NOP2 was found to be antiviral against a range of alphaviruses (Kamel et al., 2024). NOP2 has a C5 methyltransferase (m^5C) involved in ribosome biogenesis, and its role changed after infection. Interestingly previous reports have demonstrated that NOP2 methylates viral RNA for an antiviral effect (Kong et al., 2020). I established that it is an antiviral effector in viral fitness assays involving knockdowns, measurements of SINV capsid production in a knockdown background, and the rate of infection when NOP2 was knocked out. We also demonstrated that NOP2 shuttles from the nucleus to the cytoplasm after infection, and that this is necessary for its antiviral activity. We utilised iCLIP to enhance our understanding of NOP2 RNA interactors before and after

infection, to characterise its change in activity. The utility of CLIP-based methods in understanding vRNA interaction dynamics has also been demonstrated for HIV-1 (Garcia-Moreno et al., 2023), IAV (Lee et a., 2017; Williams et al., 2018) and SARS-CoV2 (Wickenhagen et al., 2022). We established that NOP2 does bind vRNA and we successfully recapitulated its binding activity to ribosomal rRNA (Liao et al., 2022). iCLIP as a method for understanding RNA modifications is a very low throughput, time and resource intensive protocol. A downside of the CLIP analysis is that it filters out ribosomal RNA as they are multi-locus genes that are incompatible with unique mapping. This led to problems in characterising the binding activities of NOP2. Looking to the future of characterising RNA modifications on viral, and cellular, RNA, RNA nanopore sequencing would be a more appropriate approach. It has been successfully used to map the m^6A profile in vivo in yeast and human RNAs, as well as in targeted non-coding RNAs (Leger et al., 2021). Furthermore, some groups have successfully utilised it to map modifications of alphaviral RNA (Tan et al., 2024) and other groups have characterised the change in the host epitranscriptome on IAV infection (Wang et al., 2024).

In the story of NOP2 we still need to investigate the mechanistic basis of what it does to exert its antiviral effects. We established that it binds viral RNA in the iCLIP experiments and that this correlates with a reduction in its binding of rRNA. But investigating what this binding of viral RNA does is the next question. Does it methylate viral RNA which recruits antiviral proteins, or is its antiviral properties not reliant on its catalytic properties? Does it instead interact with proteins that bring about the destruction of viral RNA or does it bind non-specifically and block transcription and translation of RNA? This could be addressed by sequencing experiments to verify if the vRNA is methylated by methods such as bisulfite sequencing covered in the discussion of Chapter 5 or nanopore sequencing discussed above. Protein interacting partners could be identified by performing pull down experiments or proteomic experiments. Since NOP2 demonstrated antiviral activity in the CRISPR screens in Chapter 4, it would be good to return to the viruses used in the screens, and other RNA viruses, to establish if the antiviral effect is observed against many RNA viruses.

Beyond NOP2, there are many possibilities for where this project can go next, and the RNA modifying enzyme CRISPR screening platform can be used as the basis for many

projects. RRP8 had effects against all the viruses investigated in Chapter 4 so following up the characteristics of this protein could be a whole project. Furthermore, screening many other viruses and identifying if there are other viruses that RRP8 and NOP2 affect would be interesting, but also to identify other novel RME effectors in other viral infections. I only investigated one nuclear virus (IAV) in the screens and several cytoplasmic viruses. Determining if there are proteins that only affect nuclear viruses would be interesting too. The library is documented, and analysis pipelines are established, so it will hopefully be used by other researchers to uncover new proteins and contribute to the essential knowledge of virus infection.

Understanding the mechanistic basis of viral infections is crucial for advancing medicine, public health, and our knowledge of viral interactions with host organisms. Gaining insight into these mechanisms offers several significant benefits by informing the development of effective treatments, vaccines, and diagnostic tools. By studying these interactions at a mechanistic level, we can gain valuable insights into evolutionary processes, both in terms of viral mutation and host immune adaptation. This knowledge can also predict how new viruses may evolve and interact with human populations in the future. What we have learned in this PhD contributes to research for uncovering broad acting antiviral (NOP2 and RRP8) or proviral effectors in the cell, while also having scope to identify effectors that have a narrow range of viruses they impact.

Knowledge of viral mechanisms is vital for optimising vaccine strategies and designs. This may involve tailoring vaccines to enhance immune responses, including the activation of innate immune factors like interferons. RNA modifications that stimulate an immune response could be included in RNA vaccines to boost immune responses. Moreover, a deeper understanding of conserved viral components, or viral strategies such as hijacking a common enzyme to modify their genome or sub genomic RNA or mRNA, can guide the creation of broad-spectrum vaccines, offering protection against a wide range of viruses or rapidly evolving strains (Hajnik et al., 2024). RNA modifications have been used in vaccines previously but not for their antiviral effects: the mRNA SARS-CoV-2 vaccines utilised pseudouridine for stability (Morais et al.,

2021). Perhaps future vaccines could be engineered to contain modifications that enhance immune responses.

In addition to vaccines, understanding the molecular mechanisms underlying a virus life cycle enables the identification of specific therapeutic targets. For example, by studying how antiviral proteins and enzymes inhibit viral replication or modulate the immune response, researchers can design drugs that either mimic these natural factors or enhance their activity. This approach leads to the development of more effective and precise antiviral treatments that target specific stages of the viral life cycle. Such targeted therapies reduce side effects and improve treatment outcomes compared to broad-spectrum drugs (Li et al., 2023). Perhaps treatments could be created that enhance the activity of RNA modifying enzymes, particularly those that impart modifications that result in an antiviral response. However, at this point I think RNA modifying enzymes and RNA modifications are more useful in the development of RNA vaccines. For example, if a protein like NOP2 is a key part of an innate antiviral mechanism, molecular mimics of it could be used to treat infection, however since it is not a virus specific enzyme and has cellular activities as part of its normal function, treatments would not be targeted and could have adverse effects.

The emergence of new viral pathogens, such as SARS-CoV-2, demonstrates the need for rapid scientific responses to pandemics and fundamental research can contribute to preparedness for emerging viral threats. Understanding the mechanisms of viruses allows researchers to quickly assess how different factors interact with new viruses and identify potential therapeutic strategies. For instance, basic research into how viruses stimulate the innate immune system or methods viruses use to hijack the cellular components to hide from detection, like methylating their genomes, can lead to the rapid development of treatments or vaccines that target novel pathogens. By identifying key antiviral factors early in the response to an outbreak, public health authorities can deploy targeted interventions like vaccines more effectively. A screening platform such as the one I created in this PhD project could be used in an outbreak of a novel virus to identify factors affecting infection. Having pipelines and methodologies refined for characterising previously identified factors from a range of viral studies will enable a more rapid characterisation of factors during an outbreak. During the COVID-19 pandemic, a protein called OAS1 was identified using a

previously established screening platform to have restrictive effects to SARS-CoV-2 infection. Different isoforms of the gene were identified to have differing levels of protection from viral disease in individuals (Wickenhagen et al., 2022). This knowledge could be used as a biomedical marker of potential impact of infection for a patient.

Overall, the work presented in this thesis was able to contribute to the discovery and elucidation of the role of RNA modifications in viral infection. I demonstrated the creation and use of a CRISPR platform for screening RNA modifying enzymes during infection and confirmed the utility of the platform by following up a hit from the screens, NOP2, demonstrating it has antiviral activity. The epitranscriptome is an underestimated factor in viral infection. Increasing our understanding of the dynamics of RNA modifications and what this means for viruses could be translated into therapeutics and different viral intervention strategies.

Appendix 1 CRISPR Guide Sequences

Guide	Location (5', 3' etc)	Fw sequence	Rv sequence
ADAR 1	5'	CACCgAATAGTATCCGCGCAGCACC	AAACGGTGCTGCGCGGATACTATTC
2	3'	CACCgACCCGGGACAATTCATTCCG	AAACCGGAATGAATTGTCCCGGGTC
3	mid-3'	CACCGTAGTGACAAAATCCTACGC	AAACGCGTAGGATTTTGTCACTAC
4	5'-mid	CACCgAATCCTACGCTGGAACGTGC	AAACGCACGTTCCAGCGTAGGATTC
5	mid	CACCgATCCTACGCTGGAACGTGCT	AAACAGCACGTTCCAGCGTAGGATC
6	mid-3'	CACCGACAAGCGTCAACTGGTGTC	AAACGACACCAGTTGACGCTTGTC
7	5'	CACCgCTCGGCCATTGATGACAACC	AAACGGTTGTCATCAATGGCCGAGC
ADARB1 1	3'	CACCGCTTACACAGGCGGGACGCG	AAACCGCGTCCCGCCTGTGTAAGC
2	3'	CACCgATCTTGAACGAACTGCGCCC	AAACGGGCGCAGTTCGTTCAAGATC
3	5'	CACCGGTAGGCGACTCCGCTATTG	AAACCAATAGCGGAGTCGCCTACC
4	5'	CACCAGCTGACGCTGTCTCACGCC	AAACGGCGTGAGACAGCGTCAGCT
5	5'	CACCgAATCTCGTCTCATACCTTCC	AAACGGAAGGTATGAGACGAGATTC
6	5'-mid	CACCgCAATGCGAGCATCCAAACGT	AAACACGTTTGGATGCTCGCATTGC
7	5'	CACCgACGGGATTCTTCCCACTCGG	AAACCCGAGTGGGAAGAATCCCGTC
ADAT1 1	3'	CACCgTCGGGCCATCTTGTCACTAC	AAACGTAGTGACAAGATGGCCCGAC
2	3'	CACCGCATCCGAGGACGTTCCATC	AAACGATGGAACGTCCTCGGATGC
3	3'	CACCgACAGTGCCCCTTGGCATCCG	AAACCGGATGCCAAGGGGCACTGTC
4	3'	CACCGCCGGGTGCTGCGTTTCACC	AAACGGTGAAACGCAGCACCCGGC
5	3'	CACCgTGCTCCGTTGGTGACCTCCC	AAACGGGAGGTCACCAACGGAGCAC
13	5'	CACCgTTGAACTGGTGATAATCCGG	AAACCCGGATTATCACCAGTTCAAC
7	3'	CACCGTAGTGACAAGATGGCCCGA	AAACTCGGGCCATCTTGTCACTAC
ADAT2 1	3' mid	CACCgCTCGATTGGTGTCGTCAAAG	AAACCTTTGACGACACCAATCGAGC
2	3' mid	CACCgCCAATCGAGGACCTGATCGA	AAACTCGATCAGGTCCTCGATTGGC
3	3' mid	CACCgCACTTTGACGACACCAATCG	AAACCGATTGGTGTCGTCAAAGTGC
4	5'	CACCGCTTCCTCAGCCCGATATCC	AAACGGATATCGGGCTGAGGAAGC
5	5'	CACCgCAGCACCAAAATCGAAAGTT	AAACAACTTTCGATTTTGGTGCTGC
Not made	5' mid	CACCgAAGCGGCGCGTGCTCGGTGT	AAACTATACAACCAGCGGGATTTAC

7	5' mid	CACCgTCTGCTGACCTACCAAACAC	AAACGTGTTTGGTAGGTCAGCAGAC
8	5' mid	CACCGTCTACAACAATGAAGTTGT	AAACACAACTTCATTGTTGTAGAC
ADAT3 1	mid-3'	CACCGTTTACGCACGGCGCCTGCG	AAACCGCAGGCGCCGTGCGTAAAC
2	mid-3'	CACCGCGTAAACTGGACGCAGACG	AAACCGTCTGCGTCCAGTTTACGC
3	3'	CACCgAGGGCGGCGCCTACGTGTCG	AAACCGACACGTAGGCGCCGCCCTC
4	3'	CACCGCGCACCGTAGAAGACGCGC	AAACGCGCGTCTTCTACGGTGCGC
5	mid-3'	CACCGCACGCCGTCATGGTGTGCG	AAACCGCACACCATGACGGCGTGC
6	mid-3'	CACCgCGCACACCATGACGGCGTGC	AAACGCACGCCGTCATGGTGTGCGC
7	mid	CACCGCCAGCACGCGGTCCGAGGC	AAACGCCTCGGACCGCGTGCTGGC
16	5'	CACCGCTTCTCGGACAGGACAGGG	AAACCCCTGTCCTGTCCGAGAAGC
ALKBH1 1	3'	CACCGAGGGGTCATCGACTTCTCGG	AAACCCGAGAAGTCGATGACCCCTC
2	5'	CACCGTCTACGTGGATTCCCAGTG	AAACCACTGGGAATCCACGTAGAC
3	5'	CACCGACAGTCATGTTAACACGAG	AAACCTCGTGTTAACATGACTGTC
4	5'	CACCGTGTGCATAAACATGGCCGTG	AAACCACGGCCATGTTTATGCACAC
5	5' - mid	CACCGAAACTGCGTTGGGTGACCGT	AAACACGGTCACCCAACGCAGTTTC
6	3'	CACCGTCTACCGTCAGAGCCGGCCC	AAACGGGCCGGCTCTGACGGTAGAC
7	5'	CACCGATCCTGAATTACTACCGCC	AAACGGCGGTAGTAATTCAGGATC
ALKBH5 1	3'	CACCGGGACACCACCTCGTCAATG	AAACCATTGACGAGGTGGTGTCCC
2	3'	CACCgCGCTGTTGACGAAGCCCTCG	AAACCGAGGGCTTCGTCAACAGCGC
3	3'	CACCgACTGGTTCCGACACCCGAAT	AAACATTCGGGTGTCGGAACCAGTC
4	3'	CACCGTTCAAGCCTATTCGGGTGT	AAACACACCCGAATAGGCTTGAAC
5	5'	CACCgCTACCCCTCCGCCGGTGTGT	AAACACACACCGGCGGAGGGGTAGC
6	3'	CACCGCGCTGTTGACGAAGCCCTC	AAACGAGGGCTTCGTCAACAGCGC
7	3'	CACCGGGATCTCGTCCACGTCGCC	AAACGGCGACGTGGACGAGATCCC
ALKBH8 1	Mid	CACCCgTCCGACGAGGCAACATAAC	AAACGTTATGTTGCCTCGTCGGAGC
2	5'-mid	CACCgTACCCCTTGGCCGCACATTG	AAACCAATGTGCGGCCAAGGGGTAC
3	5'-mid	CACCgACTCCACAATGTGCGGCCAA	AAACTTGGCCGCACATTGTGGAGTC
4	mid	CACCGTTGCCTCGTCGGAGTTTGC	AAACGCAAACTCCGACGAGGCAAC
5	5'	CACCGTGGAGCAAATGCGTGACAT	AAACATGTCACGCATTTGCTCCAC
6	5'-mid	CACCgCTCCACAATGTGCGGCCAAG	AAACCTTGGCCGCACATTGTGGAGC
7	5'	CACCGCTACTACGATCAAGGAAAC	AAACGTTTCCTTGATCGTAGTAGC

BUD23 1	5'	CACCGAAATACGTTCGCAAGTGAG	AAACCTCACTTGCGAACGTATTTC
2	3' mid	CACCGCCTTCGACCTTTATACCAG	AAACCTGGTATAAAGGTCGAAGGC
3	5'	CACCgCGGAAATACGTTCGCAAGTG	AAACCACTTGCGAACGTATTTCCGC
4	3'	CACCgCGCGTGGTGACTTAGAAGCG	AAACCGCTTCTAAGTCACCACGCGC
5	3'	CACCGGTTCCCATTAAGGATGTCG	AAACCGACATCCTTAATGGGAACC
(isoform issues) 8	3'	CACCgCGGCCGGTGTACTGGGTGTC	AAACGACACCCAGTACACCGGCCG
7	3'	CACCGTCACCACGCGGTTCTGGAA	AAACTTCCAGAACCGCGTGGTGAC
CDK5RAP1 1	3'	CACCGCAGTCTACCTCGAGACCTA	AAACTAGGTCTCGAGGTAGACTGC
2	5'-mid	CACCgACGGGCATATCATAGGCTGA	AAACTCAGCCTATGATATGCCCGTC
3	3'-mid	CACCgATGCCTACCGGGACCTTCCC	AAACGGGAAGGTCCCGGTAGGCATC
4	3'	CACCGCGGGGCCGCCTTGTCTTCA	AAACTGAAGACAAGGCGGCCCCGC
5	3'	CACCgTCATCCATCATGAGATAGGG	AAACCCCTATCTCATGATGGATGAC
6	3'-mid	CACCGCCTATTGCCTCCATTCTAG	AAACCTAGAATGGAGGCAATAGGC
7	3'	CACCgCTTGGAGGTTACTGGTCCGC	AAACGCGGACCAGTAACCTCCAAGC
CDKAL1 1	mid	CACCgTTCCATGAGTACGCTGTCGG	AAACCCGACAGCGTACTCATGGAAC
2	5'	CACCGTATTTCGCCTTCGTACCTT	AAACAAGGTACGAAGGCGAAATAC
3	5' - mid	CACCGCCTCGCCAGGACTACCTTA	AAACTAAGGTAGTCCTGGCGAGGC
4	5'-mid	CACCGGTTCAGCAGATAGATCGTG	AAACCACGATCTATCTGCTGAACC
5	mid	CACCgTGCCTCCGACAGCGTACTCA	AAACTGAGTACGCTGTCGGAGGCAC
6	3'	CACCgTGCTAGCGGTTTGCTGATGG	AAACCCATCAGCAAACCGCTAGCAC
7	5'	CACCgCATCGAAGATATCGTGTCTC	AAACGAGACACGATATCTTCGATGC
CTU1 1	5'	CACCGGGCGCGTAGACGCACTCCT	AAACAGGAGTGCGTCTACGCGCCC
2	5'	CACCGGAGTGCGTCTACGCGCCCG	AAACCGGGCGCGTAGACGCACTCC
3	5'	CACCgTACGCGCCCGAGGCCTTCCG	AAACCGGAAGGCCTCGGGCGCGTAC
4	3'	CACCGTGACAGGTGAGCGTAGTAC	AAACGTACTACGCTCACCTGTCAC
5	3'	CACCgCTCACCTGTCACGATGTGCG	AAACCGCACATCGTGACAGGTGAGC
6	3'	CACCgTCGTAGGCCACGACCGTGAG	AAACGTCGTAGGCCACGACCGTGAG
7	5'	CACCgACTTCCTACGGGGCGACGCG	AAACCGCGTCGCCCCGTAGGAAGTC
DIMT1 1	3' mid	CACCgCTTCAGACCACCGCCCAAGG	AAACCCTTGGGCGGTGGTCTGAAGC
2	3'	CACCgCAGGTTTTGCAACCAGTCGG	AAACCCGACTGGTTGCAAAACCTGC
3	3' mid	CACCgAGGTTCTATCCTTACAACAC	AAACGTGTTGTAAGGATAGAACCTC
4	3'	CACCgAGGTTTTGCAACCAGTCGGA	AAACTCCGACTGGTTGCAAAACCTC

5	3'	CACCgAAGAGAATTTGCCCTCCGAC	AAACGTCGGAGGGCAAATTCTCTTC
6	3'	CACCgCTCCGACTGGTTGCAAAACC	AAACGGTTTTGCAACCAGTCGGAGC
7	5'mid	CACCgTAGTAAGGATAACCTTTGTT	AAACAACAAAGGTTATCCTTACTAC
8	5'	CACCgAAGTGCAGTGCAACAACTCT	AAACAGAGTTGTTGCACTGCACTTC
DUS1L 1	3'	CACCGGCGTCGCGGACAAAGACCT	AAACAGGTCTTTGTCCGCGACGCC
2	3'	CACCgTTGTCCGCGACGCCAACTAC	AAACGTAGTTGGCGTCGCGGACAAC
3	mid	CACCGTGGGCCCGGACGTAGGACA	AAACTGTCCTACGTCCGGGCCCAC
4	3'	CACCgCCTTCCGGTAGTTGGCGTCG	AAACCGACGCCAACTACCGGAAGGC
5	5'mid	CACCgCAGCACTTACGCTTCAGAGA	AAACTCTCTGAAGCGTAAGTGCTGC
6	3'	CACCgCGTCACAGTAATCCTGAGCC	AAACGGCTCAGGATTACTGTGACGC
7	5'mid	CACCGTGGAAGGGCAAGTCGCCGG	AAACCCGGCGACTTGCCCTTCCAC
DUS2 1	3' mid	CACCgTTCGCATCCTGCCATCGGTA	AAACTACCGATGGCAGGATGCGAAC
2	3'	CACCgTGTGCCTACTAGAGTGGTGC	AAACGCACCACTCTAGTAGGCACAC
3	3'	CACCgATCGTCTGTCTGCGGAGCCA	AAACTGGCTCCGCAGACAGACGATC
4	5'	CACCgAGAGTCCCTACCCGAACCAT	AAACATGGTTCGGGTAGGGACTCTC
5	5'	CACCGAGTCCCTACCCGAACCATT	AAACAATGGTTCGGGTAGGGACTC
6	5'	CACCgAGTCCCTACCCGAACCATTG	AAACCAATGGTTCGGGTAGGGACTC
7	3'	CACCGCCTACTAGAGTGGTGCCGG	AAACCCGGCACCACTCTAGTAGGC
8	5'	CACCgTAATCCTGGCCCCAATGGTT	AAACAACCATTGGGGCCAGGATTAC
DUS3L 1	5'	CACCgTCGCGGCCCAGGTAGTAGGG	AAACCCCTACTACCTGGGCCGCGAC
2	mid	CACCgCGAAGCGCTTGCAGATCCGT	AAACACGGATCTGCAAGCGCTTCGC
3	mid	CACCgACGGATCTGCAAGCGCTTCG	AAACCGAAGCGCTTGCAGATCCGTC
4	5'	CACCgCTGCGGGACTTCACCAACTA	AAACTAGTTGGTGAAGTCCCGCAGC
5	5'	CACCgTCACCGGGATCATGATTGCC	AAACGGCAATCATGATCCCGGTGAC
6	mid	CACCGCGCTTGCAGATCCGTCGGA	AAACTCCGACGGATCTGCAAGCGC
7	5'	CACCgCAACGCGTACAAGTAGCCTC	AAACGAGGCTACTTGTACGCGTTGC
DUS4L 1	Mid	CACCgAAATCAGCGGCAACAATCAT	AAACATGATTGTTGCCGCTGATTTC
2	3'	CACCGCAAACCCGGCCATGTTTGC	AAACGCAAACATGGCCGGGTTTGC
3	mid	CACCgATAGTCTGTCCTTATGCGAA	AAACTTCGCATAAGGACAGACTATC
4	5'	CACCgCTTTGAATATCGAACCATTG	AAACCAATGGTTCGATATTCAAAGC
5	5'	CACCgACTTTGAATATCGAACCATT	AAACAATGGTTCGATATTCAAAGTC
6	3'	CACCGATTACCTTACAGACCATTA	AAACTAATGGTCTGTAAGGTAATC

7	5'	CACCgCATGCAAACGACAATATGTC	AAACGACATATTGTCGTTTGCATGC
ELP1 1	5'	CACCgATCCAAGAATCGCCGAAAAG	AAACCTTTTCGGCGATTCTTGGATC
2	5'	CACCgCTCCGCTTTTCGGCGATTCT	AAACAGAATCGCCGAAAAGCGGAGC
3	5'	CACCgTAGATGATGAGGTACCCCAC	AAACGTGGGGTACCTCATCATCTAC
4	5'	CACCgAGAATCGCCGAAAAGCGGAG	AAACCTCCGCTTTTCGGCGATTCTC
5	3'	CACCgTGGACGACTGACCGGAGCGT	AAACACGCTCCGGTCAGTCGTCCAC
6	3'	CACCgACCTCGCCTATGATTGGCAC	AAACGTGCCAATCATAGGCGAGGTC
7	5'	CACCgTCGCCACAAGAAACGTTTAT	AAACATAAACGTTTCTTGTGGCGAC
ELP4 1	5'	CACCgAGCTGTCCATTCCGCACCGA	AAACTCGGTGCGGAATGGACAGCTC
2	5'	CACCgCGGGCACGCGACCGTCGGTG	AAACCACCGACGGTCGCGTGCCCGC
3	5'	CACCgACTCGCGGCAACACTACCGC	AAACGCGGTAGTGTTGCCGCGAGTC
4	5'	CACCgCATTGCGGGCACGCGACCGT	AAACACGGTCGCGTGCCCGCAATGC
5	5'	CACCGCCGCTGTCGTTGGTCACGC	AAACGCGTGACCAACGACAGCGGC
6	5'	CACCgCGCGAGTACTGGGTCTGCAG	AAACCTGCAGACCCAGTACTCGCGC
7	5'	CACCgACGCGACCGTCGGTGCGGAA	AAACTTCCGCACCGACGGTCGCGTC
9	mid	CACCgAGTTCTGGAAATTTCGTACC	AAACGGTACGAAATTTCCAGAACTC
FTO 1	Mid	CACCgCGGTGGGTGGAACTAAACCG	AAACCGGTTTAGTTCCACCCACCGC
2	mid	CACCgACTAAACCGAGGTTGTGAAC	AAACGTTCACAACCTCGGTTTAGTC
3	mid	CACCGTTTAGTTCCACCCACCGAG	AAACCTCGGTGGGTGGAACTAAAC
4	5'	CACCgCACTTCATCTTGTCCGTTGT	AAACACAACGGACAAGATGAAGTGC
5	mid	CACCgACTTACCTCTGCCACTCGGT	AAACACCGAGTGGCAGAGGTAAGTC
6	mid	CACCgTTTTGGCCGGTTCACAACCT	AAACAGGTTGTGAACCGGCCAAAAC
7	3'	CACCGTGTCAACCCATGGCTCAAC	AAACGTTGAGCCATGGGTTGACAC
FTSJ1 1	mid	CACCgACCGTAAGAATGGTCCAGCA	AAACTGCTGGACCATTCTTACGGTC
2	3'	CACCGGTCCGAATCATAGGAGCTC	AAACGAGCTCCTATGATTCGGACC
3	mid	CACCgCACCGTAAGAATGGTCCAGC	AAACGCTGGACCATTCTTACGGTGC
4	3'	CACCGTAACTGCGGTCCGAATCAT	AAACATGATTCGGACCGCAGTTAC
5	mid	CACCgTGTAGAGGAGCGTCACATCC	AAACGGATGTGACGCTCCTCTACAC
6	mid	CACCGAACTCTAGCATCGGTCAGT	AAACACTGACCGATGCTAGAGTTC
7	3'	CACCgCATCTCGCCACCATACCAGG	AAACCCTGGTATGGTGGCGAGATGC
FTSJ2/MRM2 1	mid	CACCgAGTCGCTGCAAGAATCGGA	AAACTCCGATTCTTGCAGCGACTC

2	mid	CACCGCTTGAAGGCGCTTCGACAC	AAACGTGTCGAAGCGCCTTCAAGC
3	mid	CACCgTCGAAGCGCCTTCAAGCTCC	AAACGGAGCTTGAAGGCGCTTCGAC
4	5'	CACCgATCGAGGTCCCGGAACCCTG	AAACCAGGGTTCCGGGACCTCGATC
5	3'	CACCgCGCGGGGAACACCAATGGCG	AAACCGCCATTGGTGTTCCCCGCGC
6	5'	CACCGTCAAAGCCGTCGGTTACAG	AAACCTGTAACCGACGGCTTTGAC
7	5'	CACCgTCCGGGACCTCGATCATGAC	AAACGTCATGATCGAGGTCCCGGAC
GTPBP3 1	Mid	CACCgATCGATATAGGCCTCCACGT	AAACACGTGGAGGCCTATATCGATC
2	mid	CACCGGCCTATATCGATTTCGGCG	AAACCGCCGAAATCGATATAGGCC
3	mid	CACCgTTTCGGCGAGGATGACAACC	AAACGGTTGTCATCCTCGCCGAAAC
4	mid	CACCgATCCTCGCCGAAATCGATAT	AAACATATCGATTTCGGCGAGGATC
5	mid	CACCgCGTACTTCGATGTCGGCTGT	AAACACAGCCGACATCGAAGTACGC
6	5'	CACCgTAGCGCGAAGATGGTGGCGC	AAACGCGCCACCATCTTCGCGCTAC
7	5'	CACCgACGTGCCGCTTGGGCCGCCA	AAACTGGCGGCCCAAGCGGCACGTC
HSD17B 10 1	3'	CACCgAGAGGTGACCCCACTTACGT	AAACACGTAAGTGGGGTCACCTCTC
2	3'	CACCGACCCCACTTACGTCGGCTG	AAACCAGCCGACGTAAGTGGGGTC
3	3'	CACCgCGCCCCAGCCGACGTAAGTG	AAACCACTTACGTCGGCTGGGGCGC
4	3'	CACCgCTCCGGTTATTACCGCCACC	AAACGGTGGCGGTAATAACCGGAGC
5	3'	CACCgTTCGCCCCAGCCGACGTAAG	AAACCTTACGTCGGCTGGGGCGAAC
6	5'	CACCgTCTCGATGATGGCCTGTACG	AAACCGTACAGGCCATCATCGAGAC
7	5'	CACCgTGAGTATGCTCACCTCGTAC	AAACGTACGAGGTGAGCATACTCAC
METTL1 1	5'	CACCgCGTAGGCATATTCTGCTAGC	AAACGCTAGCAGAATATGCCTACGC
2	3'	CACCgCACGCTGCGCTAGTGAGGAG	AAACCTCCTCACTAGCGCAGCGTGC
3	5'	CACCGTATACCATAACCGATGTGC	AAACGCACATCGGTTATGGTATAC
4	3'	CACCgTCCGGCCACGTTCCGAGTCT	AAACAGACTCGGAACGTGGCCGGAC
5	mid	CACCGGGCCTGAGTGTTACCTAAC	AAACGTTAGGTAACACTCAGGCCC
6	3'	CACCgACGCTGCGCTAGTGAGGAGT	AAACACTCCTCACTAGCGCAGCGTC
7	3'	CACCGTTGCCGGTAGTAGCGCTTC	AAACGAAGCGCTACTACCGGCAAC
METTL1 4 1	3'	CACCgATAGTACAATTCGACCAGGT	AAACACCTGGTCGAATTGTACTATC
2	3'	CACCgAGAGATAGTACAATTCGACC	AAACGGTCGAATTGTACTATCTCTC
3	3'	CACCgTGTGAAGCGTAGCACAGACG	AAACCGTCTGTGCTACGCTTCACAC
4	5'	CACCgTAACACGGCACCAATGCTGT	AAACACAGCATTGGTGCCGTGTTAC
5	3'	CACCgCTGTGAAGCGTAGCACAGAC	AAACGTCTGTGCTACGCTTCACAGC

6	5'	CACCgATAGCCGCTTGCAGGAGATC	AAACGATCTCCTGCAAGCGGCTATC
7	5'	CACCGGCCGCGGACCTGCTGCGCG	AAACCGCGCAGCAGGTCCGCGGCC
METTL2A 1	5'	CACCgCTGCAGTCCTCGCCGATAAG	AAACCTTATCGGCGAGGACTGCAGC
2	5'	CACCgTTGTGGTGGAAGACGCGCGC	AAACGCGCGCGTCTTCCACCACAAC
3	5'	CACCgTACCTCCAGTATTCGGTAGG	AAACCCTACCGAATACTGGAGGTAC
4	5'	CACCGTCGGAAGAGCAAGCCGCGG	AAACCCGCGGCTTGCTCTTCCGAC
5	5'	CACCgTGTTTCCGGCTCCGGTGTCA	AAACTGACACCGGAGCCGGAAACAC
6	5'	CACCgTCCGGCTCCGGTGTCATGGC	AAACGCCATGACACCGGAGCCGGAC
7	3'	CACCgAACTGACAATGTACCGGGTT	AAACAACCCGGTACATTGTCAGTTC
METTL2B 1	5'	CACCgCTGCAATCCTCGCCGATAAG	AAACCTTATCGGCGAGGATTGCAGC
(10) 2	3'	CACCgAGATTACGGCCGCTATGACA	AAACTGTCATAGCGGCCGTAATCTC
3	3'	CACCGCCGACTGCAGGTGAACCGA	AAACTCGGTTCACCTGCAGTCGGC
4	5'	CACCgTTGTGGTGGAAGACGCGCGC	AAACGCGCGCGTCTTCCACCACAAC
5	5' mid	CACCgTACCTCCAGTATTCGGTAGG	AAACCCTACCGAATACTGGAGGTAC
6	5'	CACCGTCGGAAGAGCAAGCCGCGG	AAACCCGCGGCTTGCTCTTCCGAC
7	5'	CACCgTGTTTCCGGCTCCGGTGTCA	AAACTGACACCGGAGCCGGAAACAC
METTL31	5'	CACCgATCATTCGGACAGGCCGTAC	AAACGTACGGCCTGTCCGAATGATC
2	5'	CACCGCTCAACATACCCGTACTAC	AAACGTAGTACGGGTATGTTGAGC
3	5' mid	CACCgAAAATTTCGCTCTCGAGGTC	AAACGACCTCGAGAGCGAAATTTTC
4	5'	CACCGTAATGCAATTCAGTTACGT	AAACACGTAACTGAATTGCATTAC
5	5'	CACCGCGCATCTCATCATCTGTCA	AAACTGACAGATGATGAGATGCGC
6	5'	CACCgCTGCAACGCATCATTCGGAC	AAACGTCCGAATGATGCGTTGCAGC
7	5'	CACCgATGACTGGTGGAACGAACCT	AAACAGGTTCGTTCCACCAGTCATC
METTL61	3'	CACCgTAGCTCCTCAAACTCTCTGG	AAACCCAGAGAGTTTGAGGAGCTAC
2	5'	CACCgTCATGTACCGCCAGAGTCTG	AAACCAGACTCTGGCGGTACATGAC
3	3'	CACCGGAGCTAAGATCATGTAGAG	AAACCTCTACATGATCTTAGCTCC
4	5'	CACCgATAAAGGATTTTGCTACAGG	AAACCCTGTAGCAAAATCCTTTATC
5	3'	CACCGTTACCGTCAGTTTCAGAGA	AAACTCTCTGAAACTGACGGTAAC
6	5'	CACCgCATCTTTAGTCAGATCACAC	AAACGTGTGATCTGACTAAAGATGC
7	3'	CACCgCTGGACCACCAGAGAGTTTG	AAACCAAACTCTCTGGTGGTCCAGC
isoform specific 1	5'	CACCgTGCCAACCTCATGAAAGGTC	AAACGACCTTTCATGAGGTTGGCAC

METTL8 1	5'	CACCgCGTAAAGGTATGCTACTCC	AAACGGAGTAGCATACCTTTACGC
2	mid	CACCgAGGATCGTAATTGGCTGTTG	AAACCAACAGCCAATTACGATCCTC
3	mid	CACCgACTAGAGGTATTGTGCTCAA	AAACTTGAGCACAATACCTCTAGTC
4	mid	CACCGGATCGTAATTGGCTGTTGA	AAACTCAACAGCCAATTACGATCC
5	5'	CACCgTCGTAAAGGTATGCTACTCC	AAACGGAGTAGCATACCTTTACGAC
6	5'	CACCgTGGAGCTGTGGAGCTCGTAA	AAACTTACGAGCTCCACAGCTCCAC
7	mid	CACCgAGTTTTTCAAGGATCGTAAT	AAACATTACGATCCTTGAAAAACTC
MRM1 1	5'	CACCgACCGTCCGGGGCGCGACCTG	AAACCAGGTCGCGCCCCGGACGGTC
2	5'	CACCgCGACCGTCCGGGGCGCGACC	AAACGGTCGCGCCCCGGACGGTCGC
3	5'	CACCgAACTGCTGGGGGTCGTCGCC	AAACGGCGACGACCCCCAGCAGTTC
4	5'	CACCGCATTGCTCTCGACCGTCCG	AAACCGGACGGTCGAGAGCAATGC
5	5'	CACCgAGTTGTGGCTCGTCCTCGAT	AAACATCGAGGACGAGCCACAACTC
6	5'	CACCGCGCTGGACTTGCTGACTAC	AAACGTAGTCAGCAAGTCCAGCGC
7	5'	CACCgTGTCCCGCGCCTCGGCCATC	AAACGATGGCCGAGGCGCGGGACAC
(3 has low efficiency)10	5'	CACCGGACGAGCCACAACTGCTGG	AAACCCAGCAGTTGTGGCTCGTCC
(iso specific) MRM3 1	5'	CACCgCTACGATAAAGCTTATCCCG	AAACCGGGATAAGCTTTATCGTAGC
2	5'	CACCgCGGTCGCACGACAAACCTCG	AAACCGAGGTTTGTCGTGCGACCGC
3	5'	CACCgCGGGATGCGGACTCCTCGAG	AAACCTCGAGGAGTCCGCATCCCGC
4	5'	CACCGGTCGCACGACAAACCTCGC	AAACGCGAGGTTTGTCGTGCGACC
5	5'	CACCgCGCTACGATAAAGCTTATCC	AAACGGATAAGCTTTATCGTAGCGC
6	5'	CACCGGACCTTGACGCGAGGCGCT	AAACAGCGCCTCGCGTCAAGGTCC
7	5'	CACCGCTACGATAAAGCTTATCCC	AAACGGGATAAGCTTTATCGTAGC
MRM3 1	3'	CACCGCCACATAGACCCGAGTGTC	AAACGACACTCGGGTCTATGTGGC
2	3'	CACCgAATGTGCGCCCATACCCGCC	AAACGGCGGGTATGGGCGCACATTC
3	3'	CACCGTGATTGGCGGGGAGACCTA	AAACTAGGTCTCCCCGCCAATCAC
4	3'	CACCgCGGGTATGGGCGCACATTTC	AAACGAAATGTGCGCCCATACCCGC
5	3'	CACCgATACCCGCCCGGAGCACTTT	AAACAAAGTGCTCCGGGCGGGTATC
6	5'	CACCgAGTGTTACTCACCAAAGGTA	AAACTACCTTTGGTGAGTAACACTC
7	3'	CACCgAAACCGGAGCCAGTCAAGAT	AAACATCTTGACTGGCTCCGGTTTC
MTO1 1	5'	CACCgCCGCGTGGACACGATCGGTG	AAACCACCGATCGTGTCCACGCGGC

2	mid	CACCgTCCCTAGGGTATAAAGACGC	AAACGCGTCTTTATACCCTAGGGAC
3	5'	CACCgACGTCGAAGTGCGGAGTCCG	AAACCGGACTCCGCACTTCGACGTC
4	mid	CACCgCGGCTGGTAAACATGCGGTA	AAACTACCGCATGTTTACCAGCCGC
5	5'	CACCgCACTTCGACGTGATAGTCAT	AAACATGACTATCACGTCGAAGTGC
6	mid	CACCgCTTGCGACTGACCCGAAGAC	AAACGTCTTCGGGTCAGTCGCAAGC
7	mid	CACCGCCGGCTGTCAGCATTATCA	AAACTGATAATGCTGACAGCCGGC
NAT10 1	3'	CACCgACCGCCGTCGGAAATCTGTG	AAACCACAGATTTCCGACGGCGGTC
2	mid	CACCGTCAATCCGATACGCCCCTG	AAACCAGGGGCGTATCGGATTGAC
3	mid	CACCgAGTCAATCCGATACGCCCCT	AAACAGGGGCGTATCGGATTGACTC
4	mid	CACCgACGGCTTATGGCCCTCTACG	AAACCGTAGAGGGCCATAAGCCGTC
5	mid	CACCgAGCAGCGCGGACACTGTATG	AAACCATACAGTGTCCGCGCTGCTC
6	3'	CACCGCAAGGCTAGGAACCGCCGT	AAACACGGCGGTTCCTAGCCTTGC
7	3'	CACCGAACCGCCGTCGGAAATCTG	AAACCAGATTTCCGACGGCGGTTC
(for 5' target) 15	5'	CACCgACATGCCGAAGGTATTGCCC	AAACGGGCAATACCTTCGGCATGTC
NSUN1/ NOP2 1	3'	CACCgTACCGTATCAGCATCGTCCT	AAACAGGACGATGCTGATACGGTAC
2	3'	CACCGCCCCCGCTTCTCCTTCGTA	AAACTACGAAGGAGAAGCGGGGGC
3	mid	CACCgACGAGTTCACAAGCGGATCC	AAACGGATCCGCTTGTGAACTCGTC
4	5'	CACCGTTTTACCCGCTTTCGAGAA	AAACTTCTCGAAAGCGGGTAAAAC
5	5'	CACCgCGTCGGGTAGAACGCAGACT	AAACAGTCTGCGTTCTACCCGACGC
6	mid	CACCGATCCTTCTTGAGCCGGTTC	AAACGAACCGGCTCAAGAAGGATC
7	5'	CACCGTGTTGTGGGCAACTTGCAT	AAACATGCAAGTTGCCCACAACAC
NSUN2 1	3'	CACCgAGGCTACCCCGAGATCGTCA	AAACTGACGATCTCGGGGTAGCCTC
2	3'	CACCgTGTTCTCCTTGACGATCTCG	AAACCGAGATCGTCAAGGAGAACAC
3	5'	CACCgCCGCCATCCGCATAAGACGA	AAACTCGTCTTATGCGGATGGCGGC
4	3'	CACCGATCGTGCCCGAGGGCGAGT	AAACACTCGCCCTCGGGCACGATC
5	mid	CACCgCAGCTGCGGATTGCAACACG	AAACCGTGTTGCAATCCGCAGCTGC
6	5'	CACCgATCGTCTTATGCGGATGGCG	AAACCGCCATCCGCATAAGACGATC
7	3'	CACCgATCGTGCCCGAGGGCGAGTG	AAACCACTCGCCCTCGGGCACGATC
NSUN3 1	3'	CACCGGCTACATACATTGGGCCCC	AAACGGGGCCCAATGTATGTAGCC
2	3'	CACCgATTAAGGCCTTACGTCCTGG	AAACCCAGGACGTAAGGCCTTAATC
3	mid	CACCgCGTGTTCAAATGATCGAAGC	AAACGCTTCGATCATTTGAACACGC
4	3'	CACCgCATAGGCATGATGTTACCGT	AAACACGGTAACATCATGCCTATGC

5	3'	CACCgCCACGGTAACATCATGCCTA	AAACTAGGCATGATGTTACCGTGGC
6	3'	CACCgAAGTATCCCTCCAGGACGTA	AAACTACGTCCTGGAGGGATACTTC
7	5'	CACCGATAATTGAATCGGTTAAGC	AAACGCTTAACCGATTCAATTATC
NSUN4 1	5'	CACCGCATCGAAGGTTCGGACTGC	AAACGCAGTCCGAACCTTCGATGC
(long isoform specific)	5'	CACCGCCATATCGGCGTGCTCCAC	AAACGTGGAGCACGCCGATATGGC
2	5'	CACCgACACTAGCGTTGCTTCAGAC	AAACGTCTGAAGCAACGCTAGTGTC
3	mid	CACCGTAGTCTGGCTATTCGGGAC	AAACGTCCCGAATAGCCAGACTAC
4	mid	CACCGTTCGAGTTACCTCATGGGA	AAACTCCCATGAGGTAACTCGAAC
5	3'	CACCgCCGCCACTCCCTTCATGAGG	AAACCCTCATGAAGGGAGTGGCGGC
6	5'	CACCgAACGCTAGTGTCTTTCCCCC	AAACGGGGGAAAGACACTAGCGTTC
NSUN5 1	5' mid	CACCgTCATGGTAGCGTGGATCCGA	AAACTCGGATCCACGCTACCATGAC
2	5'	CACCgTTGAACGGGTCGAGGTGCCA	AAACTGGCACCTCGACCCGTTCAAC
3	5' mid	CACCgCTCATGGTAGCGTGGATCCG	AAACCGGATCCACGCTACCATGAGC
4	5' mid	CACCgCATGGTAGCGTGGATCCGAG	AAACCTCGGATCCACGCTACCATGC
5	5' mid	CACCgATGGTAGCGTGGATCCGAGG	AAACCCTCGGATCCACGCTACCATC
6	5'	CACCgTGCTGTAATTGAACGGGTCG	AAACCGACCCGTTCAATTACAGCAC
7	5' mid	CACCgCTCGGATCCACGCTACCATG	AAACCATGGTAGCGTGGATCCGAGC
PUS1 1	3'	CACCgCGCTCGGTGCCGATGATGGT	AAACACCATCATCGGCACCGAGCGC
2	3'	CACCgCGTGACCCGCTTCAGTCCTA	AAACTAGGACTGAAGCGGGTCACGC
3	5'	CACCgAATACAGCCTGACCGGACGA	AAACTCGTCCGGTCAGGCTGTATTC
4	5'	CACCgCCGGCGAAGAAGCTCAAGAG	AAACCTCTTGAGCTTCTTCGCCGGC
5	3'	CACCgTGACCCGCTTCAGTCCTAGG	AAACCCTAGGACTGAAGCGGGTCAC
6	3'	CACCgACCAGCGCTTTGGCAACGAT	AAACATCGTTGCCAAAGCGCTGGTC
7	5'	CACCgAGCACGATCTTCCGCTTGGG	AAACCCCAAGCGGAAGATCGTGCTC
PUS3 1	5'	CACCGTCCCCTACGTACAAAATGC	AAACGCATTTTGTACGTAGGGGAC
2	3'	CACCgTCATCAAGTCCGATGTATGA	AAACTCATACATCGGACTTGATGAC
3	5'	CACCgCATTTAGGACGGTCCATGAG	AAACCTCATGGACCGTCCTAAATGC
4	5'	CACCGGACTGTAATGACACACTAG	AAACCTAGTGTGTCATTACAGTCC
5	5'	CACCGTATAGTATGCTACAAGGAC	AAACGTCCTTGTAGCATACTATAC
6	3'	CACCgTACATCGGACTTGATGATAA	AAACTTATCATCAAGTCCGATGTAC
7	5'	CACCGCATTTAGGACGGTCCATGA	AAACTCATGGACCGTCCTAAATGC

PUS7 1	3'	CACCgACTGGTGTGTCGCTGAAACG	AAACCGTTTCAGCGACACACCAGTC
2	5'	CACCgCCTTTGAGAACGAGGTCCCC	AAACGGGGACCTCGTTCTCAAAGGC
3	3'	CACCgTGGTGTGTCGCTGAAACGTG	AAACCACGTTTCAGCGACACACCAC
4	3'	CACCgTCGGAATGCAGTCTAACCAA	AAACTTGGTTAGACTGCATTCCGAC
5	5'	CACCGGGTAGATAACATCGAAACC	AAACGGTTTCGATGTTATCTACCC
6	5'	CACCgACGAATAATGATCTTTCGGT	AAACACCGAAAGATCATTATTCGTC
7	5'	CACCGCCATGGTGGCGTAAGTAGA	AAACTCTACTTACGCCACCATGGC
RPUSD2 1	5'	CACCgAATAGGGCCGCACCTTACGC	AAACGCGTAAGGTGCGGCCCTATTC
2	5'	CACCgCTTCGAGGGCGGCCTGCGTA	AAACTACGCAGGCCGCCCTCGAAGC
3	5'	CACCgTTAGGCGCCCTAGCTTTACC	AAACGGTAAAGCTAGGGCGCCTAAC
4	5'	CACCgACCCCGGTCCGCCGCTTCTT	AAACAAGAAGCGGCGGACCGGGGTC
5	5'	CACCGTTATGTGGCTGGACCGCCG	AAACCGGCGGTCCAGCCACATAAC
6	mid	CACCgTAACTGTGTTGTGTCGGAAG	AAACCTTCCGACACAACACAGTTAC
7	mid	CACCgTTGTGTCGGAAGCGGCCACA	AAACTGTGGCCGCTTCCGACACAAC
RRP8 1	5'	CACCgTCGCCAGGGATCTTCGCCAG	AAACCTGGCGAAGATCCCTGGCGAC
2	3'	CACCGGCGGAGGTCGTGAGATTAC	AAACGTAATCTCACGACCTCCGCC
3	3'	CACCGATTACGGGCCCAAGGCCCG	AAACCGGGCCTTGGGCCCGTAATC
4	3'	CACCgTTGTTTTGCGAGGAGGCCGC	AAACGCGGCCTCCTCGCAAAACAAC
5	5'	CACCGATCTTCGCCAGCGGTGAAT	AAACATTCACCGCTGGCGAAGATC
6	3'	CACCgTTCGAACATGAGGGTCGGGA	AAACTCCCGACCCTCATGTTCGAAC
7	5'	CACCgCATTAAGCCGCAAGCAGTGG	AAACCCACTGCTTGCGGCTTAATGC
(start of 5') 9	5'est	CACCGGATGTTCGAACCTTTCTGC	AAACGCAGAAAGGTTCGAACATCC
TARBP1 1	5'	CACCGGTCGGTTTGTCGATGAGCG	AAACCGCTCATCGACAAACCGACC
2	3'	CACCgTGCGCGATCTGCTCGCCGGG	AAACCCCGGCGAGCAGATCGCGCAC
3	5'	CACCGCTTCGACCAAATTAGTACC	AAACGGTACTAATTTGGTCGAAGC
4	3'	CACCgCGGGCGCTCGGCAAATGGAG	AAACCTCCATTTGCCGAGCGCCCGC
5	3'	CACCgAGCGCGCTCGCTTGCGCGTC	AAACGACGCGCAAGCGAGCGCGCTC
6	mid	CACCgTCCAATGGAGCTACACGTAG	AAACCTACGTGTAGCTCCATTGGAC
7	5'	CACCgCGGAAACACGACTGTTCCAC	AAACGTGGAACAGTCGTGTTTCCGC
(more 5') 8	mid	CACCgTTATAGCGAACTTATCCTTG	AAACCAAGGATAAGTTCGCTATAAC
TGS1 1	5'	CACCGGCCAAAGTGAACCACGTAA	AAACTTACGTGGTTCACTTTGGCC

2	mid	CACCGTTGTAGTAGACGCATTCTG	AAACCAGAATGCGTCTACTACAAC
3	5'	CACCgCTCCATTACGTGGTTCACTT	AAACAAGTGAACCACGTAATGGAGC
4	5'	CACCgTGGTTAATCTTACCCTCAGC	AAACGCTGAGGGTAAGATTAACCAC
5	5'	CACCgACGTAATGGAGGAACCAATG	AAACCATTGGTTCCTCCATTACGTC
6	5'	CACCgTCATTGGTTCCTCCATTACG	AAACCGTAATGGAGGAACCAATGAC
7	mid	CACCgACCATTCAGTTTGCCTTAAC	AAACGTTAAGGCAAACTGAATGGTC
TRDMT1 1	5'	CACCGTATCCCACATACCGAACTC	AAACGAGTTCGGTATGTGGGATAC
2	mid	CACCgAGGTCCGTGTGCTTTACCAA	AAACTTGGTAAAGCACACGGACCTC
3	mid	CACCGCATATCGCAGCAATGACTT	AAACAAGTCATTGCTGCGATATGC
4	5'	CACCgTCCCACATACCGAACTCTGG	AAACCCAGAGTTCGGTATGTGGGAC
5	5'	CACCgTCCTCCAGAGTTCGGTATGT	AAACACATACCGAACTCTGGAGGAC
6	mid	CACCgTTGTTCAGCCCACTTGTAGA	AAACTCTACAAGTGGGCTGAACAAC
7	mid	CACCGGTCCGTGTGCTTTACCAAA	AAACTTTGGTAAAGCACACGGACC
TRMT9B 1	mid	CACCgAGTCGATTCATCCAAAGATC	AAACGATCTTTGGATGAATCGACTC
2	5'	CACCgTCAAAACGGTCCCACAGCGT	AAACACGCTGTGGGACCGTTTTGAC
3	5'	CACCgTTCAAAACGGTCCCACAGCG	AAACCGCTGTGGGACCGTTTTGAAC
4	5'	CACCgACGTGCTTGTTCCATGGAAC	AAACGTTCCATGGAACAAGCACGTC
5	3'	CACCGTAGTAGCGCATAAAGGCTG	AAACCAGCCTTTATGCGCTACTAC
6	mid	CACCgTAGGAAAATCGTTTCGTTCC	AAACGGAACGAAACGATTTTCCTAC
7	3'	CACCgTCGACAGACATTGTATCATC	AAACGATGATACAATGTCTGTCGAC
8	mid	CACCgCTTTGGATGAATCGACTCTG	AAACCAGAGTCGATTCATCCAAAGC
TRIT1 1	mid	CACCgCATCGTCAACATACGGAAGA	AAACTCTTCCGTATGTTGACGATGC
2	5'	CACCgATTGGGGATCGCGAATGGGC	AAACGCCCATTCGCGATCCCCAATC
3	5'	CACCgCATCATTGGGGATCGCGAAT	AAACATTCGCGATCCCCAATGATGC
4	3'	CACCgCAAGAGGTAGGGTCCGTTGC	AAACGCAACGGACCCTACCTCTTGC
5	3'	CACCgCGATCTCACCGCCGAGCCGC	AAACGCGGCTCGGCGGTGAGATCGC
6	3'	CACCgCCGCCACGGACGCCATCTTA	AAACTAAGATGGCGTCCGTGGCGGC
7	5'	CACCgTTCGATCACAGAGGTCACAC	AAACGTGTGACCTCTGTGATCGAAC
TRMT6 1	3'	CACCgCTAGTGTATCGTATCTCATG	AAACCATGAGATACGATACACTAGC
2	3'	CACCgACGTTGGGAAATATCCGTGC	AAACGCACGGATATTTCCCAACGTC
3	3'	CACCgCTAGCCCAGATGTTGACGTT	AAACAACGTCAACATCTGGGCTAGC
4	5'	CACCgATCTGACTTACTTTCTCCGC	AAACGCGGAGAAAGTAAGTCAGATC

5	3'	CACCGTCCATGGCAACGGTGAAGC	AAACGCTTCACCGTTGCCATGGAC
6	mid	CACCgTATTTCCCAACGTCAACATC	AAACGATGTTGACGTTGGGAAATAC
7	5'	CACCGGTCTACTGTCAGTACAAAG	AAACCTTTGTACTGACAGTAGACC
TRMO	iso specific 5'	CACCgCGGCTTAACGCAGCCGCACG	AAACCGTGCGGCTGCGTTAAGCCGC
1	mid	CACCgACGTGATCAGAGTTCCAGCG	AAACCGCTGGAACTCTGATCACGTC
2	5'	CACCgCTCATGCCGAGATGGACCTT	AAACAAGGTCCATCTCGGCATGAGC
3	3'	CACCGAGTCATACTCAGCTATGTA	AAACTACATAGCTGAGTATGACTC
4	3'	CACCgTCTGGAATTGACATGATACA	AAACTGTATCATGTCAATTCCAGAC
5	3'	CACCGTGACCAGCGACAGCTCTCA	AAACTGAGAGCTGTCGCTGGTCAC
6	5'	CACCgAGTAAACCGCACTTCTAAAG	AAACCTTTAGAAGTGCGGTTTACTC
TRMT1 1	3'	CACCGACGTGCTACAGCAAGTACG	AAACCGTACTTGCTGTAGCACGTC
2	mid	CACCgACACCTCGGAGCGGATCCGA	AAACTCGGATCCGCTCCGAGGTGTC
3	mid	CACCgCACACCTCGGAGCGGATCCG	AAACCGGATCCGCTCCGAGGTGTGC
4	5'	CACCgCAAGGCGGCCGACGAAGCTA	AAACTAGCTTCGTCGGCCGCCTTGC
5	mid	CACCGATAGTCGCTCCCGTTTCAC	AAACGTGAAACGGGAGCGACTATC
6	mid	CACCgAGTTGCGGTAAGAGCCCCTG	AAACCAGGGGCTCTTACCGCAACTC
7	5'	CACCGCGTTGACAGGTGCCCTGGT	AAACACCAGGGCACCTGTCAACGC
TRMT10A 1	3'	CACCGATGTTACGCAGAAAACCGA	AAACTCGGTTTTCTGCGTAACATC
2	3'	CACCgATGTTACGCAGAAAACCGAC	AAACGTCGGTTTTCTGCGTAACATC
3	5'	CACCgACTATCTTGCCCCAACGGAA	AAACTTCCGTTGGGGCAAGATAGTC
4	5'	CACCGATGAATAGTCGAAAAGTTT	AAACAAACTTTTCGACTATTCATC
5	3'	CACCgACAGTCAATAATAAGGCGAA	AAACTTCGCCTTATTATTGACTGTC
6	mid	CACCgTATTAGGTGAATCTGACGTA	AAACTACGTCAGATTCACCTAATAC
7	mid	CACCgTTTTACTTGACAAGCCACGG	AAACCCGTGGCTTGTCAAGTAAAAC
TRMT10B 1	mid	CACCgACGGTATGTAGTTGAATGCA	AAACTGCATTCAACTACATACCGTC
2	3'	CACCGTTGTGAGTCTCTAAGTAAG	AAACCTTACTTAGAGACTCACAAC
3	3'	CACCGACCGCACGCTTGCCAATCC	AAACGGATTGGCAAGCGTGCGGTC
4	3'	CACCgCTATATTCTTCGGAACTCAG	AAACCTGAGTTCCGAAGAATATAGC
5	5'	CACCgCGGTGAGTGCGTGAATTGCC	AAACGGCAATTCACGCACTCACCGC
6	3'	CACCGAGTCTCTAAGTAAGTGGAC	AAACGTCCACTTACTTAGAGACTC
7	mid	CACCgAACAAAGTTTACATCCTCGG	AAACCCGAGGATGTAAACTTTGTTC

TRMT10C 1	3'	CACCgCAGGTTCAGCCGTTTTGCCT	AAACAGGCAAAACGGCTGAACCTGC
2	5'	CACCGGGGGTGTACTCTCATTTTT	AAACAAAAATGAGAGTACACCCCC
3	mid	CACCGTTGTCCAAACTGCATGGCC	AAACGGCCATGCAGTTTGGACAAC
4	3'	CACCgCCAATGTTATGACTACTTTC	AAACGAAAGTAGTCATAACATTGGC
5	mid	CACCgCATGCAGTTTGGACAACCTT	AAACAAGGTTGTCCAAACTGCATGC
6	3'	CACCgCAGCCGTTTTGCCTTGGCTA	AAACTAGCCAAGGCAAAACGGCTGC
7	5'	CACCgCCCTTCTGAAGAGCTAGAGT	AAACACTCTAGCTCTTCAGAAGGGC
TRMT111	mid	CACCgACATACTCTGGCGTATACAC	AAACGTGTATACGCCAGAGTATGTC
2	5'	CACCGGCGCTACGGACTCACCGGC	AAACGCCGGTGAGTCCGTAGCGCC
3	5'	CACCgCGCTGTCGTGTACCCTTAAC	AAACGTTAAGGGTACACGACAGCGC
4	mid	CACCgTAGTCTTCCACCTAAAACGA	AAACTCGTTTTAGGTGGAAGACTAC
5	5'	CACCGCTACGGACTCACCGGCAGG	AAACCCTGCCGGTGAGTCCGTAGC
6	3'	CACCgATACTGGTCCCGATTCTGTT	AAACAACAGAATCGGGACCAGTATC
7	mid	CACCgCTAGTCTTCCACCTAAAACG	AAACCGTTTTAGGTGGAAGACTAGC
TRMT112 1	mid	CACCGGCGCGTATGATACCTAAAG	AAACCTTTAGGTATCATACGCGCC
2	mid	CACCgTGGAGGCGGCCGATAACGTG	AAACCACGTTATCGGCCGCCTCCAC
3	mid	CACCgTCATACGCGCCACGAAGTTG	AAACCAACTTCGTGGCGCGTATGAC
4	5'	CACCgCGTCTGATCCAGGTGCCGAA	AAACTTCGGCACCTGGATCAGACGC
5	mid	CACCgTCACGTTATCGGCCGCCTCC	AAACGGAGGCGGCCGATAACGTGAC
6	mid	CACCGGTAAGGATCCTCACGTTAT	AAACATAACGTGAGGATCCTTACC
7	mid	CACCgTATCACTTCCACCTGCGGGC	AAACGCCCGCAGGTGGAAGTGATAC
TRMT121	mid	CACCGATCGGTGCCAAATACACTT	AAACAAGTGTATTTGGCACCGATC
2	5'	CACCgCCCCGATCATGGCAACGGCA	AAACTGCCGTTGCCATGATCGGGGC
3	5'	CACCGGATGGCTCGGTGGCGCTAC	AAACGTAGCGCCACCGAGCCATCC
4	mid	CACCGTCCAGCGTTTGGCAAAACG	AAACCGTTTTGCCAAACGCTGGAC
5	5'	CACCgTCGGTGGCGCTACCGGTGCT	AAACAGCACCGGTAGCGCCACCGAC
6	mid	CACCgTCCAGCGTTTGGCAAAACGA	AAACTCGTTTTGCCAAACGCTGGAC
7	5'	CACCgATTTGCCCCGATCATGGCAA	AAACTTGCCATGATCGGGGCAAATC
8	5'	CACCgAGGCTGATTTGCCCCGATCA	AAACTGATCGGGGCAAATCAGCCTC
TRMT131	5'	CACCGGGTAGATGCGGTTACTATG	AAACCATAGTAACCGCATCTACCC
2	5'	CACCgCGGAGGTCGCCATAATTCTA	AAACTAGAATTATGGCGACCTCCGC

3	5'	CACCGCGGAGGTCGCCATAATTCT	AAACAGAATTATGGCGACCTCCGC
4	5'	CACCgAGGGCGATACCACACCTCCG	AAACCGGAGGTGTGGTATCGCCCTC
5	5'	CACCgTAACCGCATCTACCCTCAGC	AAACGCTGAGGGTAGATGCGGTTAC
6	5'	CACCgATAATTCTAGGGCTCGCTTC	AAACGAAGCGAGCCCTAGAATTATC
7	3'	CACCGATGGCGCTGATTGTTTGCC	AAACGGCAAACAATCAGCGCCATC
TRMT1L 1	3' mid	CACCgTGTTACATCCGTAGTGACGC	AAACGCGTCACTACGGATGTAACAC
2	3' mid	CACCGCTGCAGCCCGATGCAACAA	AAACTTGTTGCATCGGGCTGCAGC
3	5'	CACCgCATCTGTGCGTACACCCATT	AAACAATGGGTGTACGCACAGATGC
4	3' mid	CACCgTGTCCGAACTGAATATTACA	AAACTGTAATATTCAGTTCGGACAC
5	3' mid	CACCGTTACATCCGTAGTGACGCC	AAACGGCGTCACTACGGATGTAAC
6	5'	CACCGCATCTGTGCGTACACCCAT	AAACATGGGTGTACGCACAGATGC
7	5'	CACCgCGAACTCATTTTGACCCAAT	AAACATTGGGTCAAAATGAGTTCGC
TRMT2A 1	MID	CACCGATGTGCACGGTGTCAAACG	AAACCGTTTGACACCGTGCACATC
2	MID	CACCgACAGCGGTAAGGAGCCCGAG	AAACCTCGGGCTCCTTACCGCTGTC
3	MID	CACCGTCGTATGCCGAGTATGGAG	AAACCTCCATACTCGGCATACGAC
4	3'	CACCGGGCACCATGCAAAACGCGC	AAACGCGCGTTTTGCATGGTGCCC
5	3'	CACCgAAGGCCCTGCGCGTTTTGCA	AAACTGCAAAACGCGCAGGGCCTTC
6	MID	CACCGGATGTGCACGGTGTCAAAC	AAACGTTTGACACCGTGCACATCC
7	3'	CACCgAGCGACGTCCGGCGCTTCCT	AAACAGGAAGCGCCGGACGTCGCTC
17	5'	CACCgACTGGGCCCAATTGGATGCG	AAACCGCATCCAATTGGGCCCAGTC
TRMT2B 1	5'	CACCgTTACGCAGTCCGGCACGGGC	AAACGCCCGTGCCGGACTGCGTAAC
2	5'	CACCgTACGCAGTCCGGCACGGGCT	AAACAGCCCGTGCCGGACTGCGTAC
3	mid	CACCGCTCCAATGGAGACTGTCGA	AAACTCGACAGTCTCCATTGGAGC
4	5'	CACCgCATCCTTACGCAGTCCGGCA	AAACTGCCGGACTGCGTAAGGATGC
5	5'	CACCgAGCCCGTGCCGGACTGCGTA	AAACTACGCAGTCCGGCACGGGCTC
6	5'	CACCgATCCTTACGCAGTCCGGCAC	AAACGTGCCGGACTGCGTAAGGATC
7	mid	CACCgACAGTCCGCACCAATAGCCA	AAACTGGCTATTGGTGCGGACTGTC
TRMT5 1	3'	CACCGCTGATGATCTCGAAGGTTT	AAACAAACCTTCGAGATCATCAGC
2	3'	CACCGTCATGCCTCGGACATCAGA	AAACTCTGATGTCCGAGGCATGAC
3	3'	CACCgAATTGATGCGATCCCTAAAA	AAACTTTTAGGGATCGCATCAATTC
4	5'	CACCgACATCAAATAGGACATCCCC	AAACGGGGATGTCCTATTTGATGTC
5	3'	CACCgATTGATGCGATCCCTAAAAA	AAACTTTTTAGGGATCGCATCAATC

6	5'	CACCgCTGCTGAGGATGTTCGGCAA	AAACTTGCCGAACATCCTCAGCAGC
7	3'	CACCgATGCCTCGGACATCAGAAGG	AAACCCTTCTGATGTCCGAGGCATC
TRMT61A 1	5'	CACCgCATGAGCTTCGTGGCATACG	AAACCGTATGCCACGAAGCTCATGC
2	mid	CACCgCGGATGCACCTTCGACCTTG	AAACCAAGGTCGAAGGTGCATCCGC
3	3'	CACCgATGGGCGTGCCGCTGCGGAA	AAACTTCCGCAGCGGCACGCCCATC
4	5'	CACCGACCTTATCGGCCGCCCCTT	AAACAAGGGGCGGCCGATAAGGTC
5	3'	CACCGTGCGCACGTTGTAGACCTG	AAACCAGGTCTACAACGTGCGCAC
6	5'	CACCgCACGTCACCTTGGAGCCGAA	AAACTTCGGCTCCAAGGTGACGTGC
7	3'	CACCgCGTTGCACCTGCTCGATGCA	AAACTGCATCGAGCAGGTGCAACGC
TRMT61B 1	3'	CACCgAGTGACCGAGCTCCCTCGAA	AAACTTCGAGGGAGCTCGGTCACTC
2	3'	CACCgTCCCGTTCGGCAAGATCGTG	AAACCACGATCTTGCCGAACGGGAC
3	3'	CACCgATTAGCATAGTGTTTCGCGA	AAACTCGCGAAACACTATGCTAATC
4	3'	CACCgAGTCCCGTTCGGCAAGATCG	AAACCGATCTTGCCGAACGGGACTC
5	3'	CACCGTCCCGTTCGGCAAGATCGT	AAACACGATCTTGCCGAACGGGAC
6	3'	CACCgTCGAGTCCTCGAGCTCTCGA	AAACTCGAGAGCTCGAGGACTCGAC
7	3'	CACCgCTCGAGTCCTCGAGCTCTCG	AAACCGAGAGCTCGAGGACTCGAGC
15	mid 3'	CACCgTCAATGATGGATATCAACCC	AAACGGGTTGATATCCATCATTGAC
18	5'	CACCGTGTACTGGTCTAGCAACAT	AAACATGTTGCTAGACCAGTACAC
TRMU	5' excludes 1 isoform	CACCgCGCTGTCCACGCCGCCGGAC	AAACGTCCGGCGGCGTGGACAGCGC
1	5'	CACCgAGCACGTTAAGAAGCCCGAA	AAACTTCGGGCTTCTTAACGTGCTC
2	3'	CACCGGCACTAGGTGACTGACGGG	AAACCCCGTCAGTCACCTAGTGCC
3	mid	CACCgCGTCAAGGGTGACGTGTTTG	AAACCAAACACGTCACCCTTGACGC
4	3'	CACCgCTACAAGGGGGACGAGTGCC	AAACGGCACTCGTCCCCCTTGTAGC
5	3'	CACCgTCTGGTGGCGGAATCGGAAG	AAACCTTCCGATTCCGCCACCAGAC
6	5' mid	CACCgTCTTTCGTTAATCCCCCCAG	AAACCTGGGGGGATTAACGAAAGAC
TYW1 1	mid	CACCgATTACTAAGGAACCTCGAGC	AAACGCTCGAGGTTCCTTAGTAATC
2	5'	CACCGCGCATCGTGTGATGAGTCG	AAACCGACTCATCACACGATGCGC
3	5'	CACCgCGCATCGTGTGATGAGTCGA	AAACTCGACTCATCACACGATGCGC
4	5'	CACCGCATCGTGTGATGAGTCGAG	AAACCTCGACTCATCACACGATGC
5	3'	CACCGGTACAGTTTGTCCACGAGT	AAACACTCGTGGACAAACTGTACC
6	5'	CACCgCGTCAGTGTATGTCGCAACC	AAACGGTTGCGACATACACTGACGC

7	mid	CACCGTGGGCGGTCGATTTTCTTC	AAACGAAGAAAATCGACCGCCCAC
TYW3 1	mid	CACCgTGTACTCCGGACAGCCTACA	AAACTGTAGGCTGTCCGGAGTACAC
2	5'	CACCgTGAGCAAAGCGGACCTCAGC	AAACGCTGAGGTCCGCTTTGCTCAC
3	5'	CACCgAACTCCGCGCTGCGATCCAT	AAACATGGATCGCAGCGCGGAGTTC
4	5'	CACCGAACTCCGCGCTGCGATCCA	AAACTGGATCGCAGCGCGGAGTTC
5	mid	CACCgCAGGAACTCTGGCATAACGG	AAACCCGTTATGCCAGAGTTCCTGC
6	5'	CACCgTGGATCGCAGCGCGGAGTTC	AAACGAACTCCGCGCTGCGATCCAC
7	mid	CACCgAGGAACTCTGGCATAACGGT	AAACACCGTTATGCCAGAGTTCCTC
WDR4 1	3'	CACCgTCGGATCTTCTCGTCCCGGT	AAACACCGGGACGAGAAGATCCGAC
2	5' mid	CACCgCCGCAGCTTACCCGTCGCAC	AAACGTGCGACGGGTAAGCTGCGGC
3	3'	CACCgTAGCATCGAGTCCTTCTGCT	AAACAGCAGAAGGACTCGATGCTAC
4	5'	CACCgCGACGCTAAGTTGCTGATCG	AAACCGATCAGCAACTTAGCGTCGC
5	5' mid	CACCgTTTAGAAGTTTGCCGCGTCC	AAACGGACGCGGCAAACTTCTAAAC
6	5' mid	CACCGGACGCGGCAAACTTCTAAA	AAACTTTAGAAGTTTGCCGCGTCC
7	3' mid	CACCGTTTGTGAGCCGTATCTCCG	AAACCGGAGATACGGCTCACAAAC

References

Abraham S, Choi JG, Ortega NM, Zhang J, Shankar P, Swamy NM. Gene therapy with plasmids encoding IFN-β or IFN-α14 confers long-term resistance to HIV-1 in humanized mice. Oncotarget. 2016 Nov 29;7(48):78412-78420. doi: 10.18632/oncotarget.12512. PMID: 27729616; PMCID: PMC5346649.

Accola, M. A., Huang, B., Al Masri, A. & McNiven, M. A. The antiviral dynamin family member, MxA, tubulates lipids and localizes to the smooth endoplasmic reticulum. J. Biol. Chem. 277, 21829–21835 (2002).

Acheson NH, Tamm I. Replication of Semliki Forest virus: an electron microscopic study. Virology. 1967 May;32(1):128-43. doi: 10.1016/0042-6822(67)90261-9. PMID: 6067298.

Akira, S., Takeda, K. Toll-like receptor signalling. Nat Rev Immunol 4, 499–511 (2004). https://doi.org/10.1038/nri1391

Albig W, Kardalinou E, Drabent B, Zimmer A, Doenecke D. Isolation and characterization of two human H1 histone genes within clusters of core histone genes. Genomics. 1991 Aug;10(4):940-8. doi: 10.1016/0888-7543(91)90183-f. PMID: 1916825.

Alexopoulou L, Holt AC, Medzhitov R, Flavell RA. Recognition of double-stranded RNA and activation of NF-kappaB by Toll-like receptor 3. Nature. 2001 Oct 18;413(6857):732-8. doi: 10.1038/35099560. PMID: 11607032.

Almine JF, O'Hare CA, Dunphy G, Haga IR, Naik RJ, Atrih A, Connolly DJ, Taylor J, Kelsall IR, Bowie AG, Beard PM, Unterholzner L. IFI16 and cGAS cooperate in the activation of STING during DNA sensing in human keratinocytes. Nat Commun. 2017 Feb 13;8:14392. doi: 10.1038/ncomms14392. PMID: 28194029; PMCID: PMC5316833.

Alseth I, Dalhus B, Bjørås M. Inosine in DNA and RNA. Curr Opin Genet Dev. 2014 Jun;26:116-23. doi: 10.1016/j.gde.2014.07.008. Epub 2014 Aug 30. PMID: 25173738.

Amini-Bavil-Olyaee S, Choi YJ, Lee JH, Shi M, Huang IC, Farzan M, Jung JU. The antiviral effector IFITM3 disrupts intracellular cholesterol homeostasis to block viral entry. Cell Host Microbe. 2013 Apr 17;13(4):452-64. doi: 10.1016/j.chom.2013.03.006. Erratum in: Cell Host Microbe. 2013 Nov 13;14(5):600-1. PMID: 23601107; PMCID: PMC3646482.

Amos, H. & Korn, M. 5-Methyl cytosine in the RNA of Escherichia coli. Biochim. Biophys. Acta 29, 444–445 (1958).

Anderson S, Bankier AT, Barrell BG, de Bruijn MH, Coulson AR, Drouin J, Eperon IC, Nierlich DP, Roe BA, Sanger F, Schreier PH, Smith AJ, Staden R, Young IG. Sequence and organization of the human mitochondrial genome. Nature. 1981 Apr 9;290(5806):457-65. doi: 10.1038/290457a0. PMID: 7219534.

Andrejeva J, Childs KS, Young DF, Carlos TS, Stock N, Goodbourn S, Randall RE. The V proteins of paramyxoviruses bind the IFN-inducible RNA helicase, mda-5, and inhibit its activation of the IFN-beta promoter. Proc Natl Acad Sci U S A. 2004 Dec 7;101(49):17264-9. doi: 10.1073/pnas.0407639101. Epub 2004 Nov 24. PMID: 15563593; PMCID: PMC535396.

Atkins GJ, Sheahan BJ, Liljeström P. The molecular pathogenesis of Semliki Forest virus: a model virus made useful? J Gen Virol. 1999 Sep;80 (Pt 9):2287-2297. doi: 10.1099/0022-1317-80-9-2287. PMID: 10501479.

Aubert M, O'Donohue MF, Lebaron S, Gleizes PE. Pre-Ribosomal RNA Processing in Human Cells: From Mechanisms to Congenital Diseases. Biomolecules. 2018 Oct 24;8(4):123. doi: 10.3390/biom8040123. PMID: 30356013; PMCID: PMC6315592.

Bailey TL, Johnson J, Grant CE, Noble WS. The MEME Suite. Nucleic Acids Res. 2015 Jul 1;43(W1):W39-49. doi: 10.1093/nar/gkv416. Epub 2015 May 7. PMID: 25953851; PMCID: PMC4489269.

Bakkers, M.J.G., Ritschel, T., Tiemessen, M. et al. Efficacious human metapneumovirus vaccine based on AI-guided engineering of a closed prefusion trimer. Nat Commun 15, 6270 (2024). https://doi.org/10.1038/s41467-024-50659-5

Baltimore D (1970). RNA-dependent DNA polymerase in virions of RNA tumour viruses, Nature226, 1209–1211.

Barr SD, Smiley JR, Bushman FD. The interferon response inhibits HIV particle production by induction of TRIM22. PLoS Pathog. 2008 Feb 29;4(2):e1000007. doi: 10.1371/journal.ppat.1000007. PMID: 18389079; PMCID: PMC2279259.

Barrett T, Wilhite SE, Ledoux P, Evangelista C, Kim IF, Tomashevsky M, Marshall KA, Phillippy KH, Sherman PM, Holko M, Yefanov A, Lee H, Zhang N, Robertson CL, Serova N, Davis S, Soboleva A. NCBI GEO: archive for functional genomics data sets--update. Nucleic Acids Res. 2013 Jan;41(Database issue):D991-5. doi: 10.1093/nar/gks1193. Epub 2012 Nov 27. PMID: 23193258; PMCID: PMC3531084.

Batra J, Hultquist JF, Liu D, Shtanko O, Von Dollen J, Satkamp L, Jang GM, Luthra P, Schwarz TM, Small GI, Arnett E, Anantpadma M, Reyes A, Leung DW, Kaake R, Haas P, Schmidt CB, Schlesinger LS, LaCount DJ, Davey RA, Amarasinghe GK, Basler CF, Krogan NJ. Protein Interaction Mapping Identifies RBBP6 as a Negative Regulator of Ebola Virus Replication. Cell. 2018 Dec 13;175(7):1917-1930.e13. doi: 10.1016/j.cell.2018.08.044. PMID: 30550789; PMCID: PMC6366944.

Battles, M.B., McLellan, J.S. Respiratory syncytial virus entry and how to block it. Nat Rev Microbiol 17, 233–245 (2019). https://doi.org/10.1038/s41579-019-0149-x

Begik, O. et al. Quantitative profiling of pseudouridylation dynamics in native RNAs with nanopore sequencing. Nat. Biotechnol. 39, 1278–1291 (2021).

Bergstrand, S., O'Brien, E.M., Coucoravas, C. et al. Small Cajal body-associated RNA 2 (scaRNA2) regulates DNA repair pathway choice by inhibiting DNA-PK. Nat Commun 13, 1015 (2022). https://doi.org/10.1038/s41467-022-28646-5

Berke IC, Modis Y. MDA5 cooperatively forms dimers and ATP-sensitive filaments upon binding double-stranded RNA. EMBO J. 2012 Apr 4;31(7):1714-26. doi: 10.1038/emboj.2012.19. Epub 2012 Feb 7. PMID: 22314235; PMCID: PMC3321199.

Bermingham, A. & Collins, P. L. The M2-2 protein of human respiratory syncytial virus is a regulatory factor involved in the balance between RNA replication and transcription. Proc. Natl Acad. Sci. USA 96, 11259–11264 (1999).

Bhatt DM, Pandya-Jones A, Tong AJ, Barozzi I, Lissner MM, Natoli G, Black DL, Smale ST. Transcript dynamics of proinflammatory genes revealed by sequence analysis of subcellular RNA fractions. Cell. 2012 Jul 20;150(2):279-90. doi: 10.1016/j.cell.2012.05.043. PMID: 22817891; PMCID: PMC3405548.

Bhattacharya S, Qian J, Tzimas C, Baker DP, Koumenis C, Diehl JA, Fuchs SY. Role of p38 protein kinase in the ligand-independent ubiquitination and down-regulation of the IFNAR1 chain of type I interferon receptor. J Biol Chem. 2011 Jun 24;286(25):22069-76. doi: 10.1074/jbc.M111.238766. Epub 2011 May 3. PMID: 21540188; PMCID: PMC3121351.

Bhaya D, Davison M, Barrangou R. CRISPR-Cas systems in bacteria and archaea: versatile small RNAs for adaptive defense and regulation. Annu Rev Genet. 2011;45:273-97. doi: 10.1146/annurev-genet-110410-132430. PMID: 22060043.

Bitko, V. et al. Nonstructural proteins of respiratory syncytial virus suppress premature apoptosis by an NF-κB-dependent, interferon-independent mechanism and facilitate virus growth. J. Virol. 81, 1786–1795 (2007).

Blanco S, Dietmann S, Flores JV, Hussain S, Kutter C, Humphreys P, Lukk M, Lombard P, Treps L, Popis M, Kellner S, Hölter SM, Garrett L, Wurst W, Becker L, Klopstock T, Fuchs H, Gailus-Durner V, Hrabě de Angelis M, Káradóttir RT, Helm M, Ule J, Gleeson JG, Odom DT, Frye M. Aberrant methylation of tRNAs links cellular stress to neuro-developmental disorders. EMBO J. 2014 Sep 17;33(18):2020-39. doi: 10.15252/embj.201489282. Epub 2014 Jul 25. PMID: 25063673; PMCID: PMC4195770.

Blanco, S. et al. Stem cell function and stress response are controlled by protein synthesis. Nature 534, 335–340 (2016).

Bo Sun, Karin B. Sundström, Jun Jie Chew, Pradeep Bist, Esther S. Gan, Hwee Cheng Tan, Kenneth C. Goh, Tanu Chawla, Choon Kit Tang, and Eng Eong Ooi. Dengue virus activates cGAS through the release of mitochondrial DNA. Scientific Reports, 7(1):3594, June 2017.

Boccaletto, P. et al. MODOMICS: a database of RNA modification pathways. 2021 update. Nucleic Acids Res. 50, D231–D235 (2022).

Boccaletto, P., Stefaniak, F., Ray, A., Cappannini, A., Mukherjee, S., Purta, E., et al. (2022). Modomics: A database of RNA modification pathways 2021 update. Nucleic Acids Res. 50, D231–D235. doi:10.1093/nar/gkab1083

Bock, C., Datlinger, P., Chardon, F. et al. High-content CRISPR screening. Nat Rev Methods Primers 2, 8 (2022). https://doi.org/10.1038/s43586-021-00093-4

Bogorad AM, Lin KY, Marintchev A. Novel mechanisms of eIF2B action and regulation by eIF2α phosphorylation. Nucleic Acids Res. 2017 Nov 16;45(20):11962-11979. doi: 10.1093/nar/gkx845. PMID: 29036434; PMCID: PMC5714165.

Bohnsack, K. E., Höbartner, C., and Bohnsack, M. T. (2019). Eukaryotic 5-methylcytosine (m^5C) RNA methyltransferases: Mechanisms, cellular functions, and links to disease. Genes 10, 102. doi:10.3390/genes10020102

Bohnsack,K.E., Ho ̈bartner,C. and Bohnsack,M.T. (2019) Eukaryotic 5-methylcytosine (m5C) RNA methyltransferases: mechanisms, cellular functions, and links to disease. Genes (Basel), 10, 102.

Bourgeois G, Ney M, Gaspar I, Aigueperse C, Schaefer M, Kellner S, Helm M, Motorin Y. Eukaryotic rRNA Modification by Yeast 5-Methylcytosine-Methyltransferases and Human Proliferation-Associated Antigen p120. PLoS One. 2015 Jul 21;10(7):e0133321. doi: 10.1371/journal.pone.0133321. PMID: 26196125; PMCID: PMC4510066.

Brass AL, Huang IC, Benita Y, John SP, Krishnan MN, Feeley EM, Ryan BJ, Weyer JL, van der Weyden L, Fikrig E, Adams DJ, Xavier RJ, Farzan M, Elledge SJ. The IFITM proteins mediate cellular resistance to influenza A H1N1 virus, West Nile virus, and dengue virus. Cell. 2009 Dec 24;139(7):1243-54. doi: 10.1016/j.cell.2009.12.017. PMID: 20064371; PMCID: PMC2824905.

Buchbender A, Mutter H, Sutandy FXR, Körtel N, Hänel H, Busch A, Ebersberger S, König J. Improved library preparation with the new iCLIP2 protocol. Methods. 2020 Jun 1;178:33-48. doi: 10.1016/j.ymeth.2019.10.003. Epub 2019 Oct 11. PMID: 31610236.

Cai C, Tang YD, Xu G, Zheng C. The crosstalk between viral RNA- and DNA-sensing mechanisms. Cell Mol Life Sci. 2021 Dec;78(23):7427-7434. doi: 10.1007/s00018-021-04001-7. Epub 2021 Oct 29. PMID: 34714359; PMCID: PMC8554519.

Canton J, Fehr AR, Fernandez-Delgado R, Gutierrez-Alvarez FJ, Sanchez-Aparicio MT, García-Sastre A, Perlman S, Enjuanes L, Sola I. MERS-CoV 4b protein interferes with the NF-κB-dependent innate immune response during infection. PLoS Pathog. 2018 Jan 25;14(1):e1006838. doi: 10.1371/journal.ppat.1006838. PMID: 29370303; PMCID: PMC5800688.

Cao Y, et al. 2018. A comprehensive study on cellular RNA editing activity in response to infections with different subtypes of influenza a viruses. BMC Genomics 19(Suppl 1):925.

Carty M, Guy C, Bowie AG. Detection of Viral Infections by Innate Immunity. Biochem Pharmacol. 2021 Jan;183:114316. doi: 10.1016/j.bcp.2020.114316. Epub 2020 Nov 3. PMID: 33152343.

Castello, A., Sanz, M.A., Molina, S., and Carrasco, L. (2006). Translation of Sindbis virus 26S mRNA does not require intact eukariotic initiation factor 4G. J Mol Biol 355, 942–956.

Chai, J., Wang, Q., Qiu, Q. et al. YBX1 regulates the survival of chronic myeloid leukemia stem cells by modulating m6A-mediated YWHAZ stability. Cell Oncol. 46, 451–464 (2023). https://doi.org/10.1007/s13402-022-00762-w

Chan C, Kwan Sze NS, Suzuki Y, Ohira T, Suzuki T, Begley TJ, Dedon PC. Dengue virus exploits the host tRNA epitranscriptome to promote viral replication. bioRxiv [Preprint]. 2023 Nov 6:2023.11.05.565734. doi: 10.1101/2023.11.05.565734. PMID: 37986976; PMCID: PMC10659268.

Chatterjee S, Luthra P, Esaulova E, Agapov E, Yen BC, Borek DM, Edwards MR, Mittal A, Jordan DS, Ramanan P, Moore ML, Pappu RV, Holtzman MJ, Artyomov MN, Basler CF, Amarasinghe GK, Leung DW. Structural basis for human respiratory syncytial virus NS1-mediated modulation of host responses. Nat Microbiol. 2017;2:17101

Chemudupati M, Kenney AD, Bonifati S, Zani A, McMichael TM et al. 2019. From APOBEC to ZAP: diverse mechanisms used by cellular restriction factors to inhibit virus infections. Biochim. Biophys. Acta Mol. Cell Res. 1866:382–94

Chen, S. et al. N6-methyladenosine modification of HIV-1 RNA suppresses type-I interferon induction in differentiated monocytic cells and primary macrophages. PLoS Pathog. 17, e1009421 (2021).

Chen, S., Kumar, S., Espada, C. E., Tirumuru, N., Cahill, M. P., Hu, L., et al. (2021). N6-methyladenosine modification of HIV-1 RNA suppresses type-I interferon induction in differentiated monocytic cells and primary macrophages. PLoS Pathog. 17:e1009421. doi: 10.1371/journal.ppat.1009421

Chen, Y., Shen, H., Liu, T. et al. ATR-binding lncRNA ScaRNA2 promotes cancer resistance through facilitating efficient DNA end resection during homologous recombination repair. J Exp Clin Cancer Res 42, 256 (2023). https://doi.org/10.1186/s13046-023-02829-4

Chen, Y., Su, C., Ke, M., Jin, X., Xu, L., Zhang, Z., et al. (2011). Biochemical and structural insights into the mechanisms of SARS coronavirus RNA ribose 2'-O-methylation by nsp16/nsp10 protein complex. PLoS Pathog. 7, e1002294. doi:10.1371/journal.ppat.1002294

Chen, Y., Tao, J., Sun, Y., Wu, A., Su, C., Gao, G., et al. (2013). Structure-function analysis of severe acute respiratory syndrome coronavirus RNA cap guanine-N7-methyltransferase. J. Virol. 87, 6296–6305. doi:10.1128/JVI.00061-13

Chiang, J.J., Sparrer, K.M.J., van Gent, M. et al. Viral unmasking of cellular 5S rRNA pseudogene transcripts induces RIG-I-mediated immunity. Nat Immunol 19, 53–62 (2018). https://doi.org/10.1038/s41590-017-0005-y

Chin KC, Cresswell P. Viperin (cig5), an IFN-inducible antiviral protein directly induced by human cytomegalovirus. Proc Natl Acad Sci U S A. 2001 Dec 18;98(26):15125-30. doi: 10.1073/pnas.011593298. Erratum in: Proc Natl Acad Sci U S A 2002 Feb 19;99(4):2460. PMID: 11752458; PMCID: PMC64994.

Choi EJ, Wu W, Zhang K, Yuan X, Deng J, Ismail D, Buck DL, Thomason KS, Garofalo RP, Zhang S, Bao X. Parent tRNA Modification Status Determines the Induction of

Functional tRNA-Derived RNA by Respiratory Syncytial Virus Infection. Viruses. 2022 Dec 24;15(1):57. doi: 10.3390/v15010057. PMID: 36680097; PMCID: PMC9860972.

Choi, E.-J.; Wu, W.; Zhang, K.; Yuan, X.; Deng, J.; Ismail, D.; Buck, D.L.; Thomason, K.S.; Garofalo, R.P.; Zhang, S.; et al. Parent tRNA Modification Status Determines the Induction of Functional tRNA-Derived RNA by Respiratory Syncytial Virus Infection. Viruses 2023, 15, 57. https://doi.org/10.3390/v15010057

Chou Y.Y., Heaton N.S., Gao Q., Palese P., Singer R.H., Lionnet T. Colocalization of different influenza viral RNA segments in the cytoplasm before viral budding as shown by single-molecule sensitivity FISH analysis. PLoS Pathog. 2013;9:e1003358. doi: 10.1371/annotation/8f53e7f2-2348-436f-b37e-a883a01e9bbd.

Cifuentes-Muñoz N, Branttie J, Slaughter KB, Dutch RE. Human Metapneumovirus Induces Formation of Inclusion Bodies for Efficient Genome Replication and Transcription. J Virol. 2017 Nov 30;91(24):e01282-17. doi: 10.1128/JVI.01282-17. PMID: 28978704; PMCID: PMC5709606.

Ciganda,M. and Williams,N. (2011) Eukaryotic 5S rRNA biogenesis. Wiley Interdiscip. Rev. RNA, 2, 523–533.

Civril F, Deimling T, de Oliveira Mann CC, Ablasser A, Moldt M, Witte G, Hornung V, Hopfner KP. Structural mechanism of cytosolic DNA sensing by cGAS. Nature. 2013 Jun 20;498(7454):332-7. doi: 10.1038/nature12305. Epub 2013 May 30. PMID: 23722159; PMCID: PMC3768140.

Clemens, M. J. & Williams, B. R. G. Inhibition of cell-free protein synthesis by pppA2′p5′A2′p5′A: a novel oligonucleotide synthesized by interferon-treated L cell extracts. Cell 13, 565–572 (1978).

Cléry A, Senty-Ségault V, Leclerc F, Raué HA, Branlant C. Analysis of sequence and structural features that identify the B/C motif of U3 small nucleolar RNA as the recognition site for the Snu13p-Rrp9p protein pair. Mol Cell Biol. 2007 Feb;27(4):1191-206. doi: 10.1128/MCB.01287-06. Epub 2006 Dec 4. PMID: 17145781; PMCID: PMC1800722.

Cohn, W. E. Pseudouridine, a carbon–carbon linked ribonucleoside in ribonucleic acids: isolation, structure, and chemical characteristics. J. Biol. Chem. 235, 1488–1498 (1960).

Colina, R. et al. Translational control of the innate immune response through IRF-7. Nature 452, 323–328 (2008).

Cong L, Ran FA, Cox D, Lin S, Barretto R, Habib N, Hsu PD, Wu X, Jiang W, Marraffini LA, Zhang F. Multiplex genome engineering using CRISPR/Cas systems. Science. 2013;339:819–823. doi:10.1126/science.1231143

Cooper GM. The Cell: A Molecular Approach. 2nd edition. Sunderland (MA): Sinauer Associates; 2000. RNA Processing and Turnover. Available from: https://www.ncbi.nlm.nih.gov/books/NBK9864/

Courtney DG, Kennedy EM, Dumm RE, Bogerd HP, Tsai K, Heaton NS, Cullen BR. Epitranscriptomic Enhancement of Influenza A Virus Gene Expression and Replication. Cell Host Microbe. 2017 Sep 13;22(3):377-386.e5. doi: 10.1016/j.chom.2017.08.004. PMID: 28910636; PMCID: PMC5615858.

Courtney DG, Tsai K, Bogerd HP, Kennedy EM, Law BA, Emery A, Swanstrom R, Holley CL, Cullen BR. Epitranscriptomic Addition of m5C to HIV-1 Transcripts Regulates Viral Gene Expression. Cell Host Microbe. 2019 Aug 14;26(2):217-227.e6. doi: 10.1016/j.chom.2019.07.005. PMID: 31415754; PMCID: PMC6714563.

Courtney, D. G., Tsai, K., Bogerd, H. P., Kennedy, E. M., Law, B. A., Emery, A., et al. (2019). Epitranscriptomic addition of m(5)C to HIV-1 transcripts regulates viral gene expression. Cell Host Microbe 26, 217–227.e6. doi:10.1016/j.chom.2019.07.005

Cressey TN, Noton SL, Nagendra K, Braun MR, Fearns R. Mechanism for de novo initiation at two sites in the respiratory syncytial virus promoter. Nucleic Acids Res. 2018;46(13):6785–96. Epub 2018/06/07. pmid:29873775; PubMed Central PMCID: PMCPMC6061868.

Cristinelli, S., Angelino, P., and Ciuffi, A. (2022). Exploring m⁶A and m⁵C epitranscriptomes upon viral infection: An example with HIV. J. Vis. Exp. 2022. doi:10.3791/62426

Cuadrado E, Booiman T, van Hamme JL, et al. ADAR1 Facilitates HIV-1 Replication in Primary CD4+ T Cells. PLoS One. 2015;10(12):e0143613. Published 2015 Dec 2. doi:10.1371/journal.pone.0143613

Cuadrado E, Booiman T, van Hamme JL, et al. ADAR1 Facilitates HIV-1 Replication in Primary CD4+ T Cells. PLoS One. 2015;10(12):e0143613. Published 2015 Dec 2. doi:10.1371/journal.pone.0143613

Cui S, Eisenächer K, Kirchhofer A, Brzózka K, Lammens A, Lammens K, Fujita T, Conzelmann KK, Krug A, Hopfner KP. The C-terminal regulatory domain is the RNA 5'-triphosphate sensor of RIG-I. Mol Cell. 2008 Feb 1;29(2):169-79. doi: 10.1016/j.molcel.2007.10.032. PMID: 18243112.

Cui, K. et al. The chromatin-remodeling BAF complex mediates cellular antiviral activities by promoter priming. Mol. Cell. Biol. 24, 4476–4486 (2004).

Cui, L., Ma, R., Cai, J. et al. RNA modifications: importance in immune cell biology and related diseases. Sig Transduct Target Ther 7, 334 (2022).

Daffis S, Szretter KJ, Schriewer J, Li J, Youn S, Errett J, Lin TY, Schneller S, Zust R, Dong H, Thiel V, Sen GC, Fensterl V, Klimstra WB, Pierson TC, Buller RM, Gale M Jr, Shi PY, Diamond MS. 2'-O methylation of the viral mRNA cap evades host restriction by IFIT family members. Nature. 2010 Nov 18;468(7322):452-6. doi: 10.1038/nature09489. PMID: 21085181; PMCID: PMC3058805.

DaFonseca, C. J., Shu, F. & Zhang, J. J. Identification of two residues in MCM5 critical for the assembly of MCM complexes and Stat1-mediated transcription activation in response to IFN-γ. Proc. Natl Acad. Sci. USA 98, 3034–3039 (2001).

Dang Y, Li J, Li Y, Wang Y, Zhao Y, Zhao N, Li W, Zhang H, Ye C, Ma H, Zhang L, Liu H, Dong Y, Yao M, Lei Y, Xu Z, Zhang F, Ye W. N-acetyltransferase 10 regulates alphavirus replication via N4-acetylcytidine (ac4C) modification of the lymphocyte antigen six family member E (LY6E) mRNA. J Virol. 2024 Jan 23;98(1):e0135023. doi: 10.1128/jvi.01350-23. Epub 2024 Jan 3. PMID: 38169284; PMCID: PMC10805074.

Darnell, J. E. Stats and gene regulation. Science 277, 1630–1635 (1997).

Day ND, Branigan PJ, Liu C, Gutshall LL, Luo J, Melero JA, Sarisky RT, Del Vecchio AM. Contribution of cysteine residues in the extracellular domain of the F protein of human respiratory syncytial virus to its function. Virol J. 2006;3:34

de Beus E, Brockenbrough JS, Hong B, Aris JP. Yeast NOP2 encodes an essential nucleolar protein with homology to a human proliferation marker. J Cell Biol. 1994 Dec;127(6 Pt 2):1799-813. doi: 10.1083/jcb.127.6.1799. PMID: 7806561; PMCID: PMC2120275.

de Chassey B, et al. 2013. The interactomes of influenza virus NS1 and NS2 proteins identify new host factors and provide insights for ADAR1 playing a supportive role in virus replication. PLoS Pathog. 9(7):e1003440.

de Chassey, B., Aublin-Gex, A., Ruggieri, A., Meyniel-Schicklin, L., Pradezynski, F., Davoust, N., et al. (2013). The interactomes of influenza virus NS1 and NS2 proteins identify new host factors and provide insights for ADAR1 playing a supportive role in virus replication. PLoS Pathog. 9, e1003440. doi:10.1371/journal.ppat.1003440

De Vlugt, C., Sikora, D., and Pelchat, M. (2018). Insight into influenza: A virus cap-snatching. Viruses 10, 641. doi:10.3390/v10110641

De Vries DD, Went LN, Bruyn GW, Scholte HR, Hofstra RM, Bolhuis PA, van Oost BA. Genetic and biochemical impairment of mitochondrial complex I activity in a family with Leber hereditary optic neuropathy and hereditary spastic dystonia. Am J Hum Genet. 1996 Apr;58(4):703-11. PMID: 8644732; PMCID: PMC1914692.

De Wit, E., Spronken, M. I., Bestebroer, T. M., Rimmelzwaan, G. F., Osterhaus, A. D. & Fouchier, R. A. 2004. Efficient generation and growth of influenza virus A/PR/8/34 from eight cDNA fragments. Virus Res, 103, 155-61.

Decatur WA, Fournier MJ. rRNA modifications and ribosome function. Trends Biochem Sci. 2002;27:344–351.

Dede M, McLaughlin M, Kim E, Hart T. Multiplex enCas12a screens detect functional buffering among paralogs otherwise masked in monogenic Cas9 knockout screens. Genome Biol. 2020 Oct 15;21(1):262. doi: 10.1186/s13059-020-02173-2. PMID: 33059726; PMCID: PMC7558751.

Delaunay, S. & Frye, M. RNA modifications regulating cell fate in cancer. Nat. Cell Biol. 21, 552–559 (2019).

Delaunay, S., Frye, M. Localization-dictated function for METTL3. Nat Cell Biol 24, 1188–1189 (2022). https://doi.org/10.1038/s41556-022-00972-2

Delaunay, S., Helm, M. & Frye, M. RNA modifications in physiology and disease: towards clinical applications. Nat Rev Genet 25, 104–122 (2024). https://doi.org/10.1038/s41576-023-00645-2

Deng, J, Ptashkin, RN, Chen, Y, Cheng, Z, Liu, G, Phan, T et al. (2015). Respiratory syncytial virus utilizes a tRNA fragment to suppress antiviral responses through a novel targeting mechanism. Mol Ther 23: 1622–1629.

Der, S. D., Zhou, A., Williams, B. R. & Silverman, R. H. Identification of genes differentially regulated by interferon α, β, or γ using oligonucleotide arrays. Proc. Natl Acad. Sci. USA 95, 15623–15628 (1998).

Dev, R. R., Ganji, R., Singh, S. P., Mahalingam, S., Banerjee, S., and Khosla, S. (2017). Cytosine methylation by DNMT2 facilitates stability and survival of HIV-1 RNA in the host cell during infection. Biochem. J. 474, 2009–2026. doi:10.1042/BCJ20170258

Dhir A, Dhir S, Borowski LS, Jimenez L, Teitell M, Rötig A, Crow YJ, Rice GI, Duffy D, Tamby C, Nojima T, Munnich A, Schiff M, de Almeida CR, Rehwinkel J, Dziembowski A, Szczesny RJ, Proudfoot NJ. Mitochondrial double-stranded RNA triggers antiviral signalling in humans. Nature. 2018 Aug;560(7717):238-242. doi: 10.1038/s41586-018-0363-0. Epub 2018 Jul 25. PMID: 30046113; PMCID: PMC6570621.

Di Giorgio S, Martignano F, Torcia MG, Mattiuz G, Conticello SG. Evidence for host-dependent RNA editing in the transcriptome of SARS-CoV-2. Sci Adv. 2020 Jun 17;6(25):eabb5813. doi: 10.1126/sciadv.abb5813. PMID: 32596474; PMCID: PMC7299625.

Dias Junior AG, Sampaio NG, Rehwinkel J. A Balancing Act: MDA5 in Antiviral Immunity and Autoinflammation. Trends Microbiol. 2019 Jan;27(1):75-85. doi: 10.1016/j.tim.2018.08.007. Epub 2018 Sep 7. PMID: 30201512; PMCID: PMC6319154.

Diebold SS, Kaisho T, Hemmi H, Akira S, Reis e Sousa C. Innate antiviral responses by means of TLR7-mediated recognition of single-stranded RNA. Science. 2004 Mar 5;303(5663):1529-31. doi: 10.1126/science.1093616. Epub 2004 Feb 19. PMID: 14976261.

Dobin A, Davis CA, Schlesinger F, Drenkow J, Zaleski C, Jha S, Batut P, Chaisson M, Gingeras TR. STAR: ultrafast universal RNA-seq aligner. Bioinformatics. 2013 Jan 1;29(1):15-21. doi: 10.1093/bioinformatics/bts635. Epub 2012 Oct 25. PMID: 23104886; PMCID: PMC3530905.

Domingues MM, Gomes B, Hollmann A, Santos NC. 25-Hydroxycholesterol Effect on Membrane Structure and Mechanical Properties. Int J Mol Sci. 2021 Mar 4;22(5):2574. doi: 10.3390/ijms22052574. PMID: 33806504; PMCID: PMC7961727.

Dominguez D, Freese P, Alexis MS, Su A, Hochman M, Palden T, Bazile C, Lambert NJ, Van Nostrand EL, Pratt GA, Yeo GW, Graveley BR, Burge CB. Sequence, Structure, and Context Preferences of Human RNA Binding Proteins. Mol Cell. 2018

Jun 7;70(5):854-867.e9. doi: 10.1016/j.molcel.2018.05.001. Epub 2018 Jun 7. PMID: 29883606; PMCID: PMC6062212.

Dominissini D, Nachtergaele S, Moshitch-Moshkovitz S, Peer E, Kol N, Ben-Haim MS, Dai Q, Di Segni A, Salmon-Divon M, Clark WC, Zheng G, Pan T, Solomon O, Eyal E, Hershkovitz V, Han D, Doré LC, Amariglio N, Rechavi G, He C. The dynamic N(1)-methyladenosine methylome in eukaryotic messenger RNA. Nature. 2016 Feb 25;530(7591):441-6. doi: 10.1038/nature16998. Epub 2016 Feb 10. PMID: 26863196; PMCID: PMC4842015.

Doria, M., Neri, F., Gallo, A., Farace, M. G., and Michienzi, A. (2009). Editing of HIV-1 RNA by the double-stranded RNA deaminase ADAR1 stimulates viral infection. Nucleic Acids Res. 37, 5848–5858. doi:10.1093/nar/gkp604

Drygin,D., Rice,W.G. and Grummt,I. (2010) The RNA polymerase i transcription machinery: an emerging target for the treatment of cancer. Annu. Rev. Pharmacol. Toxicol., 50, 131–156.

Durbin A.F., Wang C., Marcotrigiano J., Gehrke L. RNAs containing modified nucleotides fail to trigger RIG-I conformational changes for innate immune signaling. Mbio. 2016; 7:e00833–16.

Durfee LA, Lyon N, Seo K, Huibregtse JM. The ISG15 conjugation system broadly targets newly synthesized proteins: implications for the antiviral function of ISG15. Mol Cell. 2010 Jun 11;38(5):722-32. doi: 10.1016/j.molcel.2010.05.002. PMID: 20542004; PMCID: PMC2887317.

Eckwahl, M., Xu, R., Michalkiewicz, J., Zhang, W., Patel, P., Cai, Z., et al. (2020). 5-Methylcytosine RNA modifications promote retrovirus replication in an ALYREF reader protein-dependent manner. J. Virol. 94, e00544. doi:10.1128/JVI.00544-20

Edelheit, S., Schwartz, S., Mumbach, M. R., Wurtzel, O. & Sorek, R. Transcriptome-wide mapping of 5-methylcytidine RNA modifications in bacteria, archaea, and yeast reveals m5C within archaeal mRNAs. PLoS Genet. 9, e1003602 (2013).

Eisfeld AJ, Neumann G, Kawaoka Y. Influenza A virus isolation, culture and identification. Nat Protoc. 2014 Nov;9(11):2663-81. doi: 10.1038/nprot.2014.180. Epub 2014 Oct 16. PMID: 25321410; PMCID: PMC5619698.

Evdokimova V, Ovchinnikov LP, Sorensen PH. Y-box binding protein 1: providing a new angle on translational regulation. Cell Cycle. 2006 Jun;5(11):1143-7. doi: 10.4161/cc.5.11.2784. Epub 2006 Jun 1. PMID: 16721060.

Fakruddin M, Wei FY, Suzuki T, Asano K, Kaieda T, Omori A, Izumi R, Fujimura A, Kaitsuka T, Miyata K, Araki K, Oike Y, Scorrano L, Suzuki T, Tomizawa K. Defective Mitochondrial tRNA Taurine Modification Activates Global Proteostress and Leads to Mitochondrial Disease. Cell Rep. 2018 Jan 9;22(2):482-496. doi: 10.1016/j.celrep.2017.12.051. PMID: 29320742.

Fan, X., Zhang, Y., Guo, R. et al. Decoding epitranscriptomic regulation of viral infection: mapping of RNA N6-methyladenosine by advanced sequencing

technologies. Cell Mol Biol Lett 29, 42 (2024). https://doi.org/10.1186/s11658-024-00564-y

Fearns, R. & Collins, P. L. Role of the M2-1 transcription antitermination protein of respiratory syncytial virus in sequential transcription. J. Virol. 73, 5852–5864 (1999).

Ferguson MC, Saul S, Fragkoudis R, Weisheit S, Cox J, Patabendige A, Sherwood K, Watson M, Merits A, Fazakerley JK. Ability of the Encephalitic Arbovirus Semliki Forest Virus To Cross the Blood-Brain Barrier Is Determined by the Charge of the E2 Glycoprotein. J Virol. 2015 Aug;89(15):7536-49. doi: 10.1128/JVI.03645-14. Epub 2015 May 13. PMID: 25972559; PMCID: PMC4505677.

Ficarelli M, Neil SJD, Swanson CM. Targeted Restriction of Viral Gene Expression and Replication by the ZAP Antiviral System. Annu Rev Virol. 2021 Sep 29;8(1):265-283. doi: 10.1146/annurev-virology-091919-104213. Epub 2021 Jun 15. PMID: 34129371.

Ficarelli M, Wilson H, Galão RP, Mazzon M, Antzin-Anduetza I et al. 2019. KHNYN is essential for the zinc finger antiviral protein (ZAP) to restrict HIV-1 containing clustered CpG dinucleotides. eLife 8:e46767

Finer-Moore J, Czudnochowski N, O'Connell JD 3rd, Wang AL, Stroud RM. Crystal Structure of the Human tRNA m(1)A58 Methyltransferase-tRNA(3)(Lys) Complex: Refolding of Substrate tRNA Allows Access to the Methylation Target. J Mol Biol. 2015 Dec 4;427(24):3862-76. doi: 10.1016/j.jmb.2015.10.005. Epub 2015 Oct 22. PMID: 26470919; PMCID: PMC4663122.

Flint, J., Racaniello, V.R., Rall, G.F., Hatziioannou, T. and Skalka, A.M., 2020. Principles of virology, Volume 1: Molecular biology (Vol. 1). John Wiley & Sons.

Frye, M., Harada, B. T., Behm, M. & He, C. RNA modifications modulate gene expression during development. Science 361, 1346–1349 (2018).

Furuse Y. RNA Modifications in Genomic RNA of Influenza A Virus and the Relationship between RNA Modifications and Viral Infection. Int J Mol Sci. 2021 Aug 24;22(17):9127. doi: 10.3390/ijms22179127. PMID: 34502037; PMCID: PMC8431438.

Gan SW, Tan E, Lin X, Yu D, Wang J, Tan GM, Vararattanavech A, Yeo CY, Soon CH, Soong TW, Pervushin K, Torres J. The small hydrophobic protein of the human respiratory syncytial virus forms pentameric ion channels. The Journal of biological chemistry. 2012;287(29):24671-24689

Ganti K, Bagga A, DaSilva J, Shepard SS, Barnes JR, Shriner S, Koelle K, Lowen AC. Avian Influenza A Viruses Reassort and Diversify Differently in Mallards and Mammals. Viruses. 2021 Mar 19;13(3):509. doi: 10.3390/v13030509. PMID: 33808674; PMCID: PMC8003500.

Gao G, Guo X, Goff SP. Inhibition of retroviral RNA production by ZAP, a CCCH-type zinc finger protein. Science. 2002 Sep 6;297(5587):1703-6. doi: 10.1126/science.1074276. PMID: 12215647.

Garcia-Moreno, M., Noerenberg, M., Ni, S., Jarvelin, A.I., Gonzalez-Almela, E., Lenz, C.E., Bach-Pages, M., Cox, V., Avolio, R., Davis, T., et al. (2019). System-wide Profiling of RNA-Binding Proteins Uncovers Key Regulators of Virus Infection. Mol Cell 74, 196–211 e111.

Garcia-Moreno, Manuel & Truman, Robin & Chen, Honglin & Iselin, Louisa & Lenz, Caroline & Lee, Jeff & Dicker, Kate & Noerenberg, Marko & Sohier, Thibault & Palmalux, Natasha & Järvelin, Aino & Kamel, Wael & Ruscica, Vincenzo & Ricci, Emiliano & Davis, Ilan & Mohammed, Shabaz & Castello, Alfredo. (2023). Incorporation of genome-bound cellular proteins into HIV-1 particles regulates viral infection. 10.1101/2023.06.14.544764.

Garcia, J., Garcia-Barreno, B., Vivo, A. & Melero, J. A. Cytoplasmic inclusions of respiratory syncytial virus-infected cells: formation of inclusion bodies in transfected cells that coexpress the nucleoprotein, the phosphoprotein, and the 22K protein. Virology 195, 243–247 (1993).

Garegnani L, Styrmisdóttir L, Roson Rodriguez P, Escobar Liquitay CM, Esteban I, Franco JV. Palivizumab for preventing severe respiratory syncytial virus (RSV) infection in children. Cochrane Database Syst Rev. 2021 Nov 16;11(11):CD013757. doi: 10.1002/14651858.CD013757.pub2. PMID: 34783356; PMCID: PMC8594174.

Gilman MSA, Liu C, Fung A, Behera I, Jordan P, Rigaux P, Ysebaert N, Tcherniuk S, Sourimant J, Eléouët JF, Sutto-Ortiz P, Decroly E, Roymans D, Jin Z, McLellan JS. Structure of the Respiratory Syncytial Virus Polymerase Complex. Cell. 2019;179(1):193-204.e114

Girardi E, Pfeffer S, Baumert TF, Majzoub K. Roadblocks and fast tracks: How RNA binding proteins affect the viral RNA journey in the cell. Semin Cell Dev Biol. 2021 Mar;111:86-100. doi: 10.1016/j.semcdb.2020.08.006. Epub 2020 Aug 23. PMID: 32847707; PMCID: PMC7443355.

Girardot C, Scholtalbers J, Sauer S, Su SY, Furlong EE. Je, a versatile suite to handle multiplexed NGS libraries with unique molecular identifiers. BMC Bioinformatics. 2016 Oct 8;17(1):419. doi: 10.1186/s12859-016-1284-2. PMID: 27717304; PMCID: PMC5055726.

Gizzi AS, Grove TL, Arnold JJ, Jose J, Jangra RK et al. 2018. A naturally occurring antiviral ribonucleotide encoded by the human genome. Nature 558:610–14

Gokhale, N. S., McIntyre, A. B. R., Mattocks, M. D., Holley, C. L., Lazear, H. M., Mason, C. E., et al. (2020). Altered m(6)A modification of specific cellular transcripts affects flaviviridae infection. Mol. Cell 77, 542–555.e8. doi:10.1016/j.molcel.2019.11.007

Gonatopoulos-Pournatzis T, Cowling VH. Cap-binding complex (CBC). Biochem J. 2014 Jan 15;457(2):231-42. doi: 10.1042/BJ20131214. Erratum in: Biochem J. 2014 Feb 15;458(1):185. PMID: 24354960; PMCID: PMC3901397.

Gorchakov R, Frolova E, Frolov I. Inhibition of transcription and translation in Sindbis virus-infected cells. J Virol. 2005 Aug;79(15):9397-409. doi: 10.1128/JVI.79.15.9397-9409.2005. PMID: 16014903; PMCID: PMC1181568.

Goubau D, Deddouche S, Reis e Sousa C. Cytosolic sensing of viruses. Immunity. 2013 May 23;38(5):855-69. doi: 10.1016/j.immuni.2013.05.007. PMID: 23706667; PMCID: PMC7111113.

Graham D. Williams, Dana Townsend, Kristine M. Wylie, Preston J. Kim, Gaya K. Amarasinghe, Sebla B. Kutluay, and Adrianus C. M. Boon. Nucleotide resolution mapping of influenza A virus nucleoprotein-RNA interactions reveals RNA features required for replication. Nature Communications, 9(1):465, January 2018. Publisher: Nature Publishing Group.

Grimm, S. The art and design of genetic screens: mammalian culture cells. Nat Rev Genet 5, 179–189 (2004). https://doi.org/10.1038/nrg1291

Grummt, I. and Ladurner, A. G. (2008). A metabolic throttle regulates the epigenetic state of rDNA. Cell 133, 577-580. https://doi.org/10.1016/j.cell.2008.04.026

Gu W, Gallagher GR, Dai W, Liu P, Li R, Trombly MI, Gammon DB, Mello CC, Wang JP, Finberg RW. Influenza A virus preferentially snatches noncoding RNA caps. RNA. 2015 Dec;21(12):2067-75. doi: 10.1261/rna.054221.115. Epub 2015 Oct 1. PMID: 26428694; PMCID: PMC4647461.

Guo X, Ma J, Sun J, Gao G 2007. The zinc-finger antiviral protein recruits the RNA processing exosome to degrade the target mRNA. PNAS 104:151–56

Guo X, Steinkühler J, Marin M, Li X, Lu W, Dimova R, Melikyan GB. Interferon-Induced Transmembrane Protein 3 Blocks Fusion of Diverse Enveloped Viruses by Altering Mechanical Properties of Cell Membranes. ACS Nano. 2021 May 25;15(5):8155-8170. doi: 10.1021/acsnano.0c10567. Epub 2021 Mar 3. PMID: 33656312; PMCID: PMC8159881.

Gustafson WC, Taylor CW, Valdez BC, Henning D, Phippard A, Ren Y, Busch H, Durban E. Nucleolar protein p120 contains an arginine-rich domain that binds to ribosomal RNA. Biochem J. 1998 Apr 15;331 (Pt 2)(Pt 2):387-93. doi: 10.1042/bj3310387. PMID: 9531475; PMCID: PMC1219366.

Hafner M, Maria Katsantoni, Tino Köster, James Marks, Joyita Mukherjee, Dorothee Staiger, Jernej Ule, and Mihaela Zavolan. CLIP and complementary methods. Nature Reviews Methods Primers, 1(1):20, December 2021

Hafner, M., Katsantoni, M., Köster, T. et al. CLIP and complementary methods. Nat Rev Methods Primers 1, 20 (2021). https://doi.org/10.1038/s43586-021-00018-1

Hajnik, R.L., Plante, J.A., Reddy Bonam, S. et al. Broad protection and respiratory immunity of dual mRNA vaccination against SARS-CoV-2 variants. npj Vaccines 9, 160 (2024). https://doi.org/10.1038/s41541-024-00957-2

Haller, O., Arnheiter, H., Gresser, I. & Lindenmann, J. Genetically determined, interferon-dependent resistance to influenza virus in mice. J. Exp. Med. 149, 601–612 (1979).

Haller, O., Arnheiter, H., Lindenmann, J. & Gresser, I. Host gene influences sensitivity to interferon action selectively for influenza virus. Nature 283, 660–662 (1980).

Hanson, G. & Coller, J. Codon optimality, bias and usage in translation and mRNA decay. Nat. Rev. Mol. Cell Biol. 19, 20–30 (2018).

Hao, H., Liu, W., Miao, Y., Ma, L., Yu, B., Liu, L., et al. (2022). N4-acetylcytidine regulates the replication and pathogenicity of enterovirus 71. Nucleic Acids Res. 50, 9339–9354. doi:10.1093/nar/gkac675

Harrington, EM, James C. Murphy, Julie L. Aspden, Adrian Whitehouse. EMG1 methyltransferase activity regulates ribosome occupancy at viral uORFs. bioRxiv 2024.07.23.604771; doi: https://doi.org/10.1101/2024.07.23.604771

Hatesuer B, Bertram S, Mehnert N, Bahgat MM, Nelson PS, Pöhlmann S, Schughart K. Tmprss2 is essential for influenza H1N1 virus pathogenesis in mice. PLoS Pathog. 2013;9(12):e1003774. doi: 10.1371/journal.ppat.1003774. Epub 2013 Dec 5. Erratum in: PLoS Pathog. 2014 Sep;10(9):e1004435. Pöhlman, Stefan [corrected to Pöhlmann, Stefan]. PMID: 24348248; PMCID: PMC3857797.

Hebbes, T. R., Thorne, A. W. & Crane-Robinson, C. A direct link between core histone acetylation and transcriptionally active chromatin. EMBO J. 7, 1395–1402 (1988).

Henry BA, Marchand V, Schlegel BT, Helm M, Motorin Y, Lee N. Pseudouridylation of Epstein-Barr virus noncoding RNA EBER2 facilitates lytic replication. RNA. 2022 Nov;28(11):1542-1552. doi: 10.1261/rna.079219.122. Epub 2022 Sep 13. PMID: 36100352; PMCID: PMC9745832.

Hentze MW, Castello A, Schwarzl T, Preiss T. A brave new world of RNA-binding proteins. Nat Rev Mol Cell Biol. 2018 May;19(5):327-341. doi: 10.1038/nrm.2017.130. Epub 2018 Jan 17. PMID: 29339797.

Her Z, et al. 2010. Active infection of human blood monocytes by Chikungunya virus triggers an innate immune response. J Immunol. 184(10):5903–5913.

Hocine S, Singer RH, Grünwald D. RNA processing and export. Cold Spring Harb Perspect Biol. 2010 Dec;2(12):a000752. doi: 10.1101/cshperspect.a000752. Epub 2010 Oct 20. PMID: 20961978; PMCID: PMC2982171.

Hogan CA, Gratz SJ, Dumouchel JL, Thakur RS, Delgado A, Lentini JM, Madhwani KR, Fu D, O'Connor-Giles KM. Expanded tRNA methyltransferase family member TRMT9B regulates synaptic growth and function. EMBO Rep. 2023 Oct 9;24(10):e56808. doi: 10.15252/embr.202356808. Epub 2023 Aug 29. PMID: 37642556; PMCID: PMC10561368.

Honda K, Takaoka A, Taniguchi T. Type I interferon [corrected] gene induction by the interferon regulatory factor family of transcription factors. Immunity. 2006 Sep;25(3):349-60. doi: 10.1016/j.immuni.2006.08.009. Erratum in: Immunity. 2006 Nov;25(5):849. PMID: 16979567.

Honda K, Yanai H, Negishi H, Asagiri M, Sato M, Mizutani T, Shimada N, Ohba Y, Takaoka A, Yoshida N, Taniguchi T. IRF-7 is the master regulator of type-I interferon-dependent immune responses. Nature. 2005 Apr 7;434(7034):772-7. doi: 10.1038/nature03464. Epub 2005 Mar 30. PMID: 15800576.

Hong J, Lee JH, Chung IK. Telomerase activates transcription of cyclin D1 gene through an interaction with NOL1. J Cell Sci. 2016 Apr 15;129(8):1566-79. doi: 10.1242/jcs.181040. Epub 2016 Feb 19. PMID: 26906424.

Hu, X. et al. Sensitization of IFN-γ Jak-STAT signaling during macrophage activation. Nature Immunol. 3, 859–866 (2002).

Huppertz I, Attig J, D'Ambrogio A, Easton LE, Sibley CR, Sugimoto Y, Tajnik M, König J, Ule J. iCLIP: protein-RNA interactions at nucleotide resolution. Methods. 2014 Feb;65(3):274-87. doi: 10.1016/j.ymeth.2013.10.011. Epub 2013 Oct 25. PMID: 24184352; PMCID: PMC3988997.

Hussain, S., Sajini, A.A., Blanco, S., Dietmann, S., Lombard, P., Sugimoto, Y., Paramor, M., Gleeson, J.G., Odom, D.T., Ule, J., and Frye, M. (2013). NSun2-mediated cytosine-5 methylation of vault noncoding RNA determines its processing into regulatory small RNAs. Cell. Rep. 4, 255-261.

Hutchinson JN, Ensminger AW, Clemson CM, Lynch CR, Lawrence JB, Chess A. A screen for nuclear transcripts identifies two linked noncoding RNAs associated with SC35 splicing domains. BMC Genomics. 2007 Feb 1;8:39. doi: 10.1186/1471-2164-8-39. PMID: 17270048; PMCID: PMC1800850.

Ignatiadis N, Klaus B, Zaugg JB, Huber W. Data-driven hypothesis weighting increases detection power in genome-scale multiple testing. Nat Methods. 2016 Jul;13(7):577-80. doi: 10.1038/nmeth.3885. Epub 2016 May 30. PMID: 27240256; PMCID: PMC4930141.

Imam H, Khan M, Gokhale NS, McIntyre ABR, Kim GW, Jang JY, Kim SJ, Mason CE, Horner SM, Siddiqui A. N6-methyladenosine modification of hepatitis B virus RNA differentially regulates the viral life cycle. Proc Natl Acad Sci U S A. 2018 Aug 28;115(35):8829-8834. doi: 10.1073/pnas.1808319115. Epub 2018 Aug 13. PMID: 30104368; PMCID: PMC6126736.

Isaacs A, Lindenmann J. Virus interference. I. The interferon. Proc R Soc Lond B Biol Sci. 1957 Sep 12;147(927):258-67. doi: 10.1098/rspb.1957.0048. PMID: 13465720.

Iselin L, Palmalux N, Kamel W, Simmonds P, Mohammed S, Castello A. Uncovering viral RNA-host cell interactions on a proteome-wide scale. Trends Biochem Sci. 2022 Jan;47(1):23-38. doi: 10.1016/j.tibs.2021.08.002. Epub 2021 Sep 9. PMID: 34509361; PMCID: PMC9187521.

Ishikawa, H., Barber, G. STING is an endoplasmic reticulum adaptor that facilitates innate immune signalling. Nature 455, 674–678 (2008). https://doi.org/10.1038/nature07317

Ivashkiv, L., Donlin, L. Regulation of type I interferon responses. Nat Rev Immunol 14, 36–49 (2014). https://doi.org/10.1038/nri3581

Izumikawa K, Nobe Y, Ishikawa H, Yamauchi Y, Taoka M, Sato K, Nakayama H, Simpson RJ, Isobe T, Takahashi N. TDP-43 regulates site-specific 2'-O-methylation of U1 and U2 snRNAs via controlling the Cajal body localization of a subset of C/D

scaRNAs. Nucleic Acids Res. 2019 Mar 18;47(5):2487-2505. doi: 10.1093/nar/gkz086. PMID: 30759234; PMCID: PMC6412121.

Jailson Brito Querido, Irene Díaz-López, and V. Ramakrishnan. The molecular basis of translation initiation and its regulation in eukaryotes. Nature Reviews Molecular Cell Biology, 25(3):168–186, March 2024. Number: 3 Publisher: Nature Publishing Group.

Jansens RJJ, Verhamme R, Mirza AH, Olarerin-George A, Van Waesberghe C, Jaffrey SR, Favoreel HW. Alphaherpesvirus US3 protein-mediated inhibition of the m6A mRNA methyltransferase complex. Cell Rep. 2022 Jul 19;40(3):111107. doi: 10.1016/j.celrep.2022.111107. PMID: 35858564; PMCID: PMC9347262.

Jernej Ule, Kirk Jensen, Aldo Mele, Robert B. Darnell, CLIP: A method for identifying protein–RNA interaction sites in living cells, Methods, Volume 37, Issue 4, 2005, Pages 376-386, ISSN 1046-2023, https://doi.org/10.1016/j.ymeth.2005.07.018.

Jiang F, Ramanathan A, Miller MT, Tang GQ, Gale M Jr, Patel SS, Marcotrigiano J. Structural basis of RNA recognition and activation by innate immune receptor RIG-I. Nature. 2011 Sep 25;479(7373):423-7. doi: 10.1038/nature10537. PMID: 21947008; PMCID: PMC3430514.

Jiang, Z., Wei, F., Zhang, Y. et al. IFI16 directly senses viral RNA and enhances RIG-I transcription and activation to restrict influenza virus infection. Nat Microbiol 6, 932–945 (2021). https://doi.org/10.1038/s41564-021-00907-x

Jinek, M. et al. A programmable dual-RNA-guided DNA endonuclease in adaptive bacterial immunity. Science 337, 816–821 (2012).

Johnson SM, McNally BA, Ioannidis I, Flano E, Teng MN, Oomens AG, Walsh EE, Peeples ME. Respiratory Syncytial Virus Uses CX3CR1 as a Receptor on Primary Human Airway Epithelial Cultures. PLoS Pathog. 2015;11(12):e1005318

Jonkhout N, Tran J, Smith MA, Schonrock N, Mattick JS, Novoa EM. The RNA modification landscape in human disease. RNA. 2017 Dec;23(12):1754-1769. doi: 10.1261/rna.063503.117. Epub 2017 Aug 30. PMID: 28855326; PMCID: PMC5688997.

Jønsson KL, Laustsen A, Krapp C, Skipper KA, Thavachelvam K, Hotter D, Egedal JH, Kjolby M, Mohammadi P, Prabakaran T, Sørensen LK, Sun C, Jensen SB, Holm CK, Lebbink RJ, Johannsen M, Nyegaard M, Mikkelsen JG, Kirchhoff F, Paludan SR, Jakobsen MR. IFI16 is required for DNA sensing in human macrophages by promoting production and function of cGAMP. Nat Commun. 2017 Feb 10;8:14391. doi: 10.1038/ncomms14391. PMID: 28186168; PMCID: PMC5309897.

Kamel W, Vincenzo Ruscica, Azman Embarc-Buh, Zaydah R. de Laurent, Manuel Garcia-Moreno, Yana Demyanenko, Meghana Madhusudhan, Louisa Iselin, Aino Järvelin, Maximilian Hannan, Eduardo Kitano, Samantha Moore, Andres Merits, Ilan Davis, Shabaz Mohammed, Alfredo Castello. Alphavirus infection triggers selective cytoplasmic translocation of nuclear RBPs with moonlighting antiviral roles. bioRxiv 2021.10.06.463336; doi: https://doi.org/10.1101/2021.10.06.463336

Kamel, W

Kane M, Zang TM, Rihn SJ, et al. Identification of Interferon-Stimulated Genes with Antiretroviral Activity. Cell Host & Microbe. 2016 Sep;20(3):392-405. DOI: 10.1016/j.chom.2016.08.005. PMID: 27631702; PMCID: PMC5026698.

Karikó K., Buckstein M., Ni H., Weissman D. Suppression of RNA recognition by Toll-like receptors: the impact of nucleoside modification and the evolutionary origin of RNA. Immunity. 2005; 23:165–175.

Kawai T, Akira S. Toll-like receptors and their crosstalk with other innate receptors in infection and immunity. Immunity. 2011 May 27;34(5):637-50. doi: 10.1016/j.immuni.2011.05.006. PMID: 21616434.

Kennedy EM, Bogerd HP, Kornepati AV, Kang D, Ghoshal D, Marshall JB, Poling BC, Tsai K, Gokhale NS, Horner SM, Cullen BR. Posttranscriptional m(6)A Editing of HIV-1 mRNAs Enhances Viral Gene Expression. Cell Host Microbe. 2016 May 11;19(5):675-85. doi: 10.1016/j.chom.2016.04.002. Epub 2016 Apr 21. Erratum in: Cell Host Microbe. 2017 Dec 13;22(6):830. doi: 10.1016/j.chom.2017.11.010. PMID: 27117054; PMCID: PMC4867121.

Kerr CH, Skinnider MA, Andrews DDT, Madero AM, Chan QWT, Stacey RG, Stoynov N, Jan E, Foster LJ. Dynamic rewiring of the human interactome by interferon signaling. Genome Biol. 2020 Jun 15;21(1):140. doi: 10.1186/s13059-020-02050-y. PMID: 32539747; PMCID: PMC7294662.

Khrustalev, V. V., Khrustaleva, T. A., Sharma, N., and Giri, R. (2017). Mutational pressure in Zika virus: Local ADAR-editing areas associated with pauses in translation and replication. Front. Cell. Infect. Microbiol. 7, 44–17. doi:10.3389/fcimb.2017.00044

Kim HS, Lee K, Kim SJ, Cho S, Shin HJ, Kim C, Kim JS. Arrayed CRISPR screen with image-based assay reliably uncovers host genes required for coxsackievirus infection. Genome Res. 2018 Jun;28(6):859-868. doi: 10.1101/gr.230250.117. Epub 2018 Apr 30. PMID: 29712754; PMCID: PMC5991512.

Kim, G. W., Imam, H., Khan, M., and Siddiqui, A. (2020). N(6)-Methyladenosine modification of hepatitis B and C viral RNAs attenuates host innate immunity via RIG-I signaling. J. Biol. Chem. 295, 13123–13133. doi: 10.1074/jbc.RA120.014260

Kirchdoerfer R.N., C.L. Moyer, D.M. Abelson, E.O. Saphire. The Ebola virus VP30-NP interaction is a regulator of viral RNA synthesis PLoS Pathog., 12 (2016), p. e1005937

Kiss, G. et al. Structural analysis of respiratory syncytial virus reveals the position of M2-1 between the matrix protein and the ribonucleoprotein complex. J. Virol. 88, 7602–7617 (2014).

Koepke L, Gack MU, Sparrer KM. The antiviral activities of TRIM proteins. Curr Opin Microbiol. 2021 Feb;59:50-57. doi: 10.1016/j.mib.2020.07.005. Epub 2020 Aug 20. PMID: 32829025; PMCID: PMC7440025.

Kong W, Biswas A, Zhou D, Fiches G, Fujinaga K, Santoso N, Zhu J. Nucleolar protein NOP2/NSUN1 suppresses HIV-1 transcription and promotes viral latency by competing with Tat for TAR binding and methylation. PLoS Pathog. 2020 Mar

16;16(3):e1008430. doi: 10.1371/journal.ppat.1008430. PMID: 32176734; PMCID: PMC7098636.

Kong, W., Biswas, A., Zhou, D., Fiches, G., Fujinaga, K., Santoso, N., et al. (2020). Nucleolar protein NOP2/NSUN1 suppresses HIV-1 transcription and promotes viral latency by competing with Tat for TAR binding and methylation. PLoS Pathog. 16, e1008430. doi:10.1371/journal.ppat.1008430

Konishi A, Shimizu S, Hirota J, Takao T, Fan Y, Matsuoka Y, Zhang L, Yoneda Y, Fujii Y, Skoultchi AI, Tsujimoto Y. Involvement of histone H1.2 in apoptosis induced by DNA double-strand breaks. Cell. 2003 Sep 19;114(6):673-88. doi: 10.1016/s0092-8674(03)00719-0. PMID: 14505568.

Koonin, E.V.; Gorbalenya, A.E.; Chumakov, K.M. Tentative identification of RNA-dependent RNA polymerases of dsRNA viruses and their relationship to positive strand RNA viral polymerases. FEBS Lett. 1989, 252, 42–46.

Kotenko SV, Gallagher G, Baurin VV, Lewis-Antes A, Shen M, Shah NK, Langer JA, Sheikh F, Dickensheets H, Donnelly RP. IFN-lambdas mediate antiviral protection through a distinct class II cytokine receptor complex. Nat Immunol. 2003 Jan;4(1):69-77. doi: 10.1038/ni875. Epub 2002 Dec 16. PMID: 12483210.

Kowalinski E, Lunardi T, McCarthy AA, Louber J, Brunel J, Grigorov B, Gerlier D, Cusack S. Structural basis for the activation of innate immune pattern-recognition receptor RIG-I by viral RNA. Cell. 2011 Oct 14;147(2):423-35. doi: 10.1016/j.cell.2011.09.039. PMID: 22000019.

Krishnamurthy Malathi, Takeshi Saito, Nannette Crochet, David J. Barton, Michael Gale, and Robert H. Silverman. RNase L releases a small RNA from HCV RNA that refolds into a potent PAMP. RNA (New York, N.Y.), 16(11):2108–2119, November 2010.

Kuo L, Grosfeld H, Cristina J, Hill MG, Collins PL. Effects of mutations in the gene-start and gene-end sequence motifs on transcription of monocistronic and dicistronic minigenomes of respiratory syncytial virus. Journal of virology. 1996;70(10):6892–901. pmid:8794332

Kwon, E., Todorova, K., Wang, J. et al. The RNA-binding protein YBX1 regulates epidermal progenitors at a posttranscriptional level. Nat Commun 9, 1734 (2018). https://doi.org/10.1038/s41467-018-04092-0

L. Velazquez, M. Fellous, G. R. Stark, and S. Pellegrini. A protein tyrosine kinase in the interferon alpha/beta signaling pathway. Cell, 70(2):313–322, July 1992. Velazquez L, Fellous M, Stark GR, Pellegrini S. A protein tyrosine kinase in the interferon alpha/beta signaling pathway. Cell. 1992 Jul 24;70(2):313-22. doi: 10.1016/0092-8674(92)90105-l. PMID: 1386289.

Langhendries JL, Nicolas E, Doumont G, Goldman S, Lafontaine DL. The human box C/D snoRNAs U3 and U8 are required for pre-rRNA processing and tumorigenesis. Oncotarget. 2016 Sep 13;7(37):59519-59534. doi: 10.18632/oncotarget.11148. PMID: 27517747; PMCID: PMC5312328.

Latz E, Schoenemeyer A, Visintin A, Fitzgerald KA, Monks BG, Knetter CF, Lien E, Nilsen NJ, Espevik T, Golenbock DT. TLR9 signals after translocating from the ER to CpG DNA in the lysosome. Nat Immunol. 2004 Feb;5(2):190-8. doi: 10.1038/ni1028. Epub 2004 Jan 11. PMID: 14716310.

Lee N, Le Sage V, Nanni AV, Snyder DJ, Cooper VS, Lakdawala SS. Genome-wide analysis of influenza viral RNA and nucleoprotein association. Nucleic Acids Res. 2017 Sep 6;45(15):8968-8977. doi: 10.1093/nar/gkx584. PMID: 28911100; PMCID: PMC5587783.

Leger A, Amaral PP, Pandolfini L, Capitanchik C, Capraro F, Miano V, Migliori V, Toolan-Kerr P, Sideri T, Enright AJ, Tzelepis K, van Werven FJ, Luscombe NM, Barbieri I, Ule J, Fitzgerald T, Birney E, Leonardi T, Kouzarides T. RNA modifications detection by comparative Nanopore direct RNA sequencing. Nat Commun. 2021 Dec 10;12(1):7198. doi: 10.1038/s41467-021-27393-3. PMID: 34893601; PMCID: PMC8664944.

Lekmine, F. et al. Interferon-γ engages the p70 S6 kinase to regulate phosphorylation of the 40S S6 ribosomal protein. Exp. Cell Res. 295, 173–182 (2004).

Lengyel, P. Biochemistry of interferons and their actions. Annual Review of Biochemistry, 51:251–282, 1982.

Leonard JN, Ghirlando R, Askins J, Bell JK, Margulies DH, Davies DR, Segal DM. The TLR3 signaling complex forms by cooperative receptor dimerization. Proc Natl Acad Sci U S A. 2008 Jan 8;105(1):258-63. doi: 10.1073/pnas.0710779105. Epub 2008 Jan 2. PMID: 18172197; PMCID: PMC2224197.

Lester SN, Li K. Toll-like receptors in antiviral innate immunity. J Mol Biol. 2014 Mar 20;426(6):1246-64. doi: 10.1016/j.jmb.2013.11.024. Epub 2013 Dec 3. PMID: 24316048; PMCID: PMC3943763.

Levy DE, Marié I, Smith E, Prakash A. Enhancement and diversification of IFN induction by IRF-7-mediated positive feedback. J Interferon Cytokine Res. 2002 Jan;22(1):87-93. doi: 10.1089/107999002753452692. PMID: 11846979.

Levy, D. E. & Darnell, J. E. Jr. STATs: transcriptional control and biological impact. Nature Rev. Mol. Cell Biol. 3, 651–662 (2002).

Li S, Mason CE. The pivotal regulatory landscape of RNA modifications. Annu Rev Genomics Hum Genet. 2014;15:127-50. doi: 10.1146/annurev-genom-090413-025405. Epub 2014 Jun 2. PMID: 24898039.

Li Y, Banerjee S, Wang Y, Goldstein SA, Dong B, Gaughan C, Silverman RH, Weiss SR. Activation of RNase L is dependent on OAS3 expression during infection with diverse human viruses. Proc Natl Acad Sci U S A. 2016 Feb 23;113(8):2241-6. doi: 10.1073/pnas.1519657113. Epub 2016 Feb 8. Erratum in: Proc Natl Acad Sci U S A. 2019 Jun 18;116(25):12573. doi: 10.1073/pnas.1908765116. PMID: 26858407; PMCID: PMC4776461.

Li Y, Tollefsbol TO. DNA methylation detection: bisulfite genomic sequencing analysis. Methods Mol Biol. 2011;791:11-21. doi: 10.1007/978-1-61779-316-5_2. PMID: 21913068; PMCID: PMC3233226.

Li, F., Chen, Y., Zhang, Z., Ouyang, J., Wang, Y., Yan, R., et al. (2015). Robust expression of vault RNAs induced by influenza A virus plays a critical role in suppression of PKR-mediated innate immunity. Nucleic Acids Res. 43, 10321–10337. doi: 10.1093/nar/gkv1078

Li, G., Hilgenfeld, R., Whitley, R. *et al.* Therapeutic strategies for COVID-19: progress and lessons learned. *Nat Rev Drug Discov* **22**, 449–475 (2023). https://doi.org/10.1038/s41573-023-00672-y

Li, N. & Rana, T. M. Regulation of antiviral innate immunity by chemical modification of viral RNA. Wiley Interdiscip Rev RNA. e1720 (2022).

Li, X., Peng, J. & Yi, C. The epitranscriptome of small non-coding RNAs. Noncoding RNA Res. 6, 167–173 (2021).

Li, Y. et al. Role of p38α Map kinase in type I interferon signaling. J. Biol. Chem. 279, 970–979 (2004).

Liao H, Gaur A, McConie H, Shekar A, Wang K, Chang JT, Breton G, Denicourt C. Human NOP2/NSUN1 regulates ribosome biogenesis through non-catalytic complex formation with box C/D snoRNPs. Nucleic Acids Res. 2022 Oct 14;50(18):10695-10716. doi: 10.1093/nar/gkac817. PMID: 36161484; PMCID: PMC9561284.

Lichinchi G, Gao S, Saletore Y, Gonzalez GM, Bansal V, Wang Y, Mason CE, Rana TM. Dynamics of the human and viral m(6)A RNA methylomes during HIV-1 infection of T cells. Nat Microbiol. 2016 Feb 22;1:16011. doi: 10.1038/nmicrobiol.2016.11. PMID: 27572442; PMCID: PMC6053355.

Limburg H, Harbig A, Bestle D, Stein DA, Moulton HM, Jaeger J, Janga H, Hardes K, Koepke J, Schulte L, Koczulla AR, Schmeck B, Klenk HD, Böttcher-Friebertshäuser E. TMPRSS2 Is the Major Activating Protease of Influenza A Virus in Primary Human Airway Cells and Influenza B Virus in Human Type II Pneumocytes. J Virol. 2019 Oct 15;93(21):e00649-19. doi: 10.1128/JVI.00649-19. PMID: 31391268; PMCID: PMC6803253.

Lingemann M, McCarty T, Liu X, Buchholz UJ, Surman S, Martin SE, Collins PL, Munir S. The alpha-1 subunit of the Na+,K+-ATPase (ATP1A1) is required for macropinocytic entry of respiratory syncytial virus (RSV) in human respiratory epithelial cells. PLoS Pathog. 2019;15(8):e1007963

Liu SY, Aliyari R, Chikere K, Li G, Marsden MD, Smith JK, Pernet O, Guo H, Nusbaum R, Zack JA, Freiberg AN, Su L, Lee B, Cheng G. Interferon-inducible cholesterol-25-hydroxylase broadly inhibits viral entry by production of 25-hydroxycholesterol. Immunity. 2013 Jan 24;38(1):92-105. doi: 10.1016/j.immuni.2012.11.005. Epub 2012 Dec 27. PMID: 23273844; PMCID: PMC3698975.

Liu, T., Zhang, L., Joo, D. et al. NF-κB signaling in inflammation. Sig Transduct Target Ther 2, 17023 (2017). https://doi.org/10.1038/sigtrans.2017.23

Liu, Y. et al. N (6)-methyladenosine RNA modification-mediated cellular metabolism rewiring inhibits viral replication. Science 365, 1171–1176 (2019).

Liu, Y., You, Y., Lu, Z., Yang, J., and Liu, L. (2019). N (6)-methyladenosine RNA modification-mediated cellular metabolism rewiring inhibits viral replication. Science 365, 1171–1176. doi:10.1126/science.aax4468

Long J.S., Mistry B., Haslam S.M., Barclay W.S. Host and viral determinants of influenza A virus species specificity. Nat. Rev. Microbiol. 2019;17:67–81. doi: 10.1038/s41579-018-0115-z.

López-Pelaéz, M. et al. Cot/tpl2–MKK1/2–Erk1/2 controls mTORC1-mediated mRNA translation in Toll-like receptor-activated macrophages. Mol. Biol. Cell 23, 2982–2992 (2012).

Love MI, Huber W, Anders S. Moderated estimation of fold change and dispersion for RNA-seq data with DESeq2. Genome Biol. 2014;15(12):550. doi: 10.1186/s13059-014-0550-8. PMID: 25516281; PMCID: PMC4302049.

Lu M, Zhang Z, Xue M, Zhao BS, Harder O, Li A, Liang X, Gao TZ, Xu Y, Zhou J, Feng Z, Niewiesk S, Peeples ME, He C, Li J. N6-methyladenosine modification enables viral RNA to escape recognition by RNA sensor RIG-I. Nat Microbiol. 2020 Apr;5(4):584-598. doi: 10.1038/s41564-019-0653-9. Epub 2020 Feb 3. PMID: 32015498; PMCID: PMC7137398.

Lu, M., Zhang, Z., Xue, M., Zhao, B. S., Harder, O., Li, A., et al. (2020). N(6)-methyladenosine modification enables viral RNA to escape recognition by RNA sensor RIG-I. Nat. Microbiol. 5, 584–598. doi: 10.1038/s41564-019-0653-9

Lum KK, Howard TR, Pan C, Cristea IM. Charge-Mediated Pyrin Oligomerization Nucleates Antiviral IFI16 Sensing of Herpesvirus DNA. mBio. 2019 Jul 23;10(4):e01428-19. doi: 10.1128/mBio.01428-19. PMID: 31337724; PMCID: PMC6650555.

Lundstrom K. Application of Viral Vectors for Vaccine Development with a Special Emphasis on COVID-19. Viruses. 2020 Nov 18;12(11):1324. doi: 10.3390/v12111324. PMID: 33218001; PMCID: PMC7698750.

Malakhov MP, Malakhova OA, Kim KI, Ritchie KJ, Zhang DE. UBP43 (USP18) specifically removes ISG15 from conjugated proteins. J Biol Chem. 2002 Mar 22;277(12):9976-81. doi: 10.1074/jbc.M109078200. Epub 2002 Jan 11. PMID: 11788588.

Malakhova OA, Kim KI, Luo JK, Zou W, Kumar KG, Fuchs SY, Shuai K, Zhang DE. UBP43 is a novel regulator of interferon signaling independent of its ISG15 isopeptidase activity. EMBO J. 2006 Jun 7;25(11):2358-67. doi: 10.1038/sj.emboj.7601149. Epub 2006 May 18. PMID: 16710296; PMCID: PMC1478183.

Mali P, Yang L, Esvelt KM, Aach J, Guell M, DiCarlo JE, Norville JE, Church GM. RNA-guided human genome engineering via Cas9. Science. 2013;339:823–826. doi:10.1126/science.1232033

Manuse MJ, Briggs CM, Parks GD. Replication-independent activation of human plasmacytoid dendritic cells by the paramyxovirus SV5 Requires TLR7 and autophagy pathways. Virology. 2010 Sep 30;405(2):383-9. doi: 10.1016/j.virol.2010.06.023. Epub 2010 Jul 6. PMID: 20605567; PMCID: PMC2923232.

Mao XL, Li ZH, Huang MH, Wang JT, Zhou JB, Li QR, Xu H, Wang XJ, Zhou XL. Mutually exclusive substrate selection strategy by human m3C RNA transferases METTL2A and METTL6. Nucleic Acids Res. 2021 Aug 20;49(14):8309-8323. doi: 10.1093/nar/gkab603. PMID: 34268557; PMCID: PMC8373065.

Marceau, C. D., Puschnik, A. S., Majzoub, K., Ooi, Y. S., Brewer, S. M., Fuchs, G., et al. (2016). Genetic dissection of Flaviviridae host factors through genome-scale CRISPR screens. Nature 535, 159–163. doi:10.1038/nature18631

Martin, M. Cutadapt removes adapter sequences from high-throughput sequencing reads. EMBnet.journal, 17(1):10–12, May 2011. Number: 1.

Martinez NM, Su A, Burns MC, Nussbacher JK, Schaening C, Sathe S, Yeo GW, Gilbert WV. Pseudouridine synthases modify human pre-mRNA co-transcriptionally and affect pre-mRNA processing. Mol Cell. 2022 Feb 3;82(3):645-659.e9. doi: 10.1016/j.molcel.2021.12.023. Epub 2022 Jan 19. PMID: 35051350; PMCID: PMC8859966.

Marty, A., Meanger, J., Mills, J., Shields, B. & Ghildyal, R. Association of matrix protein of respiratory syncytial virus with the host cell membrane of infected cells. Arch. Virol. 149, 199–210 (2004).

Matsukura S, Kokubu F, Kurokawa M, Kawaguchi M, Ieki K, Kuga H, Odaka M, Suzuki S, Watanabe S, Takeuchi H, Kasama T, Adachi M. Synthetic double-stranded RNA induces multiple genes related to inflammation through Toll-like receptor 3 depending on NF-kappaB and/or IRF-3 in airway epithelial cells. Clin Exp Allergy. 2006 Aug;36(8):1049-62. doi: 10.1111/j.1365-2222.2006.02530.x. PMID: 16911361.

Mauer J, Luo X, Blanjoie A, Jiao X, Grozhik AV, Patil DP, Linder B, Pickering BF, Vasseur JJ, Chen Q, Gross SS, Elemento O, Debart F, Kiledjian M, Jaffrey SR. Reversible methylation of m6Am in the 5' cap controls mRNA stability. Nature. 2017 Jan 19;541(7637):371-375. doi: 10.1038/nature21022. Epub 2016 Dec 21. PMID: 28002401; PMCID: PMC5513158.

Mazarei, M., Shahabi Rabori, V., Ghasemi, N. et al. LncRNA MALAT1 signaling pathway and clinical applications in overcome on cancers metastasis. Clin Exp Med 23, 4457–4472 (2023). https://doi.org/10.1007/s10238-023-01179-x

McFadden, M. J., McIntyre, A. B. R., Mourelatos, H., Abell, N. S., Gokhale, N. S., Ipas, H., et al. (2021). Post-transcriptional regulation of antiviral gene expression by N6-methyladenosine. Cell Rep. 34, 108798. doi:10.1016/j.celrep.2021.108798

McGivern DR, Collins PL, Fearns R. Identification of internal sequences in the 3' leader region of human respiratory syncytial virus that enhance transcription and confer replication processivity. J Virol. 2005;79(4):2449–60. pmid:15681446.

McGrath,P.C., Holley,D.T., Hamby,L.S., Mattingly,C.A. and Freeman,J.W. (1994) Prospective study correlating P120 antigen expression with established prognostic factors in breast cancer. Surg. Oncol., 3, 69–77.

McIntyre W, Netzband R, Bonenfant G, Biegel JM, Miller C, Fuchs G, Henderson E, Arra M, Canki M, Fabris D, Pager CT. Positive-sense RNA viruses reveal the complexity and dynamics of the cellular and viral epitranscriptomes during infection. Nucleic Acids Res. 2018 Jun 20;46(11):5776-5791. doi: 10.1093/nar/gky029. PMID: 29373715; PMCID: PMC6009648.

Meynier, V., Hardwick, S.W., Catala, M. et al. Structural basis for human mitochondrial tRNA maturation. Nat Commun 15, 4683 (2024). https://doi.org/10.1038/s41467-024-49132-0

Mirzalieva O, Juncker M, Schwartzenburg J, Desai S. ISG15 and ISGylation in Human Diseases. Cells. 2022 Feb 4;11(3):538. doi: 10.3390/cells11030538. PMID: 35159348; PMCID: PMC8834048.

Morais P, Adachi H, Yu YT. The Critical Contribution of Pseudouridine to mRNA COVID-19 Vaccines. Front Cell Dev Biol. 2021 Nov 4;9:789427. doi: 10.3389/fcell.2021.789427. PMID: 34805188; PMCID: PMC8600071.

Motorin, Y. & Helm, M. Methods for RNA modification mapping using deep sequencing: established and new emerging technologies. Genes 10, 35 (2019).

Murayama, A., Ohmori, K., Fujimura, A., Minami, H., Yasuzawa-Tanaka, K., Kuroda, T., Oie, S., Daitoku, H., Okuwaki, M., Nagata, K., et al. (2008). Epigenetic control of rDNA loci in response to intracellular energy status. Cell 133, 627-639. https://doi.org/10.1016/j.cell.2008.03.030

Murray, P. J. The JAK-STAT signaling pathway: input and output integration. J. Immunol. 178, 2623–2629 (2007).

N'Da Konan, S., Ségéral, E., Bejjani, F., Bendoumou, M., Ait Said, M., Gallois-Montbrun, S., et al. (2022). YTHDC1 regulates distinct post-integration steps of HIV-1 replication and is important for viral infectivity. Retrovirology 19, 4. doi:10.1186/s12977-022-00589-1

Naji S, Ambrus G, Cimermančič P, Reyes JR, Johnson JR, Filbrandt R, Huber MD, Vesely P, Krogan NJ, Yates JR 3rd, Saphire AC, Gerace L. Host cell interactome of HIV-1 Rev includes RNA helicases involved in multiple facets of virus production. Mol Cell Proteomics. 2012 Apr;11(4):M111.015313. doi: 10.1074/mcp.M111.015313. Epub 2011 Dec 15. PMID: 22174317; PMCID: PMC3322577.

Nakanishi K, Nureki O. Recent progress of structural biology of tRNA processing and modification. Mol Cells. 2005 Apr 30;19(2):157-66. PMID: 15879697.

Nasr N, Maddocks S, Turville SG, Harman AN, Woolger N, Helbig KJ, Wilkinson J, Bye CR, Wright TK, Rambukwelle D, Donaghy H, Beard MR, Cunningham AL. HIV-1 infection of human macrophages directly induces viperin which inhibits viral production. Blood. 2012 Jul 26;120(4):778-88. doi: 10.1182/blood-2012-01-407395. Epub 2012 Jun 7. PMID: 22677126.

Nazmi A, Mukhopadhyay R, Dutta K, Basu A. STING mediates neuronal innate immune response following Japanese encephalitis virus infection. Sci Rep. 2012;2:347. doi: 10.1038/srep00347. Epub 2012 Apr 2. PMID: 22470840; PMCID: PMC3317237.

Neil SJ, Zang T, Bieniasz PD. Tetherin inhibits retrovirus release and is antagonized by HIV-1 Vpu. Nature. 2008 Jan 24;451(7177):425-30. doi: 10.1038/nature06553. Epub 2008 Jan 16. PMID: 18200009.

Netzband, R., and Pager, C. T. (2020). Epitranscriptomic marks: emerging modulators of RNA virus gene expression. Wiley Interdiscip. Rev. RNA 11:e1576. doi: 10.1002/wrna.1576

Nguyen, H. A., Hoffer, E. D. & Dunham, C. M. Importance of a tRNA anticodon loop modification and a conserved, noncanonical anticodon stem pairing in tRNACGGPro for decoding. J. Biol. Chem. 294, 5281–5291 (2019).

Nishikura K. Functions and regulation of RNA editing by ADAR deaminases. Annu Rev Biochem. 2010;79:321-49. doi: 10.1146/annurev-biochem-060208-105251. PMID: 20192758; PMCID: PMC2953425.

Noton SL, Fearns R. Initiation and regulation of paramyxovirus transcription and replication. Virology. 2015 May;479-480:545-54. doi: 10.1016/j.virol.2015.01.014. Epub 2015 Feb 13. PMID: 25683441; PMCID: PMC4424093.

Noton SL, Fearns R. The first two nucleotides of the respiratory syncytial virus antigenome RNA replication product can be selected independently of the promoter terminus. Rna. 2011;17(10):1895–906. Epub 2011/09/01. rna.2813411 [pii] pmid:21878549; PubMed Central PMCID: PMC3185921

Noton SL, Nagendra K, Dunn EF, Mawhorter ME, Yu Q, Fearns R. Respiratory Syncytial Virus Inhibitor AZ-27 Differentially Inhibits Different Polymerase Activities at the Promoter. J Virol. 2015;89(15):7786–98. Epub 2015/05/23. pmid:25995255; PubMed Central PMCID: PMCPMC4505683.

Noton SL, Tremaglio CZ, Fearns R. Killing two birds with one stone: How the respiratory syncytial virus polymerase initiates transcription and replication. PLoS Pathog. 2019 Feb 28;15(2):e1007548. doi: 10.1371/journal.ppat.1007548. PMID: 30817806; PMCID: PMC6394897.

Ozanick S, Krecic A, Andersland J, Anderson JT. The bipartite structure of the tRNA m1A58 methyltransferase from S. cerevisiae is conserved in humans. RNA. 2005 Aug;11(8):1281-90. doi: 10.1261/rna.5040605. PMID: 16043508; PMCID: PMC1370811.

Pagani I, Poli G, Vicenzi E. TRIM22. A Multitasking Antiviral Factor. Cells. 2021; 10(8):1864. https://doi.org/10.3390/cells10081864

Pan, T. Modifications and functional genomics of human transfer RNA. Cell Res. 28, 395–404 (2018).

Patil, D. P., Pickering, B. F. & Jaffrey, S. R. Reading m6A in the transcriptome: m6A-binding proteins. Trends Cell Biol. 28, 113–127 (2018).

Paul AV, Wimmer E. Initiation of protein-primed picornavirus RNA synthesis. Virus Res. 2015 Aug 3;206:12-26. doi: 10.1016/j.virusres.2014.12.028. Epub 2015 Jan 12. PMID: 25592245; PMCID: PMC4476921.

Peebles, R. S. Jr & Graham, B. S. Pathogenesis of respiratory syncytial virus infection in the murine model. Proc. Am. Thorac Soc. 2, 110–115 (2005).

Pei J, Wagner ND, Zou AJ, Chatterjee S, Borek D, Cole AR, Kim PJ, Basler CF, Otwinowski Z, Gross ML, Amarasinghe GK, Leung DW. Structural basis for IFN antagonism by human respiratory syncytial virus nonstructural protein 2. Proc Natl Acad Sci U S A. 2021 118(10)

Perri S, Greer CE, Thudium K, Doe B, Legg H, Liu H, Romero RE, Tang Z, Bin Q, Dubensky TW Jr, Vajdy M, Otten GR, Polo JM. An alphavirus replicon particle chimera derived from venezuelan equine encephalitis and sindbis viruses is a potent gene-based vaccine delivery vector. J Virol. 2003 Oct;77(19):10394-403. doi: 10.1128/jvi.77.19.10394-10403.2003. PMID: 12970424; PMCID: PMC228391.

Pestka S, Krause CD, Walter MR. Interferons, interferon-like cytokines, and their receptors. Immunol Rev. 2004 Dec;202:8-32. doi: 10.1111/j.0105-2896.2004.00204.x. PMID: 15546383.

Pfaller, C. K., George, C. X., and Samuel, C. E. (2021). Adenosine deaminases acting on RNA (ADARs) and viral infections. Annu. Rev. Virol. 8, 239–264. doi: 10.1146/annurev-virology-091919-065320

Phuphuakrat, A., Kraiwong, R., Boonarkart, C., Lauhakirti, D., Lee, T. H., and Auewarakul, P. (2008). Double-Stranded RNA adenosine deaminases enhance expression of human immunodeficiency virus type 1 proteins. J. Virol. 82, 10864–10872. doi:10.1128/JVI.00238-08

Pichlmair A, Lassnig C, Eberle CA, Górna MW, Baumann CL, Burkard TR, Bürckstümmer T, Stefanovic A, Krieger S, Bennett KL, Rülicke T, Weber F, Colinge J, Müller M, Superti-Furga G. IFIT1 is an antiviral protein that recognizes 5'-triphosphate RNA. Nat Immunol. 2011 Jun 5;12(7):624-30. doi: 10.1038/ni.2048. PMID: 21642987.

Pichlmair A, Schulz O, Tan CP, Näslund TI, Liljeström P, Weber F, Reis e Sousa C. RIG-I-mediated antiviral responses to single-stranded RNA bearing 5'-phosphates. Science. 2006 Nov 10;314(5801):997-1001. doi: 10.1126/science.1132998. Epub 2006 Oct 12. PMID: 17038589.

Pichlmair, A. et al. IFIT1 is an antiviral protein that recognizes 5'-triphosphate RNA. Nature Immunol. 12, 624–630 (2011).

Piontkivska H, Wales-McGrath B, Miyamoto M, Wayne ML. ADAR Editing in Viruses: An Evolutionary Force to Reckon with. Genome Biol Evol. 2021 Nov 5;13(11):evab240. doi: 10.1093/gbe/evab240. PMID: 34694399; PMCID: PMC8586724.

Piórkowska K, Zygmunt K, Hunter W, Wróblewska K. MALAT1: A Long Non-Coding RNA with Multiple Functions and Its Role in Processes Associated with Fat Deposition. Genes. 2024; 15(4):479. https://doi.org/10.3390/genes15040479

Platanias, L. C. & Fish, E. N. Signaling pathways activated by interferons. Exp. Hematol. 27, 1583–1592 (1999).

Platanias, L. Mechanisms of type-I- and type-II-interferon-mediated signalling. Nat Rev Immunol 5, 375–386 (2005). https://doi.org/10.1038/nri1604

Powell CA, Kopajtich R, D'Souza AR, Rorbach J, Kremer LS, Husain RA, Dallabona C, Donnini C, Alston CL, Griffin H, Pyle A, Chinnery PF, Strom TM, Meitinger T, Rodenburg RJ, Schottmann G, Schuelke M, Romain N, Haller RG, Ferrero I, Haack TB, Taylor RW, Prokisch H, Minczuk M. TRMT5 Mutations Cause a Defect in Post-transcriptional Modification of Mitochondrial tRNA Associated with Multiple Respiratory-Chain Deficiencies. Am J Hum Genet. 2015 Aug 6;97(2):319-28. doi: 10.1016/j.ajhg.2015.06.011. Epub 2015 Jul 16. PMID: 26189817; PMCID: PMC4573257.

Pritlove DC, Poon LL, Fodor E, Sharps J, Brownlee GG. Polyadenylation of influenza virus mRNA transcribed in vitro from model virion RNA templates: requirement for 5' conserved sequences. J Virol. 1998 Feb;72(2):1280-6. doi: 10.1128/JVI.72.2.1280-1286.1998. PMID: 9445028; PMCID: PMC124606.

Quinlan AR, Hall IM. BEDTools: a flexible suite of utilities for comparing genomic features. Bioinformatics. 2010 Mar 15;26(6):841-2. doi: 10.1093/bioinformatics/btq033. Epub 2010 Jan 28. PMID: 20110278; PMCID: PMC2832824.

Rackham, O. & Filipovska, A. Organization and expression of the mammalian mitochondrial genome. Nat. Rev. Genet 23, 606–623 (2022).

Raychoudhuri, A. et al. ISG56 and IFITM1 proteins inhibit hepatitis C virus replication. J. Virol. 85, 12881–12889 (2011).

Ribeiro DR, Nunes A, Ribeiro D, Soares AR. The hidden RNA code: implications of the RNA epitranscriptome in the context of viral infections. Front Genet. 2023 Aug 1;14:1245683. doi: 10.3389/fgene.2023.1245683. PMID: 37614818; PMCID: PMC10443596.

Reinert, L., Lopušná, K., Winther, H. et al. Sensing of HSV-1 by the cGAS–STING pathway in microglia orchestrates antiviral defence in the CNS. Nat Commun 7, 13348 (2016). https://doi.org/10.1038/ncomms13348

Rincheval V, Lelek M, Gault E, Bouillier C, Sitterlin D, Blouquit-Laye S, Galloux M, Zimmer C, Eleouet JF, Rameix-Welti MA. Functional organization of cytoplasmic inclusion bodies in cells infected by respiratory syncytial virus. Nat Commun. 2017;8(1):563

Ringeard, M., Marchand, V., Decroly, E., Motorin, Y., and Bennasser, Y. (2019). FTSJ3 is an RNA 2'-O-methyltransferase recruited by HIV to avoid innate immune sensing. Nature 565, 500–504. doi:10.1038/s41586-018-0841-4

Roberts NJ Jr, Krilov LR. The Continued Threat of Influenza A Viruses. Viruses. 2022 Apr 24;14(5):883. doi: 10.3390/v14050883. PMID: 35632626; PMCID: PMC9143665.

Roberts, W. K., Hovanessian, A., Brown, R. E., Clemens, M. J. & Kerr, I. M. Interferon-mediated protein kinase and low-molecular-weight inhibitor of protein synthesis. Nature 264, 477–480 (1976).

Rogers RS, Horvath CM, Matunis MJ. SUMO modification of STAT1 and its role in PIAS-mediated inhibition of gene activation. J Biol Chem. 2003 Aug 8;278(32):30091-7. doi: 10.1074/jbc.M301344200. Epub 2003 May 22. PMID: 12764129.

Roundtree, I. A. et al. YTHDC1 mediates nuclear export of N6-methyladenosine methylated mRNAs. eLife 6, e31311 (2017).

Roundtree, I. A., Evans, M. E., Pan, T. & He, C. Dynamic RNA modifications in gene expression regulation. Cell 169, 1187–1200 (2017).

Sadler, A., Williams, B. Interferon-inducible antiviral effectors. Nat Rev Immunol 8, 559–568 (2008). https://doi.org/10.1038/nri2314

Sadler, A., Williams, B. Interferon-inducible antiviral effectors. Nat Rev Immunol 8, 559–568 (2008). https://doi.org/10.1038/nri2314

Safra M, Sas-Chen A, Nir R, Winkler R, Nachshon A, Bar-Yaacov D, Erlacher M, Rossmanith W, Stern-Ginossar N, Schwartz S. The m1A landscape on cytosolic and mitochondrial mRNA at single-base resolution. Nature. 2017 Nov 9;551(7679):251-255. doi: 10.1038/nature24456. Epub 2017 Oct 25. PMID: 29072297.

Sahadevan S, Sekaran T, Ashaf N, Fritz M, Hentze MW, Huber W, Schwarzl T. htseq-clip: a toolset for the preprocessing of eCLIP/iCLIP datasets. Bioinformatics. 2023 Jan 1;39(1):btac747. doi: 10.1093/bioinformatics/btac747. PMID: 36394253; PMCID: PMC9825771.

Sakai K, Ami Y, Tahara M, Kubota T, Anraku M, Abe M, Nakajima N, Sekizuka T, Shirato K, Suzaki Y, Ainai A, Nakatsu Y, Kanou K, Nakamura K, Suzuki T, Komase K, Nobusawa E, Maenaka K, Kuroda M, Hasegawa H, Kawaoka Y, Tashiro M, Takeda M. The host protease TMPRSS2 plays a major role in in vivo replication of emerging H7N9 and seasonal influenza viruses. J Virol. 2014 May;88(10):5608-16. doi: 10.1128/JVI.03677-13. Epub 2014 Mar 5. PMID: 24600012; PMCID: PMC4019123.

Samavarchi-Tehrani, Payman & Abdouni, Hala & Knight, James & Astori, Audrey & Samson, Reuben & Lin, Zhen-Yuan & Kim, Dae-Kyum & Knapp, Jennifer & St-Germain, Jonathan & Go, Christopher & Larsen, Brett & Wong, Cassandra & Cassonnet, Patricia & Demeret, Caroline & Jacob, Yves & Roth, Frederick & Raught, Brian & Gingras, Anne-Claude. (2020). A SARS-CoV-2 – host proximity interactome. 10.1101/2020.09.03.282103.

Samuel CE. Adenosine deaminase acting on RNA (ADAR1), a suppressor of double-stranded RNA-triggered innate immune responses. J Biol Chem. 2019;294(5):1710–1720. doi:10.1074/jbc.TM118.004166

Sanjana NE, Shalem O, Zhang F. Improved vectors and genome-wide libraries for CRISPR screening. Nat Methods. 2014 Aug;11(8):783-784. doi: 10.1038/nmeth.3047. PMID: 25075903; PMCID: PMC4486245.

Schindler, C., Shuai, K., Prezioso, V. R. & Darnell, J. E. Interferon-dependent tyrosine phosphorylation of a latent cytoplasmic transcription factor. Science 257, 809–813 (1992).

Schlee M, Hartmann G. Discriminating self from non-self in nucleic acid sensing. Nat Rev Immunol. 2016 Sep;16(9):566-80. doi: 10.1038/nri.2016.78. Epub 2016 Jul 25. PMID: 27455396; PMCID: PMC7097691.

Schlee M, Roth A, Hornung V, Hagmann CA, Wimmenauer V, Barchet W, Coch C, Janke M, Mihailovic A, Wardle G, Juranek S, Kato H, Kawai T, Poeck H, Fitzgerald KA, Takeuchi O, Akira S, Tuschl T, Latz E, Ludwig J, Hartmann G. Recognition of 5' triphosphate by RIG-I helicase requires short blunt double-stranded RNA as contained in panhandle of negative-strand virus. Immunity. 2009 Jul 17;31(1):25-34. doi: 10.1016/j.immuni.2009.05.008. Epub 2009 Jul 2. PMID: 19576794; PMCID: PMC2824854.

Schneider WM, Chevillotte MD, Rice CM. Interferon-stimulated genes: a complex web of host defenses. Annu Rev Immunol. 2014;32:513-45. doi: 10.1146/annurev-immunol-032713-120231. Epub 2014 Feb 6. PMID: 24555472; PMCID: PMC4313732.

Schoggins JW, et al. 2011. A diverse range of gene products are effectors of the type I interferon antiviral response. Nature 472(7344):481–485.

Schoggins JW. Interferon-Stimulated Genes: What Do They All Do? Annu Rev Virol. 2019 Sep 29;6(1):567-584. doi: 10.1146/annurev-virology-092818-015756. Epub 2019 Jul 5. PMID: 31283436.

Schroder K, Hertzog PJ, Ravasi T, Hume DA. Interferon-gamma: an overview of signals, mechanisms and functions. J Leukoc Biol. 2004 Feb;75(2):163-89. doi: 10.1189/jlb.0603252. Epub 2003 Oct 2. PMID: 14525967.

Schuberth-Wagner C, Ludwig J, Bruder AK, Herzner AM, Zillinger T, Goldeck M, Schmidt T, Schmid-Burgk JL, Kerber R, Wolter S, Stümpel JP, Roth A, Bartok E, Drosten C, Coch C, Hornung V, Barchet W, Kümmerer BM, Hartmann G, Schlee M. A Conserved Histidine in the RNA Sensor RIG-I Controls Immune Tolerance to N1-2'O-Methylated Self RNA. Immunity. 2015 Jul 21;43(1):41-51. doi: 10.1016/j.immuni.2015.06.015. Epub 2015 Jul 14. PMID: 26187414; PMCID: PMC7128463.

Shalem O, Sanjana NE, Hartenian E, Shi X, Scott DA, Mikkelson T, Heckl D, Ebert BL, Root DE, Doench JG, Zhang F. Genome-scale CRISPR-Cas9 knockout screening in human cells. Science. 2014 Jan 3;343(6166):84-87. doi: 10.1126/science.1247005. Epub 2013 Dec 12. PMID: 24336571; PMCID: PMC4089965.

Shang Z, Tan S, Ma D. Respiratory syncytial virus: from pathogenesis to potential therapeutic strategies. Int J Biol Sci. 2021 Sep 27;17(14):4073-4091. doi: 10.7150/ijbs.64762. PMID: 34671221; PMCID: PMC8495404.

Sharma S, Lafontaine DLJ. “View From A Bridge”: A New Perspective on Eukaryotic rRNA base Modification. Trends Biochem Sci. 2015;40:560–575.

Sharma, S., Langhendries, J. L., Watzinger, P., Kötter, P., Entian, K. D., and Lafontaine, D. L. J. (2015). Yeast Kre33 and human NAT10 are conserved 18S rRNA cytosine acetyltransferases that modify tRNAs assisted by the adaptor Tan1/THUMPD1. Nucleic Acids Res. 43, 2242–2258. doi:10.1093/nar/gkv075

Sharma,S., Yang,J., Watzinger,P., Ko¨tter,P. and Entian,K.D. (2013) Yeast nop2 and rcm1 methylate C2870 and C2278 of the 25S rRNA, respectively. Nucleic Acids Res., 41, 9062–9076.

Shen Z, Wei L, Yu ZB, Yao ZY, Cheng J, Wang YT, Song XT, Li M. The Roles of TRIMs in Antiviral Innate Immune Signaling. Front Cell Infect Microbiol. 2021 Mar 15;11:628275. doi: 10.3389/fcimb.2021.628275. PMID: 33791238; PMCID: PMC8005608.

Shen, LW., Qian, MQ., Yu, K. et al. Inhibition of Influenza A virus propagation by benzoselenoxanthenes stabilizing TMPRSS2 Gene G-quadruplex and hence down-regulating TMPRSS2 expression. Sci Rep 10, 7635 (2020). https://doi.org/10.1038/s41598-020-64368-8

Sheppard P, Kindsvogel W, Xu W, Henderson K, Schlutsmeyer S, Whitmore TE, Kuestner R, Garrigues U, Birks C, Roraback J, Ostrander C, Dong D, Shin J, Presnell S, Fox B, Haldeman B, Cooper E, Taft D, Gilbert T, Grant FJ, Tackett M, Krivan W, McKnight G, Clegg C, Foster D, Klucher KM. IL-28, IL-29 and their class II cytokine receptor IL-28R. Nat Immunol. 2003 Jan;4(1):63-8. doi: 10.1038/ni873. Epub 2002 Dec 2. PMID: 12469119.

Shi, T. et al. Global, regional, and national disease burden estimates of acute lower respiratory infections due to respiratory syncytial virus in young children in 2015: a systematic review and modelling study. Lancet 390, 946–958 (2017).

Sommereyns C, Paul S, Staeheli P, Michiels T. IFN-lambda (IFN-lambda) is expressed in a tissue-dependent fashion and primarily acts on epithelial cells in vivo. PLoS Pathog. 2008 Mar 14;4(3):e1000017. doi: 10.1371/journal.ppat.1000017. PMID: 18369468; PMCID: PMC2265414.

Spann, K. M., Tran, K. C. & Collins, P. L. Effects of nonstructural proteins NS1 and NS2 of human respiratory syncytial virus on interferon regulatory factor 3, NF-κB, and proinflammatory cytokines. J. Virol. 79, 5353–5362 (2005).

Stark, G. R. & Darnell, J. E. Jr. The JAK-STAT pathway at twenty. Immunity 36, 503–514 (2012).

Stark, G. R., Kerr, I. M., Williams, B. R. G., Silverman, R. H. & Schreiber, R. D. How cells respond to interferons. Annu. Rev. Biochem. 67, 227–264 (1998).

Starr R, Metcalf D, Elefanty AG, Brysha M, Willson TA, Nicola NA, Hilton DJ, Alexander WS. Liver degeneration and lymphoid deficiencies in mice lacking suppressor of cytokine signaling-1. Proc Natl Acad Sci U S A. 1998 Nov 24;95(24):14395-9. doi: 10.1073/pnas.95.24.14395. PMID: 9826711; PMCID: PMC24384.

Statello, L., Guo, C. J., Chen, L. L. & Huarte, M. Gene regulation by long non-coding RNAs and its biological functions. Nat. Rev. Mol. Cell Biol. 22, 96–118 (2021).

Su, Z., Monshaugen, I., Wilson, B. et al. TRMT6/61A-dependent base methylation of tRNA-derived fragments regulates gene-silencing activity and the unfolded protein response in bladder cancer. Nat Commun 13, 2165 (2022). https://doi.org/10.1038/s41467-022-29790-8

Sun L, Wu J, Du F, Chen X, Chen ZJ. Cyclic GMP-AMP synthase is a cytosolic DNA sensor that activates the type I interferon pathway. Science. 2013 Feb 15;339(6121):786-91. doi: 10.1126/science.1232458. Epub 2012 Dec 20. PMID: 23258413; PMCID: PMC3863629.

Suvanto MT, Uusitalo R, Otte Im Kampe E, Vuorinen T, Kurkela S, Vapalahti O, Dub T, Huhtamo E, Korhonen EM. Sindbis virus outbreak and evidence for geographical expansion in Finland, 2021. Euro Surveill. 2022 Aug;27(31):2200580. doi: 10.2807/1560-7917.ES.2022.27.31.2200580. Erratum in: Euro Surveill. 2022 Sep;27(35). doi: 10.2807/1560-7917.ES.2022.27.35.220901e. PMID: 35929430; PMCID: PMC9358406.

Suzuki, T. The expanding world of tRNA modifications and their disease relevance. Nat Rev Mol Cell Biol 22, 375–392 (2021). https://doi.org/10.1038/s41580-021-00342-0

Sze-Ling Ng, Brad A. Friedman, Sonja Schmid, Jason Gertz, Richard M. Myers, Benjamin R. Tenoever, and Tom Maniatis. IκB kinase epsilon (IKK(epsilon)) regulates the balance between type I and type II interferon responses. Proceedings of the National Academy of Sciences of the United States of America, 108(52):21170–21175, December 2011.

Takahashi K, Asabe S, Wieland S, Garaigorta U, Gastaminza P, Isogawa M, Chisari FV. Plasmacytoid dendritic cells sense hepatitis C virus-infected cells, produce interferon, and inhibit infection. Proc Natl Acad Sci U S A. 2010 Apr 20;107(16):7431-6. doi: 10.1073/pnas.1002301107. Epub 2010 Mar 15. PMID: 20231459; PMCID: PMC2867703.

Tamura T, Yanai H, Savitsky D, Taniguchi T. The IRF family transcription factors in immunity and oncogenesis. Annu Rev Immunol. 2008;26:535-84. doi: 10.1146/annurev.immunol.26.021607.090400. PMID: 18303999.

Tan L, Guo Z, Wang X, Kim DY, Li R. 2024. Utilization of nanopore direct RNA sequencing to analyze viral RNA modifications. mSystems 9:e01163-23. https://doi.org/10.1128/msystems.01163-23

Tarnow C, Engels G, Arendt A, Schwalm F, Sediri H, Preuss A, Nelson PS, Garten W, Klenk HD, Gabriel G, Böttcher-Friebertshäuser E. TMPRSS2 is a host factor that is essential for pneumotropism and pathogenicity of H7N9 influenza A virus in mice. J Virol. 2014 May;88(9):4744-51. doi: 10.1128/JVI.03799-13. Epub 2014 Feb 12. PMID: 24522916; PMCID: PMC3993819.

Te Velthuis AJ, Fodor E. Influenza virus RNA polymerase: insights into the mechanisms of viral RNA synthesis. Nat Rev Microbiol. 2016 Aug;14(8):479-93. doi: 10.1038/nrmicro.2016.87. Epub 2016 Jul 11. PMID: 27396566; PMCID: PMC4966622.

Temin HM, Mizutani S. 1970. RNA-dependent DNA polymerase in virions of Rous sarcoma virus. Nature 226:1211–13

Tenoever BR, et al. 2007. Multiple functions of the IKK-related kinase IKKepsilon in interferon-mediated antiviral immunity. Science 315(5816):1274–1278.

The ENCODE Project Consortium. An integrated encyclopedia of DNA elements in the human genome. Nature 489, 57–74 (2012). https://doi.org/10.1038/nature11247

Thery F, Eggermont D, Impens F. Proteomics Mapping of the ISGylation Landscape in Innate Immunity. Front Immunol. 2021 Aug 10;12:720765. doi: 10.3389/fimmu.2021.720765. PMID: 34447387; PMCID: PMC8383068.

Thomas S, Rai J, John L, Schaefer S, Pützer BM, Herchenröder O. Chikungunya virus capsid protein contains nuclear import and export signals. Virol J. 2013 Aug 28;10:269. doi: 10.1186/1743-422X-10-269. PMID: 23984714; PMCID: PMC3765696.

Thoresen D, Wang W, Galls D, Guo R, Xu L, Pyle AM. The molecular mechanism of RIG-I activation and signaling. Immunol Rev. 2021 Nov;304(1):154-168. doi: 10.1111/imr.13022. Epub 2021 Sep 12. PMID: 34514601; PMCID: PMC9293153.

Thuring, K., Schmid, K., Keller, P. & Helm, M. LC-MS analysis of methylated RNA. Methods Mol. Biol. 1562, 3–18 (2017).

Tian X, Zhang K, Min J, Chen C, Cao Y, Ding C, Liu W, Li J. Metabolomic Analysis of Influenza A Virus A/WSN/1933 (H1N1) Infected A549 Cells during First Cycle of Viral Replication. Viruses. 2019 Oct 31;11(11):1007. doi: 10.3390/v11111007. PMID: 31683654; PMCID: PMC6893833.

Tirumuru N, Zhao BS, Lu W, Lu Z, He C, Wu L. N(6)-methyladenosine of HIV-1 RNA regulates viral infection and HIV-1 Gag protein expression. Elife. 2016 Jul 2;5:e15528. doi: 10.7554/eLife.15528. Erratum in: Elife. 2017 Sep 13;6:e31482. doi: 10.7554/eLife.31482. PMID: 27371828; PMCID: PMC4961459.

Tong J, Zhang W, Chen Y, Yuan Q, Qin NN, Qu G. The Emerging Role of RNA Modifications in the Regulation of Antiviral Innate Immunity. Front Microbiol. 2022 Feb 3;13:845625. doi: 10.3389/fmicb.2022.845625. PMID: 35185855; PMCID: PMC8851159.

Torres AG, Piñeyro D, Filonava L, Stracker TH, Batlle E, Ribas de Pouplana L. A-to-I editing on tRNAs: biochemical, biological and evolutionary implications. FEBS Lett. 2014 Nov 28;588(23):4279-86. doi: 10.1016/j.febslet.2014.09.025. Epub 2014 Sep 27. PMID: 25263703.

Tremaglio CZ, Noton SL, Deflube LR, Fearns R. Respiratory syncytial virus polymerase can initiate transcription from position 3 of the leader promoter. J Virol.

2013;87(6):3196–207. Epub 2013/01/04. pmid:23283954; PubMed Central PMCID: PMCPMC3592119.

Tsai K, Jaguva Vasudevan AA, Martinez Campos C, Emery A, Swanstrom R, Cullen BR. Acetylation of Cytidine Residues Boosts HIV-1 Gene Expression by Increasing Viral RNA Stability. Cell Host Microbe. 2020 Aug 12;28(2):306-312.e6. doi: 10.1016/j.chom.2020.05.011. Epub 2020 Jun 12. PMID: 32533923; PMCID: PMC7429276.

Tsai, K., Jaguva Vasudevan, A. A., Martinez Campos, C., Emery, A., Swanstrom, R., and Cullen, B. R. (2020). Acetylation of cytidine residues boosts HIV-1 gene expression by increasing viral RNA stability. Cell Host Microbe 28, 306–312.e6. doi:10.1016/j.chom.2020.05.011

Turan, K. et al. Nuclear MxA proteins form a complex with influenza virus NP and inhibit the transcription of the engineered influenza virus genome. Nucleic Acids Res. 32, 643–652 (2004)

Turnbull, M. L., Wise, H. M., Nicol, M. Q., Smith, N., Dunfee, R. L., Beard, P. M., Jagger, B. W., Ligertwood, Y., Hardisty, G. R., Xiao, H., Benton, D. J., Coburn, A. M., Paulo, J. A., Gygi, S. P., Mccauley, J. W., Taubenberger, J. K., Lycett, S. J., Weekes, M. P., Dutia, B. M. & Digard, P. 2016. Role of the B Allele of Influenza A Virus Segment 8 in Setting Mammalian Host Range and Pathogenicity. J Virol, 90, 9263-84.

Turrini F, Marelli S, Kajaste-Rudnitski A, Lusic M, Van Lint C, Das AT, Harwig A, Berkhout B, Vicenzi E. HIV-1 transcriptional silencing caused by TRIM22 inhibition of Sp1 binding to the viral promoter. Retrovirology. 2015 Dec 18;12:104. doi: 10.1186/s12977-015-0230-0. PMID: 26683615; PMCID: PMC4683785.

Uddin, S. et al. Activation of the p38 Map kinase by type I interferons. J. Biol. Chem. 274, 30127–30131 (1999).

Uddin, S. et al. The Rac1/p38 Map kinase pathway is required for IFNα-dependent transcriptional activation but not serine phosphorylation of Stat-proteins. J. Biol. Chem. 275, 27634–27640 (2000).

Unterholzner L, Keating SE, Baran M, Horan KA, Jensen SB, Sharma S, Sirois CM, Jin T, Latz E, Xiao TS, Fitzgerald KA, Paludan SR, Bowie AG. IFI16 is an innate immune sensor for intracellular DNA. Nat Immunol. 2010 Nov;11(11):997-1004. doi: 10.1038/ni.1932. Epub 2010 Oct 3. PMID: 20890285; PMCID: PMC3142795.

Ushiki T, Huntington ND, Glaser SP, Kiu H, Georgiou A, Zhang JG, Metcalf D, Nicola NA, Roberts AW, Alexander WS. Rapid Inflammation in Mice Lacking Both SOCS1 and SOCS3 in Hematopoietic Cells. PLoS One. 2016 Sep 1;11(9):e0162111. doi: 10.1371/journal.pone.0162111. PMID: 27583437; PMCID: PMC5008821.

van Boxel-Dezaire AH, Rani MR, Stark GR. Complex modulation of cell type-specific signaling in response to type I interferons. Immunity. 2006 Sep;25(3):361-72. doi: 10.1016/j.immuni.2006.08.014. PMID: 16979568.

Van Damme N, Goff D, Katsura C, Jorgenson RL, Mitchell R, Johnson MC, Stephens EB, Guatelli J. The interferon-induced protein BST-2 restricts HIV-1 release and is

downregulated from the cell surface by the viral Vpu protein. Cell Host Microbe. 2008 Apr 17;3(4):245-52. doi: 10.1016/j.chom.2008.03.001. Epub 2008 Mar 13. PMID: 18342597; PMCID: PMC2474773.

Viengkhou B, White MY, Cordwell SJ, Campbell IL, Hofer MJ. A novel phosphoproteomic landscape evoked in response to type I interferon in the brain and in glial cells. J Neuroinflammation. 2021 Oct 16;18(1):237. doi: 10.1186/s12974-021-02277-x. PMID: 34656141; PMCID: PMC8520650.

Vilardo, E., Toth, U., Hazisllari, E., Hartmann, R. K. & Rossmanith, W. Cleavage kinetics of human mitochondrial RNase P and contribution of its non-nuclease subunits. Nucleic Acids Res 51, 10536–10550 (2023).

Vogel OA, et al. 2020. The p150 isoform of ADAR1 blocks sustained RLR signaling and apoptosis during influenza virus infection. PLoS Pathog. 16(9):e1008842.

Waku T, Nakajima Y, Yokoyama W, Nomura N, Kako K, Kobayashi A, Shimizu T, Fukamizu A. NML-mediated rRNA base methylation links ribosomal subunit formation to cell proliferation in a p53-dependent manner. J Cell Sci. 2016 Jun 15;129(12):2382-93. doi: 10.1242/jcs.183723. Epub 2016 May 5. PMID: 27149924.

Wang D, Booth JL, Wu W, Kiger N, Lettow M, Bates A, Pan C, Metcalf J, Schroeder SJ. Nanopore Direct RNA Sequencing Reveals Virus-Induced Changes in the Transcriptional Landscape in Human Bronchial Epithelial Cells. bioRxiv [Preprint]. 2024 Jun 28:2024.06.26.600852. doi: 10.1101/2024.06.26.600852. PMID: 38979243; PMCID: PMC11230378.

Wang H, Feng J, Zeng C, Liu J, Fu Z, Wang D, Wang Y, Zhang L, Li J, Jiang A, He M, Cao Y, Yan K, Tang H, Guo D, Xu K, Zhou X, Zhou L, Lan K, Zhou Y, Chen Y. NSUN2-mediated M5c methylation of IRF3 mRNA negatively regulates type I interferon responses during various viral infections. Emerg Microbes Infect. 2023 Dec;12(1):2178238. doi: 10.1080/22221751.2023.2178238. PMID: 36748584; PMCID: PMC9946332.

Wang X, Hinson ER, Cresswell P. The interferon-inducible protein viperin inhibits influenza virus release by perturbing lipid rafts. Cell Host Microbe. 2007 Aug 16;2(2):96-105. doi: 10.1016/j.chom.2007.06.009. PMID: 18005724.

Wang, A., Tao, W., Tong, J., Gao, J., Wang, J., Hou, G., et al. (2022). m6A modifications regulate intestinal immunity and rotavirus infection. Elife 11, e73628. doi:10.7554/eLife.73628

Wang X, Li Y, Deloria-Knoll M, Madhi SA, Cohen C, Ali A, Basnet S, Bassat Q, Brooks WA, Chittaganpitch M, Echavarria M, Fasce RA, Goswami D, Hirve S, Homaira N, Howie SRC, Kotloff KL, Khuri-Bulos N, Krishnan A, Lucero MG, Lupisan S, Mira-Iglesias A, Moore DP, Moraleda C, Nunes M, Oshitani H, Owor BE, Polack FP, O'Brien KL, Rasmussen ZA, Rath BA, Salimi V, Scott JAG, Simões EAF, Strand TA, Thea DM, Treurnicht FK, Vaccari LC, Yoshida LM, Zar HJ, Campbell H, Nair H; Respiratory Virus Global Epidemiology Network. Global burden of acute lower respiratory infection associated with human metapneumovirus in children under 5 years in 2018: a systematic review and modelling study. Lancet Glob Health. 2021 Jan;9(1):e33-e43.

doi: 10.1016/S2214-109X(20)30393-4. Epub 2020 Nov 26. PMID: 33248481; PMCID: PMC7783516.

Wang, Y., Liu, Y., Guan, Y. et al. Integrated analysis of immune-related genes in endometrial carcinoma. Cancer Cell Int 20, 477 (2020). https://doi.org/10.1186/s12935-020-01572-6

Ward SV, et al. 2011. RNA editing enzyme adenosine deaminase is a restriction factor for controlling measles virus replication that also is required for embryogenesis. Proc Natl Acad Sci USA. 108(1):331–336.

Ward, S. V., George, C. X., Welch, M. J., Liou, L. Y., Hahm, B., Lewicki, H., et al. (2011). RNA editing enzyme adenosine deaminase is a restriction factor for controlling measles virus replication that also is required for embryogenesis. Proc. Natl. Acad. Sci. 108, 331–336. doi:10.1073/pnas.1017241108

Watanabe T, Kawakami E, Shoemaker JE, Lopes TJ, Matsuoka Y, Tomita Y, Kozuka-Hata H, Gorai T, Kuwahara T, Takeda E, Nagata A, Takano R, Kiso M, Yamashita M, Sakai-Tagawa Y, Katsura H, Nonaka N, Fujii H, Fujii K, Sugita Y, Noda T, Goto H, Fukuyama S, Watanabe S, Neumann G, Oyama M, Kitano H, Kawaoka Y. Influenza virus-host interactome screen as a platform for antiviral drug development. Cell Host Microbe. 2014 Dec 10;16(6):795-805. doi: 10.1016/j.chom.2014.11.002. Epub 2014 Nov 20. PMID: 25464832; PMCID: PMC4451456.

Watkins NJ, Bohnsack MT. The box C/D and H/ACA snoRNPs: key players in the modification, processing and the dynamic folding of ribosomal RNA. Wiley Interdiscip Rev RNA. 2012;3:397–414.

Wickenhagen A, Sugrue E, Lytras S, Kuchi S, Noerenberg M, Turnbull ML, Loney C, Herder V, Allan J, Jarmson I, Cameron-Ruiz N, Varjak M, Pinto RM, Lee JY, Iselin L, Palmalux N, Stewart DG, Swingler S, Greenwood EJD, Crozier TWM, Gu Q, Davies EL, Clohisey S, Wang B, Trindade Maranhão Costa F, Freire Santana M, de Lima Ferreira LC, Murphy L, Fawkes A, Meynert A, Grimes G; ISARIC4C Investigators; Da Silva Filho JL, Marti M, Hughes J, Stanton RJ, Wang ECY, Ho A, Davis I, Jarrett RF, Castello A, Robertson DL, Semple MG, Openshaw PJM, Palmarini M, Lehner PJ, Baillie JK, Rihn SJ, Wilson SJ. A prenylated dsRNA sensor protects against severe COVID-19. Science. 2021 Oct 29;374(6567):eabj3624. doi: 10.1126/science.abj3624. Epub 2021 Oct 29. PMID: 34581622; PMCID: PMC7612834.

Wiener D, Schwartz S. The epitranscriptome beyond m6A. Nat Rev Genet. 2021 Feb;22(2):119-131. doi: 10.1038/s41576-020-00295-8. Epub 2020 Nov 13. PMID: 33188361.

Wnuk M, Slipek P, Dziedzic M, Lewinska A. The Roles of Host 5-Methylcytosine RNA Methyltransferases during Viral Infections. International Journal of Molecular Sciences. 2020; 21(21):8176. https://doi.org/10.3390/ijms21218176

Wu T, Hu E, Xu S, Chen M, Guo P, Dai Z, Feng T, Zhou L, Tang W, Zhan L, Fu X, Liu S, Bo X, Yu G. clusterProfiler 4.0: A universal enrichment tool for interpreting omics data. Innovation (Camb). 2021 Jul 1;2(3):100141. doi: 10.1016/j.xinn.2021.100141. PMID: 34557778; PMCID: PMC8454663.

Wu, S., Li, W., Bai, Z. et al. Novel heterozygous compound TRMT5 mutations associated with combined oxidative phosphorylation deficiency 26 in a Chinese family: a case report. BMC Pediatr 22, 74 (2022). https://doi.org/10.1186/s12887-022-03138-z

Wu, Y., Song, K., Hao, W. et al. Nuclear soluble cGAS senses double-stranded DNA virus infection. Commun Biol 5, 433 (2022). https://doi.org/10.1038/s42003-022-03400-1

Xia, T.-L., Li, X., Wang, X., Zhu, Y. J., Zhang, H., Cheng, W., et al. (2021). N(6)-methyladenosine-binding protein YTHDF1 suppresses EBV replication and promotes EBV RNA decay. EMBO Rep. 22, e50128. doi:10.15252/embr.202050128

Xiao, W. et al. Nuclear m6A reader YTHDC1 regulates mRNA splicing. Mol. Cell 61, 507–519 (2016).

Xie L, Zhong X, Cao W, Liu J, Zu X, Chen L. Mechanisms of NAT10 as ac4C writer in diseases. Mol Ther Nucleic Acids. 2023 Apr 3;32:359-368. doi: 10.1016/j.omtn.2023.03.023. PMID: 37128278; PMCID: PMC10148080.

Xu L, Liu X, Sheng N, Oo KS, Liang J, Chionh YH, Xu J, Ye F, Gao YG, Dedon PC, Fu XY. Three distinct 3-methylcytidine (m3C) methyltransferases modify tRNA and mRNA in mice and humans. J Biol Chem. 2017 Sep 1;292(35):14695-14703. doi: 10.1074/jbc.M117.798298. Epub 2017 Jun 27. PMID: 28655767; PMCID: PMC5582859.

Xue, M., Zhao, B.S., Zhang, Z. et al. Viral N6-methyladenosine upregulates replication and pathogenesis of human respiratory syncytial virus. Nat Commun 10, 4595 (2019). https://doi.org/10.1038/s41467-019-12504-y

Yang K, Yang J, Yi J. Nucleolar Stress: hallmarks, sensing mechanism and diseases. Cell Stress. 2018 May 10;2(6):125-140. doi: 10.15698/cst2018.06.139. PMID: 31225478; PMCID: PMC6551681.

Yao QJ, Sang L, Lin M, Yin X, Dong W, Gong Y, Zhou BO. Mettl3-Mettl14 methyltransferase complex regulates the quiescence of adult hematopoietic stem cells. Cell Res. 2018 Sep;28(9):952-954. doi: 10.1038/s41422-018-0062-2. Epub 2018 Jul 13. PMID: 30006613; PMCID: PMC6123394.

Yao, Y., Ma, W., Guo, Y. et al. USP53 plays an antitumor role in hepatocellular carcinoma through deubiquitination of cytochrome c. Oncogenesis 11, 31 (2022). https://doi.org/10.1038/s41389-022-00404-8

Ye F, Chen ER, Nilsen TW. Kaposi's Sarcoma-Associated Herpesvirus Utilizes and Manipulates RNA N6-Adenosine Methylation To Promote Lytic Replication. J Virol. 2017 Jul 27;91(16):e00466-17. doi: 10.1128/JVI.00466-17. PMID: 28592530; PMCID: PMC5533915.

Yoneyama M, Kato H, Fujita T. Physiological functions of RIG-I-like receptors. Immunity. 2024 Apr 9;57(4):731-751. doi: 10.1016/j.immuni.2024.03.003. PMID: 38599168.

Yoneyama M, Kikuchi M, Natsukawa T, Shinobu N, Imaizumi T, Miyagishi M, Taira K, Akira S, Fujita T. The RNA helicase RIG-I has an essential function in double-stranded RNA-induced innate antiviral responses. Nat Immunol. 2004 Jul;5(7):730-7. doi: 10.1038/ni1087. Epub 2004 Jun 20. PMID: 15208624.

Yongzhi Chen, Shanshan Wang, Zhaohong Yi, Huabin Tian, Roghiyh Aliyari, Yanhua Li, Gang Chen, Ping Liu, Jin Zhong, Xinwen Chen, Peishuang Du, Lishan Su, F. Xiao-Feng Qin, Hongyu Deng, and Genhong Cheng. Interferon-inducible cholesterol-25-hydroxylase inhibits hepatitis C virus replication via distinct mechanisms. Scientific Reports, 4:7242, December 2014.

You M, Yu DH, Feng GS. Shp-2 tyrosine phosphatase functions as a negative regulator of the interferon-stimulated Jak/STAT pathway. Mol Cell Biol. 1999 Mar;19(3):2416-24. doi: 10.1128/MCB.19.3.2416. PMID: 10022928; PMCID: PMC84034.

Younis S, Kamel W, Falkeborn T, Wang H, Yu D, Daniels R, Essand M, Hinkula J, Akusjärvi G, Andersson L. Multiple nuclear-replicating viruses require the stress-induced protein ZC3H11A for efficient growth. Proc Natl Acad Sci U S A. 2018 Apr 17;115(16):E3808-E3816. doi: 10.1073/pnas.1722333115. Epub 2018 Apr 2. PMID: 29610341; PMCID: PMC5910864.

Yu, L., Liu, P. Cytosolic DNA sensing by cGAS: regulation, function, and human diseases. Sig Transduct Target Ther 6, 170 (2021). https://doi.org/10.1038/s41392-021-00554-y

Zaccara, S. & Jaffrey, S. R. A unified model for the function of YTHDF proteins in regulating m6A-modified mRNA. Cell 181, 1582–1595.e18 (2020).

Zanotto, P.M.; Gibbs, M.J.; Gould, E.A.; Holmes, E.C. A reevaluation of the higher taxonomy of viruses based on RNA polymerases. J. Virol. 1996, 70, 6083–6096.

Zarember KA, Godowski PJ. Tissue expression of human Toll-like receptors and differential regulation of Toll-like receptor mRNAs in leukocytes in response to microbes, their products, and cytokines. J Immunol. 2002 Jan 15;168(2):554-61. doi: 10.4049/jimmunol.168.2.554. Erratum in: J Immunol 2002 Jul 15;169(2):1136. PMID: 11777946.

Zarnegar BJ, Flynn RA, Shen Y, Do BT, Chang HY, Khavari PA. irCLIP platform for efficient characterization of protein-RNA interactions. Nat Methods. 2016 Jun;13(6):489-92. doi: 10.1038/nmeth.3840. Epub 2016 Apr 25. PMID: 27111506; PMCID: PMC5477425.

Zhang C, Jia G. Reversible RNA Modification N1-methyladenosine (m1A) in mRNA and tRNA. Genomics Proteomics Bioinformatics. 2018 Jun;16(3):155-161. doi: 10.1016/j.gpb.2018.03.003. Epub 2018 Jun 14. PMID: 29908293; PMCID: PMC6076376.

Zhang H, Yang B, Pomerantz RJ, Zhang C, Arunachalam SC, Gao L. The cytidine deaminase CEM15 induces hypermutation in newly synthesized HIV-1 DNA. Nature.

2003 Jul 3;424(6944):94-8. doi: 10.1038/nature01707. Epub 2003 May 28. PMID: 12808465; PMCID: PMC1350966.

Zhang Q, Kang Y, Wang S, Gonzalez GM, Li W, Hui H, Wang Y, Rana TM. HIV reprograms host m6Am RNA methylome by viral Vpr protein-mediated degradation of PCIF1. Nat Commun. 2021 Sep 20;12(1):5543. doi: 10.1038/s41467-021-25683-4. PMID: 34545078; PMCID: PMC8452764.

Zhang Y, Sun S, Du C, Hu K, Zhang C, Liu M, Wu Q, Dong N. Transmembrane serine protease TMPRSS2 implicated in SARS-CoV-2 infection is autoactivated intracellularly and requires N-glycosylation for regulation. J Biol Chem. 2022 Dec;298(12):102643. doi: 10.1016/j.jbc.2022.102643. Epub 2022 Oct 26. PMID: 36309092; PMCID: PMC9598255.

Zhang Y, Wang X, Zhang X, Wang J, Ma Y, Zhang L, Cao X. RNA-binding protein YTHDF3 suppresses interferon-dependent antiviral responses by promoting FOXO3 translation. Proc Natl Acad Sci U S A. 2019 Jan 15;116(3):976-981. doi: 10.1073/pnas.1812536116. Epub 2018 Dec 27. PMID: 30591559; PMCID: PMC6338863.

Zhang Y, Zhang LS, Dai Q, Chen P, Lu M, Kairis EL, Murugaiah V, Xu J, Shukla RK, Liang X, Zou Z, Cormet-Boyaka E, Qiu J, Peeples ME, Sharma A, He C, Li J. 5-methylcytosine (m5C) RNA modification controls the innate immune response to virus infection by regulating type I interferons. Proc Natl Acad Sci U S A. 2022 Oct 18;119(42):e2123338119. doi: 10.1073/pnas.2123338119. Epub 2022 Oct 14. PMID: 36240321; PMCID: PMC9586267.

Zhang, J. J. et al. Ser727-dependent recruitment of MCM5 by Stat1α in IFN-γ-induced transcriptional activation. EMBO J. 17, 6963–6971 (1998).

Zheng G, Dahl JA, Niu Y, Fedorcsak P, Huang CM, Li CJ, Vågbø CB, Shi Y, Wang WL, Song SH, Lu Z, Bosmans RP, Dai Q, Hao YJ, Yang X, Zhao WM, Tong WM, Wang XJ, Bogdan F, Furu K, Fu Y, Jia G, Zhao X, Liu J, Krokan HE, Klungland A, Yang YG, He C. ALKBH5 is a mammalian RNA demethylase that impacts RNA metabolism and mouse fertility. Mol Cell. 2013 Jan 10;49(1):18-29. doi: 10.1016/j.molcel.2012.10.015. Epub 2012 Nov 21. PMID: 23177736; PMCID: PMC3646334.

Zheng, G. et al. ALKBH5 is a mammalian RNA demethylase that impacts RNA metabolism and mouse fertility. Mol. Cell 49, 18–29 (2013).

Zheng, Q., Hou, J., Zhou, Y., Li, Z., and Cao, X. (2017). The RNA helicase DDX46 inhibits innate immunity by entrapping m(6)A-demethylated antiviral transcripts in the nucleus. Nat. Immunol. 18, 1094–1103. doi:10.1038/ni.3830

Zhou A., Paranjape J.M., Der S.D., Williams B.R., Silverman R.H. Interferon action in triply deficient mice reveals the existence of alternative antiviral pathways. Virology. 1999;258:435–440.

Zhou H, Kimsey IJ, Nikolova EN, Sathyamoorthy B, Grazioli G, McSally J, Bai T, Wunderlich CH, Kreutz C, Andricioaei I, Al-Hashimi HM. m(1)A and m(1)G disrupt A-RNA structure through the intrinsic instability of Hoogsteen base pairs. Nat Struct Mol

Biol. 2016 Sep;23(9):803-10. doi: 10.1038/nsmb.3270. Epub 2016 Aug 1. PMID: 27478929; PMCID: PMC5016226.

Zhu Y, Chen G, Lv F, Wang X, Ji X et al. 2011. Zinc-finger antiviral protein inhibits HIV-1 infection by selectively targeting multiply spliced viral mRNAs for degradation. PNAS 108:15834–39

Zhu Y, Wang X, Goff SP, Gao G. 2012. Translational repression precedes and is required for ZAP-mediated mRNA decay. EMBO J 31:4236–46

Züst, R. et al. Ribose 2′-O-methylation provides a molecular signature for the distinction of self and non-self mRNA dependent on the RNA sensor Mda5. Nat. Immunol. 12, 137–143 (2011).